Assessment of degradation rate constants for quantitative predictions of drug-drug interactions arising from CYP450 drug metabolising enzymes

Thesis submitted in accordance with the requirements of the University of Liverpool for the degree of Doctor in Philosophy by

Christina Yik See Chan

September 2017

This thesis is the result of my own work. The material contained within the thesis has not been presented, either wholly or in part, for any other degree of qualification.

Christina Chan

This research was carried out in the

Liverpool HIV Pharmacology Group

Department of Molecular and Clinical Pharmacology

University of Liverpool

UK

Table of Contents

Acknowledgements

The research presented in this thesis was carried out in the Department of Molecular and Clinical Pharmacology, University of Liverpool. I would like to express my gratitude to the MRC and Certara (Simcyp) for providing the funding and opportunity to carry out this project.

The making of this thesis has been an incredible journey and I am thankful for everyone I met along the way who have supported and contributed to it. I would like to thank to my supervisors Prof. Andrew Owen, Dr Lisa Almond and Dr Marco Siccardi for their supervision and guidance throughout the project. Prof. Owen directed me throughout the PhD and supervised every aspect of my work - thank you you for your continued patience and for being so supportive during my many moments of 'panic'. Dr Siccardi, thank you for all your inputs and advice, especially in all things analytical. Dr Almond and Dr Garner offered invaluable advice and interesting scientific discussions during the project.

A big thank you to my colleagues (past and present) at the Liverpool HIV Pharmacology group: Owain, Louise, Rajith, Rohan, Chris, Megan, Rana, Paul, Neill, Jay, Beth, Lee, Darren, Justin, Ana, Hannah, Helen, Pedro, Henry, Alessandro, Adeniyi, Laura, Sara and Jo. Your friendship and professional wisdom (mainly imparted at the AJs) has made the last 4 years so much fun! It has been a real priveledge to work with such brilliant minds and in a culture of open knowledge sharing where no question is too silly and everyone's willing to stop what they're doing to help you in an instant. The lessons I have learnt here (not just scientifically) will stay with me for life.

I would like to thank Rohan, Ky, Katie, Georgie, Izzi, flabbies and Gab for being there for me through the highs and lows and keeping me sane throughout.

Finally, this thesis is dedicated to my family: Mum, Dad and Michael. Thank you for your unconditional love and support despite not really knowing what I've been up to in the last 4 years. Dad, you always have the words to put everything right again.

Abbreviations

^{3}H	Tritium
µCi	Microcurie(s)
µg	Microgram(s)
µl	Microliter(s)
µM	Micromolar
ADME	Absorption, distribution, metabolism, excretion
ADR	Adverse drug reaction
AhR	Aryl hydrocarbon receptor
ALD	Autophagic-lysosomal degradation
AMFR	Autocrine motility factor receptor
ANOVA	Analysis of variance
AO	Aldehyde oxidase
ARNT	Aryl hydrocarbon receptor nuclear translocator
ATCC	American type culture collection
ATG	Autophagy-related gene
ATP	Adenosine triphosphate
ATV	Atazanavir
AUC	Area under the curve
BMI	Body mass index
BSA	Bovine serum albumin
CAR	Constitutive active receptor
CCRP	Cytoplasmic CAR retention protein
cDNA	Complementary deoxyribonucleic acid
^{o}C	Degree Celsius
CHIP	C-terminus of Hsc70-interacting protein
CHRM	Cryopreserved hepatocyte recovery medium
CC_{50}	Concentration causing 50% cytotoxicity
cm	Centimetre(s)
C_{max}	Maximum plasma concentration
CNS	Central nervous system
CO_2	Carbon dioxide
CPR	Cytochrome P450 reductase

C(t)	Cycle threshold
CYP	Cytochrome P450
Cyt b_5	Cytochrome b_5
DDI	Drug-drug interaction
DEST	Aspartate (D), glutamine (E), serine (S), threonine (T)
DME	Drug metabolising enzyme
DMEM	Dulbecco's modified eagle medium
DMSO	Dimethyl sulfoxide
DNA	Deoxyribonucleic acid
E1	Ub-activating enzyme
E2	Ub-conjugating enzyme
E3	Ub-protein ligase enzyme
EC_{50}	Concentration at 50% efficacy
ECL	Enhanced chemiluminescence
EGFR	Epidermal growth factor receptor
EMA	European Medicines Agency
E_{max}	Maximum induction response
ER	Endoplasmic reticulum
ERAD	ER-associated degradation
ERAD-C	ER-associated degradation of cytosolic domain
ERAD-L	ER-associated degradation of lumenal domain
ERAD-M	ER-associated degradation of membrane domain
ES	Enzyme-substrate complex
E_{SS}	Steady-state enzyme level
e^-	Electron
FBS	Fetal bovine serum
FDA	Food and drug administration (US)
FIC	Fractional inhibitory concentration
Fm_{cyp}	Fraction metabolised by CYP enzyme
FMO	Flavin monooxygenase
GAPDH	Glyceraldehyde 3-phosphate dehydrogenase
gp78	Glycoprotein 78
GPSP	Global protein stability profiling
GSH	Glutathione

GST	Glutathione S-transferase
h	Hour(s)
H^+	Hydrogen ion
HBSS	Hank's balanced salt solution
HEPES	4-(2-hydroxyethyl)-1-piperazine ethanesulfonic acid
HPLC	High performance liquid chromatography
HPLC-UV	High performance liquid chromatography-ultraviolet
HIV	Human immunodeficiency virus
HIV-1	Human immunodeficiency virus subtype 1
HPRT1	Hypoxanthine-guanine phosphoribosyltransferase 1
HRP	Horseradish peroxidase
I	Inhibitor / inactivator
IL-6	Interleukin-6
Ind	Inducer
IC_{50}	Concentration of inhibitor resulting in 50% inhibition
iTRAQ	Isobaric tag for relative and absolute quantification
IVIVE	In vitro – in vivo extrapolation
kDa	KiloDalton(s)
k_{deg}	Degradation rate constant
kg	Kilogram(s)
K_I	Inactivation rate constant
K_{inact}	Time-dependent inhibition constant
K_m	Michaelis-Menten constant
k_{syn}	Synthesis rate constant
K_{obs}	Apparent inactivation rate constant
LC3	Microtubule-associated protein 1 light chain 3
LIR	LC3-interacting region
Lys	Lysine
MBI	Mechanism-based inhibition
MDI	Metabolism-depedent inhibition
MDZ	Midazolam
mg	Milligram(s)
$MgCl_2$	Magnesium chloride
min	Minute(s)

ml	Millilitre(s)
mM	Millimolar
mRNA	Messenger RNA
MS	Mass-spectrometry
MTT	3-(4,5-dimethylthiazol-2-yl)-2,5-diphenyltetrazolium bromide
n	Number of observations
ng	Nanogram(s)
nM	Nanomolar
nt	Nucleotide
NADH	Reduced nicotinamide adenine dinucleotide
NADPH	Reduced nicotinamide adenine dinucleotide phosphate
NAT	*N*-acetyltransferase
NBR1	Neighbour of BRCA1 gene1
NFDM	Non-fat dried milk
NME	New molecular entity
NNRTI	Non-nucleoside reverse transcriptase inhibitor
NQO1	NADPH quinone oxidoreductase 1
nt	Nucleotide
NTC	Non-targeting control
O_2	Molecular oxygen
PB	Phenobarbital
PBPK	Physiologically-based pharmacokinetic
PBREM	Phenobarbital-responsive enhancer module
PCR	Polymerase chain reaction
PD	Pharmacodynamic
pH	$-Log_{10}$ hydrogen ion concentration
PI	Protease inhibitor
PK	Pharmacokinetic
PKA	Protein kinase A
PKC	Protein kinase C
PRH	Primary rat hepatocytes
PXR	Pregnane X receptor
QC	Quality control
qPCR	Real-time polymerase chain reaction

R^2	Correlation coefficient
RIF	Rifampicin
RIS	Relative induction score
RISC	RNA-induced silencing complex
RNA	Ribonucleic acid
RNAi	RNA interference
ROS	Reactive oxygen species
RT	Room temperature
RT-PCR	Reverse-transcription polymerase chain reaction
RTV	Ritonavir
s	Second(s)
S	Substrate
SD	Standard deviation
siRNA	Small-interfering ribonucleic acid
SILAC	Stable isotope labelling by amino acid
SNP	Single nucleotide polymorphism
SQSTM1	Sequestosome-1
SULT	Sulfotransferase
$t_{1/2}$	Half-life
TBT	Thiazolyl blue tetrazolium
TDI	Time-dependent inhibition
TPMT	Thiopurine *S*-methyltransferase
T-TBS	Tween-tris buffered saline
Ub	Ubiquitin
UBC7	Ubiquitin-conjugating enzyme E2 7
UBE2G1	Ubiquitin-conjugating enzyme E2 G1
UGT	UDP-glucuronosyltransferase
UPD	Ubiquitin-proteasome degradation
V	Volt
v/v	Volume per volume
VCP	Valosin-containing protein
V_{max}	Maximal rate of enzyme reaction
XRE	Xenobiotic response element
XREM	Xenobiotic response enhancer module

Publications

Chan, C., Roberts, O., Rajoli, R., Siccardi, M., Almond, L. and Owen, A. (2017) Derivation of CYP3A4 and CYP2B6 degradation rate constants in primary human hepatocytes: A siRNA-silencing-based approach. *Drug Metabolism & Pharmacokinetics.* In production.

Chan, C., Martin, P., Liptrott, N. J., Siccardi, M., Almond, L. and Owen, A. (2017) Incompatibility of chemical protein synthesis inhibitors with accurate measurement of extended protein degradation rates. *Pharmacology Research & Perspectives.* DOI: 10.1002/prp2.359.

Communications

Chan, C. Y., Liptrott, N. J., Martin, P., Siccardi, M., Almond, L. and Owen, A. The lack of utility of pharmacological interference for the study of protein degradation. Presented at the 13th European meeting for International Society for the Study of Xenobiotics. Glasgow, UK, June 2015.

Chan, C. Y., Roberts, O., Hassan, N., Liptrott, N. J., Siccardi, M., Almond, L. and Owen, A. Use of mRNA suppression to estimate CYP3A4 protein degradation rate constant in primary human hepatocytes. *Drug Metabolism and Pharmacokinetics*, 32, S109. Presented at the 11th International meeting for International Society for the Study of Xenobiotics, Busan, South Korea, June 2016.

Abstract

The first-order degradation rate constant (k_{deg}) of drug metabolising enzymes (DMEs) is a known source of uncertainty in the prediction of time-dependent drug-drug interactions (DDIs) in physiologically-based pharmacokinetic (PBPK) modelling. There is a large disparity or paucity of published k_{deg} and related half-life ($t_{1/2}$) values for DMEs. Physiologically-relevant k_{deg} values should ideally be derived *in vivo* to facilitate accurate DDI predictions. However, direct measurement of DME degradation in humans is not routinely possible and indirect measurements utilising changes in levels of specific endogenous substrates have only been described for a few DMEs. This thesis aims to develop an *in vitro* method of measuring DME protein degradation rates to improve the prediction accuracy of time-dependent DDIs.

One *in vitro* approach of measuring protein degradation rates involves inhibiting *de novo* protein synthesis, followed by tracking residual protein or activity decline over time. Pharmacological protein synthesis inhibitor agents are commonly used for this purpose but may cause cytotoxicity. Four commonly used inhibitor agents were assessed for their capacity to inhibit protein synthesis without overt cytotoxicity. However, all selected compounds were too cytotoxic for subsequent use in k_{deg} studies. Small-interfering ribose nucleic acid (siRNA) can be added to *in vitro* systems to initiate gene-specific silencing by inhibiting messenger RNA (mRNA) translation. It was hypothesised that siRNA would inhibit *de novo* protein synthesis with less cytotoxicity owing to its specificity. CYP3A4 is the most widely studied cytochrome P450 (CYP) enzyme in terms of DDIs because of its well-recognised role in xenobiotic metabolism. Primary human hepatocytes were treated with CYP3A4-specific siRNA to suppress mRNA translation, followed by the tracking of enzyme activity and protein loss over time to derive k_{deg}. CYP3A4 k_{deg} was calculated at 0.019 (± 0.044) and 0.020 (± 0.0003) h^{-1} from protein and activity loss, respectively. These values were in good agreement with existing published values. The siRNA approach was subsequently applied to determine CYP2B6 k_{deg}. The CYP2B6 k_{deg} values derived from siRNA-treated hepatocytes were 0.081 (± 0.009) h^{-1} from protein loss and 0.058 (± 0.010) and 0.062 (± 0.006) h^{-1} from activity loss, which were assessed by different methods. The CYP2B6 k_{deg} values derived from untreated hepatocytes were similar to values in literature. This novel approach can now be used for other less well-characterised DMEs that are associated with time-dependent DDIs.

Cellular protein abundance is a balance between synthesis and degradation. Dysregulation of the lysosomal or proteasomal protein degradation mechanisms affects steady-state protein levels and impacts on overall cellular functions. It was hypothesised that single nucleotide polymorphisms (SNPs) in the CYP3A4 protein degradation machinery could affect CYP3A4 protein abundance and downstream activity. Five SNPs were investigated for associations with plasma atazanair (ATV) concentrations, which was a surrogate measure for CYP3A4 activity. No associations were found and this was likely due to the lack of clear understanding of the specific mechanisms that commits CYP proteins for degradation. Further work in this field will identify targets that may be exploited in the future for more accurate measurements of DME k_{deg}.

The data presented in this thesis enhances the understanding of methods used to study protein degradation and this can be applied to multiple fields of cellular research. Importantly, work herein has generated a novel approach to measuring k_{deg} of proteins that can be applied to other less-well characterised enzymes for better prediction of time-dependent DDIs.

CHAPTER 1

GENERAL INTRODUCTION

CONTENTS

1. INTRODUCTION

Drug-drug interactions (DDIs) occur when two or more drugs are co-administered and the perpetrator drug(s) causes changes in exposure of the concomitant (victim) drug(s), which can lead to therapeutic failure or adverse drug reaction (ADR). This is particularly relevant for treatments in cancer, human immunodeficiency virus (HIV) and psychiatric disorders, and often in elderly patients where treatments require polypharmacy and also when drugs have narrow therapeutic windows (Scripture & Figg 2006). Mathematical modelling and simulation of DDI potential are becoming increasingly important to the drug discovery and development process. Regulatory agencies such as the US Food and Drug Administration (FDA) and European Medicines Agency (EMA) have advocated for such approaches to be applied for predicting the risk and magnitude of DDIs for new molecular entities (NME) as well as approved drug compounds in the pre and post-licensing stages of drug development. This has been useful for optimising drug candidates, informing dosing regimens and clinical trials, and reducing costs of drug discovery.

Drug metabolising enzymes (DME) are amongst some of the most important components in the complex interplay of factors giving rise to DDIs. Characterising drug-induced alterations to their activity via inhibition or induction is an important focus during drug development. Reliable predictions depend on accurate kinetic drug and system parameters that are incorporated into mathematical prediction algorithms. Several sources have indicated that the uncertainty of DME degradation rate constants (k_{deg}) gives rise to error in DDI predictions when incorporated into mechanistic static and dynamic physiologically-based pharmacokinetic (PBPK) modelling to predict *in vivo* effects (Obach et al. 2006; Wang 2010; Rowland Yeo et al. 2011; Mao et al.

2013). There is a large disparity in reported k_{deg} values of DMEs and currently no consensus as to the best method of obtaining k_{deg}. This thesis aims to address this issue with the optimisation of a novel and robust method of measuring k_{deg}.

1.1. Drug-drug interactions

DDIs can be pharmacokinetic (PK), whereby alterations in drug disposition, governing processes of absorption, distribution, metabolism and/or excretion (ADME), can lead to changes in drug exposure with consequential pharmacological effects. They can also be pharmacodynamic (PD) where the effects of the administered drugs in combination can be synergistic or antagonistic. DDIs occur through PK, PD or a combination of both mechanisms. PD interactions occur when drugs or substances have similar molecular targets but do not affect the PK parameters of each other. In synergistic PD interactions, two drugs may result in better response or exacerbated toxicity through separate mechanisms of action. An example of such a reaction is in the co-administration of warfarin and aspirin where both drugs' anticoagulant activity in combination can increase the risk of spontaneous bleeding through distinct drug targets (Chan 1995).

DDIs can have various outcomes: interactions between drugs can increase or decrease therapeutic and adverse effects, or result in a completely unique response that does not occur when the agents are given individually. Various other substances and factors can alter the PK and PD of medications for example, food, drug formulation excipients, nutritional supplements, genetics and environmental factors. Drugs with narrow therapeutic windows, such as antiretrovirals, anticoagulants, carbamazepine, oestrogens and aminoglycoside antibiotics, are particularly

susceptible to DDIs because relatively small changes in drug exposure will result in increased risk of ADRs or therapeutic failure (Wienkers & Heath 2005).

PK interactions are characterised by the alteration of the disposition (ADME) of one drug by another. If the alterations to ADME are of sufficient magnitude then a significant change in exposure of the victim drug occurs leading to altered pharmacological effects. An example of PK interactions is when multiple drugs compete for the same metabolic pathway and when the pathway is inhibited the substrate drugs undergo partial metabolism at a slower rate, which results in reduced clearance and increased exposure. An example of this is in the co-administration of CYP3A4 substrates clarithromycin and simvastatin, where clarithromycin inhibition of CYP3A4 leads to increased exposure of simvastatin that in turn could potentially cause rhabdomyolysis (Lee & Maddix 2001).

Drug exposure is quantified in PK terms by the maximum plasma concentration (C_{max}) and by AUC (area under the curve); this is the area of the curve in a plasma-concentration versus time response plot. Changes in C_{max} reflects the rate and extent of absorption of an orally-given drug; therefore encompassing the effects of first-pass metabolism. AUC corresponds to overall plasma exposure and changes in AUC are dependent on the rate of elimination. If AUC is significantly increased by DDI then pharmacological effects may become exaggerated and risk of ADR potential also increases. A significant decrease in AUC can result in reduction of pharmacological effects and risk of therapeutic failure. Quantifying changes in AUC can give indication as to whether DDIs are likely to occur (Bachmann 2009a).

1.2. Cytochrome P450 enzymes

Cytochrome P450 (CYP) are functionally diverse haemoprotein enzymes found ubiquitously in nature, including bacteria, yeast, plants, fish and mammals (Danielson 2002). Human CYP enzymes constitute a major enzyme family of 57 putatively functional genes and 59 pseudogenes grouped into 18 families and 44 subfamilies and these have specific functions such as biosynthesis of steroid hormones, prostaglandins and bile acids, degradation of endogenous compounds such as fatty acids, steroids, retinoic acids as well as exogenous compounds that include drugs and carcinogens, mostly through an oxidative transformation process (Williams et al. 2000). CYP enzymes can be found in a wide variety of tissues including the intestine, kidney, lung, brain, adrenal gland, testes, heart, nasal and tracheal mucosa and skin, but the highest abundance with the largest number of isoforms occurs in the liver causing it to be the major site of xenobiotic metabolism (Pelkonen et al. 2008). The small intestines constitute the next largest site of metabolism and the relative contributions of these sites to xenobiotic biotransformation depend on its route of administration. For intravenously administered drugs the liver is likely to be the major site of biotransformation bypassing the alimentary canal, whereas orally administered drugs will first undergo intestinal absorption where a proportion of the dose is metabolised by locally present DMEs, before reaching the liver. The solubility and lipophilicity of the drug compound, as well as the interplay between uptake and efflux transporters on enterocytes and hepatocytes are some of the factors that account for the differences in drug concentrations achieved in the gut and liver, which ultimately affect the proportion of administered dose that is able to reach systemic circulation and into target sites to elicit therapeutic effects.

CYP enzymes are classified according to their genetic information and sequence homology. About a dozen enzymes belonging in the CYP- 1, 2 and 3 families and are well characterised for the metabolism of xenobiotics. An estimated 70% of all commercially used drugs undergo CYP metabolism as the main route of clearance and ten isoforms of CYP enzymes carry out the majority of CYP-mediated metabolism, these include CYPs 1A2, 2A6, 2B6, 2C8, 2C9, 2C19, 2D6, 2E1, 3A4 and 3A5 (Williams et al. 2004; Guengerich 2008). CYP3A family accounts for >30% of CYP abundance in the liver, of which the most abundant isoform is CYP3A4 that is responsible for metabolising 50% of all currently used drugs. The CYP2 family accounts for around 60% of hepatic CYPs and they also catalyse a significant number of oxidative drug biotransformation reactions (Pelkonen et al. 2008).

All CYP enzymes contain a prosthetic group consisting of a ferric Fe^{3+} chelated to an aromatic polypophorin IX ring or haem, which is linked to the protein structure via a sulphur atom from a proximal cysteine ligand. They are potent oxidants and are called monooxygenases due to their mechanism of oxidation by inserting one oxygen atom into the oxidised substrate. CYP uses molecular oxygen (O_2) by inserting one oxygen atom into a substrate (S) and reducing the second atom to a water molecule, utilising two electrons (e^-) provided by donor reduced nicotinamide adenine dinucleotide phosphate (NADPH) via a reductase protein such as cytochrome b_5 (cyt b_5) as shown in equation A (Meunier et al. 2004):

$$S + O_2 + 2e^- + 2H^+ \rightarrow SO + H_2O \qquad (A)$$

The major pathway of elimination of toxic and pharmacological agents involves the biotransformation of lipophilic compounds to readily excreted water-soluble forms. The two distinct steps involved are traditionally described as phase I

(oxidation) and phase II (conjugation) and each step is catalysed by different metabolic enzymes. CYP enzymes catalyse the majority of phase I reactions, but other enzymes in this class include esterases, hydrolases, alcohol dehydrogenase and monoamine oxidases (MAOs). The main phase II conjugating enzymes include UDP-glucuronyltransferase (UGT), sulfotransferases (SULTs) and glutathione S-transferase (GST) (Pelkonen et al. 2008). Compounds undergo either phase I or phase II, or more commonly both stages, in the pathway of elimination.

Within the liver, CYP enzymes are embedded in the endoplasmic reticulum (ER) region and the orientation of the CYP within the ER is important for their activity. The hydrophobic region in the N-terminal end forms the monotopic membrane-spanning domain anchoring the protein to the ER. The haem containing catalytic part of the CYP is oriented towards the cytoplasm. The CYP redox partners NADPH, cytochrome P450 reductase (CPR) and cyt b_5 are also anchored to the ER orientated to the cytosolic side of the membrane, readily donating electrons to CYP catalytic centre (Bachmann 2009b).

1.2.1. CYP3A4

It is estimated that CYP3A4 is involved in metabolising 50% of all currently used drugs (Zhou 2008). It is the predominant CYP isoform in the gut and constitutes over 30% of all CYPs in the liver and therefore plays a critical role in xenobiotic metabolism at both sites (Pelkonen et al. 2008). The enzyme has large substrate variability, is highly inducible and allows catalysis of multiple compounds simultaneously, rendering it the most important and widely studied in the context of DDIs. The kinetic interactions between CYP3A4 and its substrates are complex, which complicates predictions of CYP3A4-mediated DDIs (Pelkonen et al. 2008;

Galetin et al. 2005), for example the HIV protease inhibitor drug ritonavir is reported to be both an inhibitor and inducer of CYP3A in a dose and time-dependent manner (Hsu et al. 1997; Foisy et al. 2008). Moreover, CYP3A4 has a large substrate overlap with other CYP enzymes and major transporters such as P-glycoprotein (P-gp) that further incriminates its association to many clinically significant DDIs. A list of CYP3A4 substrates, inhibitors and inducers are given in Table 1.1.

Many studies collectively refer 3A4 and 3A5 isoforms as CYP3A. CYP 3A4 and 3A5 isoforms have high structural homology and substrate specificity, however expression of *CYP3A5* can vary widely between populations. Over 80% of the Caucasian population carry the *CYP3A5*3* variant in the 3A5 isoform rendering it inactive, whereas over 90% of Sub-Equatorial African populations carry the functional *CYP3A5*1* allele (Lamba et al. 2012; Bains 2013). The majority of clinically relevant CYP3A4/5 inhibitors are established as mechanism-based enzyme inhibitors (Grimm et al. 2009).

Table 1.1 CYP3A substrate, inhibitor and inducer compounds, * denotes time-dependent inhibitors (FDA, 2016)

Substrate			Inhibitor			Inducer		
Sensitive		Moderate	Weak (<2-fold ↑AUC; 20-50%↓ clearance)	Moderate (>2 and >5-fold ↑AUC; 50-80%↓ clearance)	Strong (>5-fold ↑AUC; >80%↓ clearance)	Weak (20-50% ↓AUC)	Moderate (50-80% ↓AUC)	Strong (>80%↓AUC)
Alfentanil	Simvastatin	Alprazolam	Chlorzoxazone	Aprepitant	Atazanavir	Armodafinil	Bosentran	Carbamazepine
Avanafil	Sirolimus	Aprepitant	Cilostazol	Amiodarone*	Bocepravir	Fufinamide	Efavirenz	Enzalutamide
Budesonide	Tacrolimus	Atorvastatin	Fosaprepitant	Amprenavir*	Clarithromycin*		Etravirine	Mitotane
Buspirone	Testosterone	Colchicine	Istradefylline	Azamulin*	Conivaptan		Modafinil	Phenytoin
Conivaptan	Ticagrelor	Elugistat	Ivacaftor	Cimetidine	Corbicistat			Rifampicin
Darifenacin	Tipranavir	Pimozide	Lomitapide	Ciprofloxacin	Danoprevir			St John's Wort
Darunavir	Tolvaptan	Rilpivirine	Ranitidine	Clotrimazole	Darunavir			
Dasatinib	Triazolam	Rivaroxaban	Ranolazine	Crizotinib	Diltiazem*			
Dronedarone	Vardenafil	Tadalafil	Tacrolimus	Cyclosporine	Elvitegravir			
Ebastine			Ticagrelor	Delavirdine*	Grapefruit juice*			
Eletriptan				Dronedarone	Idelalisib			
Eplerenone				Erythromycin*	Indinavir			
Everolimus				Fluconazole	Itraconazole			
Felodipine				Fluvoxamine	Ketoconazole*			
Ibrutinib				Fosamprenavir	Lopinavir*			
Indinavir				Imatinib	Nefazodone*			
Lomitapide				Miconazole	Nelfinavir*			
Lovastatin				Tofisopam	Paritaprevir			
Lurasidone				Verapamil*	Posaconazole			
Maraviroc					Ritonavir*			
Midazolam*					Saquinavir*			
Naloxegol					Telithromycin			
Nisoldipine					Telaprevir			
Quetiapine					Tipranavir			
Saquinavir					Troleandomycin*			
Sildenafil					Voriconazole			

1.2.1. CYP2B6

Until just over a decade ago, CYP2B6 was regarded as a minor human hepatic CYP accounting for <1% of total content. However, studies since conducted with improved detection methods have indicated that the isoform is highly variable between individuals, accounting for 2-10% of overall CYP abundance and an estimated 8% contribution to metabolism of all clinically used drugs (Wang & Tompkins 2008; Hedrich et al. 2016). CYP2B6 is considered highly inducible by phenobarbital-type compounds and CYP3A4 inducing drugs such as rifampicin, dexamethasone and carbamazepine (Lindley et al. 2002; Kharasch et al. 2012; Faucette et al. 2004). CYP2B6 shares mechanisms of transcriptional regulation (discussed in 1.3.2) with several other DMEs, consequently inducers of CYP2B6 have also been found to induce CYP3A4 (Kharasch et al. 2012) and UGT1A1 as well as transporters such as P-gp (Tolson et al. 2009).

Compared with CYP3A4, there has been less significant enzyme inhibition interactions identified for CYP2B6. Walsky et al. (2006) evaluated 227 clinically used drugs for their ability to inhibit CYP2B6 *in vitro*. They found that 30 of the 227 compounds displayed 50% or greater inhibition at 30 μM and identified clopidogrel and ticlopidine as potent inhibitors. However, even with this significant *in vitro* finding, these inhibitors do not fit the FDA classification of a potent inhibitor. A list of CYP2B6 substrates, inhibitors and inducers are given in Table 1.2.

CYP2B6 is highly polymorphic with over 100 single nucleotide polymorphisms (SNPs) and 63 alleles identified. Most significant is the *CYP2B6*6* (516G>T and 785A>G) allele which occur in 15-60% of various populations, the homozygous phenotype results in a non-functional allele (Zanger & Klein 2013). This variant allele has been linked to central nervous system (CNS) toxicity of efavirenz by significantly increasing plasma levels (Rakhmanina & van den Anker 2011). Efavirenz is a non-nucleoside reverse transcriptase inhibitor (NNRTI)

used widely for treatment of HIV-1; it has a narrow therapeutic index that renders the drug particularly susceptible to therapeutic failure or toxicity with altered exposure. The highly inducible and polymorphic nature of the *CYP2B6* gene contribute to the large inter-individual variability observed with PK of substrate drugs and up to 250-fold expression difference between individuals (Hedrich et al. 2016).

To date, CYP2B6 has not been implicated in causing clinically-relevant DDIs, however combining its highly inducible potential, significant impact of genetic regulations and a likelihood of interactions with other CYP enzymes and transporter proteins, there is an increased likelihood of uncovering DDIs mediated by this enzyme in the future.

Table 1.2 CYP2B6 substrate, inhibitor and inducer compounds, * denotes time-dependent inhibitors (Collated from FDA, 2016 and Hedrich et al 2016)

Substrate		Inhibitor			Inducer		
Sensitive	Moderate	Weak (<2-fold ↑AUC; 20-50%↓ clearance)	Moderate (>2 and >5-fold ↑AUC; 50-80%↓ clearance)	Strong (>5-fold ↑AUC; >80%↓ clearance)	Weak (20-50% ↓AUC)	Moderate (50-80% ↓AUC)	Strong (>80%↓AUC)
Aminopyrine Artemether Artemisinin Bupropion Clotiazepam Coumarins Cyclophosphamide Diazepam Efavirenz Ifosfamide Lidocaine Mephenytoin Mephobarbital Methadone Nevirapine Pethidine Piclamilast Propofol S-mephobarbital Selegiline Temazepam	Antipyrine Ketamine Mexiletine Nicotine Tamoxifen Tazofelone Testosterone Valproic acid	Clopidogrel* Tenofovir Ticlopidine* Voriconazole	Phencyclidine* Sertraline Thiotepa *	-	Nevirapine	Efavirenz* Rifampicin Ritonavir	Carbamazepine Phenobarbital

1.3. Relevance of cytochrome P450 enzyme turnover in drug-drug interaction predictions

CYP enzymes are estimated to metabolise over 70% of all drugs on the market (Williams et al. 2004) and they tend to have broad and overlapping substrate specificity, which renders specific CYPs particularly relevant in causing DDIs. Most drugs cleared by the CYP system are metabolised by several isoforms but drugs that are metabolised by a single isoform are more likely to be victims of DDIs compared to those with multiple metabolic pathways (Pelkonen et al. 2008). Activities of CYP enzymes are affected by genetic, endogenous and environmental factors, which causes drug metabolism to be exceedingly variable between individuals. The EMA and FDA have issued specific guidelines on characterising inhibitory and induction potential of seven major CYP isoforms, 1A2, 2B6, 2C8, 2C9, 2C19, 2D6 and 3A, by new molecular entities (NMEs) as part of the drug development process to assess potential of ADRs caused by DDIs and to recommend dosing regimens and clinical trials (EMA 2012; FDA 2012; FDA 2017).

1.3.1 Categories of CYP inhibition interactions

Inhibition of CYP enzymes is the most common cause of clinically relevant DDIs and has been the reason for withdrawal of several drugs from the market over the years. For example, the antihistamine terfenadine was removed from market due to causing QT prolongation, torsades de pointes and sudden cardiac death in patients receiving CYP3A4 inhibitors (Woosley et al. 1993; Dresser et al. 2000). Inhibition of CYP function by a perpetrator compound can lead to the reduced metabolism of a victim drug that uses the same inhibited CYP enzyme in its metabolic clearance pathway. This increases the risk of accumulation of the parent drugs leading to ADRs

or a risk of therapeutic failure if the concomitant parent drug requires biotransformation into active metabolites to exert pharmacological effects.

CYP enzyme inhibition interactions are categorised into direct and time-dependent inhibition (TDI). Direct inhibition involves the rapid reversible association and dissociation of drugs and enzymes and this can be further divided into competitive, non-competitive, uncompetitive and mixed inhibition. Competitive inhibition occurs when a substrate (inhibitor) binds to a single active site that is also the active binding site for another substrate or the inhibitor itself and the binding of the inhibitor can be reversed with increased substrate concentrations. Non-competitive inhibition occurs if the inhibitor binds at a site that is distinct from the substrate-binding site, but the binding of which slows the product formation and addition of substrate cannot overcome the inhibition. Uncompetitive inhibition occurs when a drug can only bind to the enzyme-substrate complex when a substrate is present and then cause a slowing of product formation. Finally, mixed inhibition involves a combination of competitive and non-competitive inhibition to different degrees of affinity (Zhang & Wong 2005; Bachmann 2009a).

Direct inhibition has been the most widely studied; progress in this area has led to a push to study TDI (which includes mechanism-dependent inhibition) in CYP interactions (Riley & Wilson 2015). TDI generally results from irreversible or quasi-irreversible inhibition reactions. Irreversible inhibition refers to the covalent, whereas quasi-irreversible refers to the non-covalent, binding of a chemically reactive intermediate to the enzyme that catalyses its formation, resulting in an irreversible loss of enzyme function. TDI can also result from reversible inhibition, therefore the difference between TDI and mechanism-based inhibition (MBI) ought to be recognised (Grimm et al. 2009). TDI is defined as a compound that displays an

increase to the extent of inhibition it causes when incubated with the enzyme prior to addition of substrate, therefore TDI is a definition based on the kinetics of the interaction. Whilst all MBI are quasi-irreversible and irreversible inhibition interactions, MBI can only be defined after specific biochemical studies are conducted to prove that the enzyme forms a chemically reactive metabolite as part of the inhibition mechanism (Riley & Wilson 2015).

CYP inhibition interactions can also be categorised based on the agent that is inhibiting the enzyme in question. Inhibition can occur directly from the parent compound or from its metabolite(s). Metabolism-dependent inhibition (MDI) describes inhibition interactions caused by metabolite(s) of the investigated compound and can be further divided into reversible, irreversible and quasi-irreversible MDI (Parkinson et al. 2011).

1.3.2 Relevance of enzyme turnover in time-dependent interactions

At steady-state (E_{ss}) the rate of change of active enzyme concentration (d[E]/d*t*) is considered to be a balance between *de novo* protein synthesis (k_{syn}) and protein degradation, the rate of which is called k_{deg} (enzyme degradation rate constant) and this relationship is depicted in A (Yang et al. 2008):

$$\xrightarrow{k_{syn}} \mathbf{E} \xrightarrow{k_{deg}} \quad \text{(A)}$$

$$\frac{d[E]}{dt} = k_{syn} - (k_{deg} \times [E]) \quad (1)$$

$$[E]_{SS} = \frac{k_{syn}}{k_{deg}} \quad (2)$$

When equilibrium between enzyme k_{syn} and k_{deg} is disturbed, such as in the case of irreversible inhibition or induction interactions, the abundance of active enzyme will change and reach a new steady-state. The E_{SS} level and the time taken to

reach the new steady-state level are determined by enzyme k_{syn} and k_{deg} (as described by equation 2). Induction and time-dependent DDIs are mediated by a change in enzyme level; therefore accurate estimation of enzyme turnover will affect the accuracy of predictions of these interactions (Yang et al. 2008; Almond et al. 2009). Accordingly, the predictions of time-dependent DDIs (such as MBI and time-dependent induction) are most sensitive to inaccuracies in enzyme k_{deg} (Hutzler et al. 2011).

1.3.3 Mechanism-based inhibition

A mechanism-based enzyme inhibitor is a compound that undergoes a biotransformation catalysed by the enzyme to a reactive metabolite, which in turn inactivates the enzyme by binding covalently (irreversible inhibition) or non-covalently (quasi-irreversible inhibition) (Silverman 1995). This interaction is also referred to as MDI and suicide inhibition. Mechanism-based inhibition (MBI) results in a permanent inactivation of the enzyme that can only be overcome with the synthesis of new enzyme proteins (as depicted in figure 1.1), as such, interactions often manifest as slow-onset, long-lasting and cumulative in clinical scenarios (Venkatakrishnan & Obach 2007).

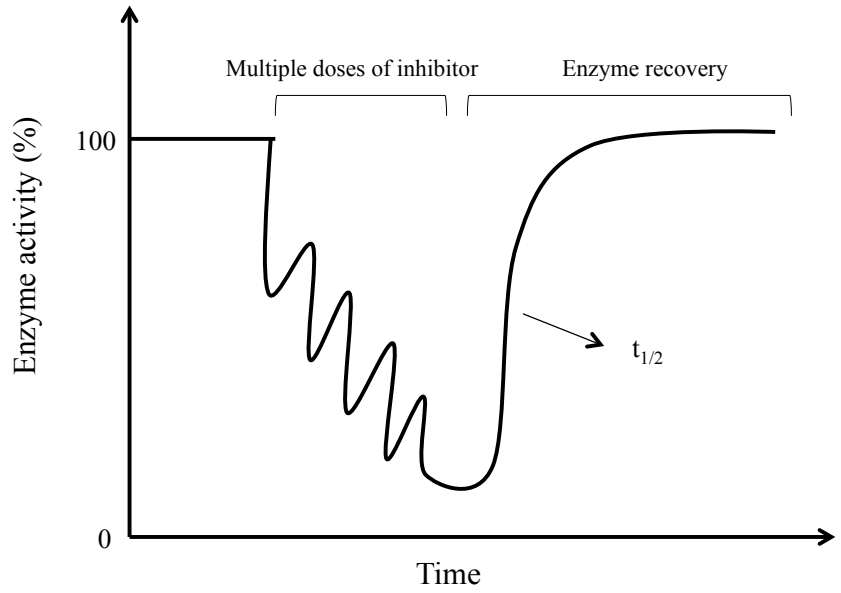

Figure 1.1 Schematic for the change in enzyme activity from baseline levels after multiple doses of a mechanism-based inhibitor. Upon removal of the inhibitor, enzyme recovery to basal levels will depend on resynthesis of the enzyme. Accordingly, the time taken to reach basal levels will depend on the rate of enzyme synthesis and degradation (that is interchangeable with $t_{1/2}$).

Predictions of DDIs based on *in vitro* models of competitive inhibition are known to underestimate the magnitude of interactions in the presence of a time-dependent inhibitor (Obach et al. 2006; Hemeryck et al. 2001). Therefore TDI require different models of kinetic interactions and TDI-specific parameters. MBI reactions, a subset of TDI, can be modelled as:

$$\mathrm{E} + \mathrm{I} \overset{k_s}{\leftrightarrow} \mathrm{EI} \overset{k_{p1}}{\longrightarrow} \mathrm{EI}' \overset{k_{p3}}{\longrightarrow} \mathrm{E_{inact}} \qquad \text{(B)}$$
$$\downarrow k_{p2}$$
$$\mathrm{E} + \mathrm{P}$$

Where *E* is the active enzyme and E_{inact} is the inactive forms of the enzyme; *I*, metabolite-dependent inactivator; *P*, product and *EI* and *EI'* are enzyme-inhibitor complexes. CYP enzymes catalyse the conversion of a mechanism-based inactivator

to the reactive form EI' with rate constant k_{p1} and this reactive metabolite is either released as a product (via k_{p2}) or react and further inactivate more enzyme, E_{inact}.

Evaluation of MBI can be divided into two categories: 1) high-throughput screening assays that rank compounds based on their TDI potential, 2) kinetic assays constructed to characterise the potency (K_I, inactivator concentration that produces 50% rate of maximal inactivation) and maximum inactivation rate (k_{inact}). These parameters are then incorporated into steady-state mechanistic or dynamic PBPK modelling to assess the potential of DDIs (Yang et al. 2005).

The *in vitro* two-step dilution approach is used to experimentally determine K_I and k_{inact}. The first step involves pre-incubating a hepatic CYP system with NADPH and a range of inactivator concentrations over varying amounts of time to determine the decrease of active enzyme over time. The second step includes a dilution of the pre-incubation mixture to quench inactivation, followed by an activity assay with an enzyme-specific probe substrate at saturating concentration (V_{max}) to track the remaining active enzyme. For each inhibitor concentration, natural log CYP activity versus pre-incubation time are plotted and the slope used for the calculation of the inactivation rate constant (k_{obs}). This is turn is fitted to the Michaelis-Menten model where the array of k_{obs} values are then plotted against inactivator concentrations to determine K_I and k_{inact} (Wong et al. 2016). The relationship between these parameters is given in the following equation:

$$k_{obs} = \frac{k_{inact} \times [I]}{K_I + [I]} \qquad (3)$$

The R value is calculated based on k_{obs} and k_{deg} and is used as an indicator for MBI potential:

$$R = \frac{k_{obs} + k_{deg}}{k_{deg}} \qquad (4)$$

The FDA draft guidance for industry regarding irreversible inhibitors recommended the use of equation 2 to assess DDI potential. If R > 1.1 (or 11 for CYP3A inhibition in the gut) then the test compound is considered likely to elicit considerable CYP MBI (FDA 2012) and warrants further investigation with a full mechanistic static model or dynamic PBPK model to predict *in vivo* DDI potential (Fujioka et al. 2012). Other methods such as the progress curve have also been suggested for assessing MBI potential (Burt et al. 2012).

1.3.3.1. Relevance of k_{deg} in mechanism-based inhibition

In the presence of an irreversible inhibitor *in vivo*, the levels of enzyme will decrease due to inactivation (described by equation 5), reaching a new steady-state level (equation 6). In steady-state CYP enzyme abundance is a balance between the rate of synthesis (k_{syn}) and rate of degradation (k_{deg}) (described by A). However, MBI will cause a secondary mechanism for loss of functional enzyme (rate constant λ) in addition to its endogenous degradation (k_{deg}), as depicted:

$$\xrightarrow{\mathbf{k_{syn}}} \mathbf{E} \xrightarrow{\mathbf{k_{deg}}} \quad \downarrow \boldsymbol{\lambda} \qquad \text{(C)}$$

K_{obs} is the inhibitory rate constant can be substituted into equations 5 and 6 to account for λ:

$$\frac{d[E]}{dt} = k_{syn} - \left(k_{deg} \times E\right) - \left(k_{obs} \times E\right) \qquad (5)$$

$$[E]_{SS} = \frac{k_{syn}}{k_{deg} + k_{obs}} \qquad (6)$$

Therefore by substituting inactivation constants, the mechanistic equation for MBI is:

$$\frac{d[E]}{dt} = k_{deg} \times E_0 - E_t \times \left(k_{deg} + \left(\frac{k_{inact} \times [I]}{K_I + [I]}\right)\right) \qquad (7)$$

Where, $k_{syn} = k_{deg} \times E_o$ and E_0 is the initial enzyme level.

From this principle, Mayhew et al. (2000) developed the following mechanistic static model equation to quantitatively assess the potential for an inactivator to cause increased exposure by MBI *in vivo*:

$$\delta AUC = \frac{1}{\left(\frac{fm_{,cyp}}{1+\frac{k_{inact} \times [I]_{in\ vivo}}{K_I \times k_{deg}}}\right)+(1-fm_{cyp})} \quad (8)$$

Where δAUC is the AUC ratio of *in vivo* exposure in the presence of inactivator compared to control state; fm_{cyp}, fraction metabolised by CYP isozyme and $[I]_{invivo}$, *in vivo* C_{max} concentration of inactivator.

Accurate predictions of DDIs arising from MBIs rely on four main parameters: 1) the *in vivo* enzyme k_{deg}, 2) *in vivo* concentration of inactivator drug available to the enzyme, 3) *in vitro* inactivation parameters k_{inact} and K_I and 4) the fraction of clearance of the affected drug mediated by the inactivated enzyme (Obach et al. 2006). Each of these parameters are potential sources of prediction errors and require further investigation.

1.3.4 Enzyme induction

Induction occurs when a perpetrating chemical compound causes an increase in the expression of enzymes in the metabolising tissue. This can result in increased CYP activity thereby enhancing clearance and reducing exposure of the victim drug and can also potentially lead to reduced therapeutic effect and/or increase in exposure to metabolites, which can in turn cause ADRs. These interactions can be clinically significant, for example in rifampicin induction of CYP3A that results in reducing the *in vivo* AUC of co-administered drug verapamil by up to 52-fold (Fromm et al. 1996), causing contraception failure if administered with oral contraceptives, organ rejection

when given with cyclosporine and failure of protease inhibitors in HIV treatments (Almond et al. 2009).

Several forms of CYP expression occur through transcription that is regulated by nuclear transcription factors including the aryl hydrocarbon receptor (AhR), pregnane X receptor (PXR) and the constitutive active receptor (CAR); the mechanisms of which are depicted in Figure 1.2. In the absence of an agonist AhR is located in the cytosol in complex with chaperone proteins Hsp90, ARA9 and p23. Upon binding, AhR undergoes conformational change that causes dissociation from chaperone proteins and nuclear translocation. Within the nucleus AhR dimerises with the AHR nuclear translocator (ARNT) and forms a DNA-binding complex. The AHR:ARNT heterodimer complex binds xenobiotic response element (XRE) and initiates transcription. CYPs 1A1, 1A2 and 1B1 are induced by this mechanism (Hewitt et al. 2007).

CYP3A induction is mediated by PXR and CAR. Following binding of an inducer to PXR, the complex translocates into the nucleus and forms a heterodimer with retinoid X receptor (RXR). The PXR:RXR heterodimer binds distal and proximal response elements in the ER6 regulatory region of the CYP3A gene, also referred as xenobiotic response enhancer module (XREM), to initiate transcription. In the absence of an activator, CAR resides in the cytosol in complex with cytoplasmic CAR retention protein (CCRP) and Hsp90. During induction, CAR pathway is activated upon binding an inducer and CAR forms a heterodimer with RXR and binds to many DNA-binding elements that are shared with PXR (Handschin & Meyer 2003).

In CYP2B6 induction, the CAR:RXR heterodimer binds to the phenobarbital-responsive enhancer module (PBREM) in the regulatory region of the CYP2B6 gene

and facilitates gene transcription. PXR has also been implicated in CYP2B6 regulation as the PXR:RXR complex is able to bind the PBREM eliciting transcription but selective activation of CAR over PXR provides preferential induction of CYP2B6 over CYP3A (Wang & Tompkins 2008; Pelkonen et al. 2008; Almond et al. 2009).

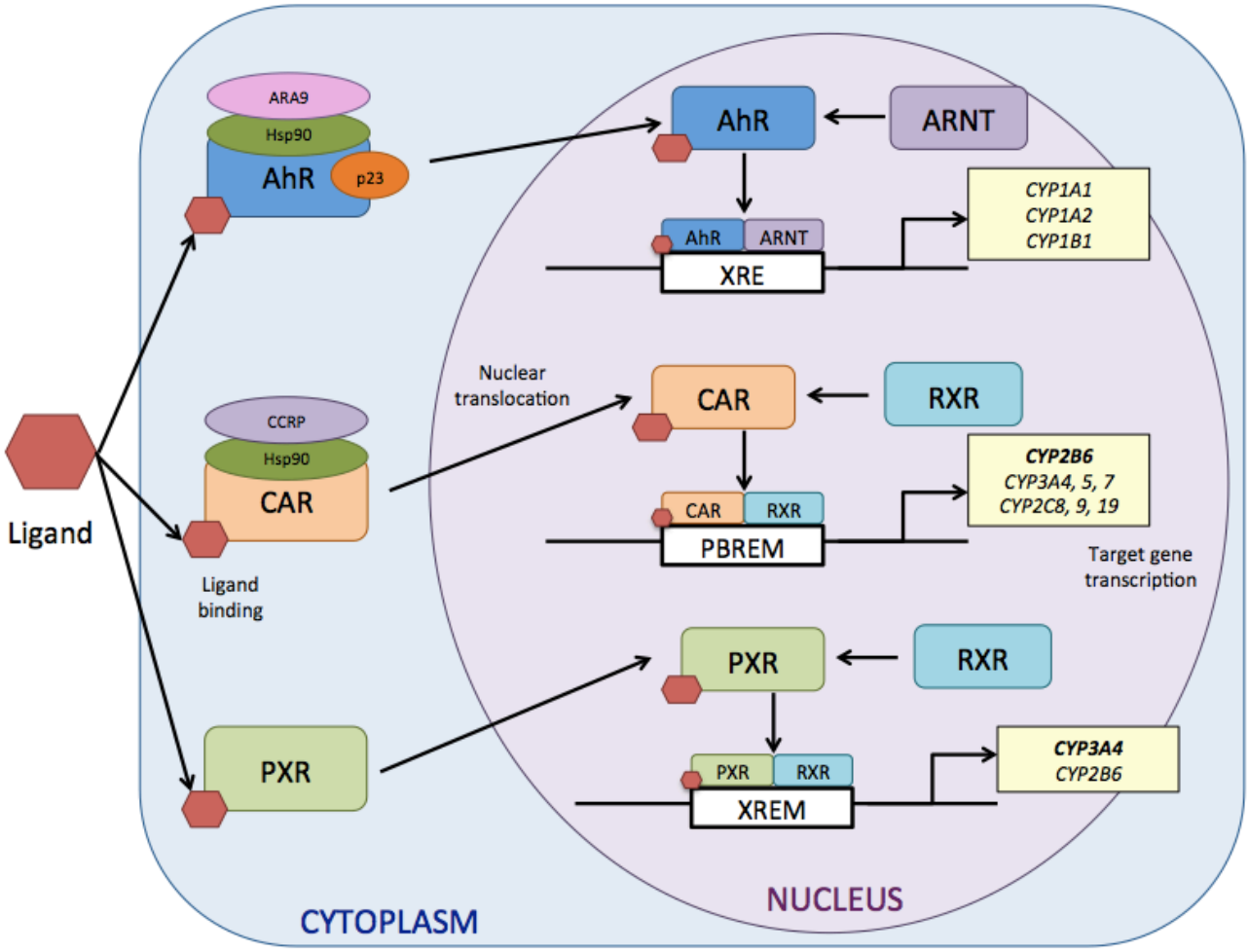

Figure 1.2 Schematic showing the activation of AhR, CAR and PXR nuclear receptor regulation pathways leading to induction of CYP enzymes. Adapted from Handschin & Meyer (2003)

CYP induction is a time and substrate concentration-dependent process. Induction occurs through binding of drugs to nuclear receptors which then activate the protein expression of a specific enzyme through an endogenous signalling pathway, therefore *in vitro* induction studies are conducted in living cells, as opposed to microsomal fractions, where these signalling mechanisms are intact. *In vitro* studies typically involve the plating and culturing of cells for 1-2 days prior to addition and incubation with a positive control and test compounds over a range of concentrations for a further few days. The magnitude of CYP increase can be detected by measuring specific enzyme activity and preferably mRNA and compared to untreated controls (Fahmi & Ripp 2010).

Several mathematical models were developed incorporating *in vitro* parameters derived from induction experiments, to assess whether a NME or drug compound is likely to cause induction DDIs. One such an approach is the relative induction score (RIS) that combines *in vitro* potency and efficacy induction parameters (E_{max} and EC_{50}, respectively) with the efficacious plasma inducer concentrations that is correlated to a calibration curve generated from known induction response:

$$\mathrm{RIS} = \frac{E_{max} \times [\mathrm{Ind}]}{EC_{50} + [\mathrm{Ind}]} \qquad (9)$$

Where E_{max} is the maximum induction response; EC_{50}, concentration at 50% of maximal induction and *[Ind]* is the concentration of inducer. If RIS > 0.1 then the compound is likely to lead to clinical DDI (Fahmi & Ripp 2010; Riley & Wilson 2015).

Another approach that is advocated by the 2012 draft FDA recommendations is the R_3-value, which is calculated by the following equation where *d* is the calibration factor (taken as 1):

$$R_3 = \frac{1}{1+\frac{d \times E_{max} \times [Ind]}{EC_{50}+[Ind]}} \quad (10)$$

If the R_3 value is < 0.9 then the investigated compound is likely to be an inducer and will require further incorporation into mechanistic static or dynamic models to assess likely magnitude of DDIs.

The RIS approach can be used where a known induction response, such as in the case of CYPs in hepatocytes, are available to generate a calibration curve to which the investigated inducer can be compared with. The R_3 approach conversely, requires generation of the entire profile of the concentration-induction curve (Kuramoto et al. 2017).

1.3.4.1 Relevance of k_{deg} in time-dependent induction

Increased abundance of enzyme levels in response to an inducer can result from either increased *de novo* protein synthesis (k_{syn}) or decrease in degradation (k_{deg}) by protein stabilisation. There will be a delay in both cases before the new equilibrium is reached and the time taken to reach this will depend on enzyme k_{deg} (depicted in Figure 1.3), therefore accurate estimation of enzyme turnover will affect the accuracy of predictions.

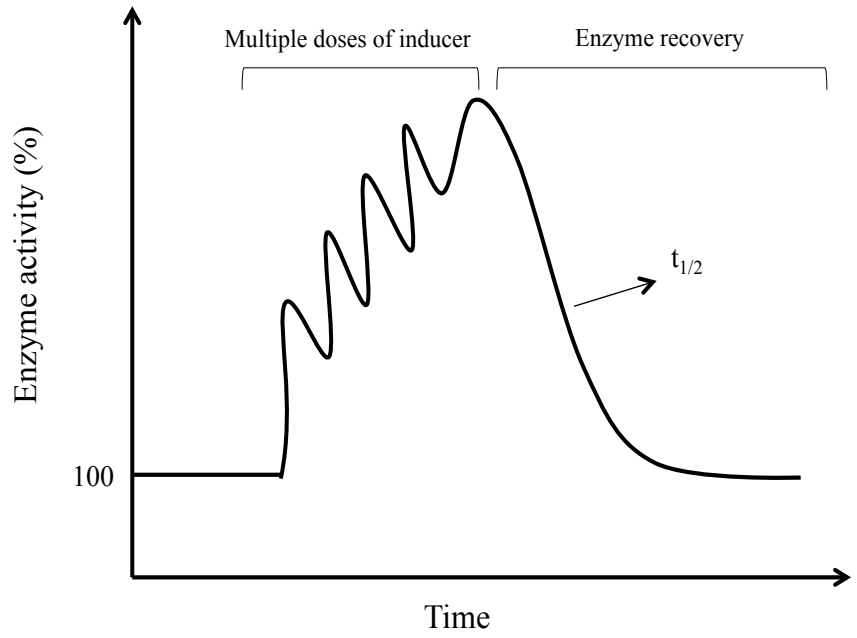

Figure 1.3 Schematic for the change in enzyme activity from baseline levels after multiple doses of an inducer. Upon removal of the inducer, the time taken to return to basal enzyme activity levels will be dependent on the rate of enzyme degradation (that is interchangeable with $t_{1/2}$).

The time taken to reach the new equilibrium is longer when k_{deg} is decreased compared to when enzyme synthesis is increased, thus enzyme k_{deg} is critical in the evaluation of time-dependent induction interactions (Almond et al. 2009). Enzyme levels will increase as described by the following equations:

$$\frac{d[E]'}{dt} = k_{syn} + k_{ind} \times [E]' - k_{deg} \times [E]' \qquad (11)$$

$$= k_{syn} + (k_{max} - k_{syn}) \times \frac{[Ind]}{EC_{50}+[Ind]} - k_{deg} \times [E]' \qquad (12)$$

A new steady state will be reached:

$$[E]'_{SS} = \frac{k_{syn}+(k_{max}-k_{syn})}{k_{deg}} \times \frac{[Ind]}{EC_{50}+[Ind]} \qquad (13)$$

Where k_{ind} is the enzyme induction rate constant; K_{max}, maximum rate of enzyme synthesis; EC_{50}, concentration of inducer at 50% of maximal induction and $[E]'_{SS}$ is the enzyme content at steady state in the presence of an inducer and *[Ind]* is the inducer concentration (Shou et al. 2008).

If the inducer only causes an increase in enzyme synthesis then the enzyme turnover (k_{deg}) does not determine the overall extent of induction. However, in the majority of time-dependent interactions the inducer is not given over sufficient time for the system to reach maximal induction and in this case the impact of interindividual variability in k_{deg} on the observed magnitude of induction will be apparent, therefore giving rise to variable DDI estimates.

1.4 Mathematical modelling for *in vivo* drug interaction predictions

Quantitative *in vitro* data describing ADME processes can be incorporated into computer-based algorithms to predict AUC changes and potential for DDIs. However, whilst many disposition interactions can be predicted qualitatively based on knowledge of ADME of interacting drugs, these quantitative changes in AUC are often insubstantial to bring about clinically-significant interactions in practice. Therefore, caution must be employed when using these prediction models because exaggeration of DDI potential can cause unnecessary attrition of potentially useful compounds (Bachmann 2009a).

1.4.1. Static mechanistic model

Fahmi et al. (2008) developed a mechanistic static model to predict the net potential for all DDIs simultaneously. This model accounts for metabolic

contributions of both the liver and the gut wall and is applicable to compounds that can act as both inhibitors and inducers of DMEs. For example, ritonavir has been demonstrated to be a potent time-dependent inhibitor of CYP3A4 as well as an activator of the PXR induction pathway (Hsu et al. 1997). Prediction of DDIs for such agents are difficult due to the challenge to determine which interaction phenomena will dominate the *in vivo* response. As such, the combined or net effect model was developed for compounds that exhibit combinations of reversible direct inhibition, TDI and/or induction (Fahmi & Ripp 2010). In this model, the AUC ratio (δAUC) can be described by:

$$\delta AUC = \frac{1}{[A_H \times B_H \times C_H] \times f_{mcyp} + (1 - f_{mcyp})} \times \frac{1}{[A_G \times B_G \times C_G] \times (1 - F_G) + F_G} \quad (14)$$

Where,

$$A = \frac{k_{deg}}{k_{deg} + \frac{k_{inact} \times [I]}{K_I + [I]}}$$

$$B = 1 + \frac{d \times E_{max} \times [Ind]}{EC_{50,Ind} + [Ind]}$$

$$C = \frac{1}{1 + \frac{[I]}{K_i}}$$

Where fm_{cyp} is the fraction metabolised by CYP enzyme; F_G, fraction of drug that escapes intestinal extraction. A, B and C are terms for TDI, induction and reversible inhibition, respectively. Subscript H and G are hepatic and gut interactions, respectively.

The FDA categorisations for changes to substrate drug are: > 5-fold increase in AUC or >80% decrease in clearance suggests a strong inhibitor, >2 but <5-fold AUC increase and 50-80% clearance decrease is a moderate inhibitor and >1.25 but <2-fold AUC increase and 20-50% clearance decrease is considered a weak inhibitor. The advantage of this model over basic models is that it incorporates both hepatic and

intestinal components as well as different mechanisms of DDIs that can improve prediction accuracy. However, predictability of the model relies on accurate estimations of additional parameters such as F_G, f_{mcyp}, dose and k_{deg}, which can introduce sources of error to the model (Fahmi & Ripp 2010).

1.4.2. Dynamic modelling

As more comprehensive compound and biological systems data have become available through the maturation of the methods of attaining them, there has been increased confidence in DDI prediction accuracy using dynamic modelling and therefore growing interests for incorporating the use of them during drug development (Riley & Wilson 2015). These simulations use PBPK and *in vitro-in vivo* extrapolation (IVIVE) methods to evaluate the relevance of inhibition and induction interactions observed *in vitro* to predict *in vivo* clinical scenarios. The FDA and EMA have advocated the use of dynamic simulations alongside the net effect model during drug development (FDA 2012; EMA 2012).

Static models assume a constant inhibitor/inducer concentration throughout the course of DDI prediction; they simply predict the change in overall exposure of victim drug from a constant concentration of perpetrator drug. However, many substrates are known to simultaneously display multiple forms of interaction including inhibition, inactivation and/or auto-activation, thus a comprehensive dynamic approach addressing the temporal changes in drug concentration as well as active enzyme levels and exposure to victim substrate should in theory improve predictions. As such, enzyme k_{deg} remains an important component in the dynamic modelling process. These models can also be semi- or whole-body PBPK and provide a physiologically-relevant framework enabling the incorporation of multiple ADME

processes, such as active transport and protein binding, as well as processes that are not yet fully characterised. However, predictability of such models relies on adequately characterised compound and biological parameters and prediction accuracy can be hampered by incorporating incorrect parameter values (Jones & Rowland-Yeo 2013).

Proprietary software programmes with in-built PBPK algorithms, such as Simcyp®, PK-Sim®, AcslXtreme® and GastroPlus™, are the most commonly used for dynamic predictions. Semi-physiological models encompassing fewer compartments provide a useful tool to examine effects within a specific tissue of interest, for example the liver or gut, and these models are simpler and less reliant on multiple accurate physiological parameters. In contrast, software such as Simcyp® requires more comprehensive input data to incorporate into the complex in-built algorithms, but the software offers the distinct advantage of incorporating parameter variability to allow for predictions of DDI magnitude in specific patient populations (Fahmi & Ripp 2010).

1.4.3. Uncertainty of k_{deg} in DDI predictions

Several sources have highlighted the sensitivity of DDI predictions in both static and dynamic models to k_{deg} values when enzyme levels change as a result of TDI or induction (Venkatakrishnan et al. 2007; Grimm et al. 2009; Fahmi & Ripp 2010; Galetin et al. 2006). Obach et al. (2006) demonstrated sensitivity of *in vivo* k_{deg} effects for accurate predictions of MBI interactions with contour mapping. Table 1.3 summarises some published studies that assessed the impact of different CYP3A k_{deg} values on DDI predictions. Different k_{deg} values have yielded varied prediction accuracies, therefore it is apparent that the choice for k_{deg} is deemed as very important

for the generation of DDI predictions. This is particularly relevant for compounds that display time-dependent mixed inhibition/induction reactions, where complex dynamic modelling is needed that relies heavily on accurate incorporation of systems parameters (Grimm et al. 2009; Prueksaritanont et al. 2013).

Table 1.3 Studies utilising different CYP3A4 k_{deg} values for DDI predictions

Study	Tested CYP3A4 k_{deg} (h^{-1}) values	Outcome	Reference
37 *in vivo* irreversible inhibition interactions with macrolides (erythromycin, clarithromycin and azithromycin) and diltiazem	0.0048 - 0.03	89% of studies predicted within 2-fold using k_{deg} of 0.0096 h^{-1}	(Galetin et al. 2006)
MBI with clarithromycin and erythromycin	0.0231, 0.0077 and 0.0026	Predicted clarithromycin inactivation rates were more sensitive to changes in k_{deg} compared with erythromycin	(Ghanbari et al. 2006)
45 *in vivo* inhibition interactions with diltiazem, erythromycin, fluconazole, fluoxetine, itraconazole, ketoconazole, paroxetine ritonavir, terbinafine and verapamil	0.0077 and 0.0193	Improved predictions of AUC for seven of nine trials when 0.0193 h^{-1} was used	(Einolf 2007)
Sensitivity analysis of erythromycin/midazolam inhibition interactions in rats	0.006 – 0.15	10-fold variation in k_{deg} resulted in midazolam AUC change from 8.3-18.8	(Zhang et al. 2010)
54 clinical interactions with clarithromycin, diltiazem, erythromycin, ritonavir, saquinavir, verapamil and fluoxetine	0.0077 and 0.03	Better prediction accuracy and less error relative to observed values when in k_{deg} of 0.03 h^{-1} was used with Simcyp.	(Wang 2010)
29 *in vivo* MBI interactions with azithromycin, clarithromycin, diltiazem, erythromycin and verapamil	0.0193 and 0.0077	Better prediction accuracy of 83 versus 59% of AUC within 1.5-fold when 0.0193 h^{-1} CYP3A4 k_{deg} was used compared to 0.0077 h^{-1}.	(Rowland Yeo et al. 2011)

Table 1.3 Continued.

Study	Tested CYP3A4 k_{deg} (h^{-1}) values	Outcome	Reference
Simcyp simulations of plasma concentration-time profiles of diltiazem and midazolam interactions	0.03 and 0.0077	Accurate Simcyp predictions (within 2-fold) were only observed when a hepatic CYP3A value of 0.03 h^{-1} was used.	(Friedman et al. 2011)
Sensitivity analysis of crizotinib-midazolam interaction predictions	0.000693 – 0.693	CYP3A4 $t_{1/2}$ of 25-35 h yielded the best prediction of crizotinib plasma concentrations whereas a $t_{1/2}$ of 30-40 h yielded the best midazolam AUC prediction. Hepatic k_{deg} of 0.019 h^{-1} yielded reasonable crizotinib interaction predictions.	(Mao et al. 2013)
Pioglitazone/midazolam and troglitazone/simvastatin DDI predictions	0.008, 0.03 and 0.019	Improved DDI predictions for both interactions with k_{deg} of 0.03 h^{-1} compared with 0.019 h^{-1} and 0.0008 h^{-1}.	(Prueksaritanont et al. 2013)
Prediction of midazolam AUC following 28 day once daily oral administration of rifampicin	0.008 and 0.03	Better prediction of observed midazolam AUC with k_{deg} of 0.08 h^{-1} compared to 0.03 h^{-1}.	(Prueksaritanont et al. 2013)

1.5 Methods of measuring CYP protein degradation rates

CYP k_{deg} is a physiological rather than drug-dependent parameter and cannot easily be directly measured *in vivo*; therefore it is often associated with uncertainty. The turnover of CYP enzymes is determined by protein degradation and, what is particularly relevant for DDI predictions, active site haem degradation. Depending on the approach of estimating k_{deg}, it is feasible that previous studies have generated $t_{1/2}$ estimates based on the protein component rather than the catalytic haem site. This will result in less relevance in terms of DDI kinetics thus introducing more uncertainty in the physiological relevance of k_{deg} for DDI predictions.

There have been several approaches used to estimate CYP k_{deg} and the most direct method is using pulse-chase tracer kinetic studies of a specific protein of interest in a living organism (Correia 1991). However, such an approach requires multiple invasive sampling of hepatic tissue over time, thus it is unsuitable for humans and has only been applied to rodent models. Half-lives of rat CYPs 1A2, 2E1 and 3A have been estimated to be 10 (Correia 1991), 6-7 (Roberts et al. 1995) and 14 hours (Watkins et al. 1985), respectively in this way. However, rat CYP enzymes have shorter half-lives compared to humans resulting in under prediction of human DDI risk when rat half-lives are used in prediction models (Iwano S 2015; Venkatakrishnan et al. 2007).

The approaches used for human estimates of human CYP k_{deg} fall into two main categories: 1) direct methods using *in vitro* models of the human liver and 2) indirect PK-based estimations based on *in vivo* animal or human systems.

Liver slices and primary cultured hepatocytes have traditionally been used as *in vitro* models to estimate human k_{deg}. Pichard et al. (1992) used a radiolabelled pulse-chase kinetic approach to estimate CYP3A4 k_{deg} in primary human hepatocytes and a

$t_{1/2}$ of 44 hours was derived. Renwick et al. (2000) derived k_{deg} estimates for several CYP enzymes through characterising the rates of loss of CYP apoprotein and CYP-specific metabolic activities in cultured human liver slices. The latter study, where pulse-chase was not conducted, is limited by the assumption that the CYP loss detected is solely due to enzyme degradation negating any *de novo* CYP synthesis that might occur during the analysis period. In both studies, the observed rate of loss of CYP may be confounded by cell death or differentiation during culture. Such caveats can result in uncertainty and lack of consensus on the optimum approach of measuring k_{deg}.

Analysis of the time-course of enzyme induction followed by tracking the de-induction profile upon removal of the inducer, or recovery profile following inactivation, may provide an indirect *in vivo* estimate of k_{deg} (as depicted in Figures 1.3 and 1.1, respectively). This is based on the assumption that steady-state enzyme levels comprise of a balance between synthesis and degradation and that CYP induction, de-induction and recovery from inactivation are all first-order processes with a rate constant equivalent to k_{deg}. The inactivator or inducer utilised in such studies must have a shorter $t_{1/2}$ than the enzyme turnover. If the inducer or inactivator has a $t_{1/2}$ longer than that of the enzyme, the $t_{1/2}$ of the drug will need to be deconvoluted from the overall process of induction, de-induction or recovery from inactivation to provide an estimate of k_{deg}. This can be done using physiologically-based modelling on the clinical PK data or via non-compartmental deconvolution (Venkatakrishnan & Obach 2007; Venkatakrishnan & Obach 2005; Venkatakrishnan et al. 2007).

Faber & Fuhr (2004) estimated human CYP1A2 $t_{1/2}$ to be 39 h from tracking the recovery of CYP1A2 activity from induced state to basal conditions following abrupt

cessation of heavy smoking. Venkatakrishnan & Obach (2005) utilised non-compartmental deconvolution of the $t_{1/2}$ of paroxetine, which was originally generated by Liston et al. (2002) who tracked the recovery time-course of CYP2D6 upon cessation of treatment of paroxetine inactivator. The deconvoluted $t_{1/2}$ of CYP2D6 was estimated to be 51 h. For CYP2E1, tracking de-induction during withdrawal phase in alcoholics derived a $t_{1/2}$ of 60 h (Lucas et al. 1995) and recovery of metabolic activity following inactivation by disulfiram have found the $t_{1/2}$ to be 51 h (Emery et al. 1999).

CYP3A (comprising 3A4 and 3A5) $t_{1/2}$ are the most extensively studied amongst CYP enzymes using indirect PK based estimations. Greenblatt (2003) tracked the recovery of midazolam oral clearance following CYP3A inactivation by grapefruit juice, which estimated the *in vivo* intestinal $t_{1/2}$ to be 23 h. For hepatic CYP3A4, the reported $t_{1/2}$ values range from 10 to 140 h (Yang et al. 2008) and these have been derived from many studies utilising a range of *in vitro* and *in vivo* approaches (Table 1.4). Earlier studies with *in vivo* rodent models estimated CYP3A $t_{1/2}$ to be 14 h (Watkins et al. 1985). At the opposite end of the spectrum, Von Bahr et al. (1998) estimated CYP3A4 $t_{1/2}$ to be 140 h from measuring nortriptyline metabolite formation *in vivo* in human subjects after dosing with pentobarbital. However, the accuracy of this estimate is likely to be limited by the fact that nortriptyline is metabolised by other CYP isozymes, primarily by CYP2D6, and the extent of metabolism can be highly variable between individuals. Several other estimates have found CYP3A4 $t_{1/2}$ to be in the region of 26 to 96 h. Table 1.4 shows a summation of the estimated turnover $t_{1/2}$ of human hepatic CYPs.

There are several caveats associated with the *in vivo* methods of deriving CYP k_{deg}. *In vivo* approaches characterise CYP activity through substrate drug turnover and

measurement of metabolite in urine or blood samples; and thus presents an indirect method of measuring k_{deg}. Such studies make the assumption that the probe substrate metabolites are produced by a single CYP isoform. However in practice, substrates such as ritonavir and midazolam are known to be metabolised by both CYP 3A4 and 3A5 (Soars et al. 2006) and chlorzoxazone has also been found to be metabolised by both CYP 1A2 and 2E1 (Ono et al. 1995). Where probe substrate compounds are used to estimate the k_{deg} for a specific CYP enzyme, the validity of k_{deg} estimate is put into question when the probe substrate is metabolised by multiple CYP isoforms. Furthermore, drugs such as ritonavir produce simultaneous auto-induction and MBI of CYP3A and therefore confounds the interpretation of k_{deg} estimates when using the model-based analysis of solely auto-induction kinetics. Estimates of k_{deg} based on *in vivo* de-induction profiles are limited by the assumption that there was no *de nov*o enzyme protein synthesis during the de-induction period. Another consideration is that *in vivo* estimates of hepatic CYP k_{deg} should take into account the relative contributions of gut disposition and metabolism of inducer/inactivator and probe substrate drug, when using PK based models for estimations with orally-dosed compounds. A combination of these caveats may give rise to the large difference between k_{deg} estimations across and within studies.

Considering the uncertainty of CYP k_{deg}, several CYP3A DDI studies have used an approach of selecting reasonable estimates of k_{deg} (for example, between 24-72 h range) for incorporation into the prediction model, followed by examining the sensitivity of the predicted interaction magnitude around the range of values used, as shown in Table 1.3 (Galetin et al. 2005; Ghanbari et al. 2006; Venkatakrishnan & Obach 2007). The sensitivity of DDI predictions to varying k_{deg} values is related to fm_{cyp} of the object drug. Prediction accuracy was found to be less sensitive to CYP

k_{deg} values when drugs had alternate clearance mechanisms (relating to a smaller fm_{cyp}) compared to those with exclusive clearance by the inactivated enzyme. As such, fm_{cyp} is incorporated into the static mechanistic models given by equations 8 and 14 (Venkatakrishnan et al. 2007; Obach et al. 2006).

Table 1.4 Human hepatic CYP turnover half-lives and corresponding k_{deg} (Updated from Yang et al. 2008)

CYP Enzyme	Source	Method	*n*	Half-life (h)	k_{deg} (h^{-1})	Reference
1A2	*In vitro*	Pulse-chase	1	51	0.014	(Diaz et al. 1990)
	In vitro	Tracking degradation over time in cultured hepatocytes	N/A	43	0.016	(Maurel 1996)
	In vitro	Tracking apoprotein over time in cultured liver slices	5	36 (8-58)	0.019	(Renwick et al 2000)
	In vivo	Tracking recovery profile following inactivation by heavy smoking	12	39 (19-143)	0.018	(Faber & Fuhr 2004)
	In vivo	Tracking autoinduction profile from carbamazepine using caffeine metabolism as probe	7	105	0.0066	(Magnusson et al. 2007)
2A6	*In vitro*	Tracking apoprotein loss over time in cultured liver slices	2	26 (19-37)	0.027	(Renwick et al 2000)
2B6	*In vitro*	Tracking apoprotein loss over time in cultured liver slices	1	32	0.022	(Renwick et al 2000)
	In vitro	De-induction profile in HepatoPac following rifampicin induction	2	68 (67-70)	0.010	(Dixit et al. 2016)
2C8	*In vitro*	Tracking apoprotein loss over time in cultured liver slices	5	23 (8-41)	0.030	(Renwick et al 2000)
	In vivo	Tracking recovery profile after gemfibrozil inactivation using repaglinide as probe	9	22 (16-28)	0.032	(Backman et al. 2009)
2C9	*In vitro*	Tracking apoprotein loss over time in cultured liver slices	5	104	0.0067	(Renwick et al 2000)
2C19	*In vitro*	Tracking apoprotein loss over time in cultured liver slices	3	26 (7-50)	0.027	(Renwick et al 2000)
2D6	*In vitro*	Tracking apoprotein loss over time in cultured liver slices	4	70	0.0099	(Renwick et al 2000)
	In vivo	Tracking recovery after MDMA inactivation using dextromethorphan as probe	12	37 (14-60)	0.019	(Yubero-lahoz et al. 2000)
	In vivo	Tracking recovery profile after paroxetine inactivation followed by non-compartmental deconvolution	13	51	0.014	(Liston et al 2002; Venkatakrishnan & Obach 2005)
	In vivo	Tracking recovery profile after MDMA inactivation and using dextromethorphan as probe	15	47 (35-58)	0.015	(O'Mathúna et al. 2008)

Table 1.4 continued

CYP Enzyme	Source	Method	*n*	Half-life (h)	k_{deg} (h^{-1})	Reference
2E1	*In vivo*	Tracking de-induction profile after alcohol induction	6	60	0.012	(Lucas et al 1995)
	In vivo	Tracking of enzyme recovery after disulfiram inactivation using chlorzoxazone as probe	13	50 (±19)	0.014	(Emery et al 1999)
	In vitro	Tracking apoprotein loss over time in cultured liver slices	5	27 (7-40)	0.026	(Renwick et al 2000)
4A11	*In vitro*	Tracking apoprotein loss over time in cultured liver slices	5	75 (56-77)	0.0092	(Renwick et al 2000)
3A4	*In vivo*	Tracking of auto-induction	6	96 (53-154)	0.0072	(Pitlick et al. 1976)
	In vivo	Tracking de-induction profile after carbamazepine induction	7	72 (20-146)	0.0096	Lai et al (1978)
	In vivo	Tracking de-induction profile after carbamazepine induction	3	(85-806)	-	(Warren et al. 1980)
	In vitro	Induction by rifampicin followed by pulse-chase tracking of de-induction in hepatocytes	1	44	0.016	(Pichard et al. 1992)
	In vivo	Tracking of auto-induction and interpreted by Yang et al 2008	13	10 (2-158)	0.069	(Boddy et al. 1995; Yang et al. 2008)
	In vitro	Tracking degradation over time in cultured hepatocytes	N/A	26	0.027	(Maurel, P 1996)
	In vivo	De-induction profile following rifampicin dosing with verapamil as probe	8	36-50	-	(Fromm et al 1996)
	In vivo	Tracking of auto-induction by ritonavir	16	85 (±61)	0.0082	(Hsu et al. 1997)
	In vivo	De-induction profile following phenobarbital dosing	6	140 (48-284)	0.0050	Von Bahr, C et al (1998)
	In vivo	Tracking of auto-induction by methadone	35	94 (62-205)	0.0074	(Rostami-Hodjegan et al. 1999)
	In vivo	Tracking de-induction after rifampicin dosage, measuring 6β-hydroxycortisol as substrate; interpreted by Yang et al.	15	72	0.0096	(Tran et al. 1999; Yang et al. 2008)
	In vitro	Tracking apoprotein loss over time in cultured liver slices	4	79	0.0088	(Renwick et al 2000)

Table 1.4 continued

CYP Enzyme	Source	Method	*n*	Half-life (h)	k_{deg} (h^{-1})	Reference
3A4	*In vivo*	Tracking autoinduction profile from carbamazepine with midazolam as probe	7	70	0.0099	(Magnusson et al 2007)
	In vivo	De-induction profile following St John's Wort induction	12	46 (20-116)	0.017	(Imai et al. 2008)
	In vivo	De-induction profile following carbamazepine induction	15	86	0.0081	(Punyawudho et al. 2009)
	In vivo	De-induction profile following rifampicin induction	11	86	0.008	(Reitman et al. 2011)
	In vitro	De-induction profile in HepatoPac following rifampicin induction	3	49 (43-56)	0.014	(Dixit et al 2015)
	In vitro	siRNA knockdown followed by metabolite detection	5	29 (22-39)	0.024	(Ramsden et al. 2015)
	In vitro	SILAC labelling in HepatoPac	4	30 (27-32)	0.023	(Takahashi et al. 2017)
3A5	*In vitro*	Tracking apoprotein loss over time in cultured liver slices	3	36 (15-70)	0.019	(Renwick et al 2000)

1.6. Mechanisms of CYP protein degradation

Protein abundance in a cellular system is a balance between the rate of synthesis and degradation. The ability of the cell to remove and replenish proteins in a dynamic state of constant turnover is paramount to maintaining essential cellular functions and all protein turnovers are regulated in a specific way. Rates of protein synthesis are readily measurable by time-course experiments utilising radioisotopes and protein quantification, but k_{deg} is often more difficult to determine especially *in vivo* (Millward et al. 1981; Pratt et al. 2002). This is due to the complex interplay between different protein degradation mechanisms and paucity in understanding the signalling mechanisms initiating specific protein degradation. The two main mechanisms of protein degradation are: lysosomal and ubiquitin-proteasomal degradation (UPD), and both pathways participate in the degradation of CYP enzymes. ER-associated degradation (ERAD) refers collectively to the mechanisms (including both lysosomal and UPD) involved in the proteolysis of ER-bound proteins (such as the CYP proteins), and thus responsible for maintaining physiological levels of CYP.

Much of what is known about ERAD is derived from studies with *Sacchromyces cerevisae* (yeast) and in rat hepatocytes, but there is a high degree of evolutionary conservation in protein degradation found in mammals and yeast. ERAD has been classed into three distinct pathways: ERAD-L for proteolysis of ER-lumenal proteins, ERAD-M for polytopic ER-membrane bound proteins and ERAD-C for monotopic ER-membrane bound proteins with cytosolic domains. CYP proteins fall under the ERAD-C category (Kim et al. 2016).

1.6.1 ERAD/ALD

Discovered in the 1950s, the lysosome was the first identified system of protein degradation. It is a vesicular organelle that occurs in the cytosol of eukaryotic cells and contains a multitude of proteases that catalyse proteolysis of intra- and extra-cellular proteins, as well as cellular organelles. The degradation process is dynamic involving many stages of lysosomal maturation together with the digestion of both exogenous and endogenous proteins and particles, through different pathways. Exogenous proteins enter the lysosome through receptor-mediated endocytosis and pinocytosis (engulfment of extracellular fluids) and particles enter by phagocytosis; all three processes are collectively known as heterophagy. Endogenous proteins and cellular organelles are targeted by microautophagy and macroautophagy, respectively (Ciechanover 2005; Eskelinen & Saftig 2009). Of these lysosomal pathways, only macroautophagy has been linked to cellular degradation of ER-bound proteins such as CYP450s (Liao et al. 2010).

The macroautophagy of CYP proteins is also referred as autophagic lysosomal degradation (ALD) or ERAD/ALD. The specific mechanisms and cellular participants of ERAD/ALD are still mostly unknown. However, macroautophagy generally involves the collaborative functions of over 35 ATG (autophagy-related genes) products that form multiprotein complexes to deliver relevant protein cargo for lysosomal degradation. This process is initiated by the formation of a phagophore, which is an isolation membrane that selectively engulfs a portion of the cytosol with intact organelles, such as the ER, to form an intracellular double-membrane vesicle called an autophagosome. The autophagosome that contains the protein cargo then fuses with the primary lysosomes to generate an autolysosome wherein lysosomal protease enzymes digest the contents and the end products are recycled or consumed

as an energy source (Correia 2003; Correia et al. 2014a; Kim et al. 2016; Bento et al. 2016).

Studies with rat liver have reported that long-lived proteins, such as ER-bound CYPs, undergo ALD in a selective process. Such as in the example of native rat CYP2E1, which undergoes biphasic degradation with a rapid phase ($t_{1/2}$ = 7 h) and a slower phase ($t_{1/2}$ = 37 h) (Correia 2003). ALD is responsible for at least some part of the slow phase of CYP2E1 degradation, as demonstrated by the accumulation of the enzyme when lysosomal degradation was inhibited by leupeptin (Ronis et al. 1991). Rat CYPs 2B1 and 2C11 are predominantly degraded by the ALD pathway (Masaki et al. 1987; Ronis & Ingelman-Sundberg 1989; Ronis et al. 1991; Murray et al. 2002).

1.6.2 ERAD/UPD

Non-lysosomal protein degradation occurs through calcium-dependent proteases and proteolytic systems found in the cytosol and in organelles, including the nucleus, ER and mitochondria. The most prominent of these is the adenosine triphosphate (ATP)/ ubiquitin (Ub)-dependent 26S proteasomal system. The cytosolic Ub/26S system is responsible for many cellular homeostatic processes including removal of erroneous proteins, processing of transcriptional protein precursors, intracellular protein trafficking and generation of peptides for antigen presentation, whereas in the nucleus it is involved in cell cycle regulation and cellular differentiation (Correia 2003). The cytosolic Ub-depdent 26S proteasomal system has been shown to participate in ER-protein degradation and is the predominant component of the CYP ERAD-C pathway (Ruggiano et al. 2014).

The majority of intracellular proteins undergo UPD and the system involves concerted actions of enzymes that link chains of Ub (a highly conserved 76-residue

protein) onto proteins to mark them for degradation. The pathway entails an ATP-dependent enzymatic conjugation of Ub to a proteolytic substrate followed by breakdown into peptides by the 26S proteasome complex. Three classes of enzymes catalyse the Ub-substrate coupling: the first is the Ub-activating enzyme (E1) that generates the Ub-thiolester ternary complex (a highly reactive form of Ub) in the presence of ATP, the second is the Ub-conjugating enzyme (E2) that shuttles the Ub-thiolester directly between the E1 enzyme and target protein and the third is the Ub-protein ligase (E3) enzyme. There are over 1000 types of mammalian E3 enzymes and they are critical for the specific recognition of target substrates in a highly regulated manner (Nakayama & Nakayama 2006). E3s catalyse the E2-mediated coupling of Ub-thiolester to target proteins via the formation of an isopeptide bond. The polyubiquitinated substrate is then targeted into the ATP-dependent multi-catalytic proteasome (26S) complex for degradation into small peptides (Ciechanover 1998; Correia 2003; Lecker 2006).

The 26S proteasome, which forms a key component of the ATP/Ub-dependent proteolysis system, is composed of a 20S catalytic core and a 19S regulatory complex. The 20S core is barrel-shaped and consists of four rings (two outer α rings and two inner β rings) containing seven distinct subunits that assemble to form stacks with a hollow cavity in which proteolysis takes place. The 19S regulatory complex caps the 20S catalytic core and regulates proteolysis by restricting barrel opening to only allow unfolded linear proteins to enter, thus preventing regular globular cellular proteins from erroneous proteasomal breakdown. The 19S complex is composed of 18 subunits with a ring of 6 homologous ATPases at its base, including Rpn (non-ATPase) subunits for polyubiquination recognition and deubiquitination, and Rpt AAA (ATPases associated with different cellular activities) ATPase subunits for

protein unfolding (Bedford et al. 2010). Altogether, the 19S regulatory complex carries out important functions such as: unfolding and translocation of proteins into the 20S core, polyubiquitin recognition for initiation of proteolysis and the de-ubiquitination and regeneration of Ub to be reused for degradation of other proteins (Lecker 2006; Kim et al. 2016).

CYP proteins are model examples of ERAD-C substrates due to their monotopic ER-topology and a cytosolic domain that is prone to oxidative/structural lesions by reactive oxygen species (ROS), due to their oxidative functions. Elucidation of rat hepatic CYP 3A and 2E1 ERAD has provided insights into CYP-specific degradation pathways. Such ERAD involves post-translational phosphorylation of the CYPs by cytosolic kinases such as protein kinase A (PKA) and C (PKC), followed by polyubiquitination by E1, E2 and E3 enzymes and 26S proteasomal degradation in the previously discussed manner. Specific but not limited to CYPs, proteins are extracted out of the ER into the cytosol by the p97/VCP (Valosin-containing protein) AAA-ATPase, an abundant cytosolic chaperone and/or the Rpt4 AAA-ATPase subunit of the 19S regulatory complex prior to proteasomal degradation (Acharya et al. 2011; Kim et al. 2016).

The specific participants of the E1, E2, E3 polyubiquinating pathways of human CYP proteins have been difficult to determine. Studies of yeast ERAD-C pathways have uncovered the Ubc6p/Ubc7p/Doa10p complex. Ubc6p and Ubc7p are ER-associated E2 enzymes that complexes with the Doa10p E3 ligase enzyme. Mammalian cells have a greater repertoire of E2/E3 complexes and the components found to be involved in ERAD include Hrd1, gp78/AMFR (autocrine motility factor receptor), TEB4/MARCH VI, RNF5/RMA1, RNF170 and CHIP (C-terminus of Hsc70-interacting protein). More than one E2/E3 Ub-ligase complex can target the

same proteins as substrates and may act synergistically, such as in the case of gp78 and CHIP in CYP3A4 ubiquitination (further discussed in Chapter 6). ERAD/UPD has also been implicated in the rapid phase of CYP2E1 degradation as well as in the biphasic degradation of CYP 2C9 and 2D6 (Kim et al. 2016).

CYP proteins have distinct half-lives suggesting different mechanisms of signalling for degradation. However, human CYPs seem to be preferentially degraded by the ERAD/UPD over the ERAD/ALD pathway. The haem and protein moieties of individual isoforms also turn over at different rates, with haem turnover being relatively more rapid and constant than that of the protein (Correia 2003). CYP protein turnover is also highly variable between different isoforms and the molecular mechanisms for this heterogeneity are yet to be clarified.

1.6.3 Targeting of CYP proteins for degradation

The mechanisms that trigger normal CYP turnover are still relatively unknown, especially the determinants that trigger the ERAD/ALD pathway. Degradation of other intracellular proteins requires specific post-translational modifications such as: Ub-conjugation, GSH-protein disulphide formation, phosphorylation and glycosylation. They may also undergo unmasking of intrinsic molecular/structural signals (also referred as 'degrons'), such as N-terminal residues, PEST/PAGE sequences, KFERQ motifs and C-terminal residues to initiate proteolysis. Understanding the processes that commit other intracellular proteins for proteolysis have provided clues for deriving determinants involved in CYP-specific degradation (Ravid & Hochstrasser 2008).

Haem modification by oxidative uncoupling or drug inactivation triggers rapid CYP degradation (Almira Correia et al. 2011). Haem modification disrupts normal

CYP conformation and renders it an aberrant protein target for disposal by the ERAD/UPD system. The rapid phase of CYP2E1 degradation is thought to result from structural damage inflicted by ROS that is generated during its futile oxidative cycling in the absence of a substrate or with a poorly fitting substrate that allows ROS leakage from the active site. CYP2E1 undergoes biphasic degradation, but substrate binding (with ethanol or acetone) can stabilise the protein by diverting it from ERAD/UPD to the slower ERAD/ALD pathway which prolongs its $t_{1/2}$ (Correia 2003; Kim et al. 2016). Studies involving the genetic knock-out of redox partner CPR in mice liver resulted in increased hepatic CYP content, thus supporting that oxidative cycling plays a major role in regulation of CYP abundance (Henderson et al. 2003). Although oxidative turnover proves to be a compelling determinant of CYP turnover, other requirements must exist as yeast cells have minimal CPR content and oxidative functions, yet ER-bound proteins do not necessarily switch to ALD as the predominant pathway.

Intrinsic structural features or 'degrons' and/or post-translational modifications are involved in CYP recognition and designation into ALD or UPD pathway. Degrons are short linear amino acid sequences (usually containing S/T-residues that undergo phosphorylation; termed phosphodegrons), structural motifs (C- or N-terminal residues) and/or cytosol-facing amino acids that engage the degradation machinery for molecular recognition and initiation of degradation. Specific ubiquitinated Lys (K) residues, along with PKA- and PKC- phosphorylated Ser and Thr residues associating with a nearby negatively charged Asp-Glu-Ser-Thr (DEST) cluster found on the CYP3A4 protein, form the 'phosphodegron' and serves as a molecular switch to enhance the gp78/CHIP (E2/E3-complex) recognition and

subsequent 26S proteasomal degradation (Correia et al. 2014b; Wang et al. 2015; Wang et al. 2011).

ALD targeting generally involves 3 mechanisms that are assumed to be relevant for CYP ERAD/ALD: (i) LC3-interacting region motifs (LIRs; LC3 referring to microtubule-associated protein 1 light chain 3); (ii) monoubiquitination or Lys_{63}-linked polyubiquitination; and (iii) cargo receptors/adapters such as p62/sequestosome-1 (SQSTM1) and/or NBR1 (neighbour of BRCA1 gene1) that contains the LIR motif to target mono- or Lys_{63}-ubiquitinated substrates to selective autophagy. The LIR is a linear 8-amino acid sequence that facilitates the docking of substrate to LC3 and subsequent targeting of the substrate to the phagophore. ALD substrates are tagged via mono- or polyubiquitination at the Lys_{63} position for the first Ub and Gly_{76} for the subsequent Ub. This K_{63}-linked ubiquitination is involved in p62/MBR-1 recruitment and specific targeting to ALD and is considered a hallmark of ALD pathway. P62/SQSTM1 and NBR1 are autophagic cargo receptors that enable selective phagosomal engulfment of the protein cargo via docking of the LIR motif. These cargo receptors are most likely to be involved in CYP ALD due to their propensity to target Lys_{63}-ubiquitinated substrates (Kim et al. 2016). CYP 2C9 and 2D6 in transfected HepG2 cells have found to undergo degradation by both ERAD/ALD and ERAD/UPD pathways and K_{63}-linked ubiquitination and LIR motifs were found in both CYPs, which supports them to be hallmarks of ALD (Wang et al. 2012; Kim et al. 2016).

The finding that CYPs undergo different pathways of degradation attests to not only to the mechanistic diversity of ER protein degradation but also the complexity. Substrate ligands can stabilise certain CYPs and induce or prolong expression by blocking post-translational modifications such as haem modification,

oxidation or phosphorylation that would normally trigger degradation of the protein. Some substrate interactions can inhibit rapid UPD and divert the CYP to the ALD pathway that prolongs its life span, such as in the case of CYP2E1. It is evident that ERAD of CYP proteins play a significant role in regulating the basal hepatic microsomal content and thus may impact on substrate PK and interactions.

CHAPTER 2

Utility of single pharmacological protein synthesis inhibitor agents for measuring protein degradation rate constants; an analysis in hepatic primary cells and tumour cell lines

CONTENTS

2.1 Introduction

The ability of the cell to remove and replenish proteins in a dynamic state of constant turnover is paramount to maintaining essential cellular functions. Mammalian protein half-lives range from minutes to years depending on the specific functions of the protein in question and protein turnover is tightly regulated through multiple molecular mechanisms. Collagen has an estimated $t_{1/2}$ of 117 years whereas regulatory proteins such as nuclear receptors are mostly estimated in the region of <5 hours (Alarid 2006; Toyama & Hetzer 2013). Characterisation of the degradation rate (k_{deg}) for specific proteins is required for better understanding of cell signalling processes involved in both normal and dysfunctional diseased cell states, thus studies of protein turnover are used in many different areas of cellular and molecular biology. In the context of PK studies for drug development, CYPs and other DME protein k_{deg} are important for the prediction of time-dependent DDIs, as discussed in Chapter 1.

Protein degradation is commonly quantified as $t_{1/2}$, the time taken for protein concentration to decrease by half (Zhou 2004; Belle et al. 2006; Zhang et al. 2007). This variable is interchangeable with k_{deg} by the following equations assuming first-order decay kinetics (Belle et al. 2006), where N is the protein intensity at time t, N_0 is the protein intensity at time T, k is the decay rate constant (and $-k$ represents k_{deg}) and $t_{1/2}$ is the half-life:

$$N_t = N_0 e^{-kt} \tag{15}$$

$$\ln(N_t) - \ln(N_0) = -kt \Rightarrow t_{\frac{1}{2}} = \frac{\ln(2)}{k} \tag{16}$$

$$-k = (\ln[N_t] - \ln[N_0]) \div t \tag{17}$$

Historically, protein degradation has been studied using methods that either measure overall protein degradation or focus on a few specific proteins. Advances in high-throughput tagging methods have allowed measurement of degradation rates of

large numbers of defined proteins but there are caveats associated with these proteome-wide approaches; such as the potential of protein tagging disrupting regular degradation pathways (Yewdell et al. 2011). Methods for measuring protein degradation and subsequent derivation of k_{deg}, generally fall into two experimental designs: i) quantifying the amount of a specific protein before and after a cell perturbation then measuring the difference in protein abundance and time between the initial and new steady-state; or ii) quantifying changes in protein abundance in real-time by time-course experiments (Alvarez-Castelao et al. 2012).

The most common approach for measuring protein degradation is the pulse-chase analysis and this method involves a 'pulse' stage of incubating cells with a radiolabelled amino acid, which allows the radiolabelled amino acids to be incorporated into newly synthesised proteins, followed by washing out of the excess unincorporated amino acids and then a 'chase' stage of incubation with unlabelled amino acids. The change in the proportion of labelled to unlabelled amino acid incorporation over time is used to calculate rate of protein degradation. Protein synthesis inhibitors, most commonly cycloheximide, are used in this method to eliminate reincorporation (Zhou 2004; Doherty et al. 2009). Another simple kinetic approach is based on inhibiting *de novo* protein synthesis with an initial cell treatment with pharmacological inhibitors or genetic interference, followed by the quantification of changes in protein content over time by immunoblotting (Alvarez-Castelao et al. 2012; Dai et al. 2013), thereby tracking the degradation of untagged proteins. However, there are concerns with using protein synthesis inhibitor agents for measuring long-lived proteins because prolonged use of these pharmacological inhibitors are likely to introduce cytotoxicity that will disrupt the regular protein turnover process. Any loss in protein could be caused by cytotoxicity rather than the

protein degradation process itself, therefore a non-cytotoxic concentration will need to be determined prior to measuring the protein degradation rate.

The more recent methods for measuring protein degradation are based on modifications to the traditional pulse-chase analysis with a focus on protein tagging to simultaneously measure the rates of a large number of proteins in a high throughput manner. For example, stable isotope labelling by amino acids (SILAC) in cell culture followed by mass-spectrometry (MS) (Mann 2006; Doherty et al. 2009; Fierro-Monti et al. 2013; Takahashi et al. 2017), isobaric tag for relative and absolute quantification (iTRAQ) (Jayapal et al. 2010) and global protein stability profiling (GPSP) utilising protein fusion constructs for reporter assays (Yewdell et al. 2011; Yen et al. 2008). The caveats of using fusion constructs to tag proteins is that any modifications to regular protein conformation may influence protein folding and any misfolding of proteins is likely to affect regular degradation pathways (Alvarez-Castelao et al. 2012; Yewdell et al. 2011).

The focus of this chapter was on the more traditional methods of measuring protein degradation by initial treatment with protein synthesis inhibitor agents followed by quantification of protein disappearance by immunoblot detection. CYP protein $t_{1/2}$ are thought to be in the medium-lived rrange of 10-140 hours (Yang et al. 2008), thus it was hypothesized that using pharmacological inhibition to stop protein synthesis followed by tracking of CYP protein disappearance over a few days was a feasible method of deriving CYP k_{deg}. Due to the cytotoxic concerns with using protein synthesis inhibiting agents, a suitable agent that provided maximum protein synthesis inhibition with minimum cytotoxicity must be defined prior to being used in a subsequent time-course immunoblot approach to derive CYP protein k_{deg}.

Table 2.1 shows some commonly used protein synthesis inhibitor agents in biology research as recommended in *Current Protocols in Cell Biology* by N. H. Cole (2001) and some examples of the use of these compounds in various *in vitro* studies to measure messenger RNA (mRNA) or protein degradation. The four protein synthesis inhibitors used in this chapter were selected based on their different mechanisms of action along the protein synthesis process, as shown in Figure 2.1, and previous use in biomedical research.

Actinomycin D (Sobell 1985) intercalates deoxyribonucleic acid (DNA) forming a stable complex with deoxyguanosine residues, thus blocking movement of RNA polymerase and subsequently transcription. Cycloheximide binds the 60S ribosomal subunit blocking the translocational step in amino acid elongation, thus inhibiting protein synthesis (Schneider-Poetsch et al. 2010). Emetine inhibits protein synthesis by binding onto the 40S subunit of ribosomes and inhibiting translocation of proteins (Akinboye 2011). Puromycin acts as an analogue of the 3′-terminal end of aminoacyl-tRNA that results in premature amino acid chain termination during translation of proteins (Azzam & Algranati 1973). The selected inhibitors actinomycin D, cycloheximide, emetine and puromycin were assessed to determine their suitability for protein degradation studies.

Leucine incorporation assays and standard 3-(4,5-dimethylthiazol-2-yl)-2,5-diphenyltetrazolium bromide (MTT) assays were conducted to determine the level of protein synthesis inhibition and cytotoxicity respectively, across a range of drug concentrations in a human hepatic immortalised cell line, HepG2, and primary rat hepatocytes (PRH). Physiologically-relevant hepatic CYP k_{deg} values should ideally be derived from primary human hepatocytes as these cells are considered to be the 'gold standard' representative of the *in vivo* human liver (LeCluyse 2001), however

the use of these cell systems are costly. Therefore, HepG2 and PRH were initially selected for the optimisation of protein synthesis inhibitor concentrations with the aim of transferring the optimised concentrations for use in primary human hepatocytes for a cost-saving optimisation approach.

The aim of this chapter was to define a single concentration of an inhibitor agent that displayed maximum protein synthesis inhibition with minimal cytotoxicity, to stop *de novo* protein synthesis, for subsequent use in measuring CYP protein $t_{1/2}$. The selected inhibitor agents were assessed for cytotoxicity by standard MTT assays and their potential to inhibit protein synthesis by leucine incorporation assay, in HepG2 and PRH cells.

Table 2.1 Protein synthesis inhibitor compounds used in cell biology research, collated from Cole (2001)

Compound	Mechanism of Action	Concentration used *in vitro* to assess mRNA or protein degradation
a-Amanitin	Acts as a potent and specific inhibitor of mRNA synthesis by binding preferentially to RNA polymerase II. At high concentrations also inhibits RNA polymerase III.	Van Nguyen et al. 1996: 5.4-108.8 μM in NIH 3T3 cells for up to 24 h; Tsao et al. 2012: 21.8 μM in COS cells for 14 h; Lugowski et al. 2017: 50 μM in HEK-293 cells for up to 24 h
Actinomycin D	Inhibits transcription by complexing with deoxyguanosine residues on DNA and blocking the movement of RNA polymerase.	Koeller et al. 1991: 4.0 μM in fibroblasts for up to 3 h; Van Nguyen et al. 1996: 15.9 μM in NIH 3T3 cells for up to 24 h; Lee & Wayne 1998: 39.8 μM in bag cell neurons up to 32 h; Takei et al. 2000: 6.0 μM for 6 h; Leclerc et al. 2002: 0.5-5 μM in CEM and Nalm6 cells for up to 24 h; Lugowski et al. 2017: 4.0 μM in HEK-293 cells for up to 24 h
Anisomycin	Inhibits protein synthesis by blocking the peptidyl transferase step during translation.	Marroquin et al. 2004: 37.7 μM in murine leukemia cells for up to 96 h
Cycloheximide	The exact mechanism of action remains to be elucidated but it has been found to inhibit translation elongation through binding to 60S ribosomal subunit.	Chang et al. 1981: 0.9 mM in CHO cells for 12 h; Welch & Wang 1992: 88.9 μM in NIH 3T3 cells for up to 60 h; Van Nguyen et al. 1996: 35.5 μM in NIH 3T3 cells for 5 h; Fayadat et al. 2000: 100 μM in CHO cells for up to 24 h; Jeong et al. 2005: 355.4 μM in HepG2 cells for 4 h; Belle et al. 2006: 124.4 μM in yeast cells for 45 min; Chen & Madura 2008: 1.8 μM in yeast cells for up to 120 h; Bouligand et al. 2010: 71.1 μM in fibroblast cells for 2 h; Tsao et al. 2012: 71.1 μM in COS cells for 14 h; Puskarjov et al. 2012: 100 μM in hippocampal slices for 4 h; Majumber et al. 2012: 248.8 μM in hippocampal neurons for up to 8 h
Emetine	Irreversibly blocks protein synthesis by inhibiting movement of ribosomes along mRNA by binding to 40S ribosomal subunit.	Chang et al. 1981: 5 μM in CHO cells for 10 h; Fayadat et al. 2000: 100 μM in CHO cells for up to 24 h; Gelman et al. 2002: 75 μM in CHO cells for 4 h; Bouligand et al. 2010: 208.1 μM in fibroblasts for 6 h; Puskarjov et al. 2012: 100 μM in hippocampal slices for 4 h; Weitzel et al. 2004: 100 μM in sea urchin egg cells for 30 min
Hygromycin	Inhibits protein synthesis at the translocation step on 70S ribosomes and causes misreading of mRNA.	Tan & Walker 2010: 94.8 μM in HEK293 cells for 24 h; Chen & Madura 2008: 0.2 mM in yeast cells for up to 120 h
Puromycin	Inhibits protein synthesis by causing premature release of nascent polypeptide chains by its addition to the growing chain end; structural analog of 3'-terminal end of the aminoacyl-tRNA.	Chang et al. 1981: 0.2 mM in CHO cells for 12 h; Liao et al. 1998: 10 μM in HepG2 cells for 10 min; Lacsina et al. 2012: 20.0 μM in 293-K^b cells for 50 min

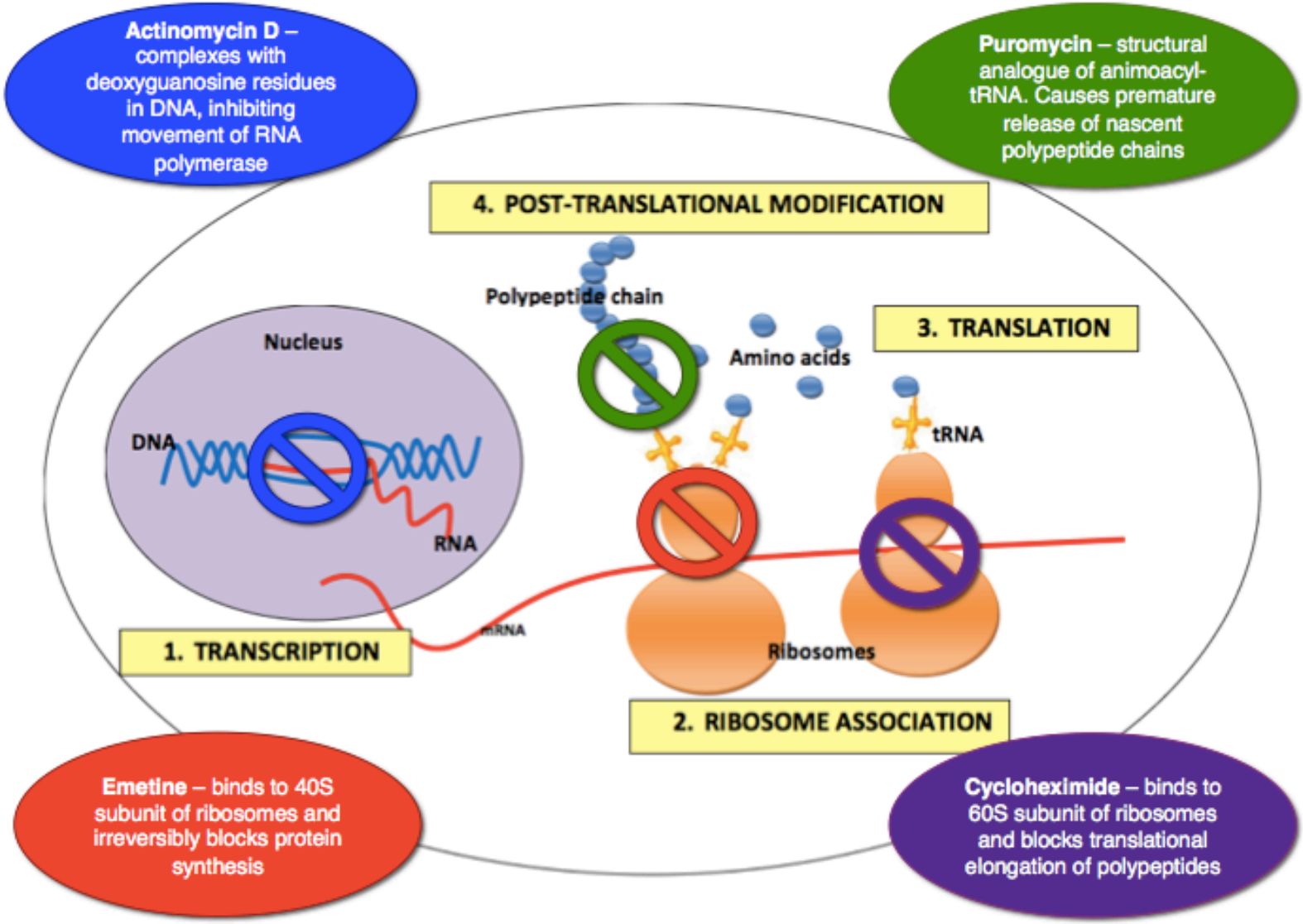

Figure 2.1 Mechanisms of action of selected protein synthesis inhibitor agents: actinomycin D, puromycin, emetine and cycloheximide.

2.2 Materials and methods

2.2.1 Materials

Dulbecco's modified eagle medium (DMEM), foetal bovine serum (FBS), trypsin-EDTA solution, Hank's balanced salt solution (HBSS), thiazolyl blue tetrazolium (TBT), sterile water (W4502) and protein synthesis inhibitors; actinomycin D (A4262), emetine dihydrochloride hydrate (E2375) and puromycin dihydrochloride (P7255), were purchased from Sigma-Aldrich (Dorset, UK). HepG2 cells were purchased from American Tissue Culture Collections (ATCC, Virginia, USA). Cryopreserved primary rat hepatocytes, William's E media, plating cocktail, maintenance cocktail, Geltrex® matrix and collagen I coated plates were purchased from Invitrogen Ltd (Paisley, UK). Cycloheximide (ab120093) was purchased from Abcam (Cambridge, UK). L-Leucine [4,5-^{3}H] (MT-672E) was obtained from Moravek (California, USA).

2.2.2 Cell line culture

HepG2 cells were maintained in DMEM medium supplemented with 10% FBS solution. Cells were seeded in T175 culture flasks and grown in a 37°C 5% CO_2 humidified incubator. The media was changed every 48 hours and cells were sub-cultured by the standard trypsin and centrifugation method when they reached approximately 80-90% confluence. The cells were discarded beyond passage 20.

2.2.3 PRH culture

Primary rat hepatocytes (PRH) were purchased from Invitrogen (Paisley, UK), isolated from male Sprague-Dawley rats at 9 weeks old (Lot. RS745). Cryopreserved

PRH were thawed in a 37°C water bath for approximately 2 mins until contents were around 90% thawed. Once thawed, the hepatocytes were added to 50 ml of pre-warmed plating media (William's E media without phenol red supplemented with 5% FBS, 1 µM dexamethasone, 1% solution of penicillin/streptomycin, 4 µg/ml Bovine insulin, 2 mM GlutaMAX™ and 15mM HEPES; CHRM® supplement A) and centrifuged for 3 min at 55 x g at 18^{o}C and the supernatant fraction discarded. The hepatocytes were then resuspended in plating media at approximately 1 x 10^{6} cells per ml density and counted.

2.2.4 Cell counting and viability

The cell numbers and viability of HepG2 and PRH were calculated using the Chemometec NucleoCounter® NC-100TM (Chemometec, Denmark). 150 µl of cell suspension was added to a fresh Eppendorf tube for total dead cells count, 50 µl of reagent A and B were added to 50 µl of cell suspension in a separate Eppendorf tube for total cell count. A cell viability of > 80% was required for experiments. Cell viability was calculated using the following equation:

$$\text{Cell viability (\%)} = 100 - \left(\frac{\text{Dead cells count}}{\text{Total cells count (Reagent A + B) x 3 (dilution factor)}}\right)$$

2.2.5 PRH plating and maintenance

PRH cells were seeded in 96-well collagen-I coated plates and were incubated in plating media for 5 h at 37°C with 5% CO_2 and 95% humidity to allow for cell adherence to culture plate. After 5 hour incubation, plating media was discarded and replaced with 0.022 mg/ml of Geltrex® Matrix in maintenance media (William's E media supplemented with 0.1 µM dexamethasone, 0.5% penicillin/streptomycin 6.25

μg/ml human recombinant insulin, 6.25 μg/ml human transferrin, 6.25 ng/ml selenous acid, 1.25 mg/ml BSA, 5.35 μg/ml linoleic acid, 2nM GlutaMAX™ and 15mM HEPES). Protein concentration for each Geltrex® Matrix lot vary and the amount of Geltrex® required for each experiment was calculated by:

$$\text{Geltrex amount (ml)} = \frac{\text{Incubation medium (mL)x 0.35(mg/mL)}}{\text{Geltrex protein concentration (mg/mL)}}$$

Geltrex® Matrix was added to maintenance media on ice. After incubation overnight, the media containing Geltrex® was removed and replaced with regular maintenance media with varying drug concentrations and controls. Maintenance media with treatment conditions were replaced every 24 hours.

2.2.6 Measuring cytotoxicity by standard MTT Assays

Standard MTT assays were performed on HepG2 and PRH cells to determine cell viability. 2 x 10^4 cells per well of HepG2 were seeded into 96-well plates in DMEM with 10% FBS and left overnight in a 37°C humidified incubator to allow cells to adhere to the plate. PRH were seeded in collagen-I coated 96-well plates at a density of 2 x 10^4 cells per well. Old media was removed and replaced with 10 concentrations between 0-300 μM diluted at third-log concentrations, of protein synthesis inhibitor drugs in fresh maintenance media and incubated for 72 hours, and the media containing treatment conditions were replaced every 24 hours. Vehicle controls and a control with no drug was included. The vehicle controls were 1% sterile water for emetine, puromycin and cycloheximide, or 1% dimethyl sulfoxide (DMSO) for actinomycin D, in cell maintenance media. Vehicle control wells required >90% cell viability for the solvent to be deemed suitable for drug dissolution. 20μl of 5mg/ml TBT in HBSS was added to each well and incubated for

2 hours. 100µl lysis buffer (50%v/v dimethylformamide and 20%v/v sodium dodecyl sulphate) was added to each well and the plate was incubated overnight at 37°C. The absorbance at 570nm, which correlated to cell viability, was determined by Tecan GENios micoplate reader (Germany).

2.2.7 Measuring protein synthesis inhibition by [^{3}H]-leucine incorporation

HepG2 cells were seeded at 2 x 10^5 cells per well on 96-well plate in DMEM supplemented with 10% FBS and the plates were incubated overnight at 37°C to allow cells to adhere. PRH cells were seeded in collagen-I coated 24-well plates at a density of 2 x 10^5 cells per well. Old media was removed and replaced with 0-100µM of protein synthesis inhibitor drugs dissolved in DMEM with 10% FBS for HepG2 cells or maintenance media for PRH and incubated for 72 hours in a 37°C humidified incubator. In the last 2 hours of incubation, cells were pulsed with 2µCi of [^{3}H]-leucine without removing the inhibitor. After 2 hours, the media containing [^{3}H]-leucine was removed by aspiration and the cells were washed twice with HBSS before removal from well by trypsinisation for 5 min at 37°C with 5% CO_2 and 95% humidity. HepG2 cells were then harvested onto a filtermat using a TomTec cell harvester. The filtermat was sealed in a sample bag with melt-on scint and the level of protein synthesis was determined by the amount of [^{3}H]-leucine incorporation measured using a MicroBeta detector (Perkin-Elmer, Cambridge, UK). PRH cells were transferred to scintillation vials following trypsinisation. 4 ml of scintillation fluid was added to each sample and radioactivity was determined using QuantaSmartTM software on Tri-Carb scintillation counter (Perkin-Elmer, Cambridge, UK).

2.2.8 Protein synthesis inhibitor drug analysis

The protein synthesis inhibitors actinomycin D, cycloheximide, emetine and puromycin were tested individually in HepG2 and PRH cells. Actinomycin D was incubated at 0-10μM and 0-0.039μM and puromycin at 0-20μM and 0-5μM for leucine incorporation assays and MTT cytotoxicity assays, respectively. Cycloheximide was incubated at 0-300μM and emetine at 0-30μM for both leucine incorporation and MTT assays. These concentration ranges were determined after initial optimization in HepG2 cells utilizing a wide range of concentrations for each inhibitor to detect a sigmoidal concentration-response.

2.2.9 IC_{50} and CC_{50} calculations

The CC_{50} (concentration causing 50% cytotoxicity) and IC_{50} (concentration causing 50% protein synthesis inhibition) for each inhibitor drug were calculated by non-linear regression of drug concentration versus % protein synthesis inhibition (as determined by level of [^{3}H]-leucine incorporation) and % cell viability (as determined by MTT assays) concentration-response graphs, respectively, using Graphpad Prism 6 software. IC_{50} and CC_{50} values could only be determined when a sigmoidal concentration-response curve was observed. Where non-sigmoidal responses were seen, experiments were repeated with a wider concentration range until a sigmoidal relationship could be observed by eye. A mean value ± standard deviation (SD) was taken over at least four replicates in at least three independent experiments.

2.2.10 Linear regression of HepG2 and PRH data

Linear regression was carried out with Graphpad Prism 6 software for HepG2 and PRH derived CC_{50} and IC_{50} for each of the protein synthesis inhibitor drugs to

determine the correlation between HepG2 and PRH derived values and suitability of these cell types for measuring k_{deg}.

2.3 Results

2.3.1 Optimisation of concentration ranges for protein synthesis inhibitor drugs in MTT assays for accurate CC_{50} measurement

A clear sigmoidal concentration-response relationship is required for accurate CC_{50} calculation by the Graphpad Prism 6 software. HepG2 cells were initially incubated with third-log dilutions of drug concentration over the range of 0-100 μM for all four protein synthesis inhibitors. Cell viability was calculated as a percentage of control, where no drug was added, and this was assumed to be to 100% viability. Figures 2.1 A and C depicting actinomycin D and emetine, respectively, did not display a sigmoidal concentration-response when the drug concentration range was at 0-100 μM. Although puromycin did display a sigmoidal curve over this concentration range, accurate CC_{50} could not be determined as there was a sharp decrease in viability between two concentrations (Figure 2.1 C). A more gradual drop in cell viability is needed to better quantify CC_{50}.

Further optimisations with narrowing drug concentration ranges deemed 0-0.039 μM for actinomycin D, 0-100 μM for cycloheximide, 0-30μM for emetine and 0-5μM for puromycin to be the ideal concentration ranges to display a sigmoidal concentration-response with standard MTT assays.

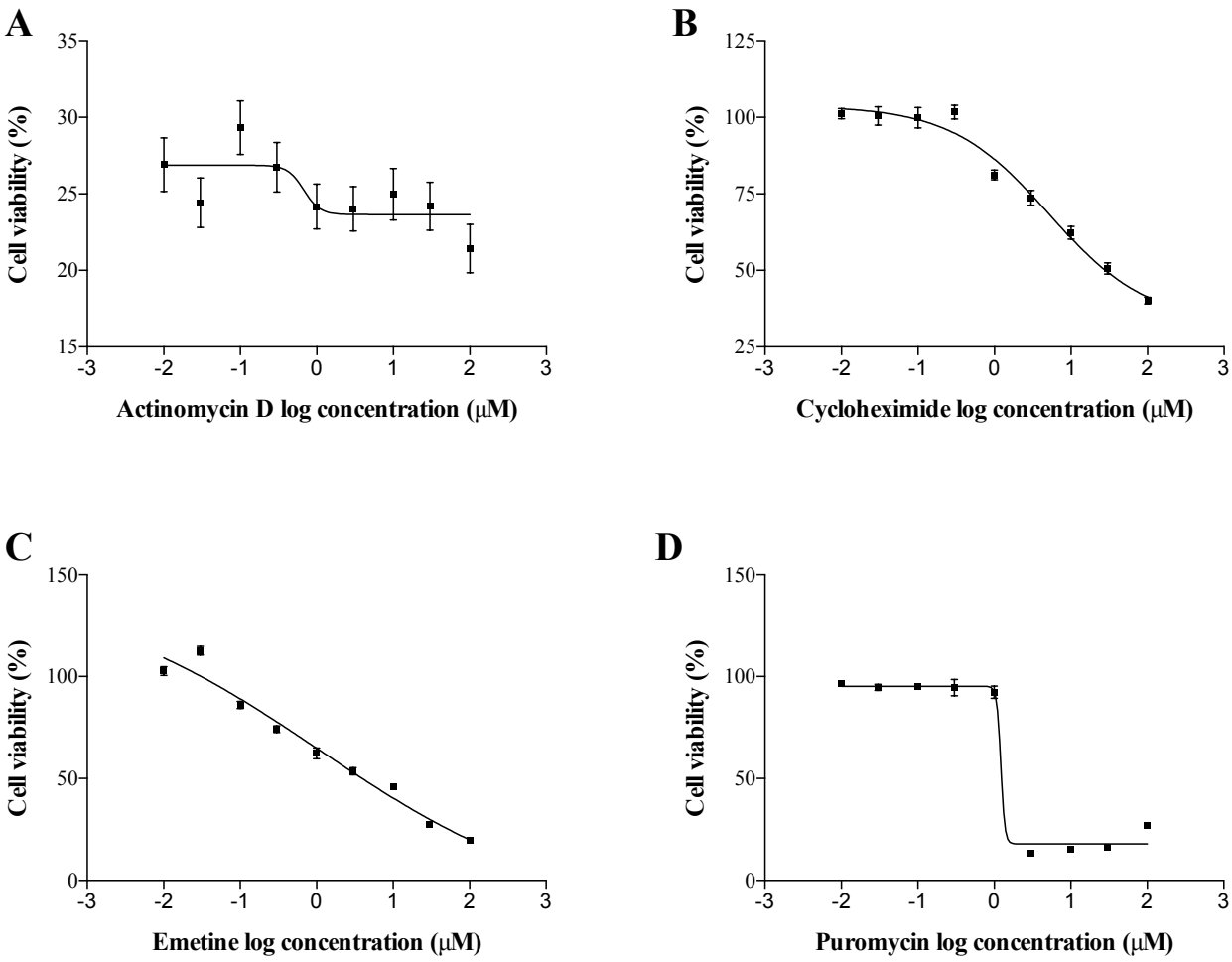

Figure 2.1 HepG2 cell viability, determined by standard MTT assays, as a response to a range of protein synthesis inhibitor concentrations. Optimisation of concentration-response assays conducted in HepG2 cell lines. **A.** actinomycin D. **B.** cycloheximide **C.** emetine and **D.** puromycin. Data are expressed as the mean of 8 technical replicates ± SD in at least 1 independent experiment.

2.3.2 Optimisation of concentration ranges for protein synthesis inhibitor drugs in [^{3}H]-leucine incorporation assays for accurate IC_{50} measurement

The Graphpad Prism 6 software was also used for calculation of IC_{50} and a clear sigmoidal concentration-response relationship was also required for accurate measurement. HepG2 cells were incubated with third-log dilutions of drug concentration over the range of 0-100 μM for all four protein synthesis inhibitor agents. The level of protein synthesis inhibition was calculated as a percentage of control, where no drug was added inhibition was assumed to be 0%. Figure 2.2.A shows that actinomycin D did not exhibit a sigmoidal concentration-response and further repeats were needed with a more narrow concentration range for emetine and puromycin, and a wider concentration range for cycloheximide. The outlier observed for 1 μM puromycin (Figure 2.2 D) futher attests to the variability in protein synthesis inhibition observed between 0.1 – 3 μM and therefore more concentrations within this range should be included to better define the concentration-response. A more gradual change in protein synthesis inhibition, than that shown in figure 2.2 were needed to accurately measure IC_{50}.

Further optimisations deemed 0-10 μM for actinomycin D, 0-300 μM for cycloheximide, 0-30 μM for emetine and 0-20μM for puromycin to be the ideal concentration range to display a sigmoidal concentration-response in protein synthesis inhibition as measured by [^{3}H]-leucine incorporation assays.

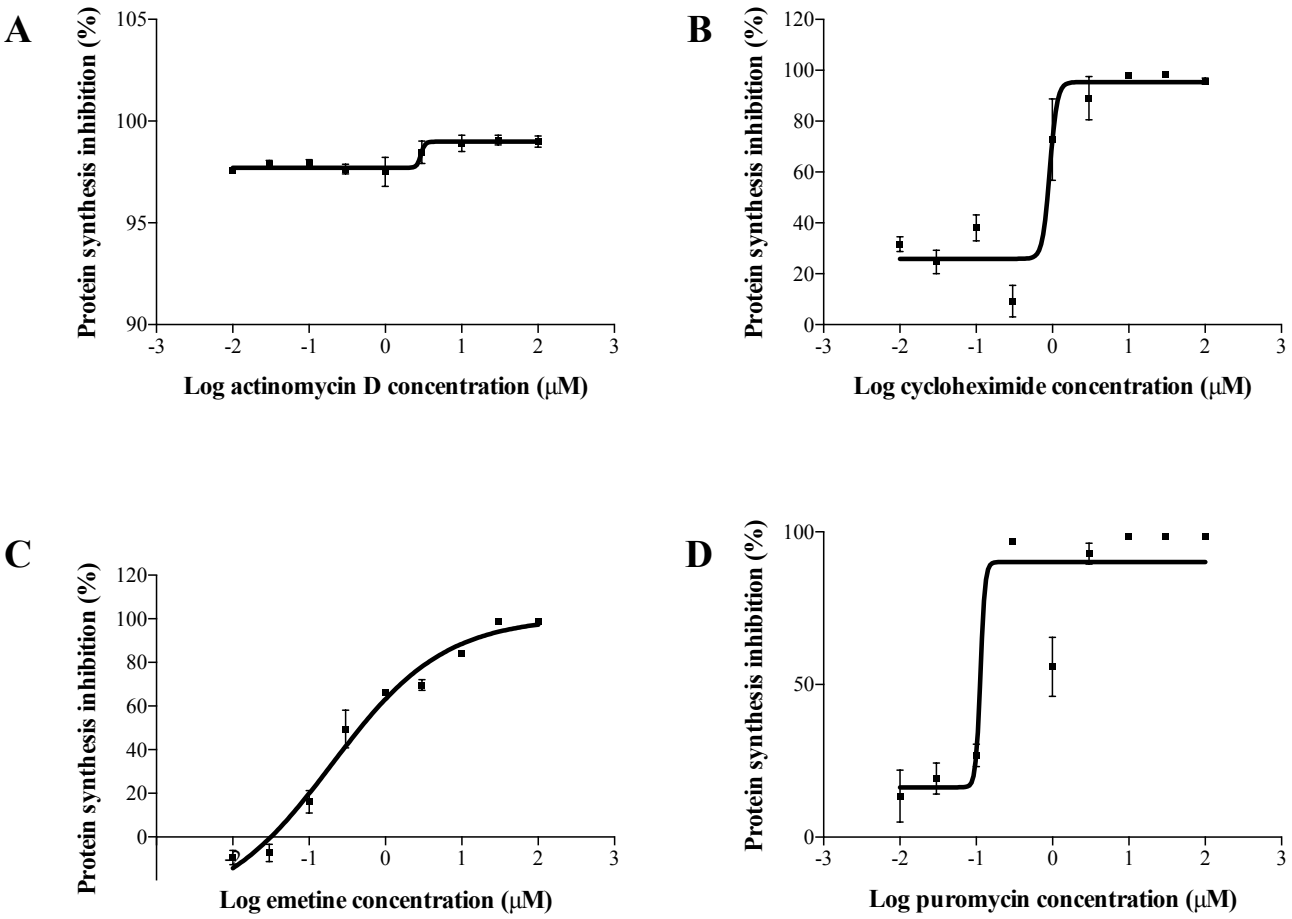

Figure 2.2 Level of protein synthesis inhibition, determined by [^{3}H]-leucine incorporation assay, as a response to incubations with a range of protein synthesis inhibitor concentrations. Optimisation of concentration-response assays conducted in HepG2 cell lines. **A.** Actinomycin D. **B.** Cycloheximide. **C.** Emetine and **D**. Puromycin. Data are expressed as the mean of 8 technical replicates ± SD in at least 1 independent experiment.

2.3.3 *CC_{50} of protein synthesis inhibitor drugs determined by standard MTT assays in HepG2 and PRH cell types*

HepG2 and PRH were incubated with the optimised protein synthesis inhibitor drug concentrations as discussed in 2.3.1. The mean ± SD CC_{50} for the four inhibitors actinomycin D, cycloheximide, emetine and puromycin were found at 0.0062 ± 0.0073, 0.57 ± 0.51, 0.081 ± 0.0090 and 1.3 ± 0.064 μM, respectively in HepG2 cells and 0.00098 ± 0.0018, 0.68 ± 1.3, 0.18 ± 0.70 and 1.6 ± 1.0 μM, respectively in PRH (Table 2.2). The CC_{50} concentrations were calculated from concentration-response graphs shown in figure 2.3. HepG2 cells were sensitive to puromycin concentrations as shown in the sharp decrease in cell viability between 1 and 2.5 μM (Figure 2.3.D).

2.3.4 *IC_{50} of protein synthesis inhibitor drugs determined by [^{3}H]-leucine incorporation assays in HepG2 and PRH cell types*

HepG2 and PRH were incubated with the optimised protein synthesis inhibitor drug concentrations as discussed in 2.3.2. The mean ± SD IC_{50} for the four inhibitors actinomycin D, cycloheximide, emetine and puromycin were calculated at 0.039 ± 0.0074, 6.6 ± 2.5, 2.2 ± 1.4 and 1.6 ± 1.2 μM, respectively, in HepG2 and 0.0017 ± 0.0018, 0.29 ± 0.090, 0.62 ± 0.92 and 2.0 ± 2.0 μM, respectively in PRH (Table 2.2). The IC_{50} concentrations were calculated from concentration-response graphs shown in figure 2.4. PRH appears to be sensitive to emetine concentrations as shown in the high variability and sharp increase in protein synthesis inhibition between 0.078 and 1.25 μM (Figure 2.4.C).

The CC_{50} concentrations were lower compared to corresponding IC_{50} values for all four inhibitor drugs except cycloheximide in PRH; this indicates that the

inhibitors were more effective in generating cell death than protein synthesis inhibition and thus unsuitable for further protein degradation studies.

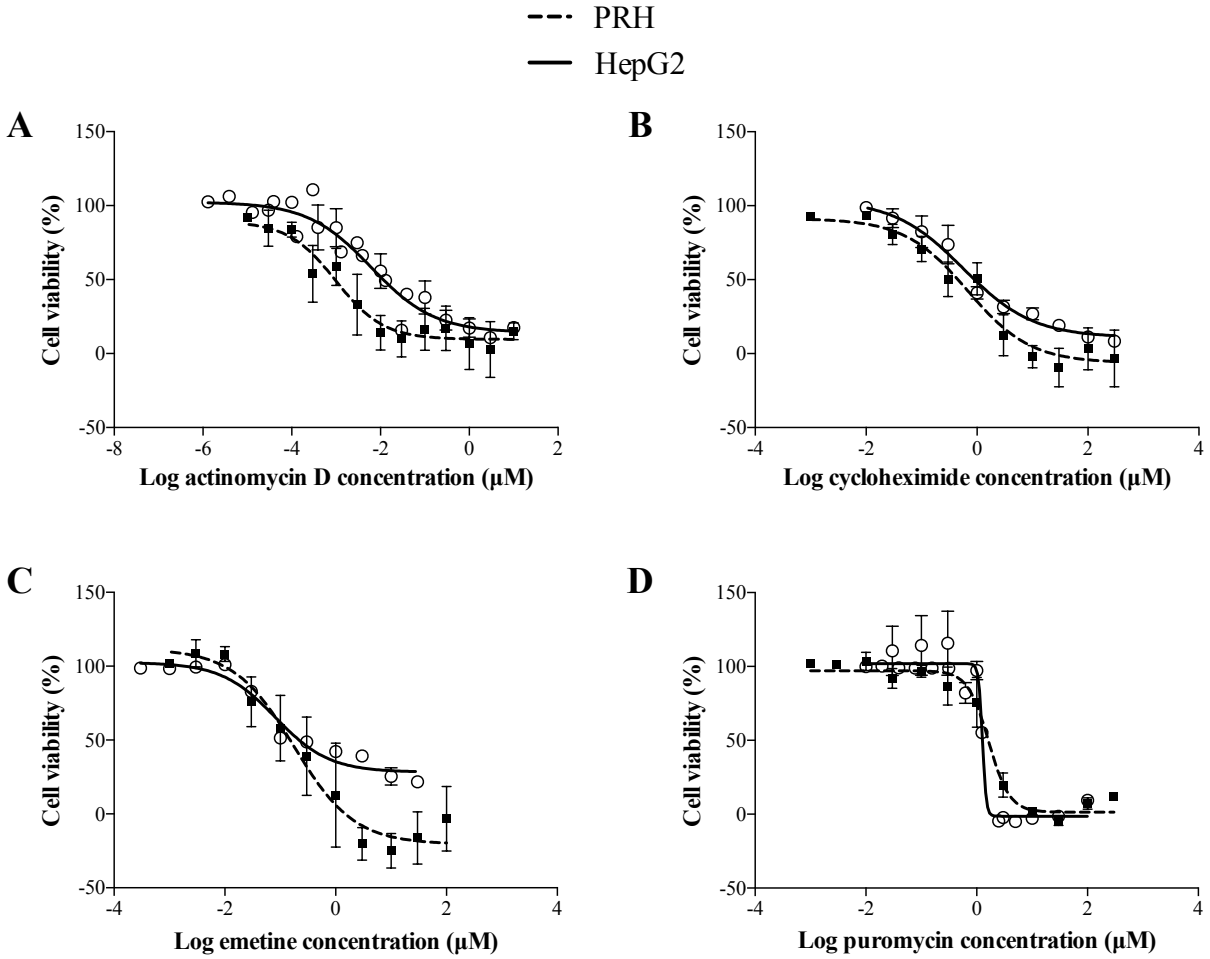

Figure 2.3 CC_{50} of the four individual protein synthesis inhibitors in HepG2 and PRH. (A-D) Cell viability across different concentrations of inhibitors was measured by MTT assays and shown as percentage of control. Dotted line shows PRH and solid line for HepG2 cells. Concentration-response curves were produced by Prism software and CC_{50} values were calculated from linear regression models. Data are shown as mean ± S.D from 4 independent experiments (n=4) carried out in 8 replicates for HepG2 and n=3 in quadruplicates in PRH.

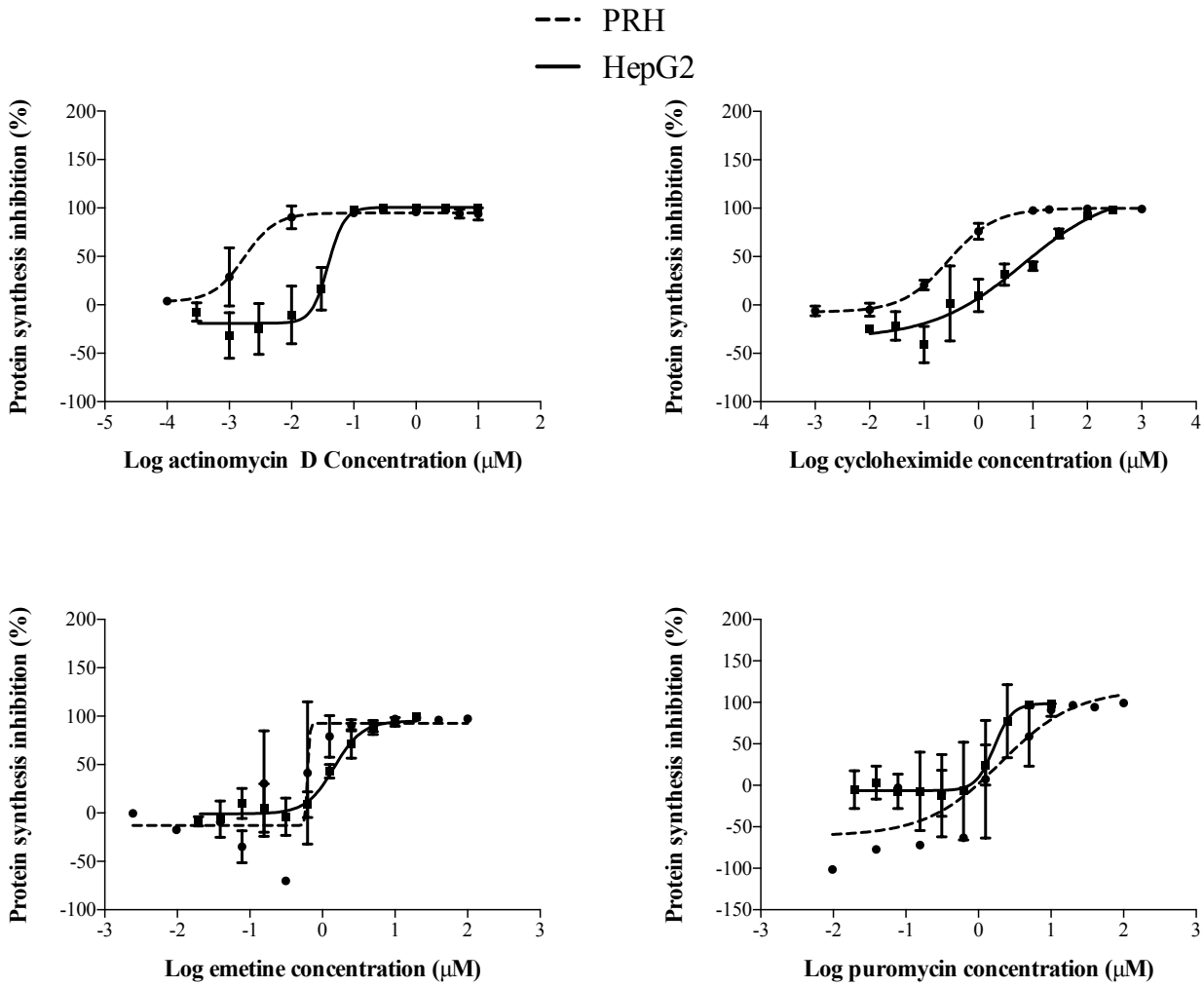

Figure 2.4 IC_{50} of the four individual protein synthesis inhibitors in HepG2 and PRH. (A-D) Protein synthesis inhibition across different concentrations of inhibitors was measured by [^{3}H]-Leucine incorporation assay and shown as percentage of inhibition of control. Dotted line shows PRH and solid line for HepG2 cells. Concentration-response curves were produced by Prism software and IC_{50} values were calculated from linear regression models. Data are shown as mean ± S.D from 4 independent experiments (n=4) carried out in 8 replicates for HepG2 and n=3 in quadruplicates in PRH.

2.3.5 *Linear regression analysis of CC_{50} and IC_{50} between HepG2 and PRH cell types*

The CC_{50} and IC_{50} values for HepG2 and PRH for each of the four selected protein synthesis inhibitors were derived from concentration-response curves shown in figures 2.3 and 2.4. These calculated values, displayed in Table 2.2, were incorporated into linear regression analyses to determine the correlation and predictability of HepG2 and PRH cell types for CC_{50} and IC_{50}.

Figure 2.5 show a linear relationship of CC_{50} between HepG2 and PRH cells for all four protein synthesis inhibitor agents at R^2=0.996. The inset graph in Figure 2.6 shows a reasonable linear correlation for actinomycin D, emetine and puromycin at R^2=0.655 when cycloheximide was omitted. The inset graph in Figure 2.7 also shows a strong linear relationship of IC_{50}:CC_{50} at R^2=0.997 when cycloheximide was omitted. Thus, cycloheximide fit in the linear relationship for cytotoxicity but not for protein synthesis inhibition. HepG2 and PRH produced CC_{50} values that were in good correlation for all four inhibitor drugs. The difference for cycloheximide in IC_{50} estimations could be due to differential mechanisms of protein synthesis inhibition between the HepG2 and PRH cell types.

Table 2.2 CC_{50}, IC_{50} and CC_{50}:IC_{50} values derived from concentration-response curves for each protein synthesis inhibitor agent in HepG2 and PRH cells.

Drug	CC_{50} (µM)		IC_{50} (µM)		Ratio IC_{50}:CC_{50}	
	HepG2	PRH	HepG2	PRH	HepG2	PRH
Actinomycin D	0.0062	0.00098	0.039	0.0017	6.2	1.8
Cycloheximide	0.57	0.68	6.6	0.29	11.6	0.42
Emetine	0.081	0.18	1.4	0.62	18.0	3.5
Puromycin	1.3	1.6	1.6	2.0	1.3	1.2

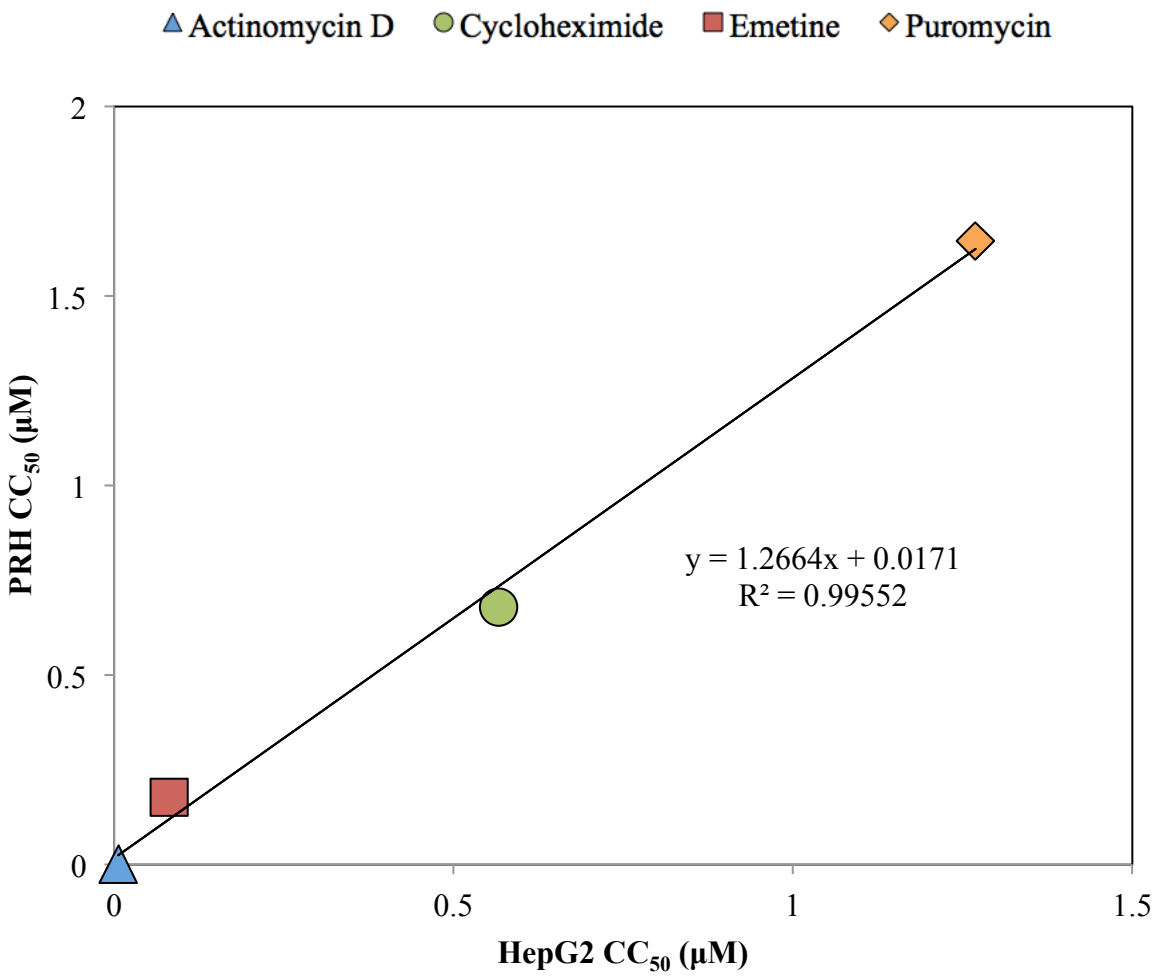

Figure 2.5 Linear regression analysis of CC_{50} between HepG2 and PRH cell types. Linear regression of the mean CC_{50} values of the four protein synthesis inhibitor drugs derived from HepG2 and PRH concentration-response cytotoxicity curves.

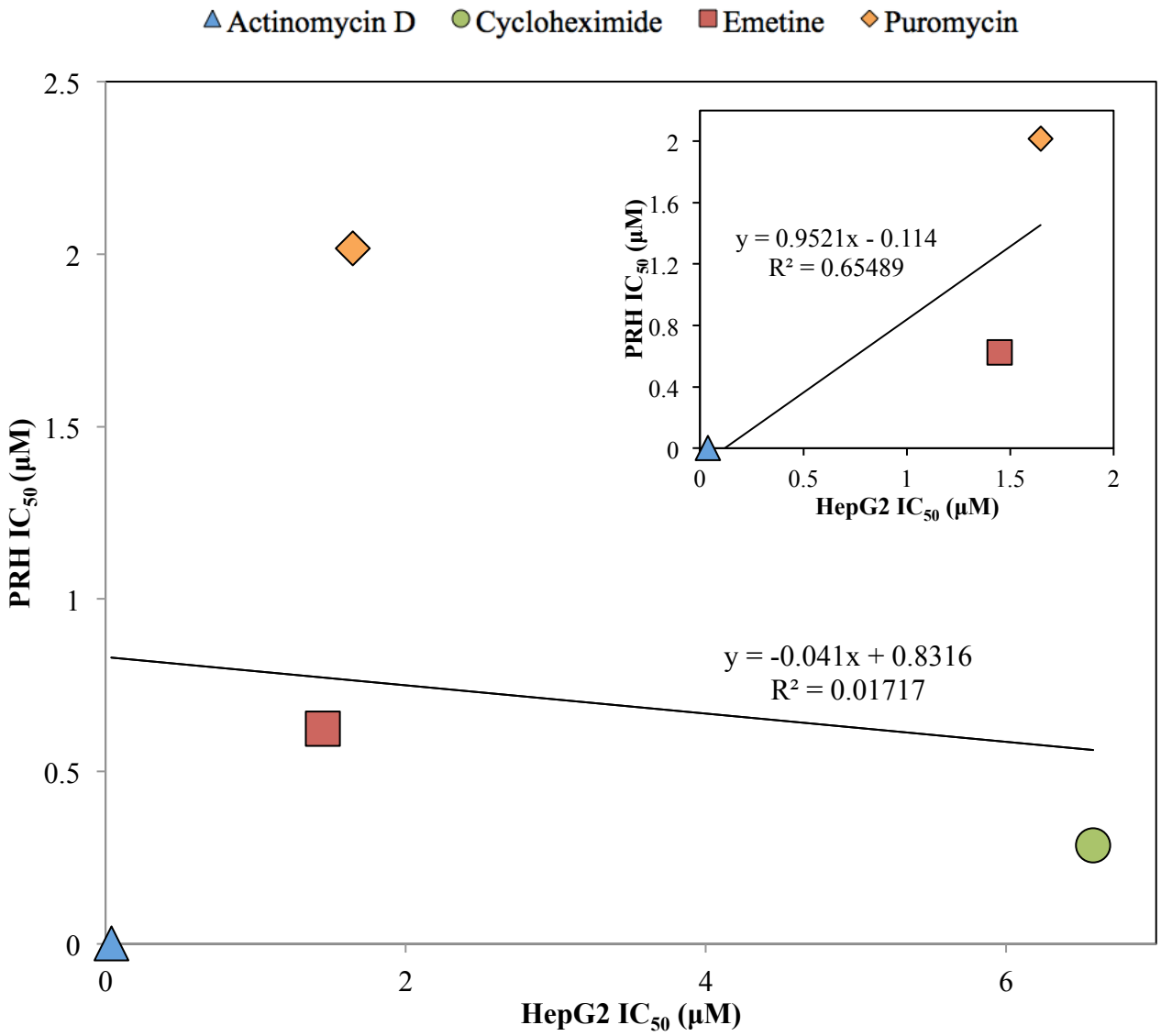

Figure 2.6 Linear regression analysis of IC_{50} between HepG2 and PRH cell types. Linear regression of the mean IC_{50} values of the protein synthesis inhibitor drugs derived from HepG2 and PRH concentration-response protein synthesis inhibition curves. Cycloheximide is omitted in the inset graph.

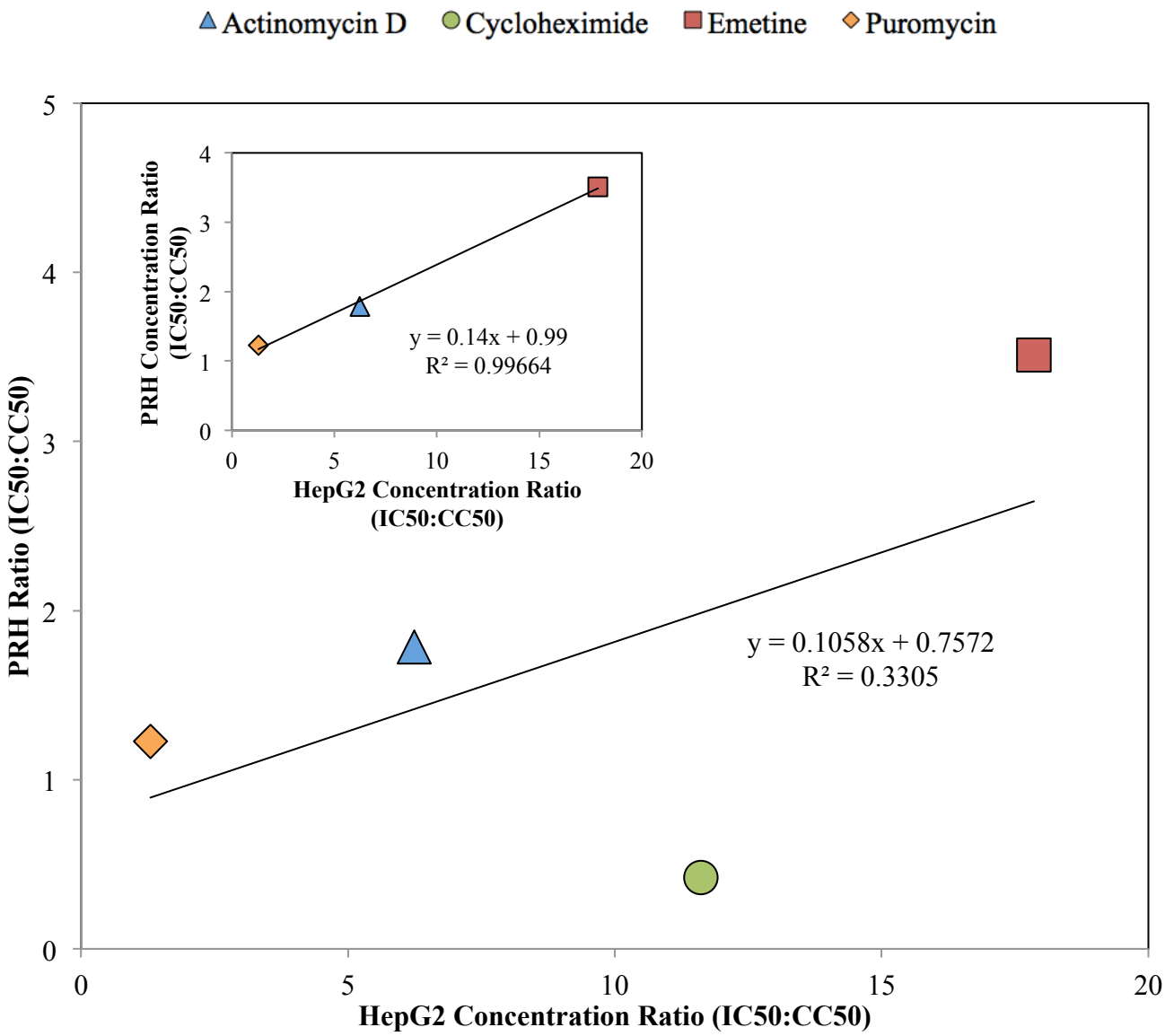

Figure 2.7 Linear regression analysis of IC_{50}:CC_{50} concentration ratio between HepG2 and PRH cell types. Linear regression of the IC_{50}:CC_{50} ratio of HepG2 and PRH cells. Cycloheximide is omitted in the inset graph.

2.4 Discussion

The use of protein synthesis inhibitors is the most common method for measuring protein degradation rates and has been documented by many sources over 4 decades (Goldberg & Dice 1974; Curfman et al. 1980; Princiotta et al. 2003; Zhou 2004; Belle et al. 2006; Delgado-Vega et al. 2012; Chistyakov et al. 2014). As discussed previously in Chapter 1, ineffective inhibition of *de novo* protein synthesis will distort the accuracy of the measured rate of protein degradation. Protein synthesis inhibitor agents universally stop protein synthesis by inhibiting fundamental gene transcription and translation processes, thus prolonged inhibition will inevitably affect proteins that are essential for cell survival. Despite their cytotoxic risks, protein synthesis inhibitors are worth exploring for their potential to use in short-term degradation rate studies as they provide the most simple, economical and readily available approach to inhibit *de novo* protein synthesis. The aim of this chapter was to define a single inhibitor at a concentration that provided maximum protein synthesis inhibition with minimal cytotoxicity, which could then be used in subsequent kinetic experiments to accurately estimate CYP protein degradation rates.

Protein synthesis inhibitors have been commonly used in previous studies of protein degradation, yet there has been little consideration for their cytotoxic effects and none have reported optimisations for a specific concentration to use. It is evident from Table 2.1 that historically, a range of different protein synthesis inhibitor compounds were used over a range of concentrations and incubation times have been used for the purpose of measuring mRNA or protein stability in different cell systems. Cycloheximide is the most commonly used of all inhibitor agents for this purpose and some previous studies have used this inhibitor with cell cultures at millimolar concentrations (Chang et al. 1981; Pan & Haines 1999; Princiotta et al. 2003; Jeong et

al. 2005; Majumder et al. 2012), which was much higher than the non-toxic concentration range found here. Moreover, Welch & Wang (1992) cultured NIH 3T3 cells with 88.9 μM for 60 h and Chen & Madura (2008) cultured yeast cells in 1.8 μM for 120 h; both of which are higher than the non-toxic concentrations reported here for cycloheximide over a long incubation period. However, it must be noted that different cellular systems may well have different tolerance of inhibitor agent-induced cytotoxicity and thus, concentrations ought to be optimised for each given cellular system.

In this chapter, the CC_{50} and IC_{50} for four protein synthesis inhibitor agents were measured in two cell types to define their potential to inhibit protein synthesis without cytotoxicity. In all cases, except for cycloheximide in PRH (as reflected in IC_{50}:CC_{50} < 1), the CC_{50} concentrations for the individual inhibitors were lower than the corresponding IC_{50} in both cell types, suggesting that protein synthesis inhibition could not be studied in the absence of an effect on other cellular functions. On closer inspection with cycloheximide in PRH, the concentration that provided 20% cytotoxicity or 80% viability (CC_{20}) was 0.11 μM and this was lower than the IC_{50} at 0.29 μM. This means that at 80% cell viability, which was considered the maximum level of acceptable toxicity, cycloheximide produced less than 50% protein synthesis inhibition and therefore insufficient for protein degradation studies. Clearly, a different approach to single protein synthesis inhibitors was needed to increase the level of target protein synthesis inhibition and reduce cytotoxicity.

Earlier studies with actinomycin D and puromycin reported toxicity in HeLa cells at concentrations within the range investigated here. Studies by Sawicki & Godman (1971) showed that at 0.08 μM actinomycin D was sufficient to cause cell toxicity in HeLa cells and the data in this chapter is in agreement with these findings. Dudani et

al. (1988) reported 79.6% protein synthesis inhibition at 0.9 mM and cytotoxicity was detected at 0.9 μM after incubation of HeLa cells with puromycin; the data presented herein agreed with these findings and suggests that puromycin is cytotoxic at concentrations lower than those required for protein synthesis inhibition.

Conversely, Low et al. (2009) conducted cytotoxicity assays Huh-7 cells that were treated with emetine and reported over 90% cell viability at 10 μM; this concentration is much higher than the cytotoxic range derived here. Although the reason for this disparity is not apparent, cytotoxicity of these inhibitors may vary between different cell types and for this reason two hepatic cell types were analysed in this Chapter.

The single drug analyses were carried out in HepG2 and PRH with reasonable agreement in protein synthesis inhibition and cytotoxicity between these cell types for actinomycin D, emetine and puromycin; as demonstrated by the linear relationship displayed in Figures 2.5 – 2.7. A strong linear correlation (R^2=0.996) was observed in the CC_{50} values derived from both cell types and also in the IC_{50}:CC_{50} (R^2=0.997) when cycloheximide was omitted, and a reasonable correlation (R^2=0.655) in IC_{50} when cycloheximide was omitted. The correlations between two cell types confirm the reliability of findings that the inhibitors were more efficacious in bringing about cytotoxicity than protein synthesis inhibition. Cycloheximide did not fit in the correlation for IC_{50}; this could perhaps be explained by differential mechanisms of protein synthesis inhibition in different species as HepG2 cell lines are of human origin. However, elucidation of this hypothesis is beyond the scope of this thesis.

Optimisation of protein synthesis inhibitor concentrations was initially carried out in HepG2 and PRH cells with the intention of transferring the optimised conditions to measure CYP k_{deg} in primary human hepatocytes. One advantage of using HepG2 (a hepatic immortalised cell line) and PRH are that they are relatively inexpensive

compared with primary human hepatocytes. HepG2 cells express similar mRNA transcripts as primary human hepatocytes and are recommended for studying DME regulation pathways (Westerink & Schoonen 2007). Unlike HepG2 cells, PRH express the full panel of phase I and II DMEs and are therefore considered a better representative model for the *in vivo* liver. However, there are reported differences between liver-specific metabolic functions across species (Vilei et al. 2001) and differential expression of CYP enzymes occur in sandwich culture between human and rat (Kern et al. 1997), therefore CYP k_{deg} derived from hepatocytes of human origin ought to provide a better representative for the human *in vivo* condition.

In summary, single protein synthesis inhibitor drugs are unsuitable for measuring protein degradation rates due to their propensity to cause cell death. Any loss of signal in subsequent protein kinetic analyses will be distorted by the loss of signal caused by cell death. The incubation time with the protein synthesis inhibitor drugs was for 72 hours in the current study and as such, measurement of degradation for proteins with medium or long (over 72 hours) half-lives, as in the case of CYP enzymes, are likely to be particularly problematic. A different approach avoiding the use of single protein synthesis inhibitor drugs, eliciting increased target protein synthesis inhibition with less cytotoxicity is needed for measurement of CYP k_{deg}. The purpose of chapter 3 was therefore to assess whether a combination of inhibitors would be more appropriate.

CHAPTER 3

Utility of multiple protein synthesis inhibitor combinations for measuring CYP protein degradation rate constant

CONTENTS

3.1 Introduction

It was concluded in Chapter 2 that individual protein synthesis inhibitor drugs, which are commonly used in processes to measure protein degradation, are likely to be unsuitable for measuring CYP degradation due to confounding cytotoxic effects when used *in vitro*. However, pharmacological interference remains the most simple and cost effective method of stopping protein synthesis and an assessment of inhibitor combinations was therefore worthy of analysis.

Combination drug therapies can increase efficacy, decrease toxicity and reduce resistance compared to monotherapy. Combination regimens are routinely used in the treatment of many diseases such as HIV, cancer and hypertension (Foucquier & Guedj 2015). This is possible due to the principles of PD interactions (Jia et al. 2009) and drug synergism in which each agent within the combination contributes to the desirable effect and so lower doses of each agent can be administered to achieve optimal efficacy, while reducing risks of toxicity. One clinical example of a synergistic dose-reduction effect is in the use of capecitabine and docetaxel in combination for treatment of advanced metastatic breast cancer (Verma et al. 2005). It was found that 1250 mg/m^2 capecitabine combined with 75 mg/m^2 docetaxel significantly improved survival compared with 100 mg/m^2 docetaxel alone (O'Shaughnessy et al. 2002). The use of combinations of antiretrovirals have been crucial in the treatment of HIV and one example, amongst many, of a clinically significant synergistic effect is in the administration of ritonavir and squinavir in combination. Ritonavir inhibits saquinavir metabolism therefore increases therapeutic effects compared to administering saquinavir alone (Merry et al. 1997).

There are several different methodologies used to assess synergism of drug combinations and the advantages and limitations between these approaches are widely

debated amongst biologists and mathematicians (Chou 2010). The most commonly used methods for assessing synergism in drug combinations fall into two main designs: effect-based and dose-effect-based approaches (Foucquier & Guedj 2015).

Effect-based approaches assess drug synergy by comparing the overall effect of a drug combination to the effects produced by the drugs individually. Dose-effect-based strategies aim to assess what amount, or the relative contribution, of each drug produces a specified quantifiable effect and such approaches rely on the principles of *Loewe Additivity* (Loewe 1926). The basis for predicting the effects of a drug combination is based on the concept of dose equivalence; this is the determination of the doses of each drug alone that give the same effect. When the ratio of equally effective dose is the same for the drugs in combination at every concentration, then drug additivity is inferred and the combination effect can be predicted. In this case, a constant relative potency occurs between the drug pairs and can be described by the following equation, where two drugs A and B are administered at doses *a* and *b*, respectively (Tallarida 2010):

$$\frac{a}{\mathrm{A}} + \frac{b}{\mathrm{B}} = 1 \qquad (33)$$

Isobolographic analysis is the most common dose-effect-based method of combination drug analysis based on the principles of *Loewe Additivity* (Loewe 1926). An isobologram is a graph that is constructed on a coordinate system with individual drug doses on the *x* and *y*-axis and a linear line of additivity that is used to differentiate synergy (superadditive) and antagonism (subadditive) from additive interactions (Tallarida 2006). The graph is produced from two drugs that produce a similar measurable effect and a dose-effect profile is produced for each drug individually. The efficacy and potency is derived from the individual concentration-effect curves for each of the drugs and allows a determination of the expected

combination effect. The expected effect is termed the ‘additive effect’ and a difference from additivity infers synergy or antagonism (Tallarida 2011). Synergy and antagonism represents greater or lesser effects for drugs in combination than the simple additive effect expected, respectively (Tallarida 2010). Additivity implies no interaction between the drug combinations, where each drug contributes to the effect according to its own potency. Figure 3.1 shows theoretical isobolograms indicating these interactions; if the curve lies below the line of additivity then a lower concentration is needed to reach a specified effect and synergy is assumed. Conversely, if it lies above then a higher dose is required and antagonism is infered.

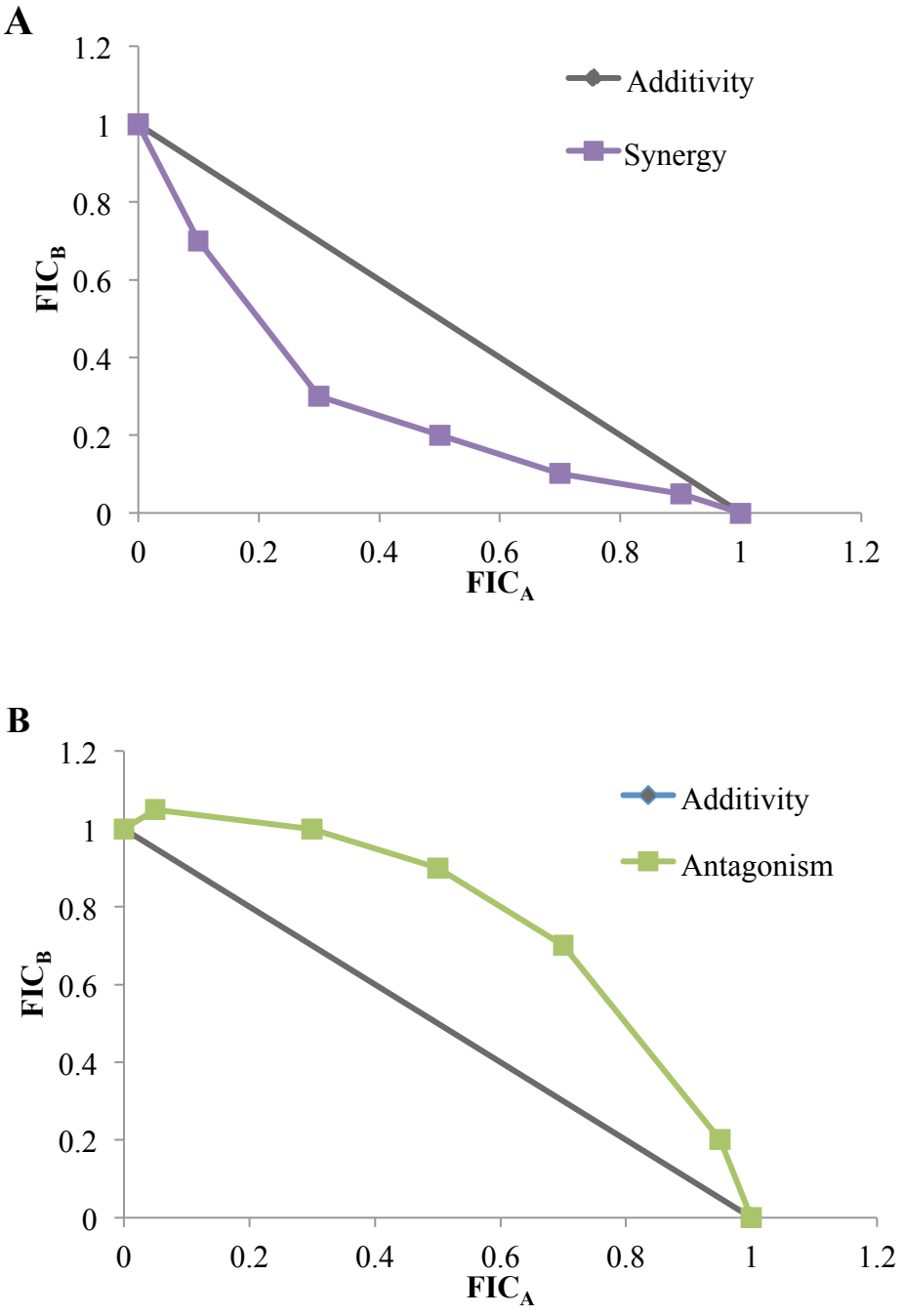

Figure 3.1 Theoretical isobolograms showing synergy (A) and antagonism (B). FIC denotes fractional inhibitory concentration of drug A or drug B (See equations 3.1-3.3). The solid black line represents the line of additivity.

Synergy for a desired effect and antagonism of an undesired effect is the ideal scenario when assessing drug combinations. Drug combination effects are often not predictable in a concentration-dependent manner as constituent concentrations of each drug within the combination may present different effects. Accordingly, different concentration ratios of the drugs in combination are assessed to determine an optimal combination at specific concentrations for synergising a desirable effect (Tallarida 2010).

MTT assays were the only form of cell viability analysis employed in Chapter 2 to determine cytotoxicity. Viable cells within culture convert MTT into a purple coloured formazan product with optimal absorbance at 570 nm. When cells die, they lose the ability to convert MTT into formazan therefore the intensity of colour formation, as determined by absorbance value, serves as a surrogate estimate for cell viability (Riss et al. 2004). The exact mechanism of MTT reduction to formazan product remains poorly understood but it is likely that reduced nicotinamide adenine dinucleotide (NADH) and NADPH electron transfer in the mitochondria are involved; thus it is widely accepted that MTT assays are a measure of mitochondrial function (Berridge & Tan 1993). Several chemical compounds, especially reducing compounds, are known to interfere with MTT assays and can produce signals by increasing absorbance values in the absence of viable cells. Consequently there are limitations to using MTT assays to alone to determine cell viability. This limitation was addressed in this chapter through the use of multiple cell viability assays, which determine cell viability through different mechanisms and using different indicators as measure of viability. As cell death can be caused by multiple mechanisms, such as those leading to apoptosis or necrosis, using a single method of determining cell viability may not be a true measure of cell death. The GSH-Glo™ glutathione assay

measures oxidative stress and the CellTiter-Glo® luminescent assay measures ATP production; both assays detect early indicators of cytotoxicity. Converesly, trypan blue exclusion tests for membrane integrity and can be considered a measure of the later stages in the cascades of cell death. The comparison of cell viability estimated from MTT assays to other established cytotoxicity assays will confirm the robustness of the data reported in Chapter 2.

The aim of this chapter was to investigate the potential for using multiple protein synthesis inhibitor drug combinations for measuring CYP protein degradation rates. The principles of concentration-effect-based combination drug analysis were employed to study the *in vitro* effects and find possible synergy in protein synthesis inhibition and antagonism in cytotoxicity in two-drug combinations of the four previously chosen protein synthesis inhibitors: actinomycic D, cycloheximide, emetine and puromycin, detailed in 2.1, for use in subsequent degradation rate studies. Three and four-drug combinations were also investigated at sub-cytotoxic concentrations for level of protein synthesis inhibition and cytotoxicity. A range of different cytotoxicity assays including GSH-Glo™ glutathione, CellTiter-Glo® luminescent and Trypan blue exclusion assays were also performed on the three and four-drug combinations to assess the robustness of using MTT assays as a measure of cell viability.

3.2 Materials and methods

3.2.1 Materials

Dulbecco's modified eagle medium (DMEM), foetal bovine serum (FBS), trypsin-EDTA solution, Hank's balanced salt solution (HBSS), dimethyl sulfoxide (DMSO), sterile water (W4502), thiazolyl blue tetrazolium (TBT) and protein synthesis inhibitors; actinomycin D (A4262), emetine dihydrochloride hydrate (E2375) and puromycin dihydrochloride (P7255), were purchased from Sigma-Aldrich (Dorset, UK). HepG2 cells were purchased from American Tissue Culture Collections (ATCC, Virginia, USA). Cycloheximide (ab120093) was purchased from Abcam (Cambridge, UK). L-Leucine [4,5-^{3}H] (MT-672E) was obtained from Moravek (California, USA). CellTiter-Glo® luminescent cell viability assay and GSH-Glo™ glutathione assay were purchased from Promega (Southampton, UK).

3.2.2 Cell culture and plating

HepG2 cell line was maintained and plated as described in 2.2.2 and 2.2.4, respectively. After overnight incubation to allow for cell adherence, old media was removed and cells were dosed with desired drug combinations. Cells were incubated for 72 h at 37 °C with 5% CO_2 and 95% humidity with drug-containing media and this media was replaced every 24 h.

3.2.3 Two-drug combination fixed-ratio isobologram analysis

The effects of two-drug combinations on HepG2 cells were assessed using a modified fixed-ratio isobologram method, published by Fivelman et al., that detects synergy, additivity or antagonism between a pair of drugs (Fivelman et al. 2004). Stock solutions of the drugs were prepared at 10 mM in sterile water or DMSO then diluted

in cell line maintenance media (DMEM with 10% FBS) to achieve desired concentration with the dissolution vehicle at <1% of final concentration. The IC_{50} and CC_{50} of the individual drugs were derived from concentration-response assays described in 2.2.9. The four protein synthesis inhibitor drugs (actinomycin D, cycloheximide, emetine and puromycin) formed six different two-drug combinations and for these combinations dilutions were made to allow the IC_{50} or CC_{50} to fall at about the fourth three-fold serial dilution. The dilutions of each of the two drugs in each combination were prepared in 7 fixed ratios 6:0, 5:1, 4:2, 3:3, 2:4, 1:5 and 0:6. These mixtures were then serially diluted three-fold in quadruplicates to generate a range of eight concentrations for each condition. Cell viability and protein synthesis inhibition assays were conducted as described in 2.2.6 and 2.2.7 to generate a concentration-response curve to calculate the CC_{50} and IC_{50}, respectively, for drug A and B in each mixture. The fractional inhibitory concentrations (FICs) were calculated using equations 3.1, 3.2 and 3.3 (Gorka et al. 2013):

$$\mathrm{FIC_A} = \frac{\mathrm{IC_{50}\ or\ CC_{50}\ of\ drug\ A\ in\ combination}}{\mathrm{IC_{50}\ or\ CC_{50}\ of\ drug\ A\ alone}} \qquad [3.1]$$

$$\mathrm{FIC_B} = \frac{\mathrm{IC_{50}\ or\ CC_{50}\ of\ drug\ B\ in\ combination}}{\mathrm{IC_{50}\ or\ CC_{50}\ of\ drug\ B\ alone}} \qquad [3.2]$$

$$\mathrm{FIC_{index}} = \mathrm{FIC_A} + \mathrm{FIC_B} \qquad [3.3]$$

Isobologram curves were generated by plotting FIC_A versus FIC_B. $FIC_{index} = 1$ was taken as indicative of an additive effect between drug A and B, $FIC_{index} < 1$ indicative of synergy and $FIC_{index} > 1$ indicative of antagonism. There were four replicates per condition and the assays were repeated four times.

3.2.4 *Measuring protein synthesis inhibition in two-drug combinations by [^{3}H]-leucine incorporation*

HepG2 cells were seeded at 2 x 10^5 cells per well on 96-well plates. Cells were then

dosed with drug-containing media in concentrations described in 3.2.3. [^{3}H]-leucine incorporation assays were conducted after 72 h incubation as described in 2.2.7 on all six two-drug combinations at each fixed-ratio to generate an IC_{50} for each drug in each mixture. Only combinations that displayed additivity or synergy in the level of protein synthesis inhibition were proceeded for analysis of cytotoxicity to determine useful two-drug combinations for protein degradation studies.

3.2.5 Measuring cytotoxicity of two-drug combinations by standard MTT assay

HepG2 cells were seeded at 2 x 10^4 cells per well on 96-well plates. Cells were then dosed with drug-containing media in concentrations described in 3.2.3. After 72 h incubation, the levels of cytotoxicity of the two-drug fixed-ratio combinations explained in 3.2.3 were determined by standard MTT assays as described in 2.2.6 to generate a CC_{50} for each drug in each mixture. Vehicle controls and a control with no drug were included. Only combinations that displayed additive or synergistic protein synthesis inhibition were included.

3.2.6 Calculation of CC_{10} concentrations for three and four-drug combination analysis

Three-drug combinations: actinomycin D, cycloheximide and emetine; actinomycin D, puromycin and emetine; actinomycin D, puromycin and cycloheximide; and puromycin, cycloheximide and emetine, and four-drug combination: actinomycin D, puromycin, cycloheximide and emetine were assessed at sub-cytotoxic concentrations of each drug (CC_{10}; concentration of inhibitor providing 10% cytotoxicity or 90% viability). The CC_{10} value was determined from the concentration-response curves derived from single drug incubation experiments in HepG2 cells shown in Figure 2.3.

The EC_{50} (concentration that gives 50% maximum response) and hill slope (H) derived from GraphPad Prism 6 software were inputted to the GraphPad calculator which calculated the CC_{10} value by the following equation:

$$EC_F = (\frac{F}{100 - F})^{1/H} \text{ x } EC_{50}$$

Where F represents the desired response percentage. The CC_{10} concentrations are shown in Table 3.1.

Table 3.1 The CC_{50}, hill slope and CC_{10} values derived in HepG2 cells in response to protein synthesis inhibitors

Drug	CC_{50} (µM)	Hill Slope	CC_{10} (nM)
Actinomycin D	0.0062	-0.61	0.17
Cycloheximide	0.57	-0.69	2.4
Emetine	0.081	-0.89	7.0
Puromycin	1.3	-13	107

3.2.7 *Measuring protein synthesis inhibition in three and four-drug combinations by [^{3}H]-leucine incorporation*

HepG2 cells were seeded at 2 x 10^5 cells per well on 96-well plates. Cells were then dosed with three or four-drug combinations made up at CC_{10} for each drug by dilution in HepG2 maintenance media to achieve final concentrations shown in Table 3.1. Cells were incubated for 72 h with drug-containing media replaced every 24 h. For each of these combinations the level of protein synthesis inhibition was assessed by [^{3}H]-leucine incorporation as described in 2.2.7.

3.2.8 *Measuring cytotoxicity of three and four-drug combinations*

Cytotoxicity of the three and four-drug combinations on HepG2 cells were determined by several different toxicity assays. Further toxicity assays, in addition to MTT (CellTiter-Glo®, GSH-Glo™ glutathione and trypan blue exclusion) were performed on three and four-drug combinations to confirm the robustness of MTT assays as a measure of cell viability.

3.2.8.1 Standard MTT assay

HepG2 cells were seeded at 2 x 10^4 cells per well onto 96-well plates. After initial incubation to allow for adherence, cells were incubated with the three and four-drug combinations described above for 72 h. Standard MTT assays were performed after 72 h using methods described in 2.2.6.

3.2.8.2 CellTiter-Glo® luminescent cell viability assay

HepG2 cells were seeded at 2 x 10^4 cells per well onto 96-well plates. CellTiter-Glo® luminescent cell viability assay were performed following 72 h incubation with three and four-drug combinations. A vehicle control and a control containing media only with no cells were included to obtain background luminescence. Plated cells and CellTiter-Glo® reagents were equilibrated at room temperature (RT) for 30 min. Equal volumes of CellTiter-Glo® substrate was added to buffer to create CellTiter-Glo® reagent. An equal volume to cell culture medium, 100 µl, of CellTiter-Glo® reagent was added to each well then mixed for 2 min on an orbital shaker. The plate was incubated for 10 min at RT to stabilise luminescent signal and then read by Tecan GENios micoplate reader (Germany). The luminescence corresponds to the amount of ATP present, which indicates the presence of metabolically active viable cells. All readouts were normalised against background fluorescence and cell viability was

determined as a percentage of control where no drug was added and viability assumed at 100%.

3.2.8.3 GSH-Glo™ glutathione assay

HepG2 cells were seeded at 1 x 10^4 cells per well on 96-well plates. After overnight incubation, cells were incubated with the three and four-drug combinations for 72 h. Vehicle controls and a control with no drug were included for background luminescence. All media was removed at 72 h and 100 µl GSH-Glo™ reagent (made up of Luciferin-NT substrate and GSH diluted 1:100 in GSH-Glo™ reaction buffer) was added to each well and then mixed for 2 min on an orbital shaker. The plate was incubated for 30 min at RT. 100 µl reconstituted luciferin detection reagent was added to each well before plates were mixed for further 2 min on an orbital shaker. The plate was incubated for 15 min at RT before luminescence was read by Tecan GENios micoplate reader (Germany). All readouts were normalised against background fluorescence and cell viability was determined as a percentage of control where no drug was added and viability assumed at 100%. GSH-Glo™ glutathione assays measures the conversion of a luciferin derivative into luciferin in the presence of glutathione and glutathione S-transferase (GST) as an indication of oxidative stress, a surrogate measure of cell death.

3.2.8.4 Trypan blue exclusion

HepG2 cells were seeded at 5 x 10^4 cells per well, left overnight and for adherence before incubation with the three and four-drug combinations for 72 h. Following incubation, the cells were washed twice with HBSS solution then either trypsinised for 5 min or incubated with cell dissociation buffer at 37°C with 5% CO_2 and 95% humidity for cell removal, before being transferred in suspension to Eppendorf tubes. 10µl of cell suspension was added to 10µl of trypan blue solution and placed on a

Countess™ slide. Cell viability was calculated using a Countess™ automated cell counter (LifeTechnologies, UK) that contained internal algorithms to determine cell viability.

3.2.9 Data Analysis

The IC_{50} and CC_{50} values in HepG2 cells derived from the single inhibitor analyses (Table 2.2) were used for two-drug combination fixed-ratio isobologram analyses. Concentration-response curves were created individually for each drug (A and B) in the two-drug combination at each of the 7 fixed ratios to generate IC_{50} and CC_{50} values to calculate FIC values for isobolograms. All concentration-response curves were generated in GraphPad Prism 6 software as described in 2.2.9.

Statistical analyses of the three and four-drug combinations were completed using SPSS software, whereby a Shapiro-Wilk test was used to test for normality followed by unpaired T-test for normal populations and Mann-Whitney tests used for non-normal populations. $P<0.05$ was taken as significant.

3.3 Results

3.3.1 Antagonistic two-drug protein synthesis inhibitor combinations

The fixed-ratio isobologram method was employed to assess additivity, synergy or antagonism in both protein synthesis inhibition and cytotoxicity between drug pairs. Figure 3.2 shows a typical concentration-response curve produced by the fixed-ratio method to generate IC_{50} and CC_{50} values for each individual drug within the drug pairs at each fixed-ratio concentrations. The IC_{50} and CC_{50} values of the drugs alone and in combination were used to calculate the FIC_{index}, which is plotted in an isobolographic analysis (Figures 3.3, 3.4 and 3.5).

All six combinations of drug pairs for the four inhibitors were analysed for protein synthesis inhibition. Three of the six two-drug combinations: cycloheximide and emetine; cycloheximide and puromycin; emetine and puromycin, showed antagonism for protein synthesis inhibition at all ratios (Figure 3.3). This meant the drugs showed decreased efficacy in inhibiting protein synthesis in combination than with the inhibitors alone, therefore these drug pairs were deemed unsuitable for protein degradation studies. As such, isobolograms to assess cytotoxicity were not carried out for these combinations.

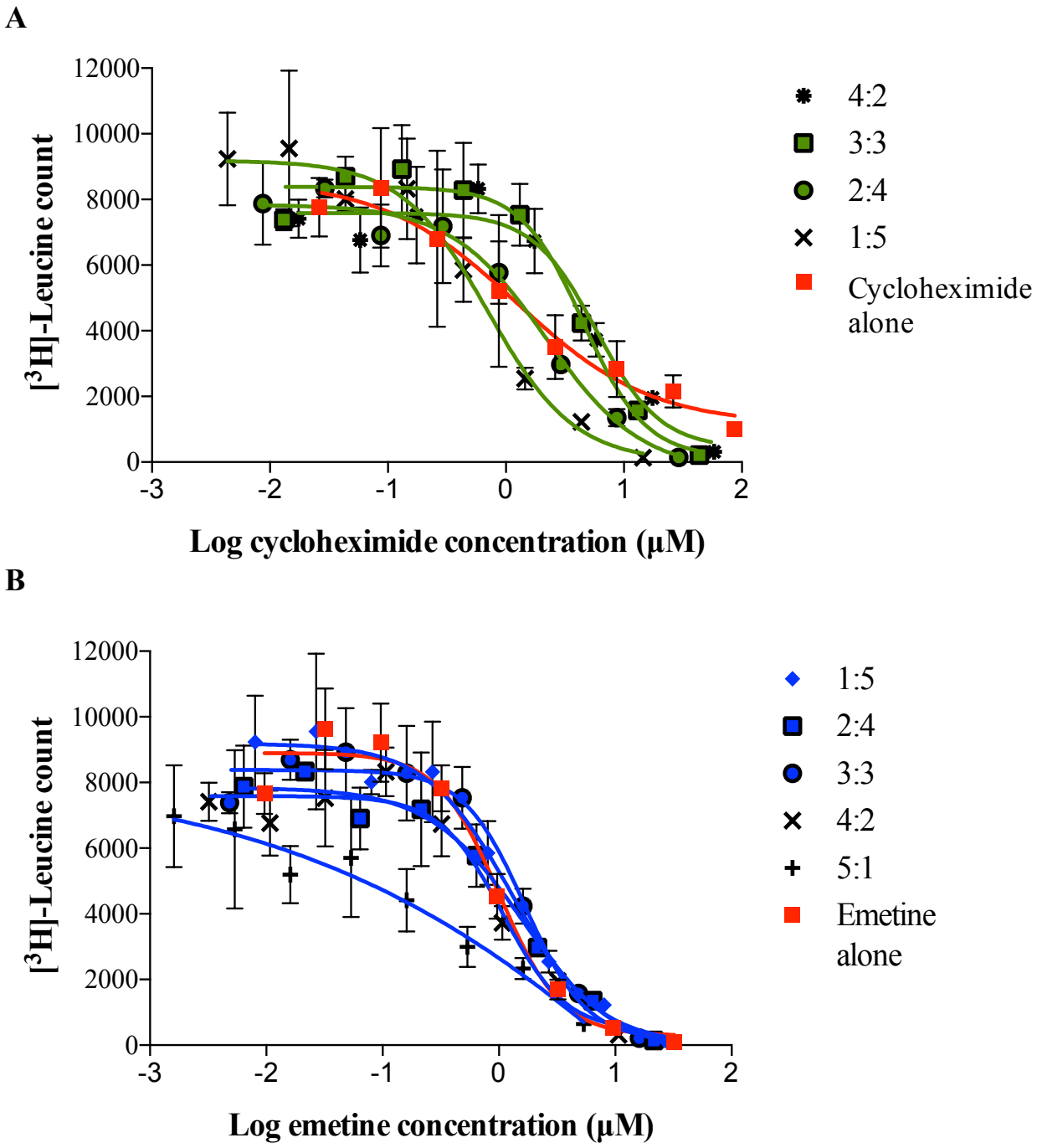

Figure 3.2 Typical concentration-response curves produced by the fixed-ratio method. Cycloheximide and emetine drug pair is shown for analysis of protein synthesis inhibition in HepG2 cells. A. Cycloheximide concentration-response. Ratios Drug A : Drug B represent cycloheximide : emetine. **B.** Emetine concentration-response. Ratios Drug A : Drug B represent emetine : cycloheximide. Individual IC_{50} values are derived for the individual drugs in each fixed-dose ratio to calculate corresponding FIC values for isobolographic analysis. N = 4.

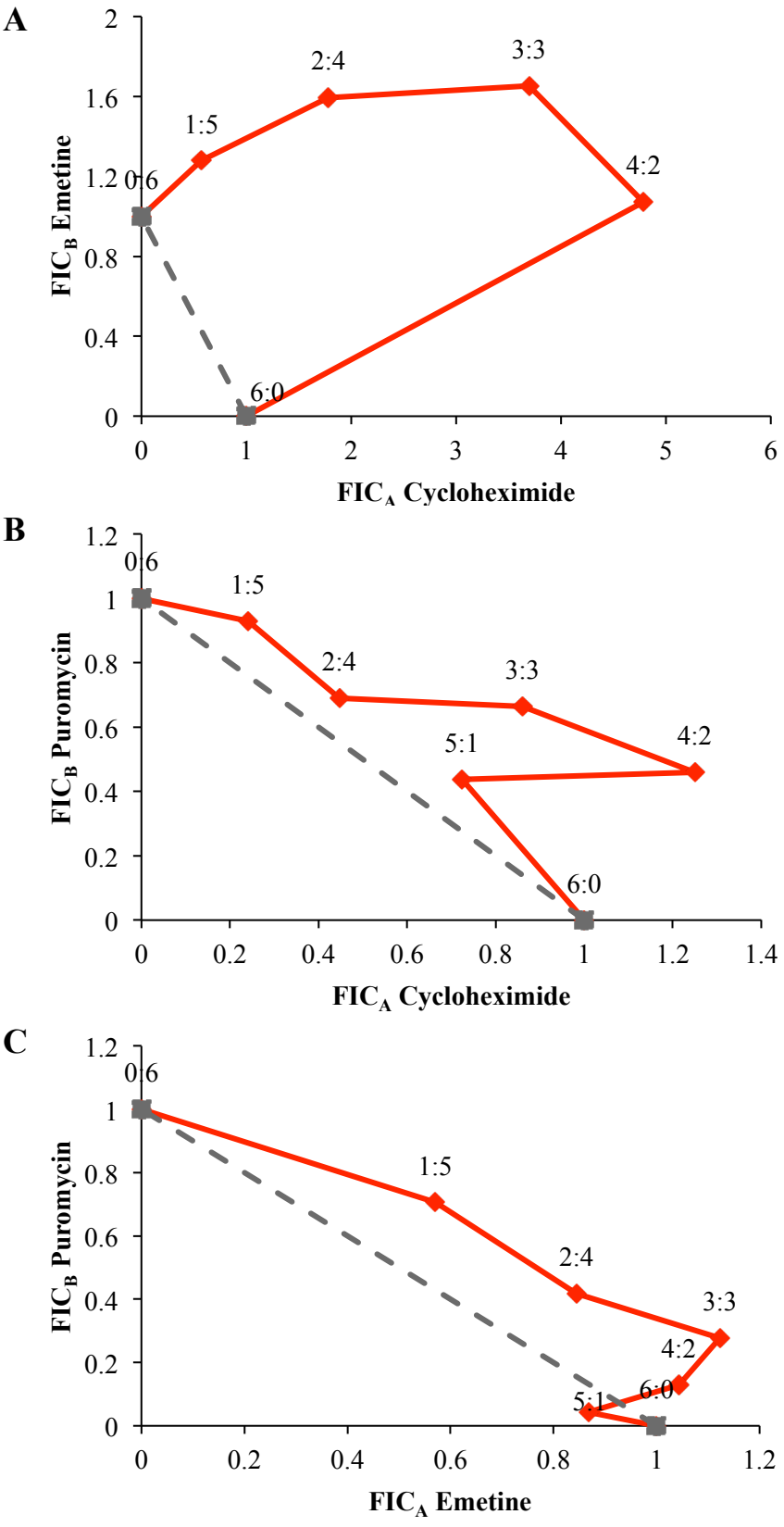

Figure 3.3 Isobolograms showing antagonistic interactions for protein synthesis inhibition in HepG2 cells. **A.** cycloheximide and emetine **B.** cycloheximide and puromycin and **C.** emetine and puromycin. Dotted line represents the line of additivity. Red line corresponds to drug pair interactions for protein synthesis inhibition. FIC_A and FIC_B correspond to the fractional inhibitory concentrations of the first and second drugs in each drug pair listed.

3.3.2 Additive two-drug protein synthesis inhibitor combination

As seen in Figure 3.4, actinomycin D and emetine showed additivity (no interaction) between the drugs for protein synthesis inhibition and was investigated for interactions in cytotoxicity. The drug pair showed synergy at all ratios for cytotoxicity, indicating that actinomycin D and emetine in combination did not improve efficacy in protein synthesis inhibition but increased cytotoxic effects compared to the drugs alone. As such, this combination was also deemed unsuitable for measuring CYP protein degradation rates.

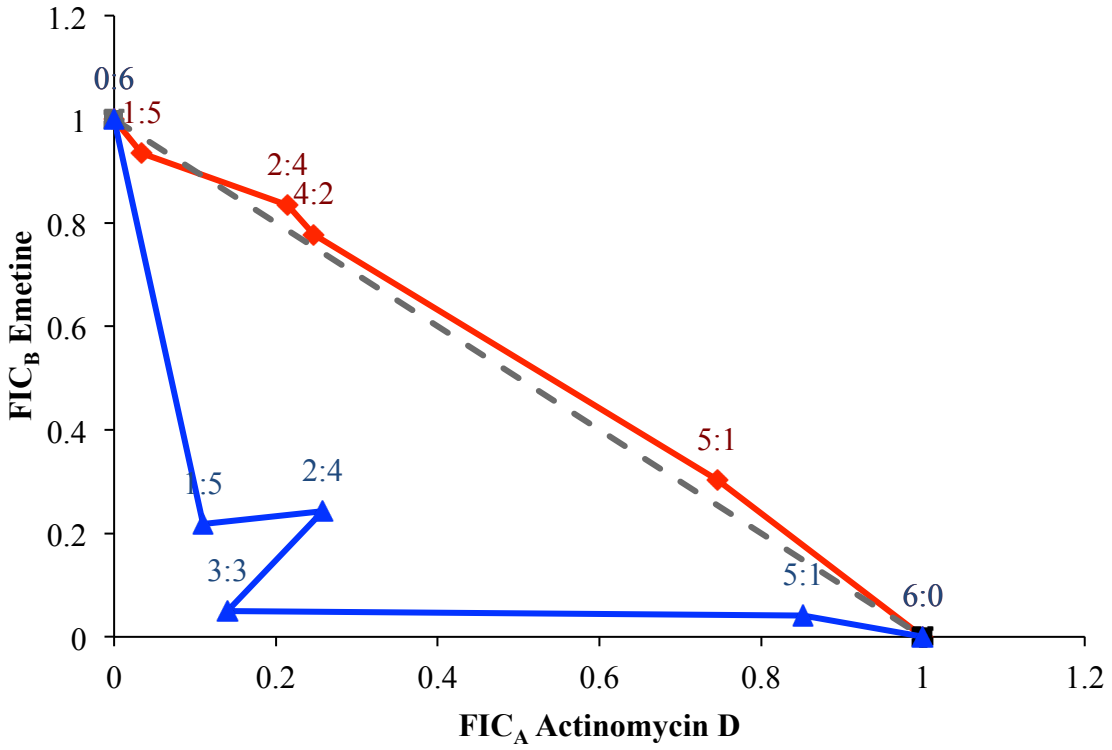

Figure 3.4 Isobolograms showing protein synthesis inhibition and cytotoxicity interactions for actinomycin D and emetine in HepG2 cells. Dotted line represents the line of additivity. Red line corresponds interactions for protein synthesis inhibition. Blue line corresponds to interactions for cytotoxicity. FIC_A and FIC_B correspond to the fractional inhibitory concentrations of the first and second drug in each drug pair listed in the ratio.

3.3.3 Synergistic two-drug protein synthesis inhibitor combinations

Two of the six combinations: actinomycin D and cycloheximide, and actinomycin D and puromycin, showed desirable synergy for protein synthesis inhibition at most ratios, therefore these combinations were investigated for interactions in cytotoxicity. However, upon analysis of cytotoxicity both of these combination also displayed strong synergy for cytotoxicity as shown in Figure 3.5. This suggests that although in combination the drugs showed increased efficacy for protein synthesis inhibition, they also demonstrated strong undesirable synergy for producing cytotoxicity.

Interestingly, at ratios of 5:1 and 4:2 for actinomycin D : cycloheximide and actinomycin D : puromycin, these combinations were synergistic for protein synthesis inhibition and antagonistic for cytotoxicity as seen in Figure 3.5. The IC_{50} and CC_{50} values at these ratios were investigated and shown in Table 3.2. However, despite the synergy for protein synthesis inhibition and antagonism for cytotoxicity at these ratios, the CC_{50} values for these drug pairs in combination were still lower than the IC_{50} values and thus cytotoxicity was observed at lower concentrations than those required to inhibit protein synthesis. The CC_{50} concentrations for actinomycin D in combination with cycloheximide at 5:1 and 4:2 ratios were 0.012 and 0.014 μM and the corresponding IC50 concentrations were 0.028 and 0.035 μM, respectively. The CC_{50} values for cycloheximide in combination with actinomycin D at 5:1 and 4:2 ratios were 0.026 and 0.012 μM and the corresponding IC_{50} concentrations were 2.5 and 1.3 μM, respectively. For actinomycin D and puromycin, the CC_{50} concentrations for actinomycin D at 5:1 and 4:2 ratios were 0.0098 and 0.0081 μM and the corresponding IC_{50} concentrations were 0.016 and 0.021 μM respectively. As for puromycin the CC_{50} values at 5:1 and 4:2 ratios were 0.060 and 0.020 μM and the corresponding IC_{50} concentrations were 0.69 and 0.36 μM, respectively, as shown in

Table 3.2. Even for two-drug combinations at ratios that showed desirable synergy in protein synthesis inhibition and antagonism for cytotoxicity, such combinations were still more potent in bringing about cytotoxicity. Therefore all two-drug combinations of the four protein synthesis inhibitor drugs assessed were unsuitable for subsequent analysis of protein degradation.

Table 3.2 IC_{50} and CC_{50} of protein synthesis inhibitor drug combinations at ratios that showed synergy for protein synthesis inhibition and antagonism for cytotoxicity

Drug Combination (A and B)	Ratio	Protein synthesis inhibition (μM)		Cytotoxicity (μM)	
		FIC_{50} of drug A	FIC_{50} of drug B	FCC_{50} of drug A	FCC_{50} of drug B
Actinomycin D and cycloheximide	4:2	0.028	2.5	0.012	0.026
	5:1	0.035	1.3	0.014	0.012
Actinomycin D and puromycin	4:2	0.016	0.69	0.0098	0.060
	5:1	0.021	0.36	0.0081	0.020

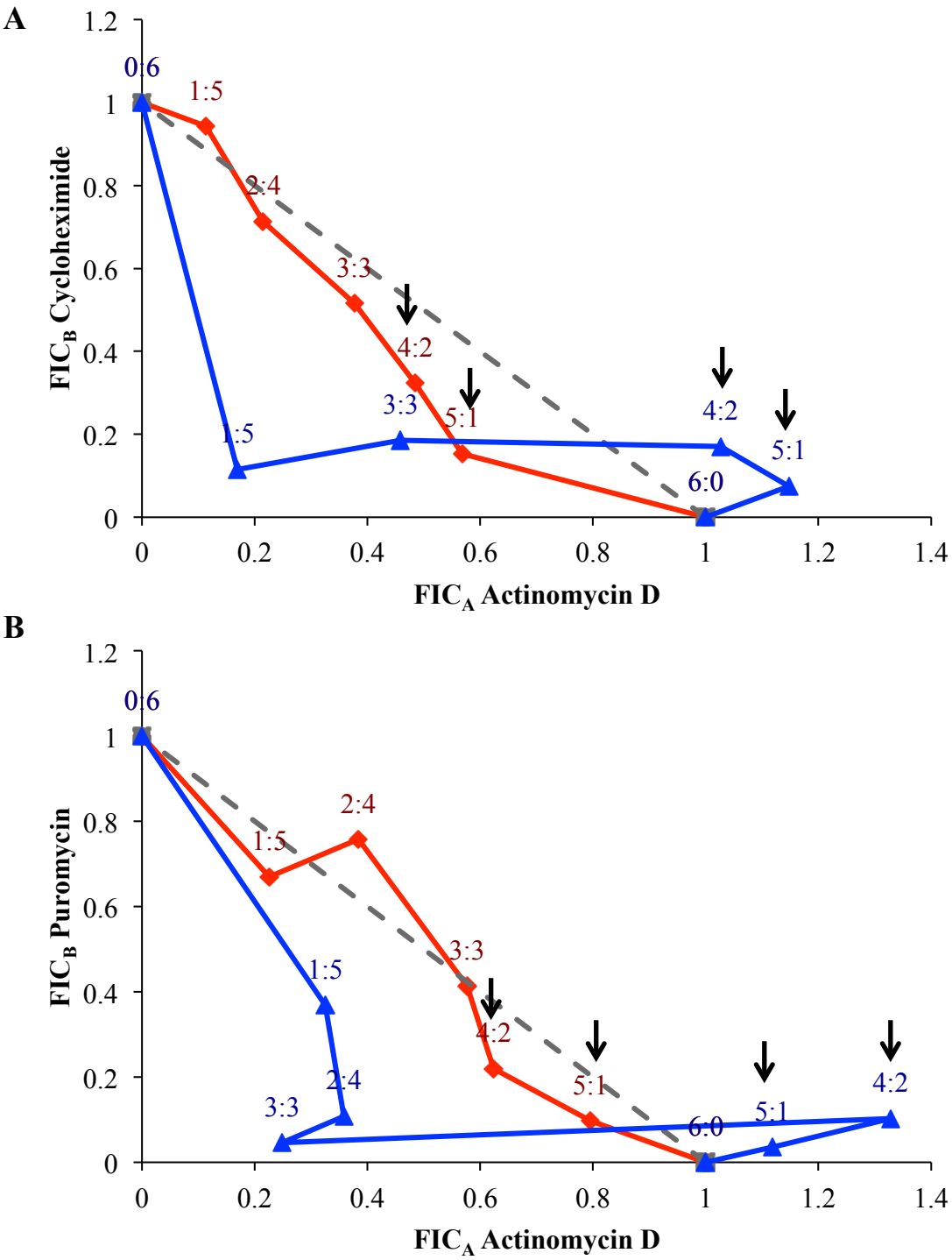

Figure 3.5 Isobolograms showing protein synthesis inhibition and cytotoxicity interactions in HepG2 cells. A. actinomycin D and cycloheximide. **B.** actinomycin D and puromycin. Dotted line represents the line of additivity Red line corresponds interactions for protein synthesis inhibition. Blue line corresponds to interactions for cytotoxicity. FIC_A and FIC_B correspond to the fractional inhibitory concentrations of the first and second drug in each drug pair listed in the ratio. Arrows indicate drug pair ratios that showed synergism for protein synthesis inhibition or antagonism for cytotoxicity.

3.3.4 Three and four-drug combination analysis for protein synthesis inhibition

Three and four-drug combinations at sub-toxic concentrations (CC_{10} of each when incubated alone) were assessed to investigate whether protein synthesis inhibition could be achieved at concentrations lower or equal to those causing cytotoxicity. The CC_{10} (90% cell viability concentration) were calculated for each drug to be 0.17, 24, 7.0 and 110 nM for actinomycin D, cycloheximide, emetine and puromycin in HepG2 cells, respectively (Table 3.1). Figure 3.6 shows that three and four-drug combinations exhibited < 50% leucine incorporation and therefore insufficient levels of protein synthesis inhibition was achieved in all combinations for subsequent use in protein degradation studies.

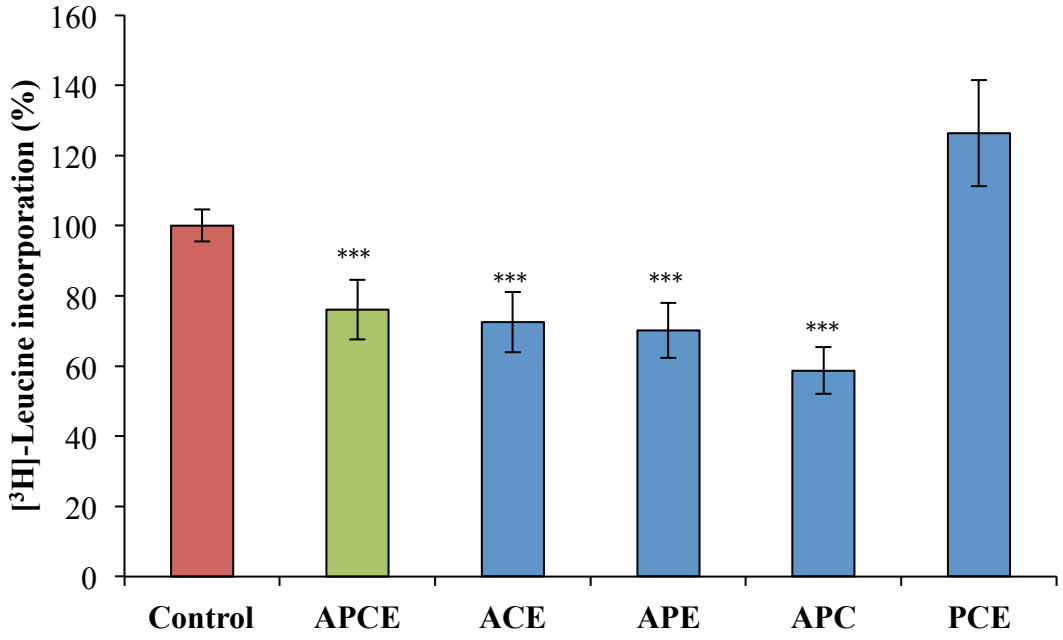

Figure 3.6 Level of [^{3}H]-Leucine incorporation for three and four inhibitor combinations at sub-cytotoxic concentrations (CC_{10}) in HepG2 cells. APCE corresponds to actinomycin D, puromycin, cycloheximide and emetine, respectively. ***P<0.001 significance was calculated compared to control group. Data are shown as mean ± S.D from n=3 experiments carried out in triplicates.

3.3.5 Three and four-drug combination analysis for cytotoxicity

HepG2 cell viability in response to incubation with three and four-drug combinations at CC_{10} of each inhibitor was assessed with several different toxicity assays. Figure 3.7 shows that over 50% cell death occurred across all drug combinations except for puromycin, cycloheximide and emetine (PCE). However, this combination was also ineffective at inhibiting protein synthesis, as shown in Figure 3.6, where level of leucine incorporation was higher than control.

There was good agreement between the different toxicity assays in relation to the level of cytotoxicity measured as a response to the three and four-drug combinations, with the exception of GSH-Glo™, which consistently measured a higher viability across all combinations. Overall, three and four-drug combinations of the selected protein synthesis inhibitors were deemed to be unsuitable for further protein degradation studies even at low concentrations due to high cytotoxicity levels and low protein synthesis inhibition potential.

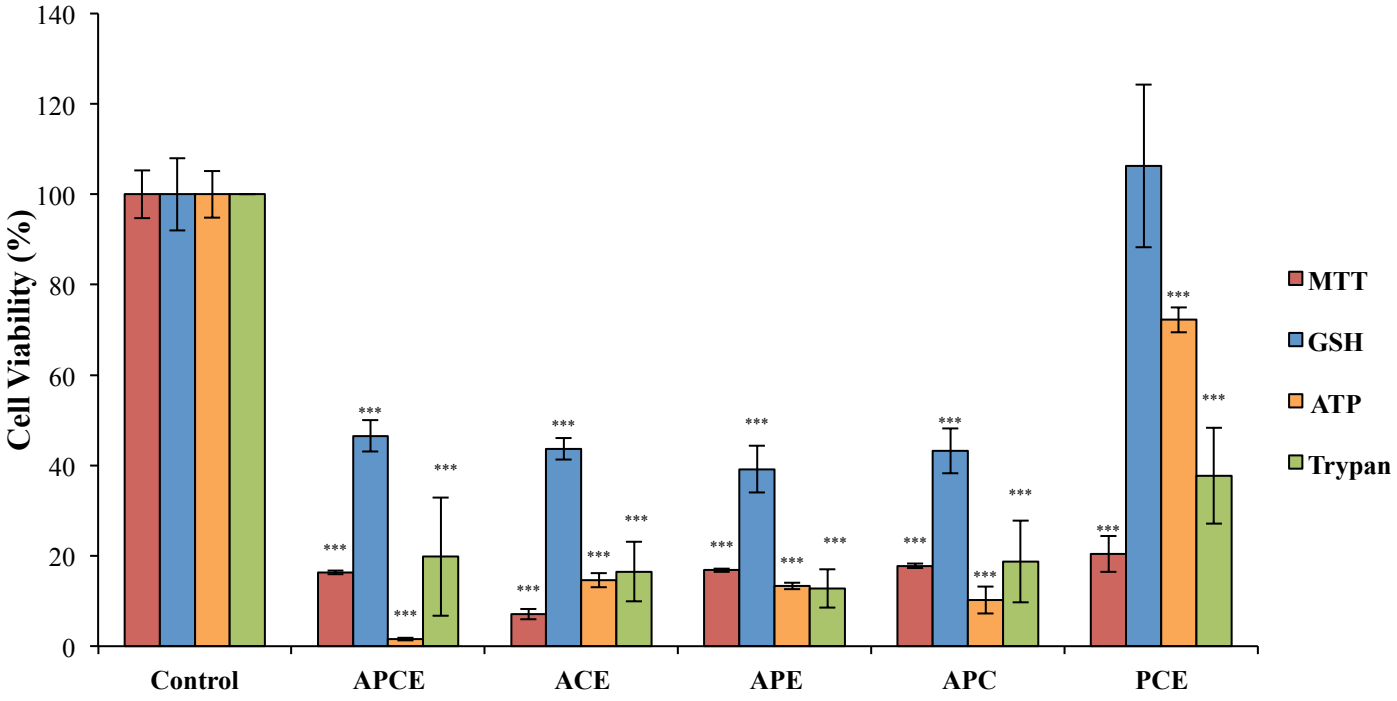

Figure 3.7 Cytotoxicity for three and four inhibitor combinations at sub-cytotoxic concentrations (CC_{10}). Three and four inhibitor combinations were prepared at CC_{10} concentrations. A range of cytotoxicity assays including standard MTT, GSH, ATP and trypan blue exclusion assays were conducted on HepG2 cells. APCE corresponds to actinomycin D, puromycin, cycloheximide and emetine, respectively. ***P<0.001 significance was calculated compared to corresponding control. Data are shown as mean ± S.D from n=3 experiments carried out in triplicates.

3.4 Discussion

Pharmacological interference through protein synthesis inhibitor drugs is the most common and inexpensive method of achieving protein synthesis inhibition for subsequent use in methods for measuring rates of protein degradation (Alvarez-Castelao et al., 2012). In Chapter 2, four protein synthesis inhibitor drugs were deemed individually unsuitable for assessing protein degradation due to overt cytotoxicity. However, it is known that drug combinations that exhibit similar effects can sometimes produce synergy and any inhibitor combination that was able to produce improved protein synthesis inhibition and reduced cytotoxicity was worth investigating. The aim of this chapter was to assess the utility of multiple inhibitor drugs at all possible combinations from the four selected protein synthesis inhibitor drugs used in Chapter 2. Ideally, a drug combination that provided synergy for protein synthesis inhibition and antagonism for cytotoxicity would be the most suitable for subsequent use in quantifying CYP protein degradation rate. However, even through rigorous investigation of all possible combinations, no inhibitor combination was able to generate sufficient protein synthesis inhibition in the absence of cytotoxicity. This study supports the previously reported concerns over pharmacological inhibitors being too disruptive to normal cellular function to measure natural rates of protein turnover (Yewdell et al. 2011; Eden et al. 2011).

Protein synthesis inhibitor drugs bring about inhibition of universal protein synthesis by inhibiting fundamental protein transcription and translation machinery; it is therefore unsurprising that such drugs are cytotoxic as proteins vital for cell survival will also be affected in prolonged inhibition. MTT assays were the only method used to derive CC_{50} across the four individual protein synthesis inhibitor drugs in Chapter 2. Since MTT assays specifically assess the formazan production

pathway as a measure of cellular mitochondrial damage (Berridge & Tan 1993), other forms of cytotoxicity assays including CellTiter-Glo®, GSH-Glo™ and trypan blue exclusion, which assess other mechanisms of cytotoxicity, were carried out to validate the findings. The CellTiter-Glo® luminescent cell viability assay is a form of ATP-assay, where ATP present in viable cells convert luciferin substrate into luciferase that emits light photons. The intensity of light photons emitted, measured as a luminescent signal, is an indicator of cell viability as only viable cells are able to produce ATP (Posimo et al. 2014; Riss et al. 2004). The GSH-Glo™ glutathione assay is another commercially available assay based on the detection of glutathione (GSH) levels as a measure of oxidative stress, potentially leading to cell death. Luciferin derivative is converted to luciferin in the presence of GSH and GST and the luciferin is then converted to luciferase in the presence of ATP and O_2 and light is generated. The luminescent signal detected is directly proportional to the amount of GSH present and this is an indicator of cytotoxicity (Promega). The Trypan Blue exclusion test of cell viability measures viable cells through principles of dye exclusion. Live cells with intact cell membranes do not take up Trypan Blue dye whereas dead cells with permeable membrane stain blue. By calculating the proportion of dead stained cells in a total cell count, the amount of viable cells in a sample can be calculated (Strober 2001). Each of the cytotoxicity assays measure a specific indicator of cytotoxicity however, the assays alone may not definitively show cell death therefore a range of toxicity assays were utilised for the same concentrations in the same cell type to confirm the robustness of the assays individually as a measure of cell death.

Good agreement across cytotoxicity assays in response to most three and four-drug combinations were observed, with the exception of puromycin, cycloheximide and emetine in which higher cellular toxicity was detected in MTT than other assays.

The GSH-Glo™ assay generally derived higher cell viability across the different drug combinations; this is perhaps due to GSH being a measure of oxidative stress, which is a surrogate indicator of cell death and GSH may not be fully depleted even as cells die via a different mechanism. It should be noted that GSH-Glo™ assays alone could not be used to predict the CC_{50} because they were in disagreement with the other assays that clearly demonstrated cytotoxicity. Interestingly, all three and four-drug combinations involving actinomycin D showed significant cytotoxicity across all viability assays which is consistent with the synergy in cytotoxicity observed in all two-drug combinations involving this drug. Therefore, actinomycin D was clearly the most cytotoxic of the four drugs in HepG2 cells. In this study, cell viability was determined through several different cytotoxicity assays that utilise different mechanisms and indicators of cell death. The reasonably good agreement across assays confirmed that MTT was a robust method of measuring of cell viability in chapter 2.

No two-drug combinations, even at ratios that appeared to be synergistic for protein synthesis inhibition and antagonistic for cytotoxicity, were suitable for use in protein degradation analysis. This highlights a need for caution when interpreting data from isobolograms because on closer inspection of such seemingly suitable combinations the CC_{50} at these ratios were still less than corresponding IC_{50}, which means that the combinations were still more potent in generating toxicity than protein synthesis inhibition. It is important to compare the source data rather than drawing conclusions based upon the interaction. The requirements and limitations of using isobolograms for assessing drug combinations have been discussed in detail by several sources (Tallarida 2006; Li et al. 2011; Chou 2010; Foucquier & Guedj 2015; Zhou et al. 2016; Matthews et al. 2017). Isobolograms do not provide the exact extent

of synergy nor statistical differentiation and their effective use is limited by inconsistencies in mathematical definitions of additive, syngergistic and antagonistic interactions.

For all drug combinations, the data suggest that inhibiting mechanisms of protein synthesis by pharmacological interference (even with lower concentration combinations) is not a physiologically appropriate method of measuring k_{deg} because all protein systems, including those essential for cell survival are likely to be affected. Furthermore, several studies have shown that cycloheximide causes disruption to protein degradation machinery affecting both lysosomal (Thoene et al. 1985) and UPD (Hanna et al. 2003; Dai et al. 2013) protein degradation pathways. Other protein synthesis inhibitors including emetine and puromycin have also been reported to impact on lysosomal degradation (Thoene et al 1985). Guzelian and Barwick suggested that cycloheximide directly inhibits CYP degradation machinery in PRH (Guzelian & Barwick 1979). In support of this, Tokunaga et al. found that cycloheximide and puromycin suppressed ERAD (discussed in Chapter 1) in baby hamster kidney cells (Tokunaga et al. 2003). ERAD is a recognised pathway of CYP protein degradation therefore these inhibitors are particularly unsuitable for use in measuring CYP k_{deg} as they will likely affect normal CYP turnover.

Consistent with Chapter 2, 72 h was selected to be the incubation time point due to the likelihood of CYP $t_{1/2}$ fitting within this time course (Yang et al 2008) and indeed other studies have conducted cell incubations with cycloheximide beyond 72 h (Chen & Madura 2008). Clearly, 72 h incubation with protein synthesis inhibitors was too long as demonstrated by the overt cytotoxicity detected for all combinations. However, it may be possible to use synergistic combinations for protein synthesis inhibitors on a shorter time frame for measuring degradation of proteins with a shorter

$t_{1/2}$ but further optimisation would be needed to define a cut-off point. A potential limitation of this study is that protein binding was not assessed. However, it should be recognised that protein binding would be expected to impact both cytotoxicity and protein synthesis inhibition by impacting free-drug concentration. In taking protein binding into account, lower concentrations for potency would be anticipated but the ratio would not be expected to be different.

There have been recent reports of protein synthesis inhibitors actively inducing a range of protein mRNA production that also impact accuracies for calculating protein degradation rates downstream (Chen & Feigelson 1979; Hattori & Gross 1995; Schuetz et al. 1995; Stordeur et al. 1995). Furthermore, Joiakim et al. (2004) reported superinduction of CYP1A1 mRNA in MCF10A cell line cultures in response to multiple protein synthesis inhibitors including cycloheximide, anisomycin and puromycin; further supporting the notion that these inhibitor drugs are unsuitable especially for use in measuring CYP degradation. Taken collectively with the data presented in this chapter, the use of protein synthesis inhibitors for CYP enzyme k_{deg} estimation is not recommended. As such, further work with these inhibitors was not conducted.

Despite the wide-ranging importance of protein degradation, there has been no single recognised method for its measurement. However, the use of protein synthesis inhibitors, whether alone or in combination, should be avoided particularly for medium and long $t_{1/2}$ proteins. Protein synthesis inhibitor drugs not only impact on essential cell survival proteins but are also known to induce mRNA of several different genes and affect protein degradation machinery, which would in turn dramatically impact any protein degradation rate derived downstream. The more recent methods of measuring rates of degradation focus on high-throughput

approaches aiming to quantify many different proteins in parallel; these involve metabolic labelling of proteins of interest followed by MS analysis (Doherty & Beynon 2006; Yewdell et al. 2011). Newly developed quantitative proteomic methods provide an important alternative to chemical inhibition, but reproducibility across different experiments and the impact of protein labelling on endogenous protein degradation warrants full investigation.

CHAPTER 4

Using mRNA suppression to estimate CYP3A4 degradation rate constant in primary human hepatocytes

CONTENTS

3.4 Discussion

4.1 Introduction

CYP enzymes are important DMEs indicated in many clinically-relevant DDIs. Any alterations to their activity through induction, inactivation or inhibition can manifest as changes in PK profiles of the victim substrate drug(s) (Tanaka 1998; Chu et al. 2009). DDIs can cause an increase or decrease of exposure and thus a change in therapeutic effect and/or increased potential for adverse effects. Approaches to assessing DDI potential for a new drug candidate have traditionally been conducted *in vitro* using animal and human samples, which require the translation to the human *in vivo* situation. Where preclinical studies indicate DDI liability, DDI studies have also been carried out *in vivo* in humans by measuring PK profiles in clinical trials, but these studies invoke huge costs and require ethical approval (Kuhlmann & Mück 2001). Increasingly, regulators have advocated the use of *in silico* approaches to DDI prediction as an alternative or alongside clinical studies (Yeo et al. 2013; Zhao et al. 2012; Leong et al. 2012). Such methods include PBPK modelling which integrates physiological system-specific parameters with drug-specific parameters derived from *in vitro* and *in vivo* experiments. Once the model has been adequately verified and deemed 'fit-for-purpose', the impact of intrinsic and extrinsic sources of variability in PK can be predicted, including DDIs (Einolf 2007; Rostami-Hodjegan 2012).

At the kinetic level, CYP protein abundance at steady-state comprises of a continuous turnover of proteins that balance *de novo* synthesis at zero-order and degradation at first-order (Belle et al. 2006). However, many endogenous factors such as drugs, hormones and foods can induce or inhibit CYP expression (Zanger & Schwab 2013), thus disrupting the steady-state abundance and accordingly, the time required to return to steady-state is partially dependent on its rate of degradation (Yang et al 2008). As previously mentioned, the enzyme P450 degradation rate

constant, k_{deg}, is an important system parameter that gives rise to the timescale of interactions, which is required for predicting time-dependent DDIs such as those arising from MBI and induction of enzymes (Yang et al 2008).

Owing to the challenges with methodology and sample size there is a lack of consensus on CYP turnover half-lives, which places a significant limitation on the accurate prediction of changes in drug concentration-time profiles associated with interactions involving enzyme MBI and/or induction (Almond et al. 2009). Consequently, there is a paucity of reported k_{deg} values for many of the CYP enzymes that are involved in clinically relevant DDIs. As such, inaccurate k_{deg} continues to be a source of error in metabolic time-dependent DDIs and several sources have documented the importance of accurate k_{deg} values in facilitating accurate predictions of DDI magnitudes (Houston & Galetin 2010; Lutz et al. 2013; Almond et al. 2009).

The measurement of k_{deg} values should ideally be achieved by specific labelling of enzymes in humans *in vivo*, but this direct method has proven to be understandably difficult and surrogate k_{deg} values derived from *in vitro* approaches are needed. As discussed previously in Chapter 1, CYP3A4 is involved in the metabolism of around 50% of all marketed drugs and due to this wide specificity; the enzyme has been most widely implicated in DDIs. Examples of inhibitors, inducer and substrates of CYP3A4 are given in Table 1.1 and classic examples drug that cause clinically-significant CYP3A4 TDIs include diltiazem, verapamil, erythromycin and troleandomycin (Grimm et al. 2009; Chen et al. 2011). As such, CYP3A4 has been the most extensively studied of all CYP enzymes with the reported half-life values ranging from 10 to 140 hours (Yang et al. 2008). These half-life values were derived by a plethora of different *in vivo* and *in vitro* methods.

The three main *in vitro* approaches include: (i) measuring CYP apoprotein expression loss in liver models without treatment over time (Maurel 1996; Renwick et al. 2000), (ii) induction of CYP enzymes followed by tracking of de-induction and recovery profiles (Maurel 1996; Dixit et al. 2016) and (iii) Pulse-chase analysis after de-induction (Pichard et al. 1992). Many *in vitro* studies have shown that CYP apoprotein and enzyme levels decline differentially over time in culture (Guillouzo et al. 1985; Paine 1990; Morel et al. 1990) thus, enzyme degradation rates can be derived from tracking the loss of expression assuming that the changes are caused solely by endogenous enzyme degradation mechanisms. However, this method is limited by the assumption that there is no *de novo* enzyme synthesis and that the decline in cell viability does not contribute to the enzyme expression loss observed.

In the second aforementioned approach, enzyme turnover is estimated from measuring the increased level of activity instigated by incubation of liver with multiple doses of a known inducer compound to reach a maximally induced new steady-state, then removing the inducer and measuring the time taken to return to the basal non-induced enzyme level using probe substrates. The main caveats to this approach include, again, the assumption that there is no *de novo* CYP protein synthesis and the interindividual variability in the inducibility of CYP enzymes between donor livers.

The pulse-chase method is frequently used to predict turnover and half-life of various proteins (Belle et al. 2006; Montgomery et al. 2003; Boisvert et al. 2012) and typically the protein of interest is labelled with a radioactive amino acid precursor during pre-incubation followed by a chase period where an excess of non-radioactive amino acid is added to the culture to prevent further incorporation of radiolabelled precursor amino acid. Cells are then harvested and the radioactivity determined over

several time points to measure rate of protein disappearance to determine half-life (Zhou 2004; Jansens & Braakman 2003). This technique is limited by the potential of isotope labelling distorting normal CYP degradation mechanisms thereby producing an inaccurate degradation rate constant value.

Another simple kinetic approach circumventing the problem of radiolabelling the protein of interest, involves inhibiting *de novo* protein synthesis by treatment with pharmacological inhibitors, followed by the quantification of changes in protein content over time by immunoblotting (Alvarez-Castelao et al., 2012; Dai et al., 2013). However as deduced in Chapters 2 and 3, the use of pharmacological inhibitors should be avoided due to their cytotoxic effects precluding the propensity for protein synthesis inhibition (Chan et al. 2017). More recently, based on the principle of inhibiting *de novo* protein synthesis, Ramsden et al. (2015) utilised RNA interference (RNAi) and interleukin-6 (IL-6) to specifically knockdown CYP3A4 gene expression *in vitro* in the HepatoPac model, followed by tracking its degradation and recovery profile to estimate k_{deg}.

siRNAs are short 20-30 nt (nucleotide) sequences of non-coding RNA that regulate the genome mainly through inhibitory effects by silencing the translation of the regulated parts of the genome via the RNAi pathway (Carthew & Sontheimer 2009). The mechanism of siRNA gene silencing is depicted in Figure 4.1. In eukaryotic cells the RNase-III-type enzyme Dicer cleaves long double-stranded siRNA into short 21-26 nt siRNA duplexes. Components of the RNAi machinery then recognise the siRNA duplex and incorporate a single strand of siRNA into the RNA-induced silencing complex (RISC). The argonaute 2 protein within RISC unwinds the siRNA and cleaves off the passenger or sense strand. The activated RISC complex containing the antisense siRNA strand binds and cleaves mRNA at the site that

contains the complementary sequences to the single antisense strand, therefore inhibiting subsequent gene translation (Dorsett & Tuschl 2004; Whitehead et al. 2009). The activated RISC complex continues to destroy more mRNA targets, further propagating the gene-silencing response. siRNA occurs endogenously within cells as a mechanism of genetic regulation but it can also be synthetically produced and introduced experimentally via transfection vectors, circumventing the Dicer process (Whitehead et al 2009). Increasingly, siRNA has been exploited *in vitro*, enabling the knockdown of genes to analyse specific gene functions. RNAi has also been used as a therapeutic approach in the treatment of diseases including cancer and autoimmune disorders (Aagaard & Rossi 2007; Wittrup & Lieberman 2015). For DME k_{deg} investigations, it was hypothesised that by introducing target gene-specific siRNA, the translation of target protein is specifically silenced without impacting on regular cellular survival and protein degradation mechanisms. This circumvents the previously encountered problems of cytotoxicity and *de novo* protein synthesis during analysis of degradation rates.

Based on the findings from Ramsden et al. (2015), the aim of this Chapter was to investigate the utility of CYP3A4-specific siRNA, as an alternative *in vitro* approach to protein synthesis inhibitors, for suppressing synthesis of CYP3A4 mRNA and protein. CYP3A4 k_{deg} was derived by tracking activity and protein expression loss over time in cryopreserved primary human hepatocytes.

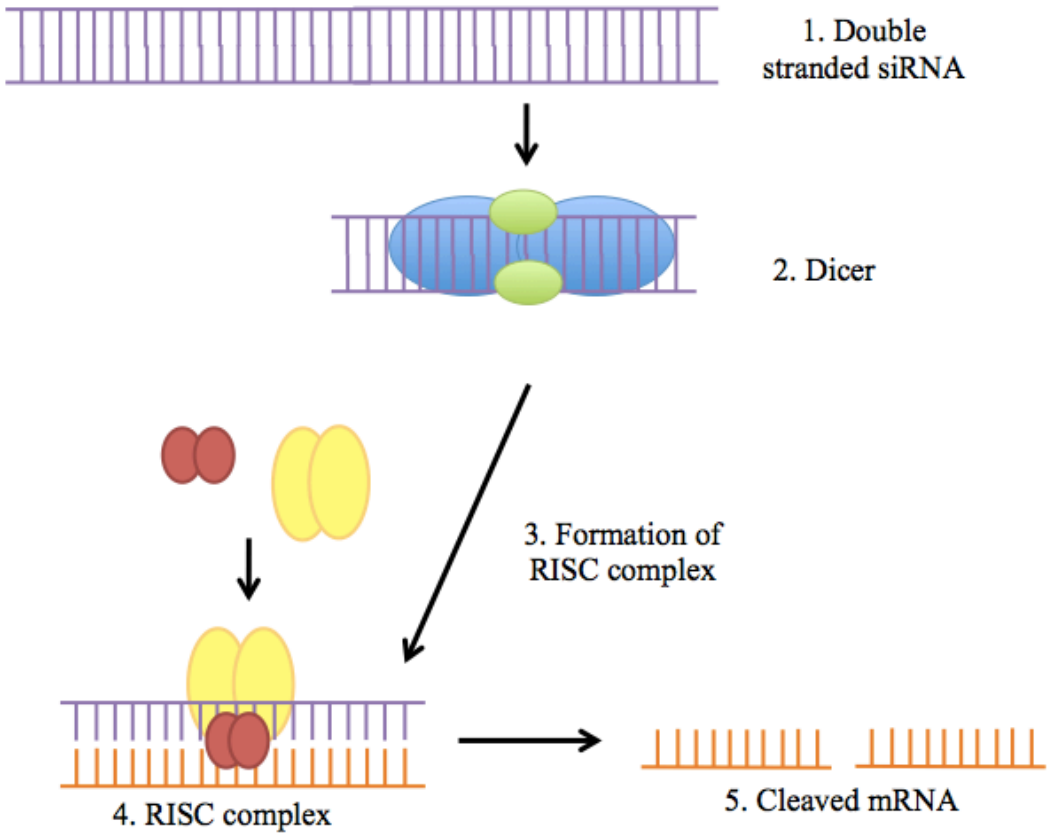

Figure 4.1 Mechanism of siRNA gene silencing. Adapted from Dorsett et al (2004).

4.2 Materials and methods

4.2.1 Materials

Plateable cryopreserved primary human hepatocytes (HMCPIS Lot. Hu1591, Hu1824 and Hu8241), CHRM® media, William's E media, thawing and plating supplements (CM3000), maintenance supplements (CM4000), 24-well collagen I coated plates and opti-MEM® I media were purchased from Invitrogen Ltd (Paisley, UK). TaqMan® reverse transcription reagents, TaqMan® gene expression assays for CYP3A4 (Hs00604506_m1), glyceraldehyde 3-phosphate dehydrogenase (GAPDH; Hs02758991_g1) and hypoxanthine-guanine phosphoribosyltransferase 1 (HPRT1; Hs02800695_m1), TaqMan® gene expression master mix, PrestoBlue® cell viability reagent, CYP3A4 (P2377) and control (P2315) BACULOSOMES® plus reagent, Lipofectamine® RNAiMAX reagent, NuPAGE® Western blot materials and TRIzol® reagent were purchased from ThermoFisher Scientific Inc. (Loughborough, UK). ON-TARGETplus human CYP3A4 SMARTpool, GAPD control pool and non-targeting pool siRNA were purchased from GE Healthcare Dharmacon™ (UK). Western blot primary and secondary antibodies: anti-CYP3A4 (ab3572), anti-beta actin (ab6276), anti-GAPDH (ab181602), goat polyclonal anti-mouse IgG1 (ab97240) and goat polyclonal to rabbit IgG (ab97080) were purchased from Abcam (Cambridge, UK). Luminata™ Forte Western HRP substrate was bought from Millipore (Watford, UK). TWEEN®20, Bradford Reagent, urea solution, CelLytic™ M, protease inhibitor cocktail, 1'-hydroxymidazolam, RNase-free water and other Western blot buffer ingredients were purchased from Sigma-Aldrich (Dorset, UK). Midazolam hydrochloride was purchased from Tocris (Bristol, UK).

4.2.2 Cryopreserved primary human hepatocyte culture

4.2.2.1 Cell thawing

Cryopreserved primary human hepatocytes were thawed in a 37 °C water bath for approximately 2 min until contents were around 90% thawed. Once thawed, the hepatocytes were added to 50 ml of pre-warmed plating media (William's E media without phenol red supplemented with 5% FBS, 1 μM dexamethasone, 1% solution of penicillin/streptomycin, 4 μg/ml Bovine insulin, 2 mM GlutaMAX™ and 15mM HEPES; CHRM® supplement A) and centrifuged for 10 min at 100 x g at 18^{o}C and the supernatant fraction discarded. The hepatocytes were then resuspended at approximately 1 x 10^6 cells per ml density in plating media, which was prepared as Williams E media without phenol red supplemented with 1μM dexamethasone, 1% solution of penicillin-streptomycin, 4 μg/ml insulin, 5% FBS, 2 mM GlutaMAX™ and 15 mM HEPES (CM3000, supplement A). The donor demographics are given in Table 4.1.

4.2.2.2 Cell counting and plating

The cell viability and count were determined as described in 2.2.4. Primary human hepatocytes were seeded at 500 μl per well on 24-well collagen-I coated plates at a density of 3 x 10^5 viable cells/well for CYP3A4 metabolism activity and protein expression analyses. Cells were incubated with plating media for 5 hours at 37°C with 5% CO_2 and 95% humidity to allow cell adherence prior to siRNA transfection. After 5 hours of incubation, the plating media was replaced with maintenance media (William's E media supplemented with 0.1 μM dexamethasone, 0.5% penicillin/streptomycin 6.25 μg/ml human recombinant insulin, 6.25 μg/ml human transferrin, 6.25 ng/ml selenous acid, 1.25 mg/ml BSA, 5.35 μg/ml linoleic acid, 2nM GlutaMAX™ and 15 mM HEPES) for untreated control or dosed with varying siRNA

conditions in optiMEM® I reduced serum media. Following siRNA transfection, maintenance media was replaced every 24 hours. The use of Geltrex™ matrix overlay is generally recommended for primary hepatocytes to maintain phenotype during culture. However, after private correspondence with authors of the publication by Vozza-Brown et al. they advised against the use of Geltrex™ as it was found that the matrix interfered with siRNA delivery, consequently Geltrex™ was not used in conjunction with siRNA experiments.

Table 4.1 Donor demographics of the cryopreserved primary human hepatocytes

Demographics	Donor 1	Donor 2	Donor 3
Donor ID	Hu1591	Hu1824	Hu8241
Age	29	66	60
Gender	Male	Female	Male
Ethnicity	Caucasian	Caucasian	Caucasian
Characteristics	Rare alcohol user. No tobacco or drug use reported	Tobacco use. No alcohol or drug use	Tobacco and alcohol user. No drug use
Cause of death	Not reported	Not reported	Cardiac related
Cell viability	91%	93%	94%

4.2.3 Small-interfering RNA (siRNA) treatment

CYP3A4 siRNA experiments were conducted by modification of the knockdown protocol published by Vozza-brown et al. (2005). 5X siRNA buffer (300 mM KCl, 30 mM HEPES-pH 7.5, 1.0 mM $MgCl_2$) was prepared and diluted to 1X concentration with RNAse-free water. siRNA was stored at 10 μM stock concentration in 1X siRNA buffer at -20°C until use.

After 5 hours incubation with hepatocyte plating media, cells were washed and treated with Dharmacon ON-TARGETplus human CYP3A4 SMARTpool

siRNA. Positive ON-TARGETplus GAPD human control pool and negative control ON-TARGETplus non-targeting pool were also included. The sequences of the siRNA used are shown in Table 4.2. 1.25 µl of transfection reagent Lipofectamine RNAiMAX™ was complexed with ON-TARGETplus siRNA in reduced serum opti-MEM® I media for 30 minutes prior to addition to cell culture. Hepatocytes were exposed to the siRNA overnight for 15 hours before the cells were washed and media replaced with standard hepatocyte maintenance media. Cells were subsequently incubated at 37°C with 5% CO_2 and 95% humidity for a range of time post CYP3A4 siRNA treatment. CYP3A4 metabolic activity, mRNA and protein expression were assessed at specific time points. Time 0 hours was taken at 5 hours incubation with plating media, prior to siRNA transfection and maintenance media replacement.

Table 4.2 siRNA sequences.

siRNA	Sequence
ON-TARGETplus human CYP3A4 SMARTpool	5'-CAUCCCAAUUCUUGAAGUA-3' 5'-GUGGAAAACUCAAGGAGAU-3' 5'-GAACUGAAGCUCUUAUUAU-3' 5'-CCAACUGUCUCGAUGCAAU-3'
ON-TARGETplus human GAPD control pool	5'-GUCAACGGAUUUGGUCGUA-3' 5'-CAACGGAUUUGGUCGUAUU-3' 5'-GACCUCAACUACAUGGUUU-3' 5'-UGGUUUACAUGUUCCAAUA-3'
ON-TARGETplus Non-targeting pool	5'-UGGUUUACAUGUCGACUAA-3' 5'-UGGUUUACAUGUUGUGUGA-3' 5'-UGGUUUACAUGUUUUCUGA-3' 5'-UGGUUUACAUGUUUUCCUA-3'

4.2.4 Cytotoxicity determined by PrestoBlue™ cell viability reagent

PrestoBlue™ reagent is a resazurin-based cell viability assay that is able to monitor live cells not requiring lysis at the final stage of analysis and therefore, appropriate for detecting cytotoxicity caused by siRNA and transfection reagent in primary human hepatocytes following knockdown. Due to the expense of primary human hepatocytes, PrestoBlue™ assay optimisation was initially conducted in HepG2 cells because they displayed concentration-dependent toxicity in Chapter 2 in response to actinomycin D.

4.2.4.1. Optimisation of PrestoBlue™ assay in HepG2 cells

HepG2 cell line was maintained and plated as described in 2.2.2 and 2.2.4, respectively. Cells were seeded at $3x10^5$ per well on 24-well culture plates and incubated with 0.0001-10 μM actinomycin D dissolved in cell line maintenance media. Drug dissolution vehicle and cells with no drug treatment were included as controls. The assay was carried out in triplicates. HepG2 cells were incubated with varying concentrations of actinomycin D at 37°C with 5% CO_2 and 95% humidity for 72 hours, with media replaced every 24 hours. At the end of incubation, 50 μl of 10X PrestoBlue™ reagent was directly added to each well and fluorescence was read at 10 min intervals for 80 min with excitation at 560 nm and 590 nm emission on a CLARIOstar® microplate reader (BMG LABTECH, Aylesbury, UK). Final readings were taken at a time point before signal saturation and normalised against background fluorescence.

4.2.4.2. Determination of siRNA and transfection reagent inflicted cytotoxicity

Following siRNA treatment and cell incubation to a designated time point, 50 μl of 10X PrestoBlue™ reagent was directly added to each well. Media only with no cells,

cells incubated with transfection reagent and cells with no treatment were included as controls. Fluorescence was read with excitation at 560 nm and 590 nm emission at 10 min intervals for 60 min on a CLARIOstar® microplate reader (BMG LABTECH, Aylesbury, UK). Final readings were taken at a time point before signal saturation and normalised against background fluorescence. The media containing PrestoBlue™ reagent was washed off the cells 3 times with HBSS prior to proceeding with further experimental procedures.

4.2.5 CYP3A4 mRNA knockdown quantification

The magnitude of siRNA knockdown was determined by quantifying gene expression by reverse-transcription polymerase chain reaction (RT-PCR) following a designated time of incubation.

4.2.5.1 Total mRNA isolation

After siRNA treatment and incubation, total RNA isolation was carried out using the standard TRIzol® reagent extraction protocol by Ambion/Life Technologies. Media was discarded and hepatocytes were treated with 1 ml TRIzol® reagent and homogenised for 5 min at RT. The cell lysates were transferred to 1.5 ml centrifuge tubes and samples were vortexed with chloroform at 0.2 ml per 1 ml of TRIzol® and incubated for 2 min at 30°C before centrifugation at 13,200 x g for 15 min at 4°C. The aqueous phase of the samples were transferred into new centrifuge tubes. 0.5 ml per 1ml TRIzol® of 100% isopropanol was added and incubated for 10 min at RT before centrifugation at 12,000 x g for 10 min at 4°C. The supernatant fraction was then removed leaving the mRNA pellet that was washed with 1 ml of 75% ethanol per 1 ml of TRIzol® used. The samples were vortexed with 75% ethanol then centrifuged at 7500 x g for 5 min at 4°C. The supernatant fraction was then discarded and mRNA

pellet left to dry. The mRNA pellet was resuspended in 30 µl RNase-free water and incubated on a heat block at 60°C for 15 min. The isolated mRNA was stored at -80°C until analysis. Total mRNA was quantified by NanoDrop™ 1000 spectrophotometer with an average purity ($A_{260/280}$) of >1.80.

4.2.5.2 cDNA synthesis

Complementary DNA (cDNA) synthesis was performed using Taqman® reverse transcription kit. 2 µg of total mRNA was reverse transcribed with 3 µl 10X Taqman® RT buffer, 1.75 mM $MgCl_2$, 0.5 mM dNTP mix, 1.0 U/µl RNase inhibitor, 2.5 U/µl MultiScribe™, 2.5 µM random hexamers and reaction mixes were made up to 50 µl per sample with RNase-free water. cDNA amplification was performed in a GeneAmp® PCR 9700 thermocycler (Applied Biosystems, UK) with cycling conditions of 25°C for 10 min, 37°C for 30 min and 95°C for 5 min. The cDNA samples were kept at 4°C overnight for analysis the following day. Total cDNA was quantified by NanoDrop™ 1000 spectrophotometer with an average purity ($A_{260/280}$) of >1.80, then diluted to produce a working stock of 5 ng/µl.

4.2.5.3 Gene amplification by RT-PCR

Real-time PCR (qPCR) were developed for quantification relative to HPRT1, housekeeping gene; assays were conducted according to Taqman® gene expression protocol. All samples were completed in quadruplicate. A 25 µl reaction mix consisting of 1.25 µl of 20X Taqman® custom gene CYP3A4 (assay ID, Hs00604506_m1), GAPDH (Hs02758991_g1) or HPRT1 (Hs02800695_m1) assay, 40 ng cDNA in 8 µl, 3.25 µl RNase free water and 12.5 µl of 2X Taqman® Master Mix were dispensed into a 96-well plate. Negative controls where RNase-free water was added in place of cDNA was included. The plates were then covered with Microseal® adhesive PCR plate sealing film and centrifuged briefly up to 2000 rpm

to mix the reaction contents to eliminate air bubbles from the solution mix. PCR conditions were run at 95°C for 10 min, followed by 40 cycles of 95°C for 15 s and 60°C for 1 min.

4.2.5.4 Calculating relative expression

Relative CYP3A4 and GAPDH mRNA expression against housekeeping gene HPRT1 were performed in an Opticon2™ Fluorescence Detector (MJ Research, UK). The cycle threshold [C(t)] was set to ignore any aberrant fluorescence to ensure that only gene amplification was measured. Data was normalised to the primary hepatocyte vehicle control or untreated control sample collected at time 0 (T0) and relative expression was derived using two methods: the comparative C(t) method given by the following equation,

$$C_t = 2^{-\Delta\Delta C_{(t)}}$$

or the Pfaffl method (Pfaffl 2001), given by the following equation:

$$\text{Relative expression ratio} = \frac{(\mathrm{E_{target}})^{\Delta \mathrm{CP_{target}}(\text{control}-\text{sample})}}{(\mathrm{E}_{ref})^{\Delta \mathrm{CP_{ref}}(\text{control}-\text{sample})}}$$

Where E_{target} is the qPCR efficiency from target gene; E_{ref} is qPCR efficiency of reference gene; ΔCP_{target} is the deviation of control-sample of target gene to test sample and ΔCP_{ref} is the deviation of control-sample of reference gene to test sample.

4.2.6 CYP3A4 protein quantification

4.2.6.1 Protein extraction

Two different established methods of protein extraction were carried out to determine a suitable method for maximum extraction of proteins.

(i) Modified TRIzol® protein extraction method

The efficiency of protein extraction by TRIzol® reagent using the method published by Ambion/LifeTechnologies is known to be limited by problems of protein

resolubilisation (Hummon et al. 2007). Therefore, a modified version with improved resolubilisation was conducted as detailed in a publication by Simões et al. (2013).

Following phase separation and removal of the aqueous phase containing mRNA as detailed in 4.2.5.1, protein separation and isolation were conducted as follows: 300 µl of 100% ethanol was added to tube containing the interphase and phenol-chloroform phase. The tube was mixed by inversion then incubated for 2-3 min at RT before centrifugation at 2000 x g for 5 min at 4°C to pellet the DNA. The phenol-ethanol supernatant layer containing protein was transferred into a new centrifuge tube. 1.5 ml of 100% isopropanol was then added and samples incubated for 10 min RT. The samples were then centrifuged at 12,000 x g for 15 min at 4°C to pellet the protein. The supernatant was discarded and washed 3 times with 2 ml 0.3 M guanidine hydrochloride in 95% ethanol with 20 min incubation at RT between washes. The samples were then centrifuged at 7,500 x g for 5 min at 4°C. 2 ml of 100% ethanol was then added, vortexed and left to incubate for 20 min RT. Samples were centrifuged at 7,500 x g for 5 min at 4°C and ethanol wash supernatant discarded. 1.5 ml of 1:1 solution of 8 M urea (in Tris-Hcl 1 M, pH 8.0) and 1% sodium dodecyl sulphate (SDS) was added to the cell pellet and vortexed to resuspend pellet in solution. The solution was then sonicated for 5 cycles of 15 s and placed on ice for 30 s to solubilise the protein. The mixture was then centrifuged at 3,200 x g for 10 min at 4°C to sediment any insoluble material. The supernatant containing the dissolved protein was transferred to a new centrifuge tube and stored at -80°C until analysis.

(ii) CelLytic™ M protein extraction method

CelLytic™ M protein extraction was conducted according to manufacturer's recommendations. A separate sample from which mRNA was extracted by TRIzol®

reagent was included for CelLytic™ M protein extraction. After siRNA treatment and cell incubation, media was discarded from culture dish and cells were washed four times with HBSS before removal from well by trypsinisation for 5 min at 37°C with 5% CO_2 and 95% humidity. 1 ml of cell maintenance media was added to neutralise the trypsin-EDTA solution and the cells in solution were transferred to 1.5 ml centrifuge tubes. The samples were centrifuged at 4,500 x g for 5 min at 4°C to pellet cells. The supernatant was discarded and cells were resuspended in 1 ml HBSS before further centrifugation at 2,000 x g for 5 min at 4°C to wash cells. The supernatant was then discarded. 125 µl of CelLytic™ M lysis solution and 12.5 µl protease inhibitor cocktail (which was stored on ice during use) was added to cell pellet and mixed vigorously to lyse cells. The samples were then incubated on an oscillating table for 15 min before centrifugation at 13,900 x g for 15 min at 4°C. The supernatant containing protein samples were collected and stored at -80°C until analysis.

4.2.6.2 Quantification of extracted protein by Bradford assay

Protein concentrations of the isolated samples were determined by the Bradford reagent assay according to protocol provided by Sigma-Aldrich. Bovine serum albumin (BSA) standards were prepared at 8 concentrations at two-fold dilutions in the range of 0-1.5 mg/ml in CelLytic™ M buffer with 10% protease inhibitor cocktail. Protein standards were made to 20 µl per well on a 96-flat well plate with buffer. Protein samples were added at 1, 2.5 or 5 µl in 20 µl per well CelLytic™ M buffer with 10% protease inhibitor cocktail. Conditions were performed in duplicates. 250 µl of 1X Bradford Reagent was added to each well at RT, mixed for 30 s on orbital shaker then incubated in darkness for 30 min. The absorbance of the samples were measured at 595 nm on a CLARIOstar® microplate reader (BMG LABTECH, Aylesbury, UK). Protein concentrations of the samples were determined by

comparing the net A_{560} values against the standard curve and only plates with standard curve where $R^2 \geq 0.99$ were included.

4.2.6.3 Protein quantification by Western blotting

20 µg of total protein, as determined by Bradford assay, and 0.5 µl CYP3A4 BACULOSOMES® plus reagent (positive control) was added to 5 µl of 4X NuPAGE® LDS sample buffer, 2 µl of NuPAGE® reducing agent and made up to 21 µl volume using deoinised water. Samples were heated at 100°C for 5 min. 20 µl of sample and 3 µl of Kaleidoscope™ prestained protein standard (Bio-Rad, UK) were loaded onto a NuPAGE® 4-12% Bis-Tris Gel with 200 µl NuPAGE® antioxidant and electrophoresed for 1 hour 30 min at 150 V. Following electrophoresis, the proteins were blotted onto a Amersham Protran 0.45 nitrocellulose membrane using a Criterion™ blotter method (Bio-Rad, UK) run at 30 V for 60 min.

After protein transfer, the membrane was blocked in 5% non-fat dried milk (NFDM) or BSA in 0.01% Tween-tris buffered saline (T-TBS) for 2 hours RT, washed with 0.01% T-TBS solution 3 times for 5 min, followed by incubation with primary antibody (anti-cytochrome P450 3A4, ab3572) at 1/2000 dilution in 2% NFDM or BSA in 0.01% T-TBS overnight at 4°C. The following day, the membrane was washed 3 times with 0.01% T-TBS for 5 min then incubated with secondary antibody (goat polyclonal secondary antibody to rabbit IgG, ab97080) at 1/5000 in 2% NFDM or BSA in 0.01% T-TBS for 2 hours at 4°C. For detection of loading control β-actin, the membrane was blocked with 10% NFDM or BSA in 0.01% T-TBS overnight at 4°C. The following day, membranes were washed 3 times with 0.01% T-TBS for 5 min before incubation with primary antibody (anti-β-actin antibody, ab6276) at 1/5000 in 2% NFDM or BSA in 0.01% T-TBS for 2 hours at 4°C. After primary antibody incubation, membrane was washed 3 times with 0.01%

T-TBS for 5 min before incubation with secondary antibody (goat polyclonal secondary antibody to mouse IgG1, ab97240) at 1/2000 in 2% NFDM or BSA in 0.01% T-TBS for 1 hour at 4°C. For GAPDH loading control, membranes were initially blocked with 10% BSA in 0.01% T-TBS overnight before GAPDH was probed for using primary antibody (anti-GAPDH, ab181602) at 1/10,000 for 2 hours at 4ºC and secondary antibody (ab97080) at 1/10,000 dilution incubated for 1 hour RT in 2% BSA in 0.01% T-TBS. Following incubation with secondary antibodies, membranes were washed 3 times in 0.01% T-TBS for 5 min followed by 2 times 20 min wash in 0.01% T-TBS.

Between the detection of each protein, the membrane was stripped and re-probed. After enhanced chemiluminescence (ECL) detection, membranes were washed for 5 min in 0.01% T-TBS, then 2 times 20 min with acidic glycine stripping buffer, followed by 2 times 10 min 1X Tris-buffer saline (TBS) solution and 2 times 10 min 0.01% T-TBS. The membranes were then blocked and probed for a new protein as indicated above.

Protein bands were visualised by ECL detection. Following the final wash, the membrane was blotted dry and incubated with 3 ml Luminata™ Forte Western Horseradish Peroxidase (HRP) substrate solution for 5 min. Excess substrate was drained and membrane placed under plastic wrap. Detection was carried out in the dark room where an X-ray film was placed on the blot and the film was exposed between 10-600 s for CYP3A4, β-actin and GAPDH protein band detection. The X-ray film was then placed in a developing solution for approximately 30 s for the image to appear before immersing in fixing solution for 30 s followed by water for 30 s. Quantification of protein bands were achieved using GS-800™ calibrated densitometer (Bio-Rad, Hercules, CA) and ImageJ software (NIH). Relative protein

quantification was determined by normalising CYP3A4 band against β-actin or GAPDH loading control band density.

4.2.7 Assessment of CYP3A4 activity by probe substrate turnover

Midazolam (MDZ) and 1'hydroxymidazolan were dissolved in high performance liquid chromatography (HPLC) grade 100% methanol to form a stock solution at 1 mM that was stored at -20°C until use. The probe substrate selected for CYP3A4 activity was 3.4 μM MDZ (the concentration was chosen based on recommendations from personal communications with Dr Beth Williamson) and the probe substrate compound was prepared in hepatocyte maintenance media in <0.5% methanol. In the final hour of incubation in control and siRNA-treated samples, cells were spiked with MDZ to a final concentration of 3.4 μM and incubated for 60 min at 37°C with 5% CO_2 and 95% humidity. CYP3A4 activity was measured as 1'-hydroxymidazolam metabolite formation following incubation with MDZ at 0, 48, 72 and 96 hours after CYP3A4 siRNA transfection. After 60 min incubation with MDZ, the media was removed and immediately stored at -80°C to terminate further activity until analysis. 1'-hydroxymidazolam metabolite was extracted from cell maintenance media matrix and analysed by high performance liquid chromatography-ultraviolet (HPLC-UV).

4.2.7.1 Drug extraction from media matrix

Extraction of 1'-hydroxymidazolam metabolite involved addition of acetone (5:1 v/v) to 400 μl of media sample. The samples were then mixed on a turntable for 30 min at RT followed by centrifugation at 13,000 x g for 30 min at 4°C. The metabolite-containing supernatant fraction was then removed and transferred to a glass tube. The samples were dried overnight in a Savant SpeedVac rotary evaporator (Thermo

Scientific, UK). The resulting dried compounds were reconstituted in 150 µL mobile phase A with 20% acetonitrile (ACN) v/v.

4.2.7.2 Metabolite quantification by HPLC-UV

MDZ and 1'-hydroxymidazolam were chromatographically separated and quantified by HPLC with ultraviolet detection (HPLC-UV). 100 µL of reconstituted sample was injected into a Dionex HPLC system (Thermo, UK). Two mobile phases were used for the chromatographic run and the run was conducted using a using a multi-step gradient with a reverse-phase Fortis® column (3 µM, C18, 100 x 4.6 mm; Fortis® Technologies Ltd., Neston, UK). The conditions were as follows:

Mobile phase A	80% 25 mM KH_2PO_4 in ddH_2O, 20% ACN, pH 3.14
Mobile phase B	100% ACN
Wash	50% H_2O, 50% MeOH
Internal wash reservoir	100% H_2O
Flow rate	1 $ml.min^{-1}$
Injection volume	100 µl
Run time	9.18 min
Retention time of 1'-hydroxymidazolam	4.88 min
Detection wavelength	235 nm

The gradient mobile phase run conditions are as follows:

Time (min)	Mobile phase A (%)	Mobile phase B (%)
0.0	80	20
1.0	80	20
1.1	60	40
6.0	55	45
6.1	20	80
8.0	20	80
8.1	80	20
9.0	80	20

Calibration curves were prepared with 10 concentrations including blank media with no drug and a range of 1'-hydroxymidazolam concentrations between 0.04-20 μM. A linear calibration curve with $R^2 \geq 0.999$ was required for quantification. Precision and accuracy were determined using 3 sets of quality controls (QCs; including low, 0.5 μM; medium, 3 μM and high, 10 μM) in each run, on 3 consecutive days. Accuracy was defined as the percentage deviation from the nominal concentration and precision determined by SD at each QC concentration. Average recovery of 1'-hydroxymidazolam was determined by comparing peak area of the drug extracted from 3 QCs against samples directly injected with no extraction procedure taken to be 100%. The recovery for 1'-hydroxymidazolam was calculated at >90% in all replicates.

4.2.8 CYP3A4 k_{deg} and $t_{1/2}$ calculations and statistical analyses

K_{deg} and half-life were calculated using GraphPad Prism 6 software (GraphPad Software, CA). Linear regression was used and the percentage of metabolite, fluorescence unit or normalised protein expression, relative to untreated control at each time point post siRNA treatment, was transformed by taking the natural logarithm (*Ln*). Half-life values for CYP3A4, representative of k_{deg}, were derived from the slope (*k*) of linear regression using the following equation as described in 2.1:

$$t_{\frac{1}{2}} = \frac{\ln(2)}{k}$$

Data was plotted with *Ln* percentage on the *y*-axis and incubation time (h) on the *x*-axis and k_{deg} taken from the slope (*k*). All statistical analyses were carried out using GraphPad Prism 6 software.

4.3 Results

4.3.1 Optimisation of PrestoBlue™ reagent for cell viability analysis

The PrestoBlue™ cell viability reagent detected concentration-dependent cytotoxicity in response to incubation with varying actinomycin D concentrations in HepG2 cells, as shown in Figure 4.2. and the CC_{50} was 0.0009 μM. This is consistent with the findings in Chapter 2 and therefore confirms the utility of PrestoBlue™ reagent for detecting live cell cytotoxicity. PrestoBlue™ reagent was subsequently used to determine cytotoxicity for the optimisation of siRNA experiments.

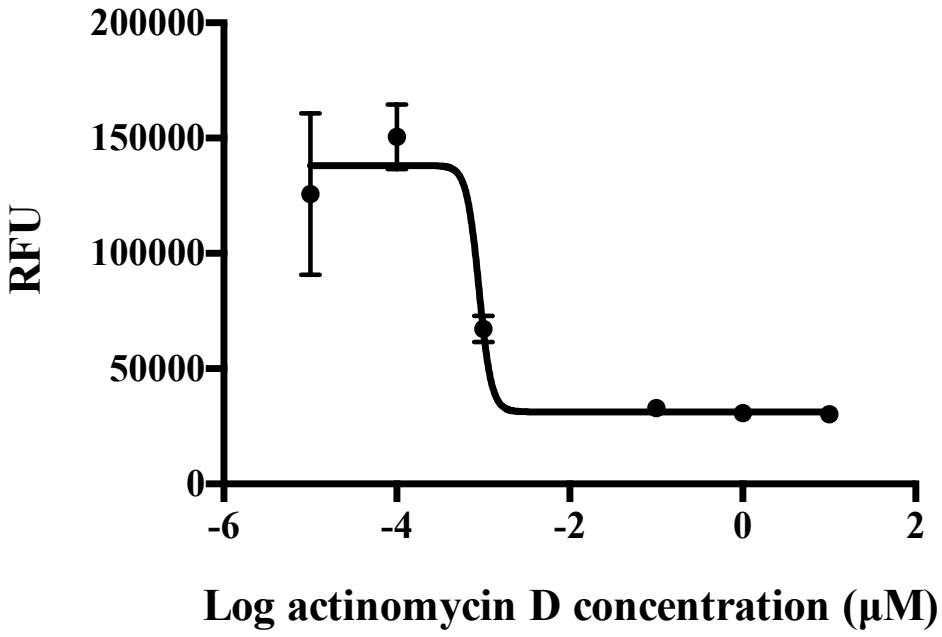

Figure 4.2. HepG2 cytotoxicity in response to actinomycin D dose. HepG2 cells were incubated with varying concentrations of actinomycin D for 72 hours to confirm utility of PrestoBlue™ assay for determination of cytotoxicity. Fluorescence reading shown was taken at 10 min incubation with PrestoBlue™ reagent. Data shown as mean ±SD of 3 replicates from N=1 experiment.

4.3.2 Optimisation of mRNA knockdown time-course and siRNA dosage

Primary human hepatocytes were initially treated with 50 or 100 nM concentrations of siRNA and incubated for 24, 48 and 72 h to determine the achievable level of mRNA knockdown after a single siRNA dose. Figure 4.3 shows that over 50% CYP3A4 knockdown was achieved at 48 h with both 50 and 100 nM siRNA. GAPDH mRNA expression was also successfully reduced by GAPD-targeting siRNA. CYP3A4 expression in non-targeting control (NTC) samples remained high as expected. No statistically significant mRNA knockdown was achieved in untreated, optiMEM and NTC control conditions compared with the corresponding vehicle control and therefore confirms the validity and specificity of CYP3A4 siRNA for target gene knockdown experiments.

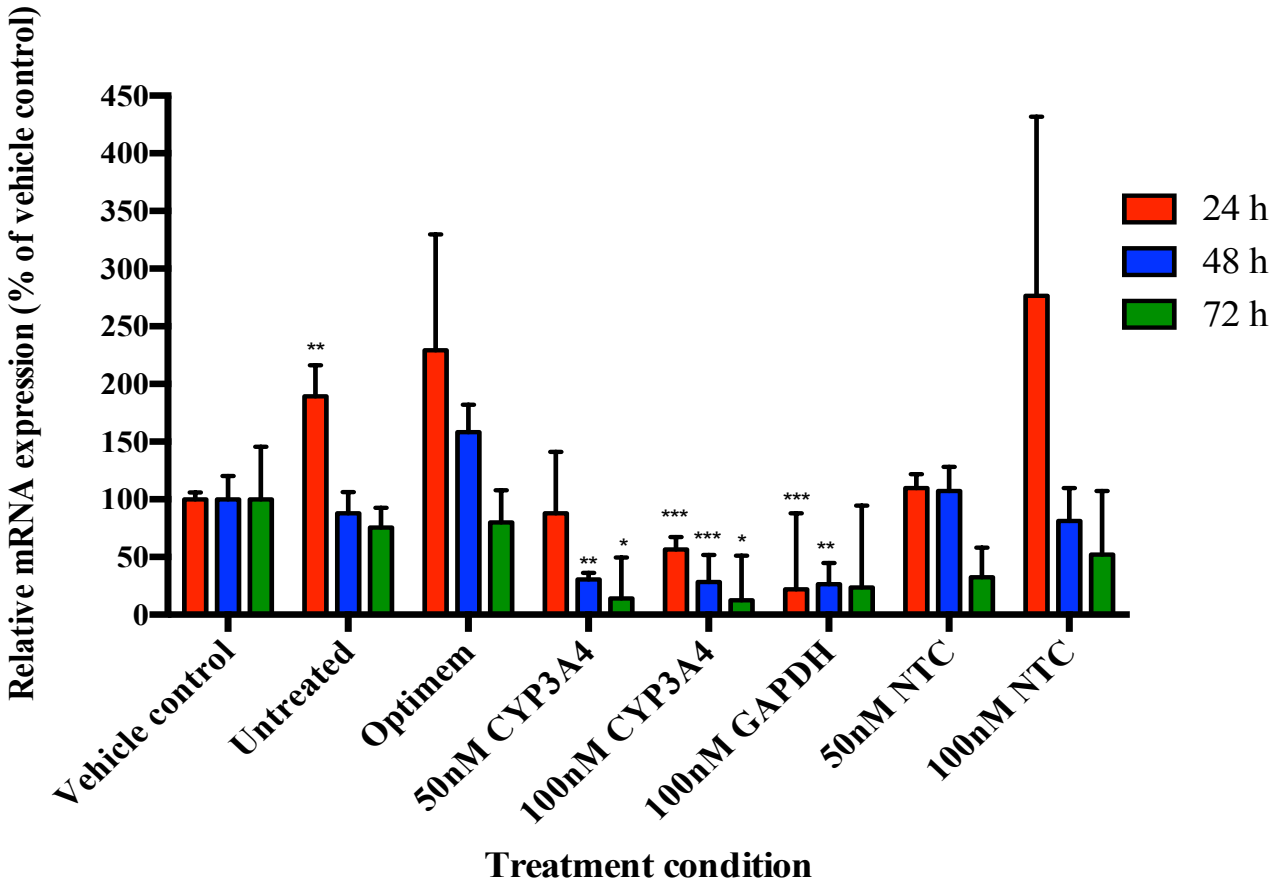

Figure 4.3 Relative mRNA knockdown following siRNA treatment and 24-72 h incubation in primary human hepatocytes (Hu1591). CYP3A4 and NTC siRNA treatment corresponds with CYP3A4 mRNA and GAPDH siRNA treatment corresponds to GAPDH mRNA expression relative to HPRT1 housekeeping gene. Data analysed by comparative C(t) method and expressed as mean ±SD as percentage of vehicle control of each time point of 4 replicates from N=1 experiment. Unpaired t-test were performed between each treatment condition against the corresponding vehcle control where, *P<0.05, **P<0.01 and ***P<0.001.

As CYP3A4 mRNA was still detectable after 72 h incubation, hepatocytes were cultured up to 96 h with 10, 50 and 100 nM siRNA dosage to determine the time-course of knockdown. Cell viability was determined at 72 and 96 h to ensure that siRNA was not causing cytotoxicity to mask any mRNA knockdown effects. As such, siRNA and vehicle control (RNAiMAX™ transfection reagent) treatments, as shown in Figure 4.4, caused no significant cytotoxicity as viability remained above 75% of untreated control in all treatment conditions.

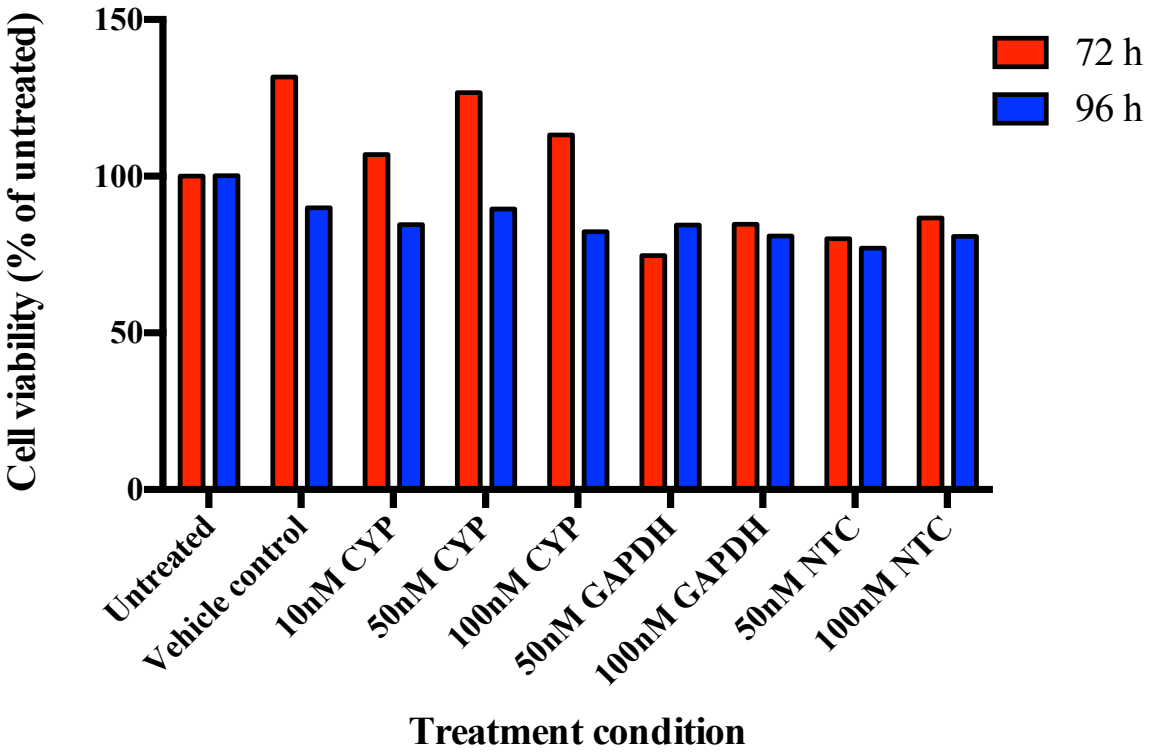

Figure 4.4 Primary human hepatocyte (Hu1591) cell viability after siRNA treatment and culture over 72 and 96 h. Cell viability was determined by PrestoBlue™ live cell assay. Fluorescence readings were taken at designated incubation time points after 10 min incubation with PrestoBlue™ reagent. Cell viability was calculated as the fluorescence measured as a percentage of the untreated sample at each time point from N=1 experiment.

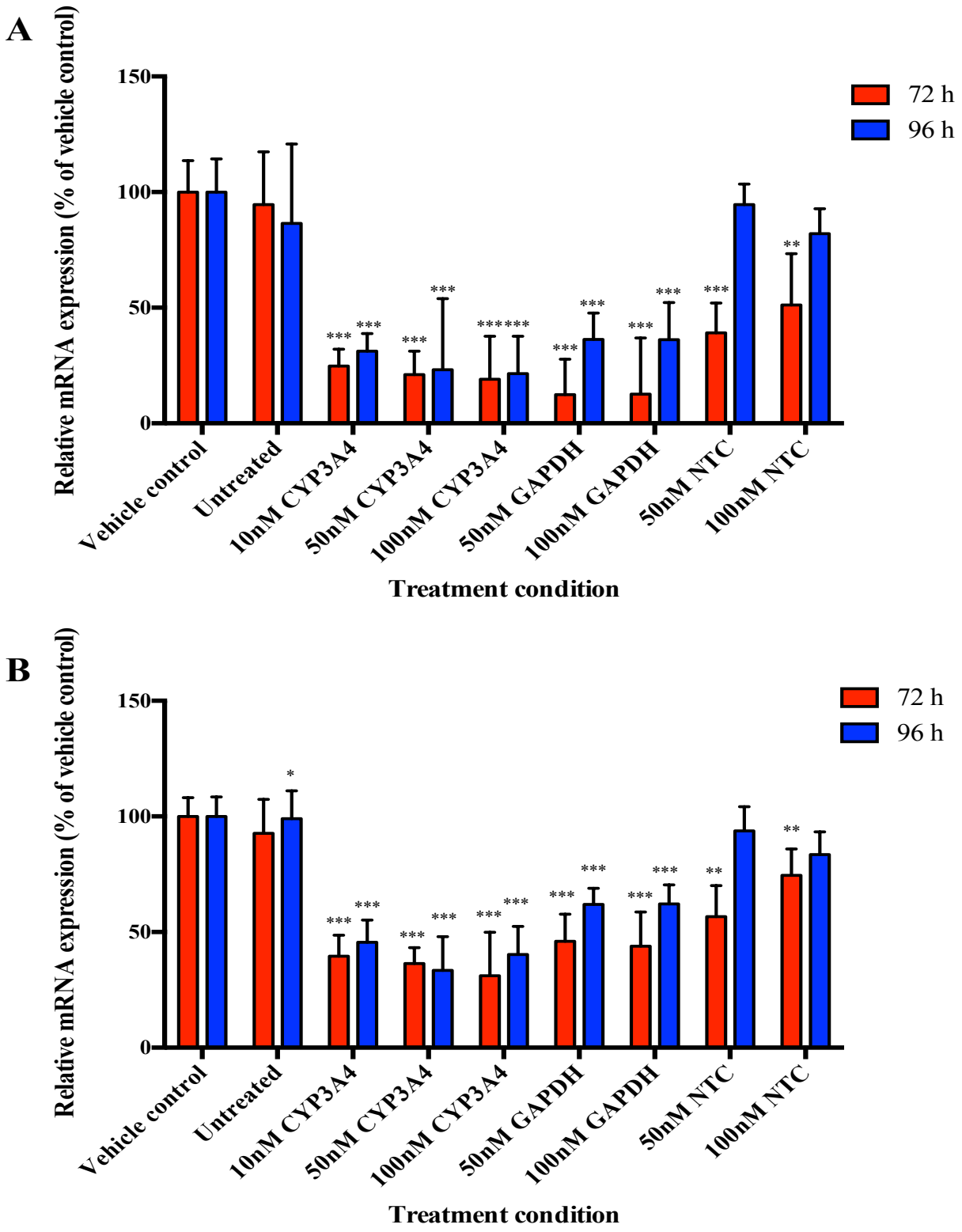

Figure 4.5 Relative mRNA knockdown following siRNA treatment and 72 and 96 h incubation, data analysed by two methods. A. Comparative CT method. **B.** Pfaffl method. CYP3A4 and non-targeting control (NTC) siRNA treatment corresponds with CYP3A4 mRNA and GAPDH siRNA treatment corresponds to GAPDH mRNA expression relative to HPRT1 housekeeping gene. Data expressed as mean ±SD as percentage of vehicle control from 4 replicates from N=1 indepdendent experiment. Where, *P<0.05, **P<0.01 and ***P<0.001.

Figure 4.5 shows the CYP3A4 and GAPDH mRNA knockdown over the incubation of 72 and 96 h after a single dose of siRNA. The data was analysed by 2 different methods. Over 50% knockdown (compared to vehicle control) was achieved for CYP3A4 mRNA in CYP3A4 siRNA treated samples up to 96 h. This confirms the use of a single siRNA dose for prolonged knockdown. Similar levels of knockdown were achieved with 50 and 100 nM siRNA concentrations, which were slightly more than with 10 nM CYP3A4 siRNA. The data was analysed using two different methods as a comparison. The Pfaffl method of gene expression analysis takes into account the efficiency of qPCR reactions. Both comparative C(t) and Pfaffl methods produced a similar trend for the same data. However, Figure 4.5 shows that the range of SD was smaller for Pfaffl analysis. Therefore, the Pfaffl method will be used for all subsequent gene expression analyses.

In order to optimise the dosage of siRNA for knockdown experiments, mRNA expression was analysed at the 48 h time-point as shown in Figure 4.6 Around 70% reduction in CYP3A4 mRNA expression was detected after 50 and 100 nM CYP3A4 siRNA treatment, whereas knockdown was not achieved with 10 nM siRNA. Interestingly, GAPDH did not show a dose-dependent level of knockdown as lower mRNA expression was detected at 50 nM than 100 nM of GAPDH siRNA in both Figures 4.5 and 4.6. This confirms the need for dose optimisation in siRNA experiments.

ON-TARGETplus siRNA complexed with 1.25 µl RNAiMAX® transfection reagent appeared to be non-toxic for primary human hepatocytes. A 50 nM dose of siRNA and time-course of 48, 72 and 96 h incubation were selected for subsequent siRNA experiments to derive CYP3A4 k_{deg}.

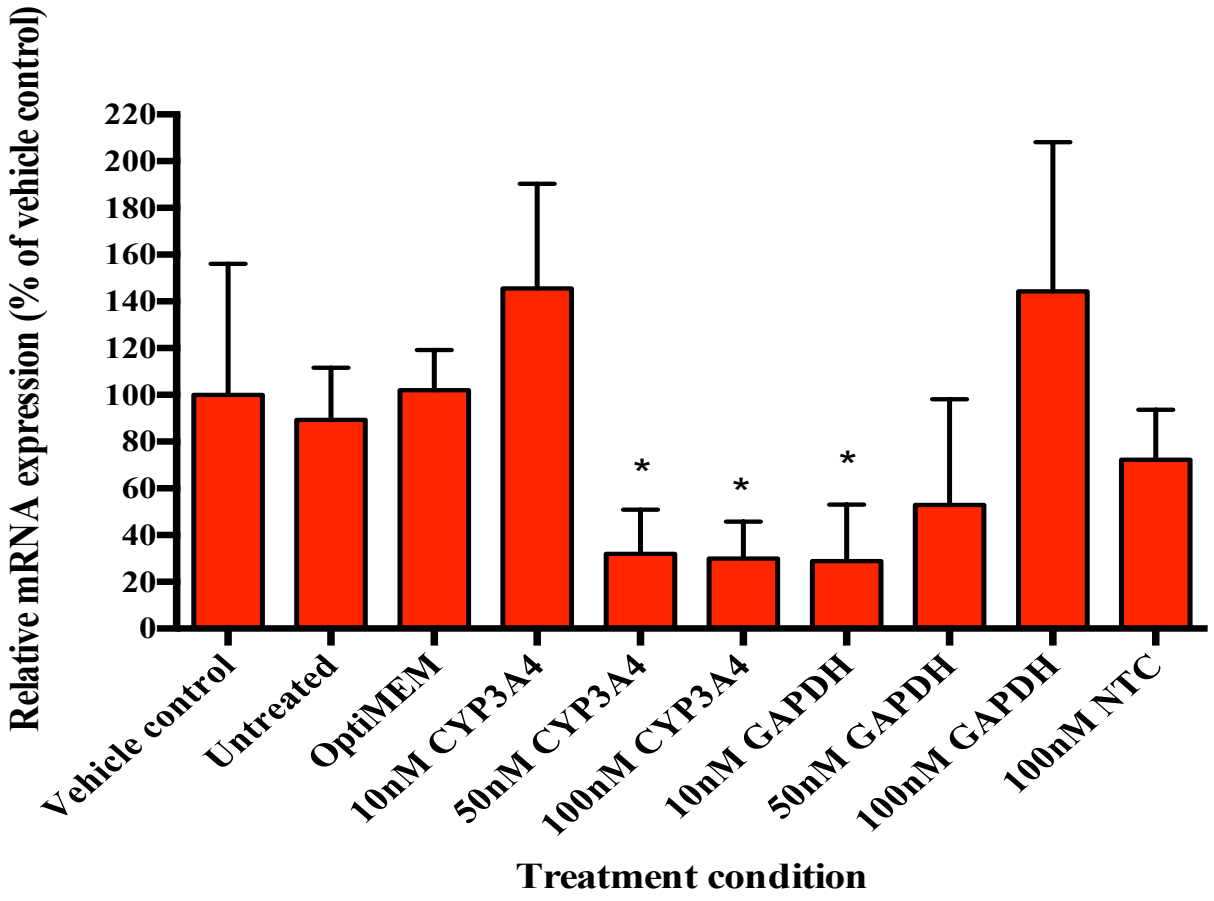

Figure 4.6 Relative mRNA expressions after 48 h incubation with varying siRNA concentrations and treatment conditions. CYP3A4 and NTC siRNA treatment corresponds with CYP3A4 mRNA and GAPDH siRNA treatment corresponds to GAPDH mRNA expression relative to HPRT1 housekeeping gene. Data analysed by comparative C(t) method and expressed as mean ±SD as percentage of vehicle control from 4 technical replicates in N=4 independent experiments in primary human hepatocytes (Hu1591). Unpaired t-test was performed between each treatment condition with vehicle control where *P<0.05.

4.3.3 Development of Western blotting conditions

Non-specific protein bands often appear on Western blots that make identification of target protein difficult, therefore a positive control is recommended (Mahmood & Yang 2012). Varying volumes of CYP3A4 and control (which is transfected with WT baculovirus) BACULOSOME® plus reagent were blotted for CYP3A4 protein expression to validate the use and concentration of this reagent for a positive control. Figure 4.7 shows a strong protein band detected at above 50 kDa for CYP3A4 BACULOSOME® samples, this band was likely to be for CYP3A4 protein that was expected at 57 kDa. Although a band was seen at 0.5 and 1 µl of the control reagent, these bands were likely due to the overspill of the adjacent CYP3A4 BACULOSOME® sample as no strong bands were detected with neighbouring wells with increasing volumes of control. Clearly, a volume of 0.5 µl or less of CYP3A4 BACULOSOME® reagent was needed for subsequent experiments as the streaky blot suggested that too much protein was present. The contrast between CYP3A4 protein detection in CYP3A4 and control reagents validate the use of CYP3A4 BACULOSOME® plus reagent as a positive control.

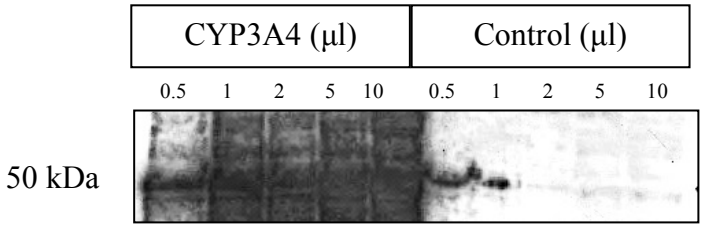

Figure 4.7 Detection of CYP3A4 protein expression in varying quantities of CYP3A4 and Control BACULOSOME® plus reagent.

Cellular protein was extracted by CelLytic™ M lysis and TRIzol® reagents to compare their uses. Successful TRIzol® protein extraction would reduce the need for a separate culture well for mRNA and protein analysis, however several sources have reported problems of solubility of the extracted protein pellet using this method (Hummon et al 2007). Figure 4.8 shows that under the same siRNA treatment conditions and incubation times, protein was not detected beyond 72 h incubation with protein extracted with TRIzol®. Therefore, a separate culture well utilising CelLytic™ M lysis reagent was required and will be used for all subsequent protein extraction from primary human hepatocytes.

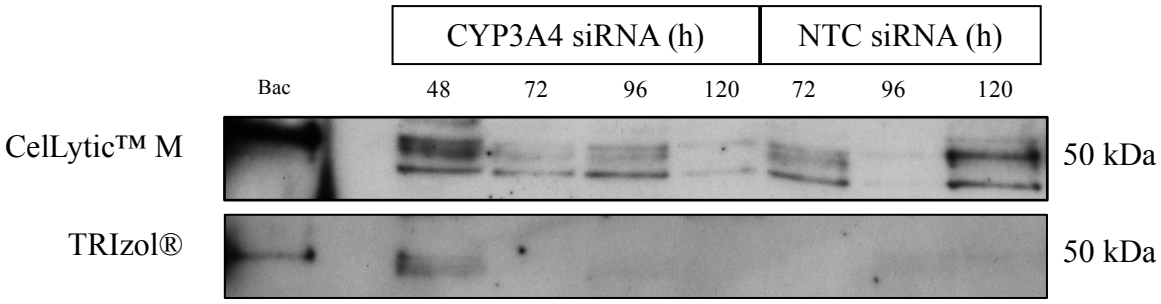

Figure 4.8 Comparison of CelLytic™ M and TRIzol® protein extraction methods in siRNA-treated primary human hepatocytes (Hu1591). Primary human hepatocytes were treated with 50 nM CYP3A4 and NTC siRNA for 48-120 h prior to protein extraction by CelLytic™ M or TRIzol® reagents. CYP3A4 protein detection was carried out by Western blotting as detailed in 4.2.6.

All protein bands were normalised to a housekeeping gene as a loading control for determination of relative protein expression. GAPDH and β-actin are common choices for Western blotting loading controls in mammalian cell types. Figure 4.9 shows that GAPDH expression was more consistent across all treatment conditions and time compared to β-actin, furthermore previous publications have demonstrated variability of housekeeping protein expression amongst different tissue types (Kim et al. 2014). All CYP3A4 protein bands were therefore normalised to GAPDH expression to determine relative expression and protein abundance.

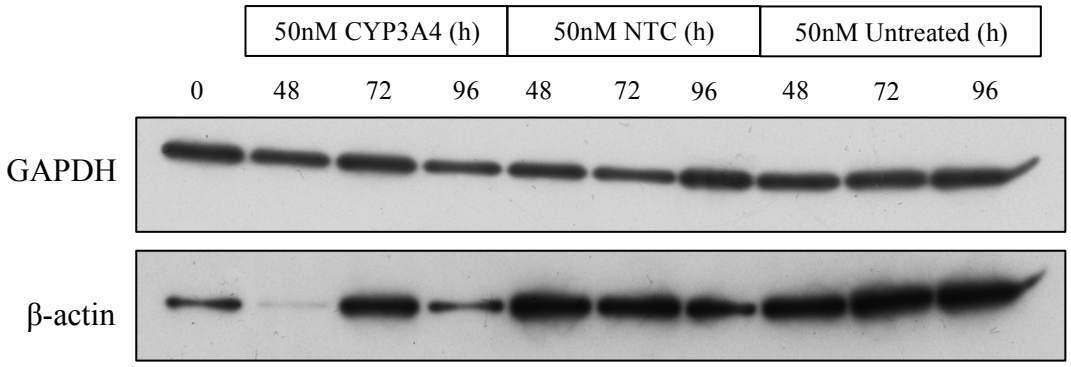

Figure 4.9 Comparison of GAPDH and β-actin expression in siRNA treated and untreated primary human hepatocytes. Cryopreserved primary human hepatocytes were treated with 50 nM CYP3A4 or NTC siRNA, or left untreated and incubated for 48-96 h. After incubation period, protein was isolated by CelLytic™ M lysis buffer and protein detection was carried out by Western blotting utilising both GAPDH and β-actin as comparison with expression quantified by ImageJ software as detailed in 4.2.6.

4.3.4 Optimisation of HPLC-UV conditions for 1'-hydroxymidazolam detection

The standards extracted from primary hepatocyte maintenance media showed good linearity over the concentration range of 0.04 to 20 µM ($R^2 \geq 0.999$) for 1'-hydroxymidazolam. As the MDZ parent drug was detected simultaneously with 1'-hydrozymidazolam metabolite to determine level of CYP3A4 activity in hepatocyte cultures, a clear separation between the two drug peaks was required. Figure 4.10 shows a representative chromatogram in the co-detection of MDZ and metabolite and the calibration curve for 1'-hydroxymidazolam.

A

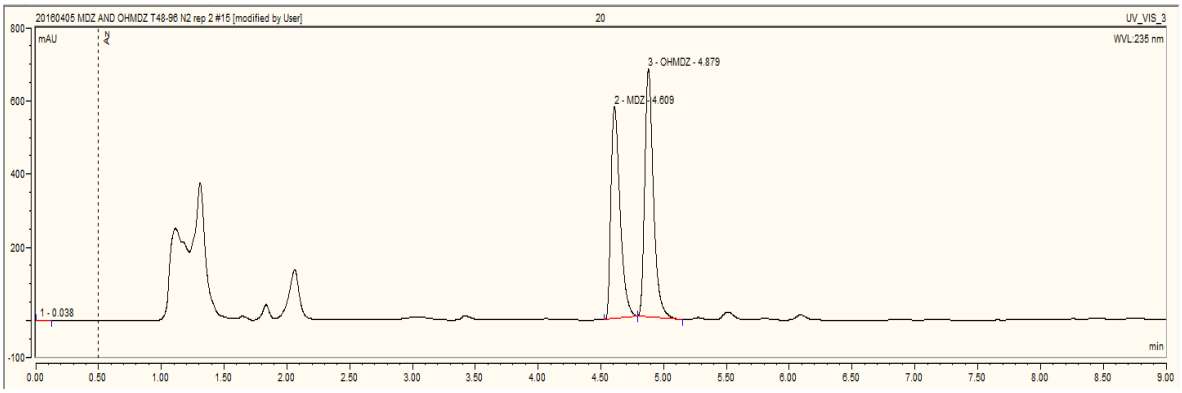

B

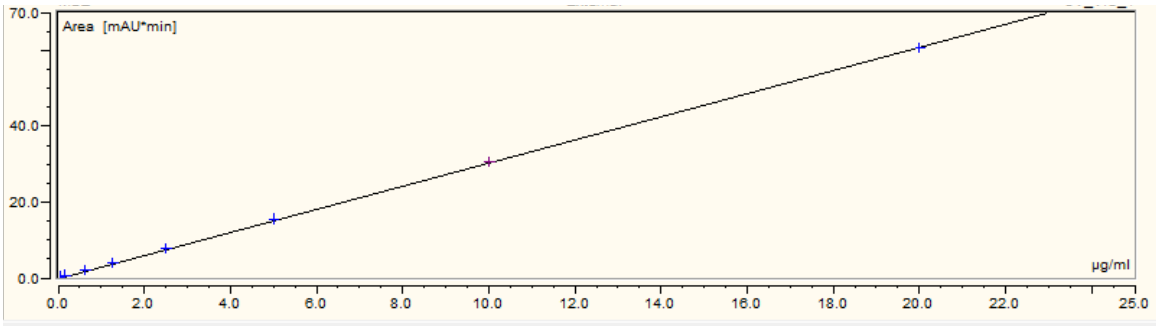

Figure 4.10 A. Representative chromatogram for the co-detection of MDZ and 1'-hydroxymidazolam. **B.** Representative calibration curve of extracted standards of 1'-hydroxymidazolam over the concentration range of 0.04 to 20 µM.

Precision and accuracy of the 1'-hydroxymidazolam detection assay were assessed and the percentages are shown in Table 4.3 for each individual run. The percentage error of accuracy and precision was below 15% for all 3 repeats at all 3 QC concentrations. Interestingly, 1'hydroxymidazolam eluted before the parent MDZ compound, which is unexpected for reverse-phase chromatography. However, the chemical components of the mobile phases and their pH may alter the retention of the compounds.

Table 4.3 shows the accuracy and precision of 3 repetitions of the assay. Accuracy and precision were assessed in triplicate at 3 levels low (0.5 μM), medium (3 μM) and high (10 μM) in 3 independent experiments.

	Low QC (0.5 μM)	**Medium QC (3 μM)**	**High QC (10 μM)**
Assay 1			
Amount detected (μM)	0.55	2.94	10.56
Variance of accuracy (%)	11.0	-2.02	5.59
Variance of precision (%)	13.0	5.08	2.62
Assay 2			
Amount detected (μM)	0.56	3.12	10.41
Variance of accuracy (%)	12.7	4.07	4.06
Variance of precision (%)	2.99	2.81	2.84
Assay 3			
Amount detected (μM)	0.44	3.06	9.85
Variance of accuracy (%)	-12.44	2.07	-1.50
Variance of precision (%)	2.47	1.69	1.47

4.3.5 Magnitude of CYP3A4 mRNA knockdown

Following incubation of primary human hepatocytes with CYP3A4 SMARTpool siRNA (50 nM) for 0-96 h, 60 (± 9.4) %, 70 (± 6.7) % and 66 (± 6.7) % CYP3A4 mRNA knockdown was achieved after 48, 72 and 96 hours of incubation, as shown in Figure 4.11. The 24 hour incubation time point was not included because previous optimisations, as shown in Figure 4.3, did not show significant CYP3A4 mRNA knockdown at this time point, therefore any subsequent detection of decrease in CYP3A4 protein or activity may not be due solely to degradation. Figure 4.11 ahows that siRNA specific for CYP3A4 elicited significant prolonged mRNA suppression following a single dose over the course of 96 hours.

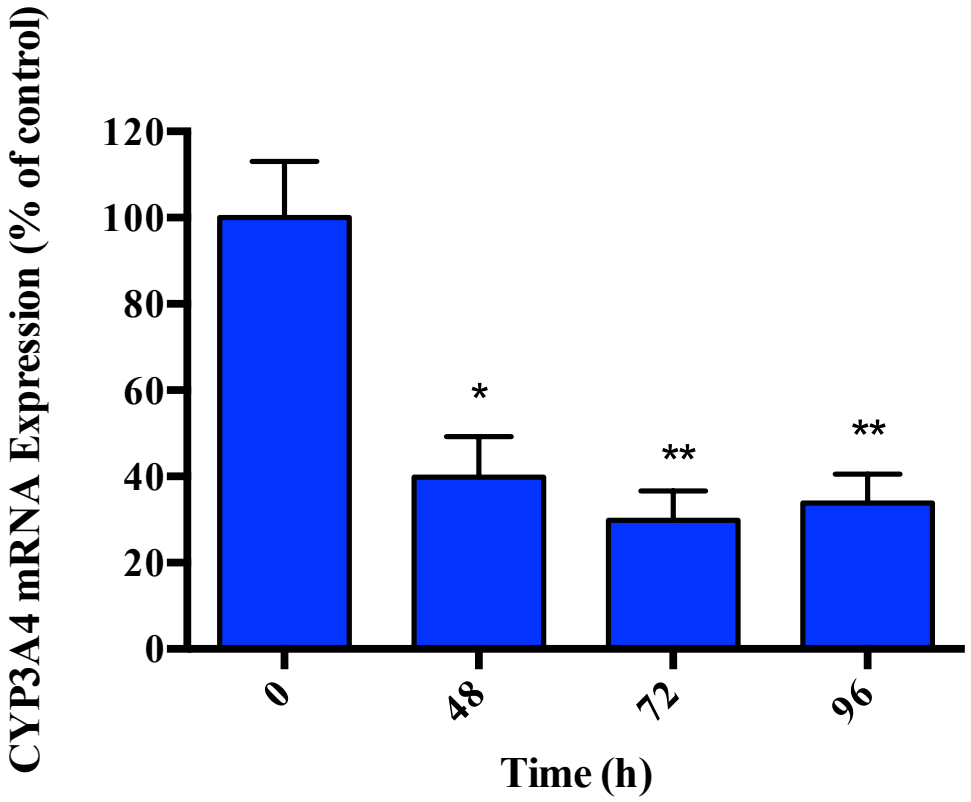

Figure 4.11 Impact of siRNA on CYP3A4 mRNA expression. Primary human hepatocytes were dosed and incubated with 50nM CYP3A4 SMARTpool siRNA for 15 h in reduced serum optiMEM™ I media. After siRNA incubation, media was replaced and cells were incubated for 48, 72 and 96 hours in 37^{o}C 5% CO_2 after initial dosing. CYP3A4 mRNA expression was determined by RT-PCR. The level of CYP3A4 expression is given as a percentage of untreated control at each time point and time 0 was taken after initial cell plating prior to siRNA treatment. Data represents mean ± SD from n=3 donors. Unpaired t-test was performed between each incubation time point and T0 where *P<0.05, **P<0.01 and ***P<0.001.

4.3.6 *Deriving CYP3A4 k_{deg} from protein expression after siRNA treatment*

The CYP3A4 protein degradation rate constant was derived with two methods: (1) from tracking differential CYP3A4 protein decline in untreated hepatocytes and (2) tracking protein decline after siRNA treatment. The relative CYP3A4 expression normalised to GAPDH was calculated (Figure 4.12) and the protein density at each time point compared to control (T0) was fit to a linear regression model and the slope is taken as rate of degradation (Figure 4.13). NTC was not included in the blot shown in Figure 4.12A because there were not enough wells on the electrophoresis gel to accommodate the NTC samples. The CYP3A4 protein k_{deg} values derived by the two methods are summarised in Table 4.4. Overall, k_{deg} derived from untreated hepatocytes resulted in a longer half-life than siRNA-treated.

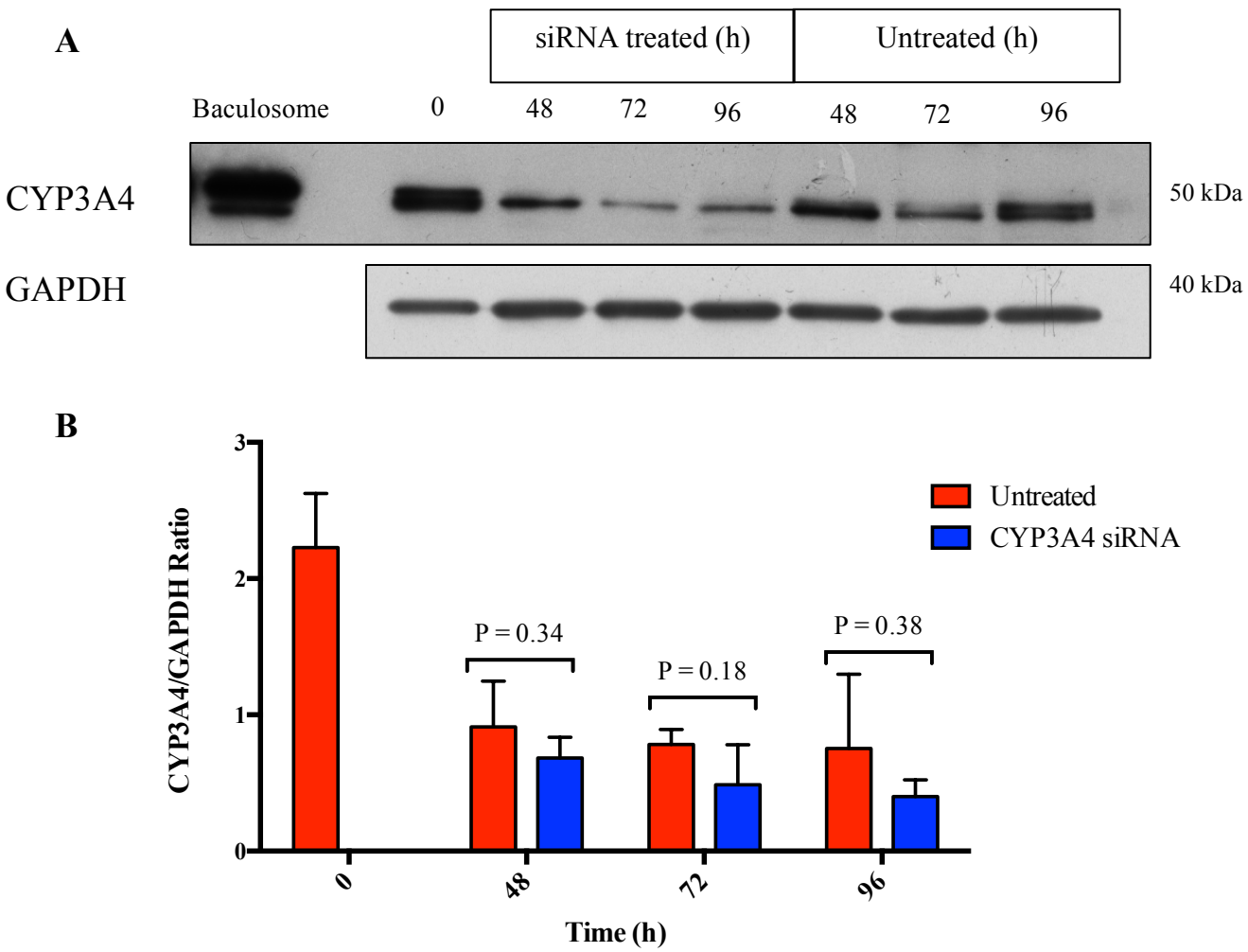

Figure 4.12 Quantification of CYP3A4 protein by Western blotting. A. Representative Western blot of Hu1591. The CYP3A4 protein density was normalised to GAPDH. **B.** The CYP3A4 protein density ratio normalised to GAPDH shown for siRNA-treated hepatocytes and corresponding untreated control. Data represents mean ± SD of 1 replicate from N=3 donors. Unpaired t-test was performed between the siRNA-treated and corresponding untreated hepatocytes at each time point.

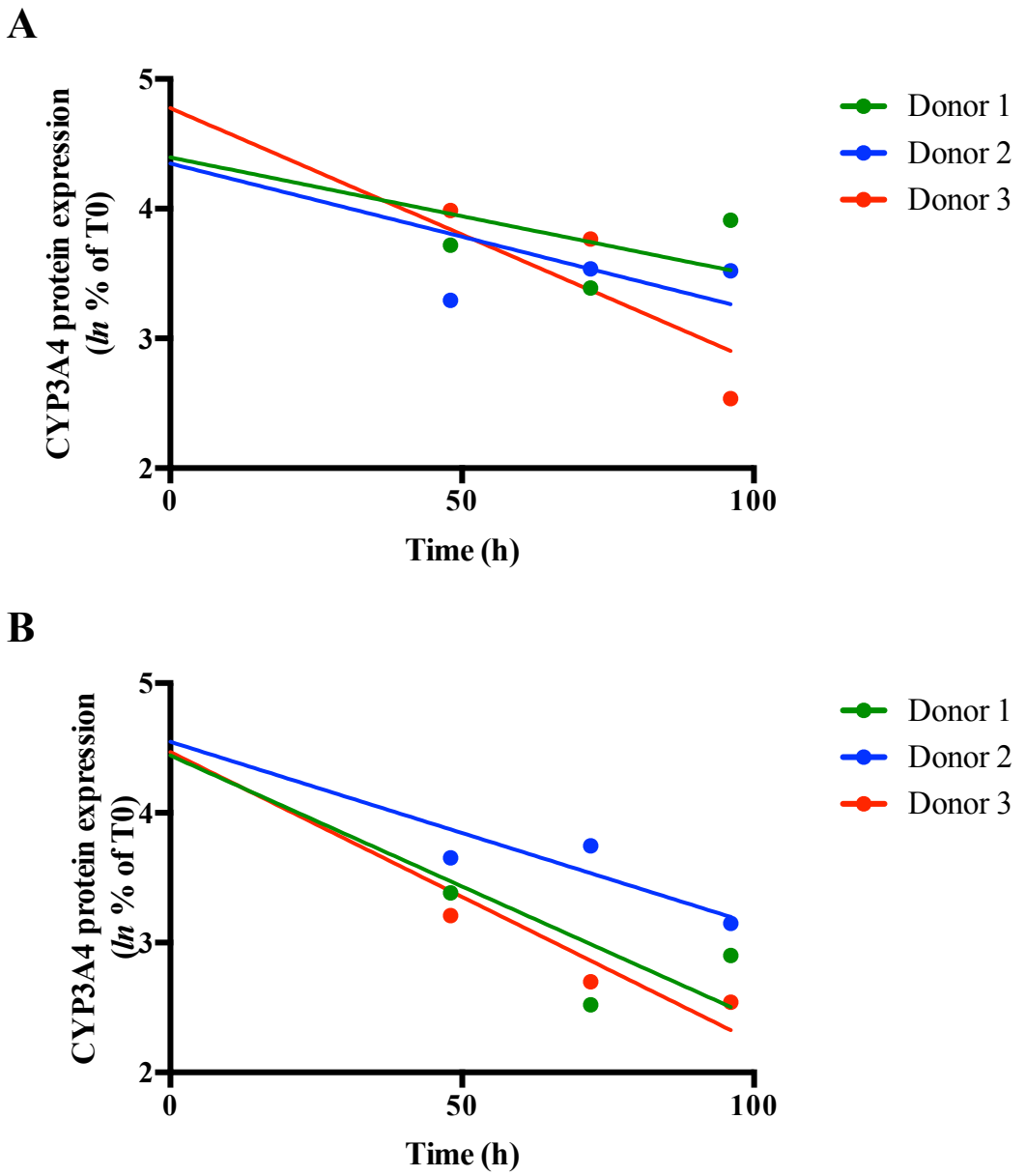

Figure 4.13. Determination of the CYP3A4 degradation rate constant by protein analysis. CYP3A4 protein degradation over time was quantified by Western blot. CYP3A4 protein density was normalized to GAPDH and is expressed as a percentage of T0. **A.** CYP3A4 k_{deg} derived from untreated hepatocytes. **B.** CYP3A4 k_{deg} derived from siRNA-treated hepatocytes. The natural logarithm of the percent of T0 is given and the slope of the loss of enzyme protein expression is used to calculate the protein half-life, which is equal to the rate of degradation. Data represents 1 replicate from N=3 donors.

4.3.7 Deriving CYP3A4 k_{deg} from activity after siRNA treatment

After exposure to CYP3A4 targeting siRNA for 48, 72 or 96 hours, 1'-hydroxymidazolam metabolite formation was quantified to determine CYP3A4 activity. Figure 4.14 shows that concentration of 1'-hydroxymidazolam detected was lower for CYP3A4 siRNA-treated hepatocytes compared with untreated and NTC-treated. Interestingly, in untreated and NTC-treated conditions there appears to be an increase in activity between 72 and 96 h, however the rebound in activity is not as significant in siRNA treated condition implicating sustained mRNA suppression by siRNA.

The percentage of activity at each time point compared to T0 was fit to linear regression models based on assumed first-order enzyme degradation kinetics as shown in Figure 4.15 to calculate k_{deg}. The CYP3A4 k_{deg} values were derived by tracking the decline of CYP3A4 activity in siRNA-treated samples and the average k_{deg} from the 3 donors were calculated to be 0.0202 (± 0.00026) h^{-1} and $t_{1/2}$ of 34.2 (± 0.49) h. Unlike protein samples, the k_{deg} was not able to be calculated from untreated samples as there were no decline in metabolite production observed over time (Figure 4.15.A).

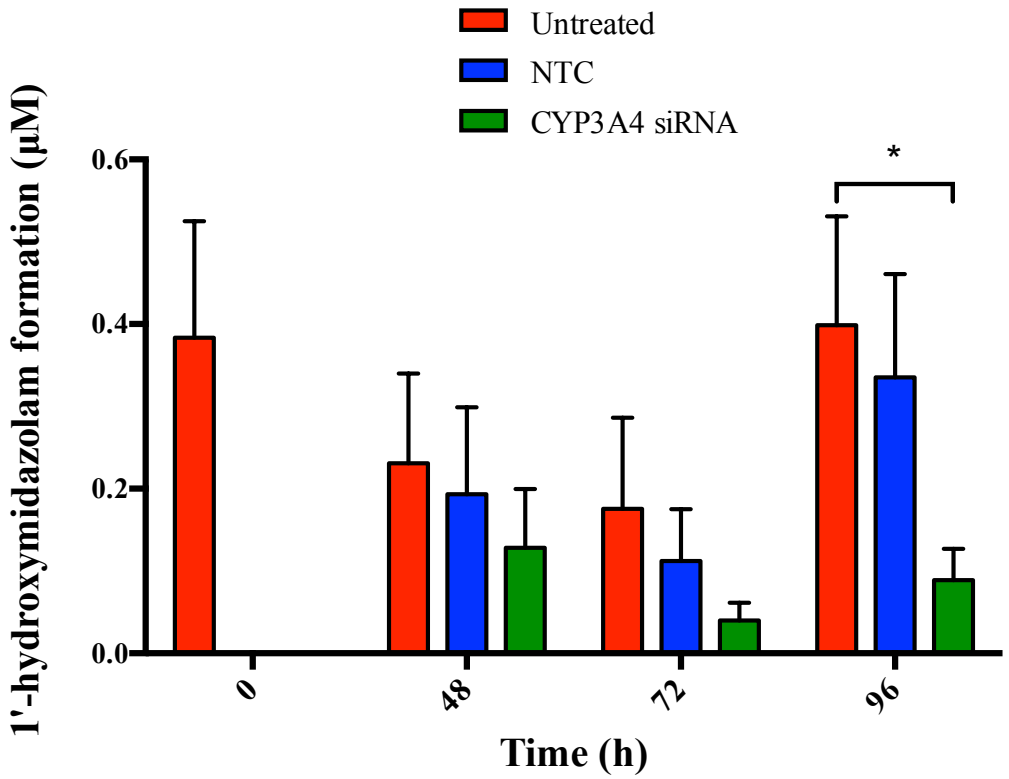

Figure 4.14 Determination of CYP3A4 activity by formation of probe substrate metabolite. Primary human hepatocytes were treated with CYP3A4 or non-targeting control (NTC) siRNA and incubated over 48, 72 and 96 h. Formation of 1'-hydroxymidazolam after 60 min incubation with 3.4 µM MDZ was quanified with HPLC-UV. Data represents mean ± SD from n=3. Unpaired t-test was performed between each treatment condition with corresponding untreated control where *P<0.05.

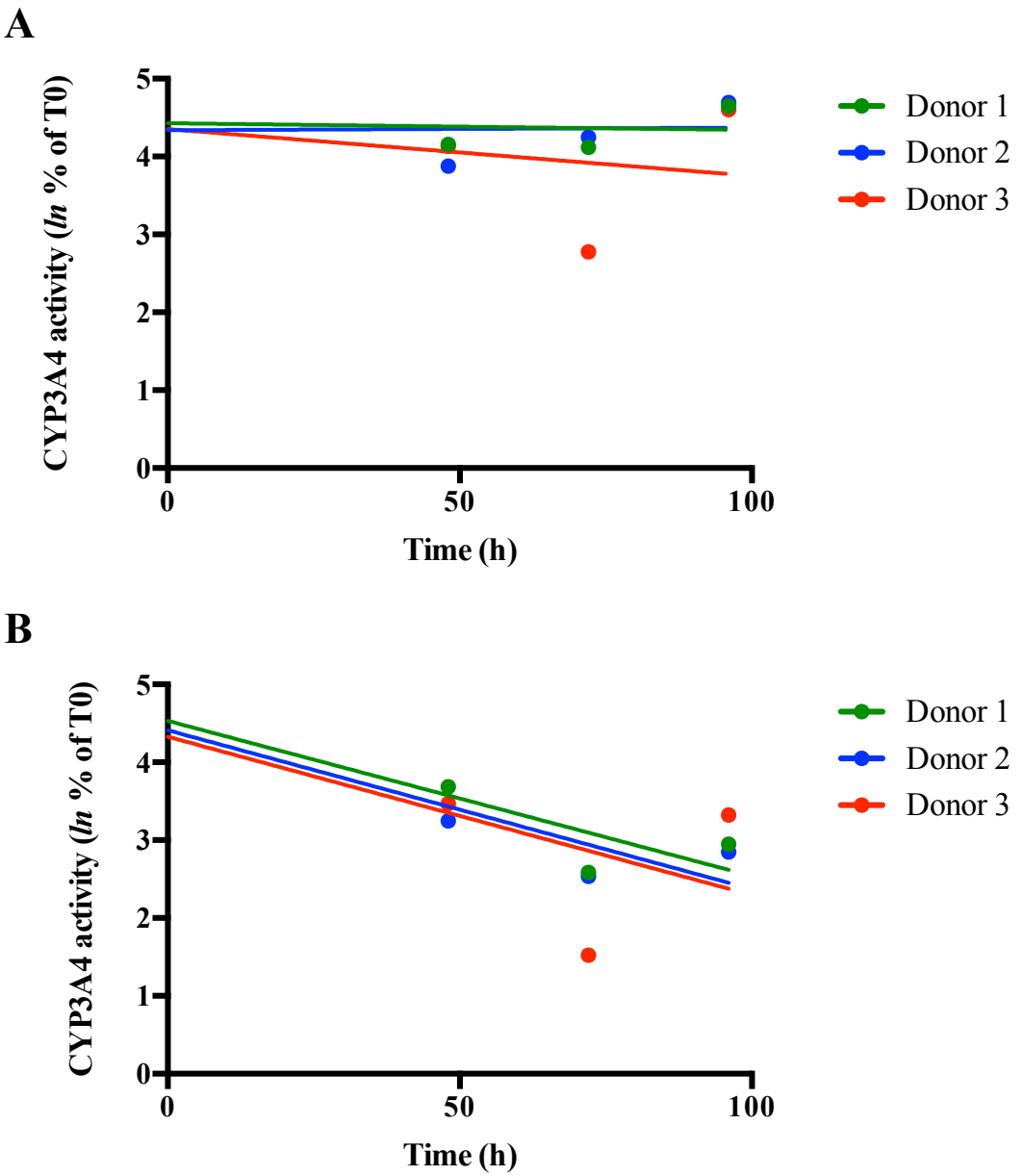

Figure 4.15 Determination of the CYP3A4 degradation rate constant by activity analysis. CYP3A4 activity was determined by formation of 1'-hydroxymidazolam. CYP3A4 activity is expressed as a percentage of T0. **A.** CYP3A4 k_{deg} derived from untreated hepatocytes. **B.** CYP3A4 k_{deg} derived from siRNA-treated hepatocytes. The natural logarithm of the percent of T0 is given and the slope of the loss of enzyme activity is used to calculate the protein half-life, which is equal to the rate of degradation. Data represents 1 replicate from N=3 donors.

A summary of the k_{deg} and $t_{1/2}$ values calculated from protein and activity methods are given in Table 4.4. Mean values were derived from one experimental replicate of hepatocytes from three donors.

Table 4.4 Summary of the k_{deg} and $t_{1/2}$ values derived from protein and activity methods of analysis using untreated and siRNA treated samples.

Parameter	Donor 1	Donor 2	Donor 3
$t_{1/2}$ (h) derived from protein determined by Western blot in untreated samples	76.4	61.3	35.5
k_{deg} (h^{-1}) derived from protein determined by Western blot in untreated samples	0.0090	0.0113	0.0195
Average $t_{1/2}$ (h)	57.7 (± 20.7)		
Average k_{deg} (h^{-1})	0.0132 (± 0.0055)		
$t_{1/2}$ (h) derived from protein determined by Western blot in siRNA treated samples	34.3	49.3	31.0
k_{deg} (h^{-1}) derived from protein determined by Western blot in siRNA treated samples	0.0202	0.0141	0.0223
Average $t_{1/2}$ (h)	38.2 (± 9.8)		
Average k_{deg} (h^{-1})	0.0189 (± 0.0043)		
$t_{1/2}$ (h) derived from activity determined by probe substrate metabolite formation in siRNA treated samples	34.8	33.9	34.0
k_{deg} (h^{-1}) derived from activity determined by probe substrate metabolite formation in siRNA treated samples	0.0199	0.0204	0.0203
Average $t_{1/2}$ (h)	34.2 (± 0.49)		
Average k_{deg} (h^{-1})	0.0202 (± 0.00026)		

4.4 Discussion

Physiologically relevant k_{deg} values of DMEs are important for the accurate prediction of time-dependent DDIs in PBPK modelling. There are currently large disparities or missing values published for the enzymes most involved in clinically significant DDIs and no agreement on the best method of assessment (Yang et al. 2008). Traditional approaches of measuring CYP enzyme degradation rates are limited by the *de novo* protein synthesis in the duration of degradation measurement. There is a general consensus that steady-state protein abundance is a dynamic balance between protein synthesis and degradation (Gottesman & Maurizi 1992), such that unaccounted levels of protein synthesis during the assessed time period will distort the degradation rate calculated in such approaches. Other common methods for measuring protein degradation rates utilise protein synthesis inhibitor drugs such as cycloheximide and actinomycin D which inhibits cellular protein synthesis mechanisms to stop universal protein production, followed by tracking the disappearance of specific target protein with pulse-chase analysis (Alvarez-Castelao et al. 2012; Yewdell et al. 2011; Zhou 2004). The concern with such an approach is that the chemical inhibitor drugs are cytotoxic and will disrupt normal cellular function including protein degradation pathways that will in turn distort degradation rates and this is demonstrated with findings in Chapters 2 and 3. Ramsden et al. (2015) used siRNA and IL-6 to specifically inhibit CYP3A4 protein synthesis without impacting on regular cellular mechanisms and a similar siRNA-silencing approach was used in this Chapter to specifically target CYP3A4 protein circumventing the concern of cytotoxicity. This study demonstrated that utilising gene-specific siRNA produced significant knockdown of CYP3A4 mRNA and protein with minimal cytotoxicity. CYP3A4 was knocked down at the functional protein level as shown in

Figure 4.14 where CYP activity was lower for siRNA-treated hepatocytes compared with untreated and NTC.

A consensus value of hepatic CYP3A4 k_{deg} for use in PBPK models has been investigated (as summaried in Table 1.3) and subsequently evolved based upon new techniques and on prediction accuracy. For example, 0.0077 h^{-1} (corresponding to half-life of 90 hours) was derived from meta-analysis of all the published CYP3A values until 2008 (Yang et al. 2008). However, Wang et al. (2010) found better prediction accuracy for 54 DDIs involving CYP3A mechanism-based inhibition interactions using 0.03 h^{-1} as the k_{deg} value compared to 0.0077 h^{-1}. Other subsequent studies also found superiority with 0.03 h^{-1} compared with 0.0077 h^{-1} (Friedman et al. 2011; Yamashita et al. 2013). Rowland Yeo et al. (2011) reported that 0.0193 h^{-1} produced decreased bias and increased precision in 29 time-dependent metabolic inhibition DDIs compared with 0.0077 h^{-1} and Mao et al. (2013) further validated this value and reported that a CYP3A4 half-life of between 25-35 hours (0.019 - 0.027 h^{-1} k_{deg}) yielded the most accurate crizotinib drug interaction predictions. Subsequently, this value has been used in numerous published examples of DDI prediction (Peters et al. 2012; Ke et al. 2016; Xu et al. 2015).

Interestingly, the CYP3A4 k_{deg} values of 0.019 h^{-1} ($t_{1/2}$ of 36.4 hours) and 0.020 h^{-1} ($t_{1/2}$ of 34.3 hours) derived from siRNA-treated hepatocytes in loss of protein method and tracking activity decline, respectively, were in close agreement to the 25-35 hour $t_{1/2}$ range reported by Mao et al. (2013) and was closer than the k_{deg} value derived by tracking protein disappearance in untreated hepatocytes (0.013 h^{-1}; $t_{1/2}$ of 53.3 hours) as shown in Table 4.4. This suggests that derivation of k_{deg} from siRNA-treated samples was the more robust method. Moreover, the k_{deg} values derived from both protein and activity in siRNA-treated hepatocytes were in close

agreement to each other. Understanding the potential of *de novo* protein synthesis distorting overall measurement of enzyme degradation during the analysis period, this is perhaps unsurprising. However, whether the difference between the values derived from protein and activity assays will impact on DDI predictions will require further modelling to confirm the best method.

Extraction of RNA and proteins from a single sample is beneficial for accurate correlations between response in the transcriptome and proteome (Hummon et al. 2007; Simões et al. 2013). However, the method of standard TRIzol® extraction of proteins was insufficient due to problems of protein resolubilisation and therefore two separate methods of protein isolation including a modified TRIzol® extraction protocol published by Simões et al. (2013) and a standard whole-cell protein extraction method utilising CelLytic™ M detergent solution according to manufacturer's protocol, were tested. It was found that a separate sample extracted by CelLytic™ M lysis buffer yielded more protein which attests to the limitations of using Western blotting to derive rates of protein degradation. However, Takahashi et al. (2017) recently reported a CYP3A4 k_{deg} value of 0.026 h^{-1} derived from SILAC and specific protein quantifications with mass spectrometry. Therefore, deriving k_{deg} by quantification of proteins over activity is likely to be possible with sensitive protein quantification methods. Simple semi-quantitative protein detection by methods such as Western blotting may not be optimal due to insufficient sensitivity and variability in detection between experiments.

It should be noted that there may be differential expression of CYP enzymes between cell types within an individual and this may impact upon k_{deg}. For example, the Simcyp default hepatic 3A4 k_{deg} is 0.0193 h^{-1} whilst the intestinal value is 0.030 h^{-1}. The faster rate of intestinal turnover of CYP3A4 is likely to be due to the turnover

of the enterocyte itself in which the enzyme resides, as the reported human intestinal epithelia complete turnover is estimated to be around 3.5 days (Darwich et al. 2012). Intestinal drug metabolism is known to contribute to exposure of orally administered drugs and several DDI prediction strategies incorporate the estimated contribution of gut metabolism (Almond et al. 2016; Xie et al. 2016). Other CYP enzymes detected in human small intestine include CYP 1A1, 1B1, 2C9, 2C19 2D6, 2E1, 2J2 and 3A5, with 3A4/5 accounting for 80% and 2C for around 18% abundance (Paine et al. 2006). Since protein turnover rates can vary between tissue types as well as species (Waterlow 1984; Millward et al. 1981), the established method here should be verified in intestinal cells for the relevant CYP enzymes detected in the gut, especially when the expected protein turnover rate is less than that of the enterocyte. Intestinal k_{deg} values for that of CYPs 2C8 and 2C19, with estimated $t_{1/2}$ of 23 and 26 h, respectively (Table 1.4), should be determined in the relevant cell systems for incorporation into time-dependent DDI prediction models.

A potential limitation to the accuracy of the hepatic CYP3A4 k_{deg} derived here is that the study was conducted in only three hepatocyte donors. Hepatic CYP3A4 expression is subject to genetic polymorphisms (Lamba et al. 2010) and it would therefore be of interest to capture inter-individual variability in k_{deg} through the study of as many donors as possible or through the use of pooled hepatocytes to generate an average k_{deg} value representative of a wider population. CYP3A4 is the most extensively studied in terms of k_{deg} and DDIs whereas values for other CYPs implicated in time-dependent interactions remain scarce (as shown in Table 1.4). The cost-effective *in vitro* method described in this Chapter can be applied to measure degradation rates for other less well-characterised CYPs.

CHAPTER 5

Using mRNA suppression to estimate CYP2B6 degradation rate constant in primary human hepatocytes

CONTENTS

5.3.8 Deriving CYP2B6 k_{deg} from P450-Glo™ activity assay

5.3.9 Deriving CYP2B6 k_{deg} from probe substrate metabolite formation

6.4 Discussion

5.1 Introduction

As discussed in Chapter 4, the k_{deg} of DMEs is a known source of error in the prediction of time-dependent DDIs in PBPK modelling. Previous attempts at quantifying this kinetic parameter have focused primarily on CYP3A4 with highly variable estimates and little consensus as to which methods yield the most physiologically-relevant values (Yang et al 2008). Methods of quantifying protein degradation rates traditionally involve using radiolabelled isotopes for tagging the protein of interest or tracking protein loss over time by immunoblotting (Yewdell et al 2011; Alvarex-Castelao et al 2012). The caveats of these approaches, as discussed in Chapter 4, are that the degradation rates derived do not account for *de novo* protein synthesis during the period of investigation, which would distort the overall level of protein abundance and impact upon the accuracy of the measured degradation rate.

Other *in vitro* approaches that address this caveat incorporate the use of protein synthesis inhibitor drugs to pharmacologically inhibit universal protein synthesis in the given test cell system (Zhou et al 2004; Belle et al 2006). However, as demonstrated in Chapters 2 and 3, protein synthesis inhibitor drugs instigate protein inhibition by acting on fundamental protein synthesis machinery that are essential for cell survival, consequently they generate high levels of cytotoxicity even at low concentrations in most cell types. Furthermore, they can also affect protein degradation processes (Dai et al 2013) and are therefore unsuitable for measuring endogenous protein degradation rates. It was demonstrated in Chapter 4 that using CYP3A4-specific siRNA, *de novo* protein production was reduced without overt cytotoxicity and k_{deg} values were derived that were in good agreement with published values. The k_{deg} values derived from siRNA-treated hepatocytes also seemed to be more consistent with literature compared to k_{deg} derived from untreated hepatocytes.

To date, k_{deg} for CYP3A4 is the most extensively studied amongst all DMEs due to the well established importance of CYP3A4 in xenobiotic metabolism. K_{deg} values for other CYP and non-CYP enzymes remain scarce, yet many other CYP isoforms, such as CYP2B6, CYP2C8, CYP2C9 and CYP2D6, are implicated in time-dependent DDIs (Riley & Wilson 2015). There are currently large disparities or missing values published for the enzymes most involved in complex DDIs.

There is currently a growing interest in CYP2B6 as this CYP isoform is inducible with highly variable expression levels between individuals, accounting for 2-10% of overall CYP abundance and an estimated 8% contribution to metabolism of all clinically-used drugs (Wang & Tompkins 2008; Hedrich et al 2016). As the list of identified CYP2B6 substrates is growing (Table 1.2), so is the enzyme's importance in propagating DDIs, especially in time-dependent induction interactions due to its highly inducible nature (Faucette et al. 2004). Clearly, an accurate k_{deg} value for CYP2B6 will be important for the predictions of DDIs propagated by this enzyme.

The objectives of this Chapter were two-fold. The first was to induce CYP2B6 expression in HepG2 and Caco-2 cell lines from which optimisations of CYP2B6 protein and activity detection could be carried out. Previously, Martin et al. (2008) reported CYP2B6 induction in HepG2 and Caco-2 cell lines at both the mRNA and protein level. We hypothesised that increasing the expression of CYP2B6 in cancer cell lines would provide a sufficient level of activity from which the turnover of probe substrate to metabolite can be detected by HPLC-UV. Thus, the induced cell lines can be used as a cheaper system compared with primary human hepatocytes in which the HPLC-UV detetction of probe substrate metabolite can be optimised. The second objective for this Chapter was to determine the k_{deg} of the CYP2B6 enzyme by utilising the approach validated in Chapter 4 for measuring CYP3A4 k_{deg}. This

approach involved using siRNA for suppression of mRNA followed by the tracking of enzyme activity and protein loss over time in primary human hepatocytes. An additional method of activity detection, using CYP2B6-Glo™ assay, was employed for studying CYP2B6 as the enzyme expression levels were expected to be low and therefore the HPLC-UV instrument may have insufficient sensitivity to detect the production of probe substrate metabolite.

5.2 Materials and methods

5.2.1. Materials

HepG2 and Caco-2 cell lines were obtained from ATCC (Virginia, USA). Plateable cryopreserved primary human hepatocytes (HMCPIS Lot. Hu1591, Hu1824 and Hu8241), CHRM® media, William's E media, thawing and plating supplements (CM3000), maintenance supplements (CM4000), 24-well collagen I coated plates and opti-MEM® I media were purchased from Invitrogen Ltd (Paisley, UK). TaqMan® reverse transcription reagents, TaqMan® gene expression assays for CYP2B6 (Hs04183483_g1) and GAPDH (Hs02758991_g1), TaqMan® gene expression master mix, CYP2B6 (P3028) and control (P2315) BACULOSOMES® plus reagent, Lipofectamine® RNAiMAX reagent, NuPAGE® Western blot materials and TRIzol® reagent were purchased from ThermoFisher Scientific Inc. (Loughborough, UK). ON-TARGETplus human CYP2B6 SMARTpool and non-targeting pool siRNA were purchased from GE Healthcare Dharmacon™ (UK). Western blot antibodies: anti-CYP2B6 (VMA00041) and goat polyclonal anti-mouse IgG (STAR207P) were purchased from Bio Rad (Oxford, UK), anti-CYP2B6 (ab198870 and ab140609), anti-GAPDH (ab181602) and goat polyclonal to rabbit IgG (ab97080) were bought from Abcam (Cambridge, UK). Luminata™ Forte Western HRP substrate was obtained from Millipore (Watford, UK). DMEM, FBS, TWEEN®20, Bradford Reagent, CelLytic™ M, protease inhibitor cocktail, salicylamide, rifampicin (RIF), phenobarbital (PB), bupropion hydrochloride, (2S,3S)-hydroxybupropion, RNase-free water and other Western blot buffer ingredients were purchased from Sigma-Aldrich (Dorset, UK). P450-Glo™ CYP2B6 assay was from Promega (Southampton, UK).

5.2.2 CYP induction in tumour cell lines

5.2.2.1 Caco-2 and HepG2 cell line culture

HepG2 and Caco-2 cells were cultured as detailed in section 2.2.2. HepG2 cells were maintained in DMEM medium supplemented with 10% FBS solution and Caco-2 cells were cultured in DMEM supplemented with 15% FBS. Cell lines were passaged or plated at 80% confluence and discarded beyond passage 20.

5.2.2.2 Induction of CYP3A4 and CYP2B6 in HepG2 and Caco-2 cell lines

HepG2 and Caco-2 cells were seeded at 3 x 10^5 cells per well in 24-well plates in DMEM medium supplemented with 10% or 15% FBS solution, respectively, and incubated overnight in a 37^{o}C 5% CO_2 humidified incubator overnight to allow cells to adhere to the plate bottom. The following day, cells were dosed with 2, 10 and 20 μM RIF and 100, 500 and 1000 μM PB and incubated for 24, 48 and 72 hours to determine the time and level of maximum induction. A vehicle control containing 1% methanol, an untreated control and controls consisting of RNA extracted from a primary human hepatocyte sample at 0 and 24 h (positive control) after plating (described in 4.2.3) were also included. The control and drug-containing media were removed and replaced every 24 h.

5.2.2.3. Magnitude of mRNA induction quantified by RT-PCR

After 24, 48 and 72 h incubation, total RNA was isolated, using TRIzol® reagent, and quantified as described in section 4.2.5.1. cDNA was synthesised from the isolated RNA with Taqman® reverse transcription kit as detailed in 4.2.5.2. The magnitude of mRNA induction at each incubation time-point was determined by quantifying CYP3A4 and CYP2B6 mRNA expression relative to the housekeeping gene GAPDH by qPCR. The protocols for CYP3A4 and CYP2B6 quantification are as detailed in 4.2.5 and 5.2.5, respectively. Data was normalised to the primary hepatocyte control

sample collected at time 0 (T0) and relative expression was derived using the Pfaffl method (Pfaffl 2001) as explained in 4.2.5.4.

5.2.2.4. Magnitude of induced CYP2B6 activity determined by P450-Glo™ assay and UV-HPLC analysis in Caco-2 cell line

Caco-2 cells were induced as described in 5.2.2.2 with 10 μM RIF; the level of induced activity was determined by two methods: the CYP2B6 P450-Glo™ assay and via bupropion probe substrate metabolite formation by UV-HPLC. In the first aforementioned method, the CYP2B6 P450-Glo™ assay was conducted as described in 5.2.7. For probe substrate metabolite detection, the protocol was as follows: 2 hours prior to the designated incubation time-point, Caco-2 cells were dosed with 500 μM of bupropion and incubated for 2 h at 37°C, 5% CO_2 in a humidified incubator. The bupropion probe concentration used was described previously (Levy et al. 2015; Zhang et al. 2016). Cell culture media containing probe and metabolite were removed and immediately stored at -80°C to stop any further reaction until analysis. (2S,3S)-hydroxybupropion metabolite was extracted from the culture media as described in 5.2.8.2 and quantified as detailed in 5.2.8.3.

5.2.3 Cryopreserved primary human hepatocyte culture

Cryopreserved primary human hepatocytes were thawed and plated as described in section 4.2.2. The donor demographics are given in Table 5.1; three hepatocyte donors were used and CYP2B6 k_{deg} were derived from 1 experiment from the three donors. Hepatocytes were seeded on 24-well collagen-I coated plates at a density of 3 x 10^5 viable cells per well for CYP2B6 metabolism activity and protein expression analyses. Hepatocytes were seeded at 1 x 10^5 viable cells/well for mRNA and P450-Glo™ CYP2B6 analyses. The media volume used was 500 μl per well. Cells were incubated with plating media for 5 hours at 37°C with 5% CO_2 and 95% humidity to

allow cell adherence prior to siRNA transfection. After 5 hours of incubation, the plating media was replaced with maintenance media for untreated control or dosed with varying siRNA conditions in optiMEM media. Following siRNA transfection, maintenance media was replaced every 24 hours for the duration of the experiment.

Table 5.1 Donor demographics of the cryopreserved primary human hepatocytes

Demographics	Donor 1	Donor 2	Donor 3
Donor ID	Hu1591	Hu1824	Hu8241
Age	29	66	60
Gender	Male	Female	Male
Ethnicity	Caucasian	Caucasian	Caucasian
Characteristics	Rare alcohol user. No tobacco or drug use reported	Tobacco use. No alcohol or drug use	Tobacco and alcohol user. No drug use
Cause of death	Not reported	Not reported	Cardiac related
Cell viability	91%	93%	94%

5.2.4 Small-interfering RNA treatment

Experiments using siRNA to suppress CYP2B6 expression were conducted following a modified knockdown protocol published by Vozza-brown et al. (2005). CYP2B6 siRNA was prepared and stored at 10 μM stock concentration in 1X siRNA buffer (as described in 4.2.3) at -20°C until use.

After 5 hours incubation with hepatocyte plating media, cells were washed with HBSS and then treated with Dharmacon ON-TARGETplus human CYP2B6 SMARTpool siRNA. Negative control of ON-TARGETplus non-targeting pool and untreated and vehicle controls were also included. The sequences for the siRNA are given in Table 5.2. 1.25 μl of transfection reagent Lipofectamine RNAiMAX™ was complexed with siRNA in reduced serum opti-MEM® I media for 30 minutes prior to

addition to the cells. Hepatocytes were exposed to the siRNA overnight for 15 hours before the cells were washed and replaced with standard hepatocyte maintenance media. Cells were subsequently incubated at 37°C with 5% CO_2 and 95% humidity after CYP2B6 siRNA treatment. CYP2B6 metabolic activity, mRNA and protein expression were assessed at specific time points. Time 0 hours was taken at 5 hours incubation with plating media, prior to siRNA transfection and maintenance media replacement.

Table 5.2 siRNA sequences.

siRNA	Sequence
ON-TARGETplus human CYP2B6 SMARTpool	5'-GGGGAUAUGGUGUGAUCUU -3' 5'-GGGAGAUUGAACAGGUGAU -3' 5'-UGCAGGAAAUCAAUGCUUA -3' 5'-AAACAUCUCUAAAGCCUGA -3'
ON-TARGETplus Non-targeting pool	5'-UGGUUUACAUGUCGACUAA-3' 5'-UGGUUUACAUGUUGUGUGA-3' 5'-UGGUUUACAUGUUUUCUGA-3' 5'-UGGUUUACAUGUUUUCCUA-3'

5.2.5 CYP2B6 mRNA knockdown quantification

Total RNA was isolated with TRIzol® reagent using the protocol described in 4.2.5.1 and cDNA was synthesised from the isolated RNA as described in 4.2.5.2 with Taqman® reverse transcription kit.

The magnitude of siRNA knockdown at each incubation time-point was determined by quantifying CYP2B6 mRNA expression relative to housekeeping gene GAPDH by qPCR. The protocol is as follows: a 25 µl reaction mix consisting of 1.25

µl of 20X Taqman® custom gene CYP2B6 (assay ID, Hs04183483_g1) or GAPDH (Hs02758991_g1) assay, 40 ng cDNA in 8 µl, 3.25 µl RNase free water and 12.5 µl of 2X Taqman® Master Mix were dispensed into a 96-well plate. All samples were completed in triplicate. Negative controls with RNase-free water added in place of cDNA were also included. The plates were then covered with Microseal® adhesive PCR plate sealing film and centrifuged briefly up to 2000 rpm to mix the reaction contents to eliminate air bubbles from the solution mix. PCR conditions were run at 95°C for 10 min, followed by 40 cycles of 95°C for 15 s and 60°C for 1 min.

Determination of the relative CYP2B6 mRNA expression against GAPDH was performed in an Opticon2™ Fluorescence Detector (MJ Research, UK). The cycle threshold [C(t)] was set to ignore any aberrant fluorescence to ensure that only gene amplification was measured. Data was normalised to the primary hepatocyte vehicle control or untreated control sample collected at time 0 (T0) and relative expression was derived using the Pfaffl method (Pfaffl 2001) as described in 4.2.5.4.

5.2.6 CYP2B6 protein quantification

5.2.6.1 Protein extraction and quantification

Cellular protein was extracted using CelLytic™ M lysis buffer with extraction protocol as described in 4.2.6.1(ii). Quantification of the extracted protein was determined by Bradford assay as explained in 4.2.6.2.

5.2.6.2. Protein detection by Western blotting

20 µg of total protein, as determined by Bradford assay, and CYP2B6 BACULOSOMES® plus reagent (positive control) was added to 5 µl of 4X NuPAGE® LDS sample buffer, 2 µl of NuPAGE® reducing agent and made up to 21 µl volume using deoinised water. Samples were heated at 100°C for 5 min. 20 µl of

sample and 3 µl of Kaleidoscope™ prestained protein standard (Bio-Rad, UK) were loaded onto a NuPAGE® 4-12% Bis-Tris Gel with 200 µl NuPAGE® antioxidant and electrophoresed for 1 hour 30 min at 150 V. Following electrophoresis, the proteins were blotted onto a nitrocellulose membrane using a Criterion™ blotter method (Bio-Rad, UK) run at 30 V for 60 min.

After protein transfer, the membrane was blocked in 5% BSA in 0.01% Tween-tris buffered saline (T-TBS) for 2 hours RT, washed with 0.01% T-TBS solution 3 times for 5 min, followed by incubation with primary antibody anti-cytochrome P450 2B6 (ab198870 at 1/500, ab140609 at 1/1000 or VMA00171 at 1/1000 dilution) in 2% BSA in 0.01% T-TBS overnight at 4°C. The following day, the membrane was washed 3 times with 0.01% T-TBS for 5 min then incubated with secondary antibody (goat polyclonal to rabbit IgG [ab97080] at 1/2000 corresponding to ab198870 and ab140609 or goat polyclonal secondary antibody to mouse IgG, [STAR207P] at 1/5000 corresponding to VMA00171) in 2% BSA in 0.01% T-TBS for 2 hours at 4°C. For detection of loading control GAPDH, the membrane was blocked with 10% BSA in 0.01% T-TBS overnight at 4°C. The following day, membranes were washed 3 times with 0.01% T-TBS for 5 min before incubation with primary antibody (anti-GAPDH antibody, ab181602) at 1/10,000 in 2% BSA in 0.01% T-TBS for 2 hours at 4°C. After primary antibody incubation, membrane was washed 3 times with 0.01% T-TBS for 5 min prior to incubation with secondary antibody (goat polyclonal to rabbit IgG, ab97080) at 1/10,000 in 2% BSA in 0.01% T-TBS for 1 hour RT. Following incubation with secondary antibodies, membranes were washed 3 times in 0.01% T-TBS for 5 min followed by 2 times for 20 min.

Between the detection of each protein, the membrane was stripped and re-probed. After enhanced chemiluminescence (ECL) detection of CYP2B6 protein,

membranes were washed for 5 min in 0.01% T-TBS, then 2 times 20 min with acidic glycine stripping buffer, followed by 2 times 10 min 1X Tris-buffer saline (TBS) solution and 2 times 10 min 0.01% T-TBS. The membranes were then blocked and probed for the GAPDH control protein, as indicated above.

Protein bands were visualised by ECL detection. Following the final wash, the membrane was blotted dry and incubated with 3 ml Luminata™ Forte Western Horseradish Peroxidase (HRP) substrate solution for 5 min. Excess substrate was drained and membrane placed under plastic wrap. Detection was carried out in the dark room where an X-ray film was placed on the blot and the film was exposed between 10-600 s for CYP2B6 and GAPDH protein band detection. The X-ray film was then placed in a developing solution for approximately 30 s for the image to appear before immersing in fixing solution for 30 s followed by water for 30 s. Quantification of protein bands were achieved using GS-800™ calibrated densitometer (Bio-Rad, Hercules, CA) and ImageJ software (NIH). Relative protein quantification was determined by normalising CYP3A4 band against GAPDH loading control band density.

5.2.7 CYP2B6 activity assessment by P450™ Glo assay

CYP2B6 are reported to be lowly expressed at around 2-10% of total hepatic CYP abundance (Wang & Tompkins 2008), thus in anticipation of insufficient probe metabolite formation detectable by UV-HPLC, CYP2B6-Glo™ assay was employed to act as comparison to probe substrate activity assays. 3 M salicylamide stock was prepared in DMSO, as and stored at -20ºC until use. Salicylamide was added to inhibit phase II conjugation of the CYP2B6-metabolised product.

Primary human hepatocytes were seeded at 1 x 10^5 cells per well in 24-well collagen-coated plates and treated with siRNA. At 0, 12, 24, 36, 48 and 60 hours post siRNA dosing, CYP2B6 activity was determined using the P450™ Glo assay (Promega, UK). At these incubation time points, the culture medium was removed and cells were washed twice with 500 µl HBSS, then 3 µM of luciferin-2B6 (1 in 1000 dilution) containing 3 mM salicylamide dissolved in HBSS was added to each well and incubated for 90 min at 37°C with 5% CO_2 and 95% humidity, according to manufacturer's instructions. Untreated, vehicle-treated and no cell controls were included. Luciferin detection reagent was equilibrated to RT and made up to 1:1 of reconstitution buffer and detection reagent supplied by the kit. 150 µl of the incubated media containing luciferin-2B6 and salicylamide was transferred to a new opaque 24-well plate and 150 µl of the luciferin detection reagent was added to the media. The plate was then left to incubate for 20 min at RT in the dark prior to reading luminescence on a CLARIOstar® microplate reader (BMG LABTECH, Aylesbury, UK). The background luminescence (no cell control) value was subtracted from all treated and untreated conditions containing primary human hepatocytes.

5.2.8 Assessment of CYP2B6 activity by probe substrate turnover

5.2.8.1 Buproprion probe substrate dosing

Bupropion hydrochloride and (2S,3S)-hydroxybupropion were dissolved in HPLC grade 100% methanol to form a stock solution at 100 mM that was stored at -20°C until use. The probe substrate for CYP2B6 activity was 500 µM bupropion prepared in hepatocyte maintenance media in <0.5% methanol. The bupropion probe concentration used was described previously (Levy et al. 2015; Zhang et al. 2016). In the final 2 hours of incubation in control and siRNA-treated samples, cells were

spiked with bupropion to a final concentration of 500 μM and incubated for 2 h at 37°C with 5% CO_2 and 95% humidity. CYP2B6 activity was measured as (2S,3S)-hydroxybupropion metabolite formation following incubation with bupropion at 0, 12, 24, 48 and 60 hours after siRNA transfection. After 2 h incubation with bupropion, the media was removed and immediately stored at -80°C until analysis, to terminate further metabolism.

5.2.8.2 Metabolite extraction from media matrix

Two approaches for hydroxybupropion extraction from hepatocyte culture media was carried out to determine a suitable method for maximum recovery; the first involved using a range of organic solvents and the second included a protocol modified from Loboz et al. (2005).

In the first approach, 1 ml of organic solvent including methanol, ACN, ethyl acetate, acetone or heptane were added 5:1 v/v to 200 μl of metabolite-containing media sample. The samples were then mixed on a turntable for 30 min at RT followed by centrifugation at 13,000 x g for 30 min at 4°C. The metabolite-containing supernatant fraction was removed and transferred to a 5 ml round-bottom glass tube. The supernatant fraction was dried overnight with no heat in a Savant SpeedVac rotary evaporator (Thermo Scientific, UK). The resulting dried compounds were reconstituted in 150 μL mobile phase A with 20% acetonitrile v/v.

The second approach involved adding 100 μl of 0.5 M carbonate buffer (pH 10.8) with 1.5% isoamyl alcohol and 1 ml heptane to 400 μl of media sample. The samples were vortexed for 20 s, mixed on a turntable for 20 min and followed by centrifugation at 1,500 x g for 15 min. The organic supernatant layer was transferred to a new 1.5 ml Eppendorf tube containing 100 μl of 0.1 M HCl. The samples were then vortexed for 20 s, mixed on a turntable for 20 min and centrifuged at 1,500 x g,

as before. The organic supernatant layer was then discarded and the drug-containing aqueous layer was transferred to a 5 ml round-bottom glass tube and dried in a Savant SpeedVac rotary evaporator (Thermo Scientific, UK) overnight with no heat. The dried compounds were reconstituted in 150 µL mobile phase A (with 20% ACN v/v) and 100 µL was injected into a Dionex HPLC system (Thermo, UK).

5.2.8.3 Metabolite quantification by UV-HPLC

Bupropion and (2S,3S)-hydroxybupropion were chromatographically separated and quantified by HPLC-UV. 100 µL of reconstituted sample was injected into a Dionex HPLC system (Thermo, UK). Two mobile phases were used for the chromatographic run and the run was conducted using a using a multi-step gradient with a reverse-phase Fortis® column (3 µM, C18, 100 x 4.6 mm; Fortis® Technologies Ltd., Neston, UK). The conditions were as follows:

Mobile phase A	80% 10 mM KH_2PO_4 in ddH_2O, 20% ACN, pH 5.5
Mobile phase B	100% ACN
Wash	50% H_2O, 50% MeOH
Internal wash reservoir	100% H_2O
Flow rate	1 $ml.min^{-1}$
Injection volume	100 µl
Run time	8.1 min
Retention time of (2S,3S)-hydroxybupropion	4.22 min
Detection wavelength	214 nm

The gradient mobile phase run conditions are as follows:

Time (min)	Mobile phase A (%)	Mobile phase B (%)
0.0	80	20
0.5	80	20
5.0	40	60
5.0	20	80
7.0	20	80
7.1	80	20
8.1	80	20

Calibration curves were prepared with 10 concentrations including blank media with no drug and a range of (2S,3S)-hydroxybupropion concentrations between 0.02-20 μM. A linear calibration curve with $R^2 \geq 0.999$ was required for the assay run to be deemed acceptable. Precision and accuracy were determined using 3 sets of quality controls (QCs; including low, 0.1 μM; medium, 0.5 μM and high, 3 μM) in each run, on 3 consecutive days. The average recovery of (2S,3S)-hydroxybupropion was determined by comparing peak area of the drug extracted from 3 QCs against samples directly injected with no extraction procedure taken to be 100%. The recovery for (2S,3S)-hydroxybupropion was calculated at >90% in all replicates for the extraction method using carbonate buffer and isoamyl alcohol (method 2).

5.2.9 CYP2B6 k_{deg} and $t_{1/2}$ calculations and statistical analyses

CYP2B6 k_{deg} and $t_{1/2}$ were calculated as detailed in 4.2.8. Statistical analyses were carried out using GraphPad Prism software.

5.3 Results

5.3.1 Inducibility of CYP2B6 mRNA in HepG2 and Caco-2 cell lines

CYP3A4 and CYP2B6 mRNA were not detected in HepG2 cells after 24, 48 and 72 h incubation with RIF and PB despite detection of GAPDH across all conditions. CYP3A4 and CYP2B6 mRNA was detected across all time points in untreated samples of primary human hepatocytes.

CYP3A4 mRNA was not detected in Caco-2 cells after incubation with RIF and PB over 72 h. Low levels of CYP2B6 mRNA expression was observed in Caco-2 after 48 h incubation with RIF and PB at all concentrations as shown in Figure 5.1. Interestingly after 72 h of culture, CYP2B6 was detected at low levels in untreated and 1% MeOH treated Caco-2 cells.

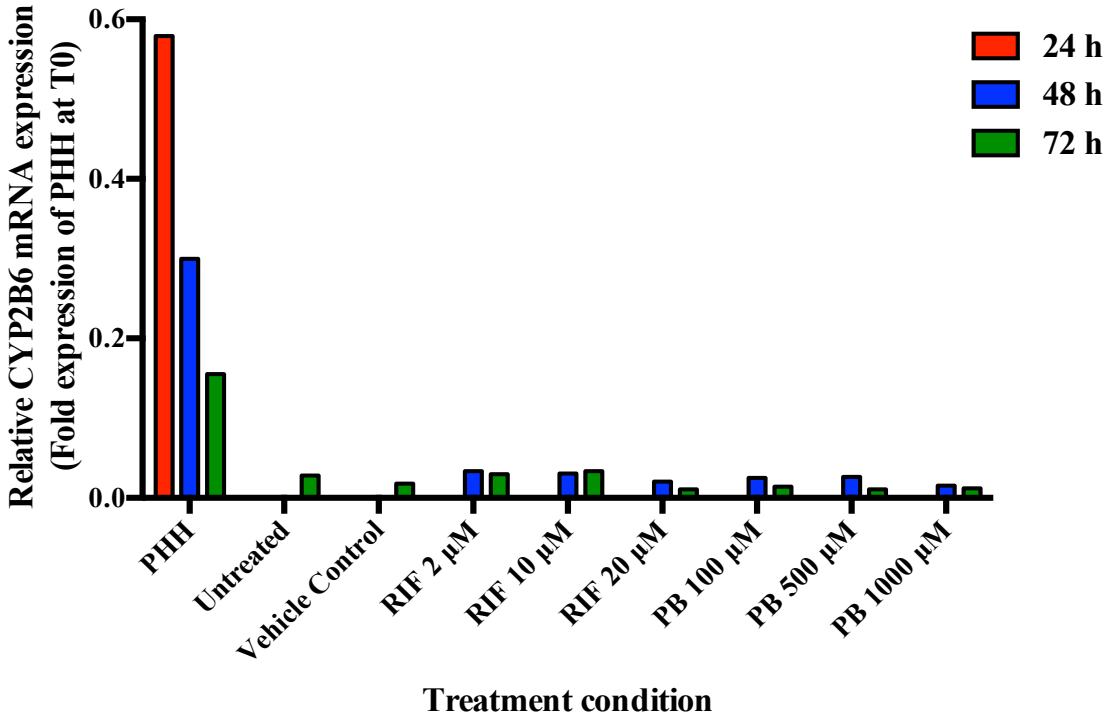

Figure 5.1 Relative induction of CYP2B6 mRNA in Caco-2 cell line after treatment with RIF and PB over 72 h. Data analysed by Pfaffl method and expressed as the mean fold expression relative to primary human hepatocyte (PHH) obtained at time 0. Positive control is untreated PHH collected at each incubation time-point. N=1 independent experiment with 3 technical replicates.

5.3.2 Optimisation of HPLC-UV conditions for (2S,3S)-hydroxybupropion detection

Two extraction methods were employed to determine the maximum recovery of (2S,3S)-hydroxybupropion metabolite from Willam's E primary human hepatocyte maintenance culture medium. A higher percentage of recovery was achieved with Method 2 (protocol adapted from Loboz et al 2005) compared with Method 1 even at lower concentrations, as shown in Table 5.3. Therefore, Method 2 was employed for all subsequent (2S,3S)-hydroxybupropion metabolite extraction for HPLC-UV detection for CYP2B6 activity analysis. Method 2 consistently gave over 100% recovery at all three concentrations, which suggests possible differences in compound stability between control standards and etracted samples. However the maximum variance from the 100% recovery value was observed at the low QC at 114.8%, which was within the acceptable limits of 15% variation to account for human error.

Table 5.3. (2S,3S)-hydroxybupropion extraction efficiency from William's E medium using two methods of extraction.

Recovery (%)				
Method 1 (N=1)	**Organic Solvent**	**Low (0.5 µM)**	**Medium (3 µM)**	**High (10 µM)**
	Acetone	N/A	114.0	79.5
	Heptane	36.7	44.3	33.8
	Ethyl acetate	73.9	58.5	46.2
	Methanol	N/A	108.1	97.7
	Acetonitrile	N/A	119.8	96.0
Recovery (%)				
		Low (0.1 µM)	**Medium (0.5 µM)**	**High (3 µM)**
Method 2 (N=3)		114.8 (±12.7)	108.8 (±1.6)	104.9 (±3.1)

The standards extracted from primary hepatocyte maintenance media using Method 2 showed good linearity over the concentration range of 0.02 to 20 µM ($R^2 \geq 0.999$) for (2S,3S)-hydroxybupropion. As the bupropion parent drug was detected simultaneously with (2S,3S)-hydroxybupropion metabolite to determine level of CYP2B6 activity in hepatocyte cultures, a clear separation between the two drug peaks was required. Figure 5.3 shows a representative chromatogram in the co-detection of buproprion and metabolite and a representative calibration curve for (2S,3S)-hydroxybupropion.

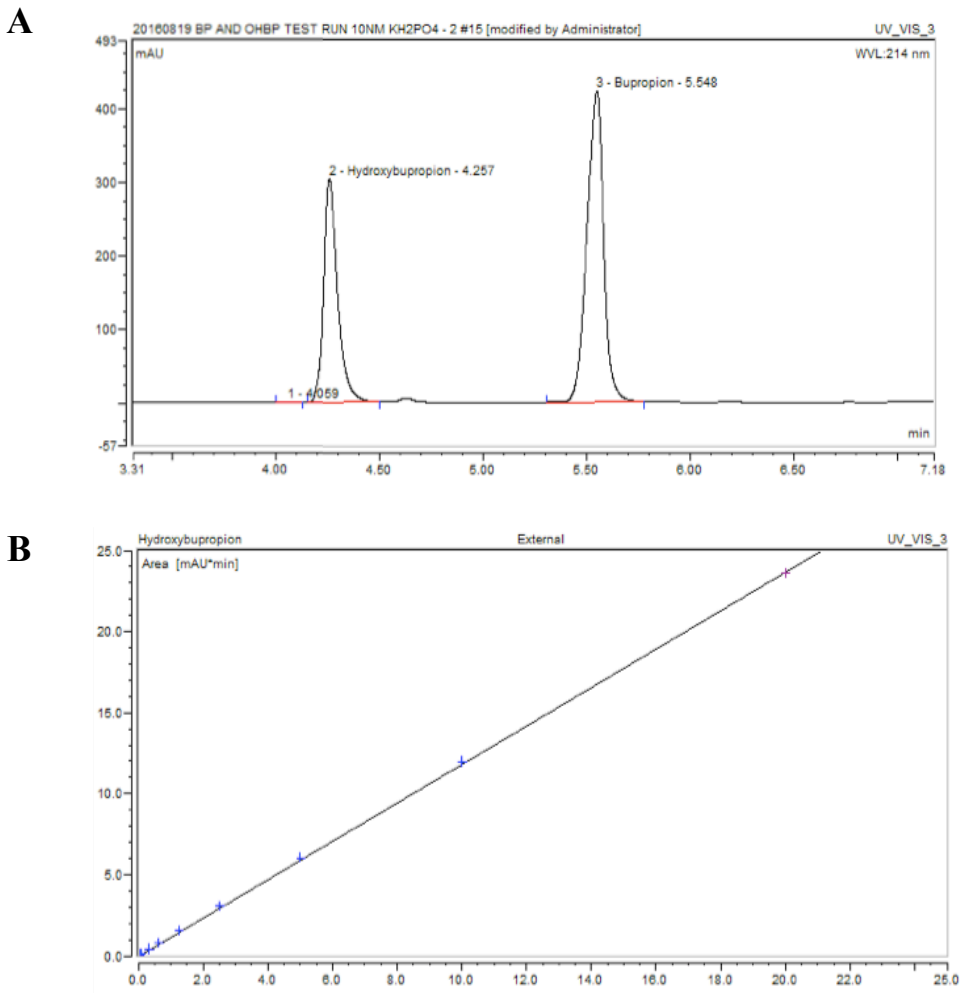

Figure 5.3 A. Representative chromatogram for the co-detection of bupropion and (2S,3S)-hydroxybupropion. **B.** Representative calibration curve of extracted standards of (2S,3S)-hydroxybupropion over the concentration range of 0.02 to 20 µM.

Precision and accuracy of the (2S,3S)-hydroxybupropion detection assay were assessed and the percentage deviation are shown in Table 5.4 for each individual run. The percentage error of accuracy and precision was below 15% for all 3 repeats at all 3 QC concentrations.

Table 5.4 shows the accuracy and precision of 3 repetitions of the assay. Accuracy and precision were assessed in triplicate at 3 levels at low (0.1 μM), medium (0.5 μM) and high (3 μM).

	Low QC (0.1 μM)	**Medium QC (0.5 μM)**	**High QC (3 μM)**
Assay 1			
Amount detected (μM)	0.09	0.51	3.01
Variance of accuracy (%)	-13.00	2.12	0.50
Variance of precision (%)	13.51	7.41	6.18
Assay 2			
Amount detected (μM)	0.11	0.52	3.18
Variance of accuracy (%)	10.27	4.89	5.91
Variance of precision (%)	2.68	1.34	1.73
Assay 3			
Amount detected (μM)	0.11	0.51	3.01
Variance of accuracy (%)	8.50	2.05	0.48
Variance of precision (%)	8.75	1.37	4.53

5.3.3 Inducibility of CYP2B6 activity in Caco-2 cell lines

CYP2B6 probe substrate metabolite was not detectable in Caco-2 cells with HPLC-UV after induction with 10 μM RIF for 72 h (data not shown), despite this treatment condition generating the highest level of CYP2B6 mRNA expression detected, as shown in Figure 5.1. The Caco-2 cell line was therefore inappropriate for use in optimising CYP2B6 activity detection by HPLC-UV for subsequent siRNA investigations. However, minor CYP2B6 enzyme activity was detected in Caco-2 cells by the P450-Glo™ assay in untreated and induction with 10 μM RIF treatment conditions as shown in Figure 5.4.

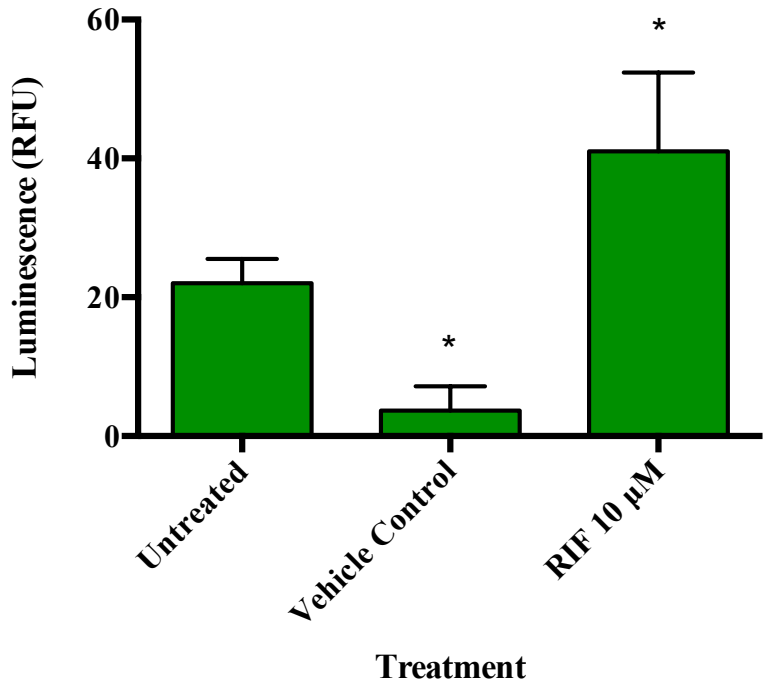

Figure 5.4. Effect of RIF on CYP2B6 enzyme activity in Caco-2 cell line determined by P450-Glo™ assay. Caco-2 cells were seeded at 3 x 10^5 per well and incubated with 10 μM RIF for 72 h. CYP2B6 P450-Glo™ assay was conducted to determine CYP2B6 activity. Data shows mean ± SD of three replicates from one independent experiment corrected for background luminescence, where *P<0.05 compared with untreated cells.

5.3.4 Optimisation of mRNA knockdown time-course and siRNA dosage

Primary human hepatocytes were treated with varying concentrations of CYP2B6 siRNA for 15 h and then incubated over 120 h to determine the achievable level of mRNA knockdown and the optimum time-course for prolonged knockdown after a single dose of siRNA. CYP2B6 mRNA expression declined over time without any siRNA treatment, as shown in Figure 5.5. This decline in untreated primary human hepatocytes was utilized to calculate k_{deg} in subsequent experiments.

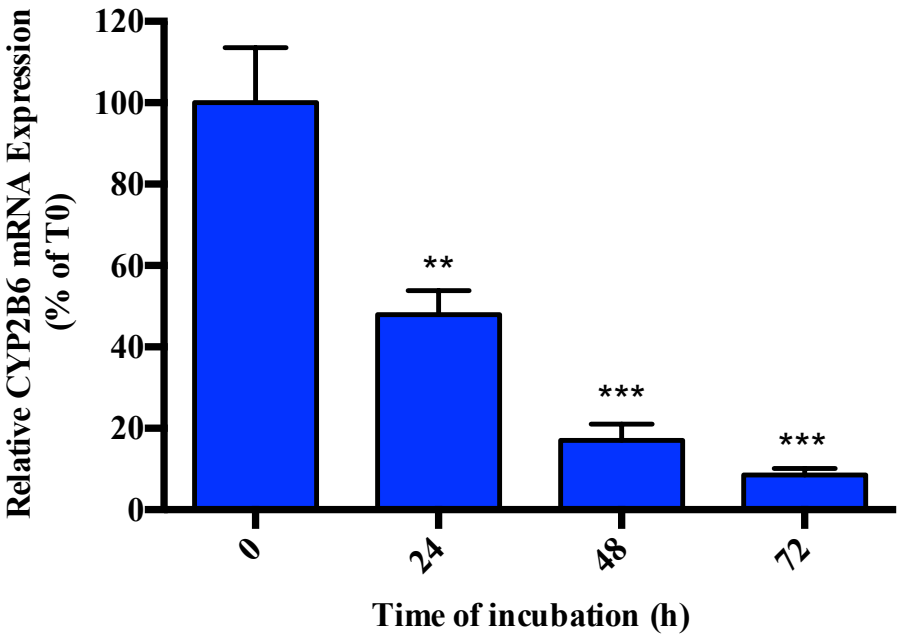

Figure 5.5 Relative CYP2B6 mRNA expression in untreated samples incubated over 72 h. Cryopreserved primary human hepatocytes (Hu1824) were seeded at 1 x 10^5 per well and incubated over 72 h with culture medium replaced every 24 h. Relative CYP2B6 mRNA expression was calculated by Pfaffl method and expressed as percentage expression of hepatocytes at time 0 with mean ± SD across 3 technical replicates with N=1 independent experiment. Unpaired t-test was performed between each incubation time point and T0 where *P<0.05, **P<0.01 and ***P<0.001.

Figure 5.6 shows that in optimisation experiments a statistically significant level of mRNA knockdown was achieved with CYP2B6-targeting siRNA. Over 50% CYP2B6 mRNA knockdown was detected in hepatocytes between 48-72 h incubation at all siRNA concentrations, with the exception of 50 nM CYP2B6 siRNA at 72 h. CYP2B6 mRNA expression resumed to over 90% of corresponding untreated controls at 120 h, suggesting that at 10 and 50 nM, siRNA was no longer silencing mRNA expression after 120 h from initial dosing (data not shown). CYP2B6 mRNA expression in non-targeting control (NTC) samples remained high across all time points and siRNA concentrations; the expected high expression for control conditions confirm the validity of using siRNA for specific gene knockdown.

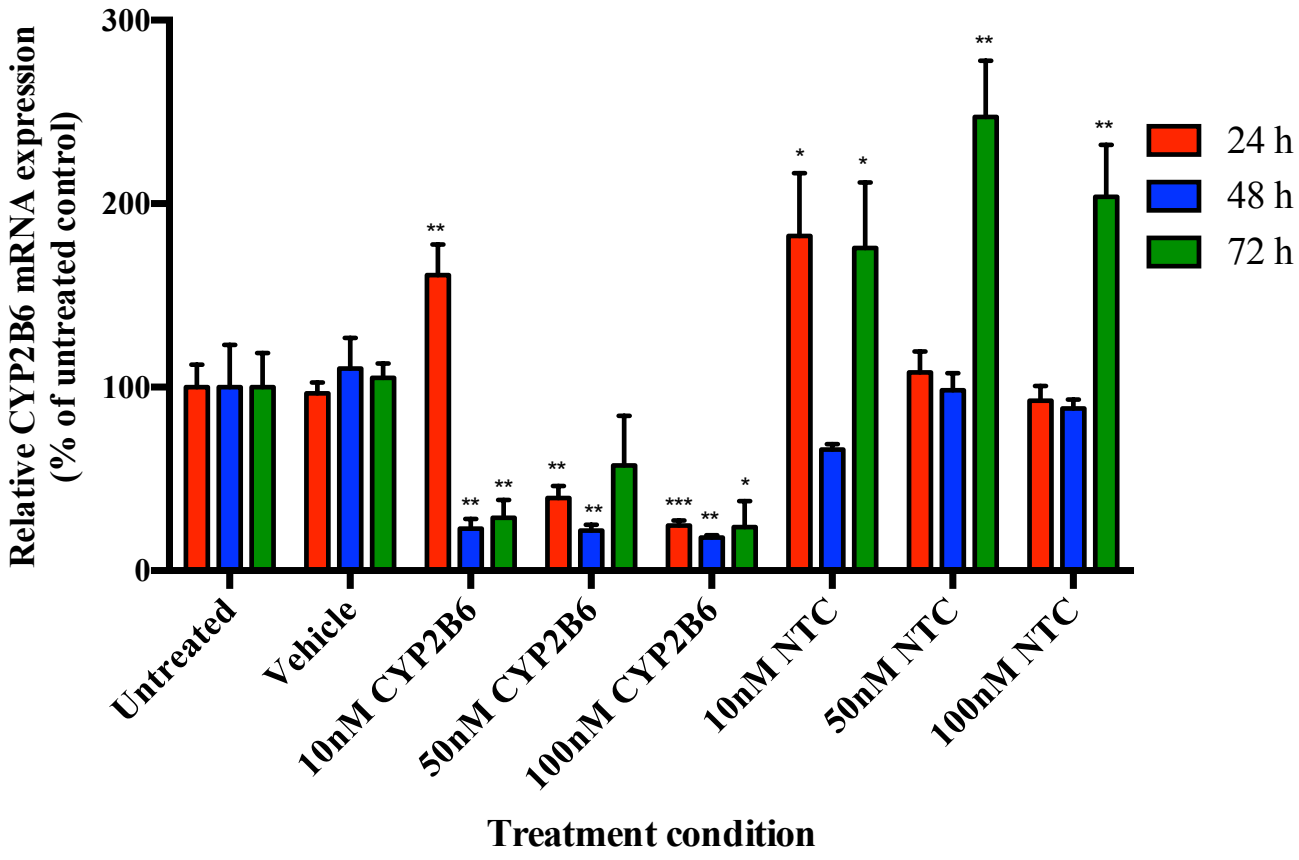

Figure 5.6 Relative CYP2B6 mRNA expression after treatment with a single siRNA dose followed by incubation over 72 h. Data was analysed by Pfaffl method and CYP2B6 expression was normalised to GAPDH. NTC refers to the non-targeting siRNA negative control. CYP2B6 mRNA is expressed as the relative expression of untreated hepatocytes at each incubation time point. Data displayed as mean ±SD from 3 technical replicates from 1 independent experiment from donor Hu1824. Unpaired t-test was performed between each treatment condition and corresponding untreated control, at each time point, where *P<0.05, **P<0.01 and ***P<0.001.

In order to optimise the siRNA concentration needed to achieve maximum mRNA knockdown, primary human hepatocytes were dosed with 10, 50 or 100 nM of CYP2B6 SMARTpool siRNA for 15 h before it was removed and cells were incubated over 120 h. Figure 5.7 shows that 100 nM of siRNA consistently achieved over 65% mRNA knockdown across all time-points from 24-72 h incubation. At 120 h, CYP2B6 mRNA showed rebound and recovered to that of untreated control levels across all siRNA concentrations. Therefore, 100 nM CYP2B6 siRNA over the course of 60 h was selected as the optimum treatment conditions to derive CYP2B6 k_{deg} in subsequent protein and activity experiments.

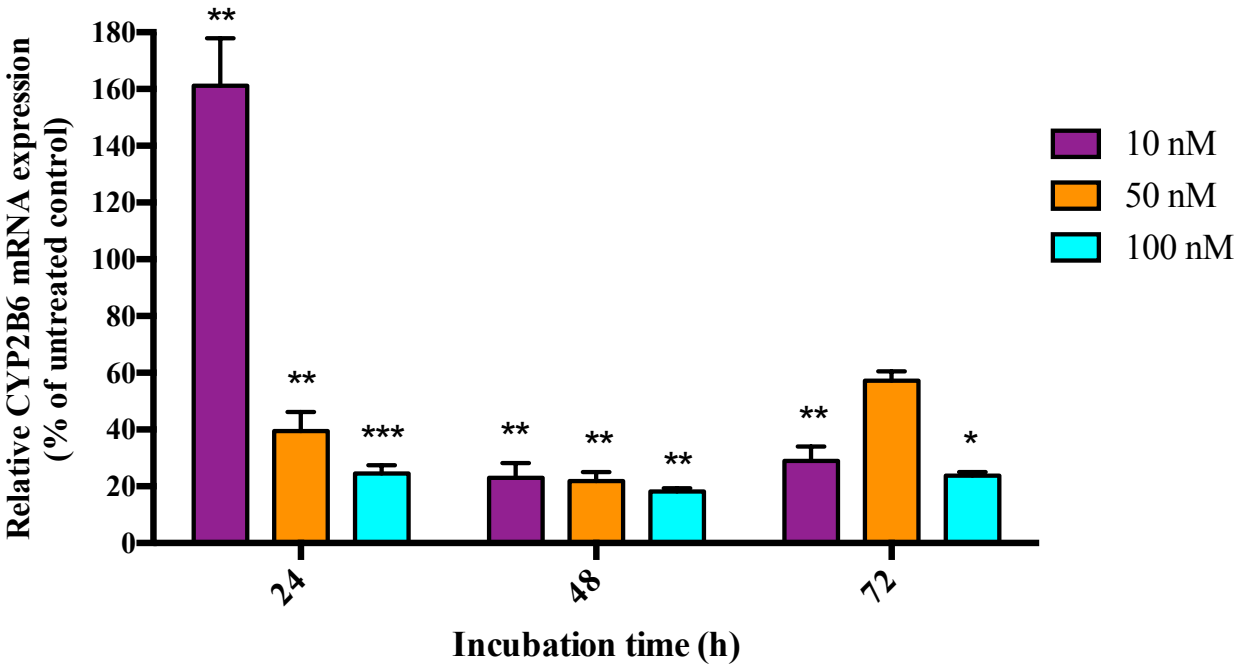

Figure 5.7 Relative CYP2B6 mRNA expression after dosing with different siRNA concentrations and incubation over 72 h. Primary human hepatocytes (Hu1824) were seeded at 1 x 10^5 cells per well and dosed with 10, 50 or 100 nM CYP2B6 SMARTpool siRNA for 15 h. siRNA was then removed and hepatocytes were incubated with culture medium over 120 h. Data expressed as relative CYP2B6 expression to GAPDH control, calculated by Pfaffl method. Expression is shown as % of untreated at each time point with mean ± SD from 3 technical replicates of 1 independent experiment. Unpaired t-test was performed between each treatment condition and corresponding untreated control, at each time point, where *P<0.05, **P<0.01 and ***P<0.001.

5.3.5 Optimisation of Western blotting for CYP2B6 protein detection

As discussed in Chapter 4, a positive control is required to identify the protein band of interest from other bands detected by non-specific binding in Western blotting. CYP2B6 BACULOSOME® plus reagent was included and blotted at 25 and 250 nl to identify the optimum concentration to use as the positive control. Figure 5.8 shows a strong protein band at around 50 kDa for CYP2B6 BACULOSOME® and this was likely to be for CYP2B6 protein expected at 56 kDa, however CYP2B6 protein was not clearly detected in primary human hepatocytes as there were no corresponding bands shown for untreated primary human hepatocytes even at time 0 where high levels of CYP2B6 would be expected. It is evident from Figure 5.8 that 25 nl of CYP2B6 BACULOSOME® reagent was the more appropriate volume to use for positive control in subsequent blots.

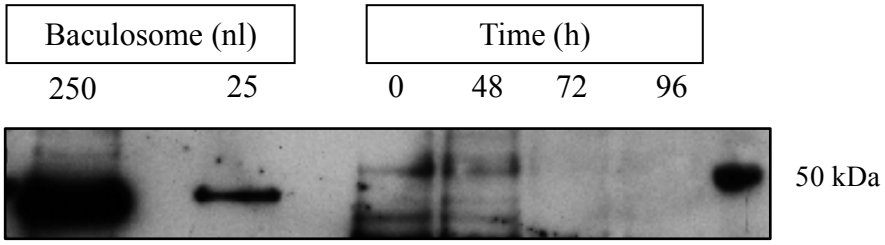

Figure 5.8 CYP2B6 protein expression in varying volumes of CYP2B6 BACULOSOME® plus reagent and in untreated primary human hepatocytes (Hu1824) incubated over 96 h. Untreated control primary human hepatocytes were incubated over 96 h time course before total protein was extracted using CelLytic™ M and quantified by Bradford assay. Protein was detected after incubation with primary anti-CYP2B6 antibody (ab198870) at 1/500 and secondary antibody (ab97080) at 1/2000 dilution.

Three different primary CYP2B6 antibodies (ab198870, ab140609 and VMA00171) were used for optimisation to blot for CYP2B6 protein. Figure 5.9 shows that no corresponding CYP2B6 protein band to the baculosome control was detected with ab198870. With the same protein sample, VMA000171 was able to detect a corresponding protein band to baculosome that displayed a reduction in abundance across time-points as expected, whereas ab140609 did not detect this. Low expression at time 0 was detected with ab140609 where the highest CYP2B6 expression was expected. VMA00171 was therefore used as the primary anti-CYP2B6 antibody for all subsequent Western blotting for CYP2B6 protein.

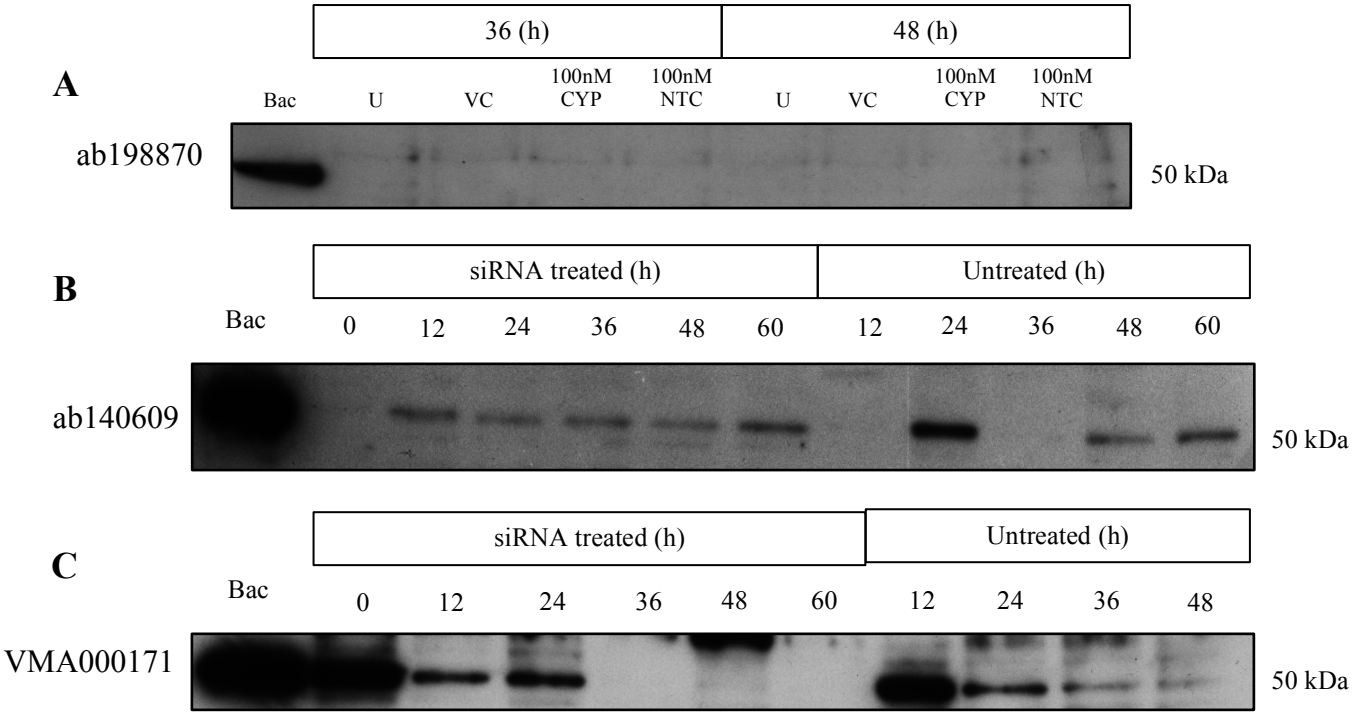

Figure 5.9 Representative Western blots showing CYP2B6 protein expression in primary human hepatocytes detected by different primary monoclonal antibodies. 250 nl baculosome (Bac) included as positive control. **A.** CYP2B6 protein detected by ab198870 antibody in hepatocytes following treatment with various siRNA and control conditions over 36 and 48 h. VC; vehicle control. **B.** CYP2B6 protein expression detected by ab140609 or **C**. VMA000171 antibody in hepatocytes following 100 nM CYP2B6 siRNA treatment or no treatment and incubated over 0-60 h.

5.3.6 Magnitude of CYP2B6 knockdown

Following incubation of primary human hepatocytes with 100 nM of CYP2B6 SMARTpool siRNA for 0-60 h, 19 (± 20.5) %, 74 (± 13) % and 97 (± 4.7) % mRNA knockdown was achieved at 12, 24 and 60 hours, respectively. Figure 5.10 shows that at 36 and 48 hours of incubation, CYP2B6 mRNA was undetectable. Incubating primary human hepatocytes for 15 h with 100 nM CYP2B6 SMARTpool siRNA showed prolonged mRNA suppression following a single dose over the course of 60 h. Figure 5.10 shows that at 60 h, CYP2B6 mRNA recovery was observed.

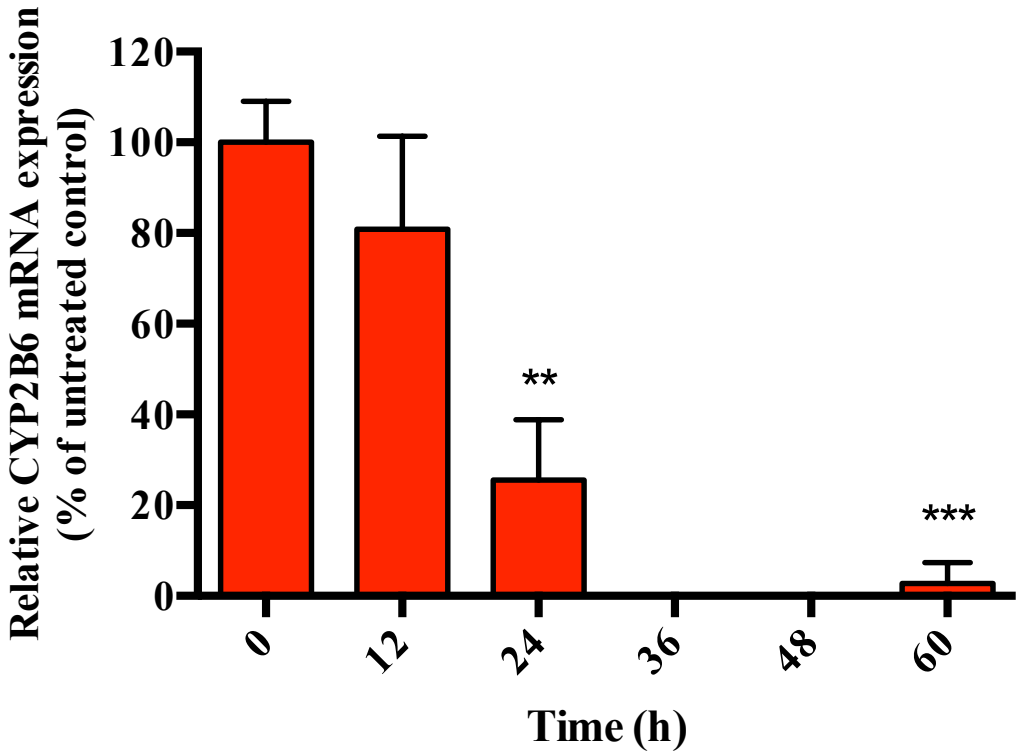

Figure 5.10 Impact of siRNA on CYP2B6 mRNA expression. Primary human hepatocytes were dosed and incubated with 100nM CYP2B6 SMARTpool siRNA for 15 h in reduced serum optiMEM™ I media. After siRNA incubation, media was replaced and cells were incubated for 12, 24, 36, 48 and 60 h in 37^{o}C 5% CO_2. CYP2B6 mRNA expression was determined by RT-PCR. The level of CYP2B6 expression is given as a percentage of untreated control at each time point and time 0 was taken after initial cell plating. Data represents mean ± SD from n=3 independent experiments. Unpaired t-test was performed between each incubation time point and T0 where *P<0.05, **P<0.01 and ***P<0.001.

5.3.7 Deriving CYP2B6 k_{deg} from protein expression after siRNA treatment

The CYP2B6 protein degradation rate constant was derived with two methods, as described in 4.3.6; from tracking protein loss in untreated hepatocytes and in siRNA-treated hepatocytes over time. The relative CYP2B6 expression normalised to GAPDH was calculated (Figure 5.11) and the protein density at each time point compared to control (T0) was fit to a linear regression model as shown in Figure 5.12. The slope was taken as the rate of degradation, which is inversely proportional to $t_{1/2}$. NTC was not included in the blot shown in Figure 5.11A because there were not enough wells on the electrophoresis gel to accommodate all the NTC samples. Multiple protein bands were observed for CYP2B6 and possible explanations for this include degradation of the protein samples during handling or non-specificity of the primary detection antibody. Care was taken to reduce artefacts caused by protein degradation, including the use of protease inhibitors, keeping protein samples on ice during handling and minimising freeze-thaw cycles.

The CYP2B6 protein k_{deg} values derived by the two methods are summarised in Table 5.5. The average k_{deg} from the 3 donors derived from untreated samples was calculated to be 0.048 (± 0.031) h^{-1} and $t_{1/2}$ of 26.0 (± 26.7) h. The average k_{deg} derived from siRNA treated samples was 0.081 (± 0.009) h^{-1} and $t_{1/2}$ of 8.63 (± 0.948) h. Overall, k_{deg} derived from untreated hepatocytes resulted in a longer average half-life compared with siRNA-treated.

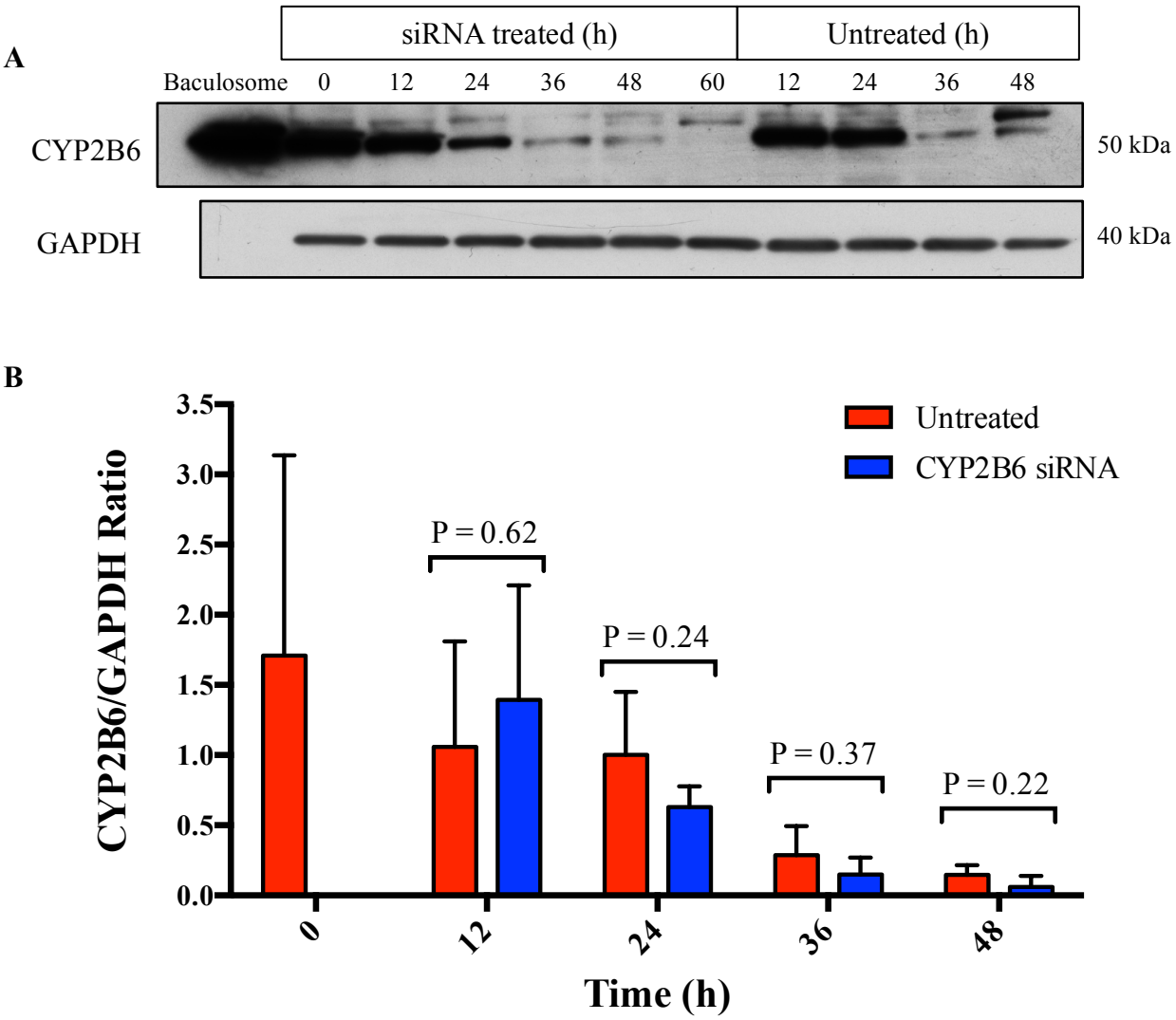

Figure 5.11 Determination of CYP2B6 degradation rate constant by protein analysis. A. Representative Western blot of donor Hu8241, CYP2B6 protein density was normalised to GAPDH. **B.** The CYP2B6 protein density ratio normalised to GAPDH shown for siRNA-treated hepatocytes and corresponding untreated control. Data represents mean ± SD of 1 replicate from N=3 donors. Unpaired t-test was performed between the siRNA-treated and corresponding untreated hepatocytes, at each time point.

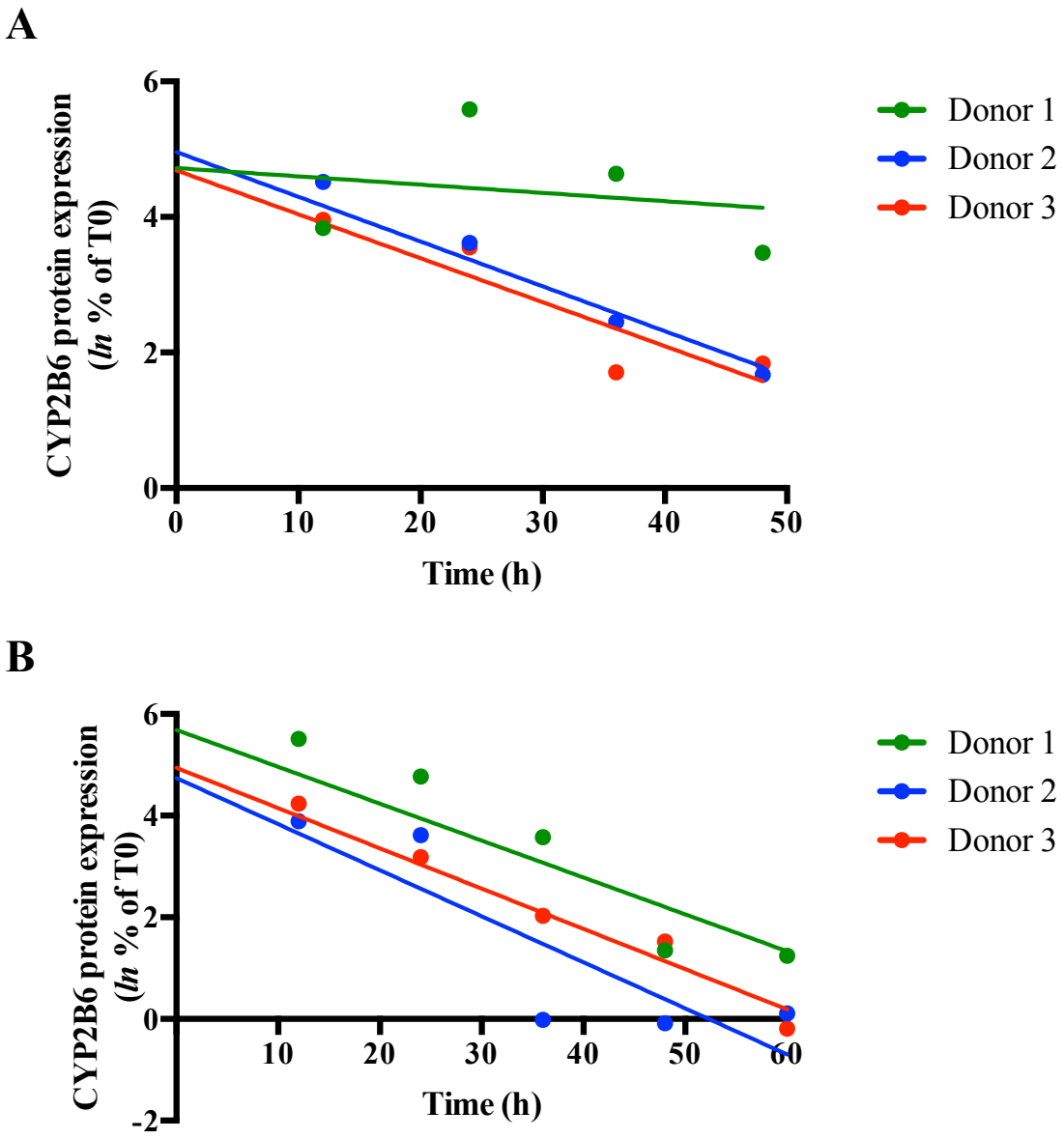

Figure 5.12. Determination of CYP2B6 degradation rate constant by protein analysis. CYP2B6 protein degradation over time was quantified by Western blot. CYP2B6 protein density was normalized to GAPDH and is expressed as a percentage of T0. **A.** CYP2B6 k_{deg} derived from untreated hepatocytes. **B.** CYP2B6 k_{deg} derived from siRNA-treated hepatocytes. The natural logarithm of the percent of T0 is given and the slope of the loss of enzyme protein expression is used to calculate the protein half-life, which is equal to the rate of degradation. Data represents 1 replicate from N=3 donors.

5.3.8 Deriving CYP2B6 k_{deg} from P450-Glo™ activity assay

CYP2B6 enzyme activity was determined by P450-Glo™ assay at 0, 12, 24, 36, 48 and 60 h incubation following initial siRNA dosing. The percentage of activity at each time point compared to T0 was fit to linear regression models (Figure 5.13) based on first-order enzyme degradation kinetics. K_{deg} was taken as the slope of the curve as described previously.

Table 5.5 shows that the average k_{deg} from the 3 donors derived from untreated samples was 0.029 (± 0.007) h^{-1} and $t_{1/2}$ of 24.6 (± 6.24) h. The average k_{deg} derived from siRNA treated samples were 0.058 (± 0.010) h^{-1} and $t_{1/2}$ of 12.3 (± 2.26) h. Overall, k_{deg} derived from untreated hepatocytes resulted in a longer average half-life compared with siRNA-treated.

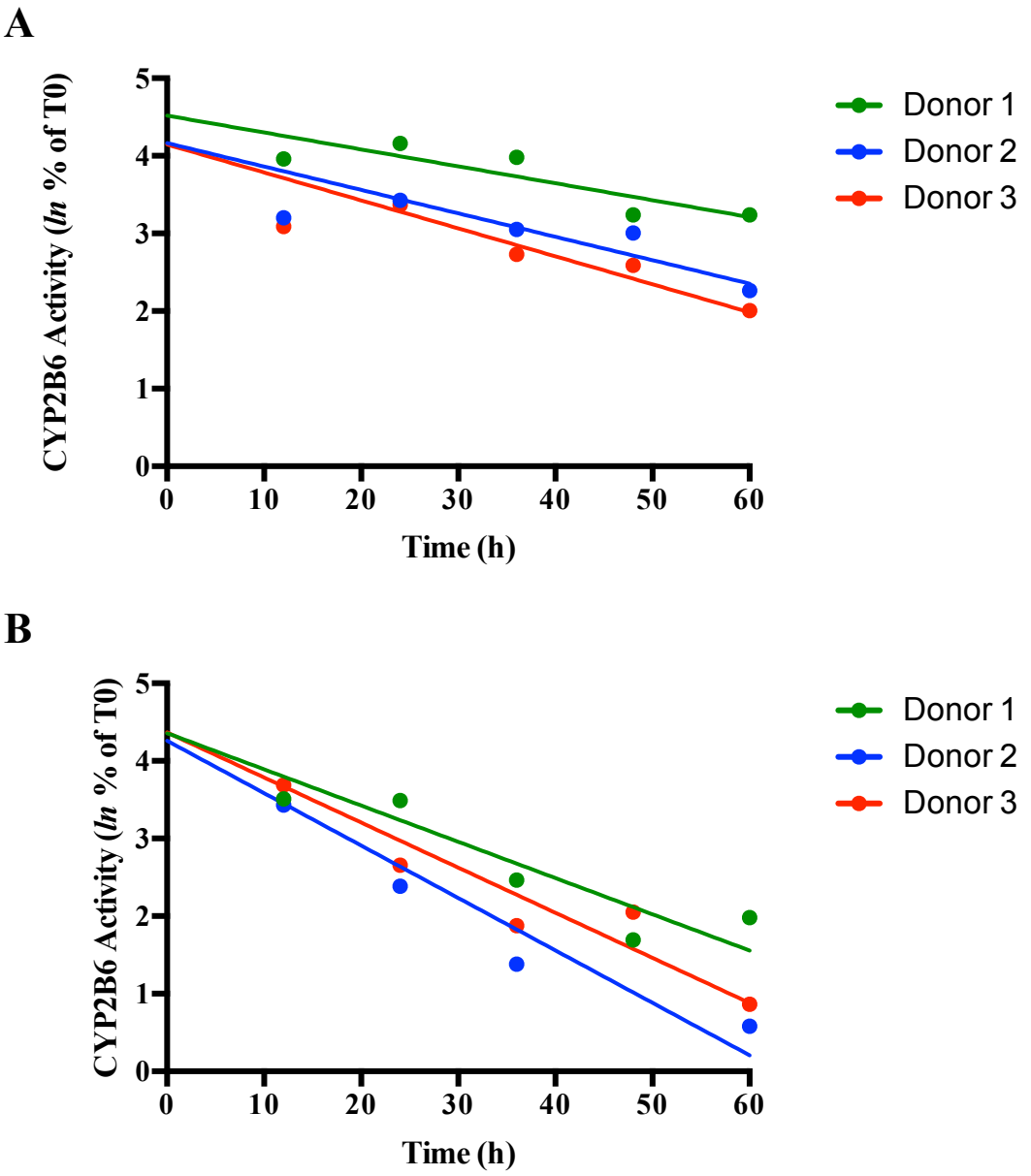

Figure 5.13 Determination of CYP2B6 k_{deg} by CYP2B6 P450-Glo™ assay. Primary human hepatocytes were treated with siRNA and incubated over 0-60 h. CYP2B6 enzyme activity was quantified by Promega CYP2B6 P450-Glo™ assay at designated time points according to manufacturer's protocol. **A.** CYP2B6 k_{deg} derived from untreated hepatocytes. **B.** CYP2B6 k_{deg} derived from siRNA-treated hepatocytes. The natural logarithm of the percent of T0 is given and the slope of the loss of activity curve is used to calculate the enzyme half-life, which is equal to the rate of degradation. Data represents 1 replicate from N=3 donors.

5.3.8 Deriving CYP2B6 k_{deg} from probe substrate metabolite formation

CYP2B6 activity was measured by bupropion probe substrate turnover. The amount of (2S, 3S)-hydroxybupropion metabolite formation was measured at 12, 24, 36, 48 and 60 hours after incubation with CYP2B6 targeting siRNA. Figure 5.14 shows that concentration of (2S,3S)-hydroxybupropion detected was lower for CYP2B6 siRNA-treated hepatocytes compared with untreated and NTC-treated. However, statistically significant differences were not detected when unpaired t-test was performed between untreated and siRNA treated conditions.

The percentage of activity at each time point compared to T0 was fit to linear regression models based on assumed first-order enzyme degradation kinetics as shown in Figure 5.15 to calculate k_{deg}. The CYP2B6 k_{deg} values were derived by tracking the decline of CYP2B6 activity in both untreated and siRNA-treated samples. The average k_{deg} from the 3 donors derived from untreated samples were calculated to be 0.036 (± 0.007) h^{-1} and $t_{1/2}$ of 15.2 (± 3.81) h. The average k_{deg} derived from siRNA treated samples were 0.062 (± 0.006) h^{-1} and $t_{1/2}$ of 11.3 (± 1.10) h. Overall, k_{deg} derived from untreated hepatocytes resulted in a longer average half-life compared with siRNA-treated.

A summary of the k_{deg} and $t_{1/2}$ values calculated from protein and activity methods are given in Table 5.5. Mean values were derived from one experimental replicate of hepatocytes from three donors.

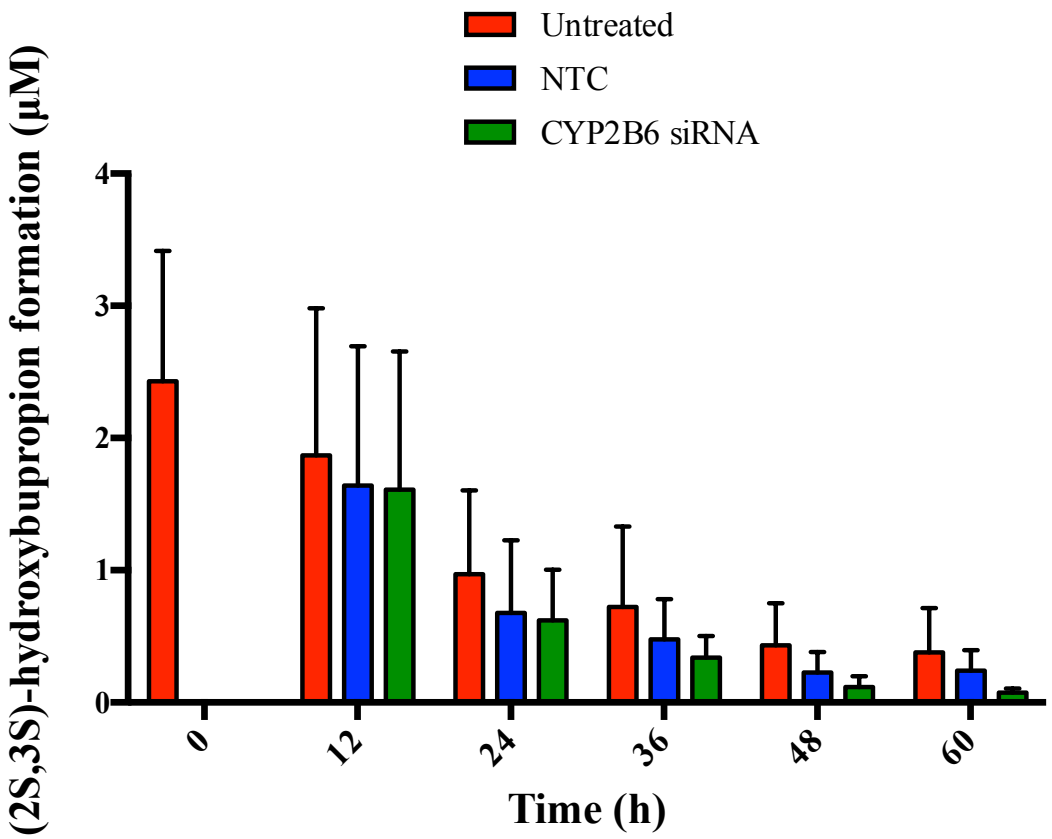

Figure 5.14 Determination of CYP2B6 activity by formation of probe substrate metabolite. Primary human hepatocytes were treated with CYP2B6 or non-targeting control (NTC) siRNA and incubated over 12, 24, 36, 48 and 60 h. Formation of (2S,3S)-hydroxybupropion after 2 h incubation with 500 µM buproprion was quanified with HPLC-UV. Data represents mean ± SD from n=3.

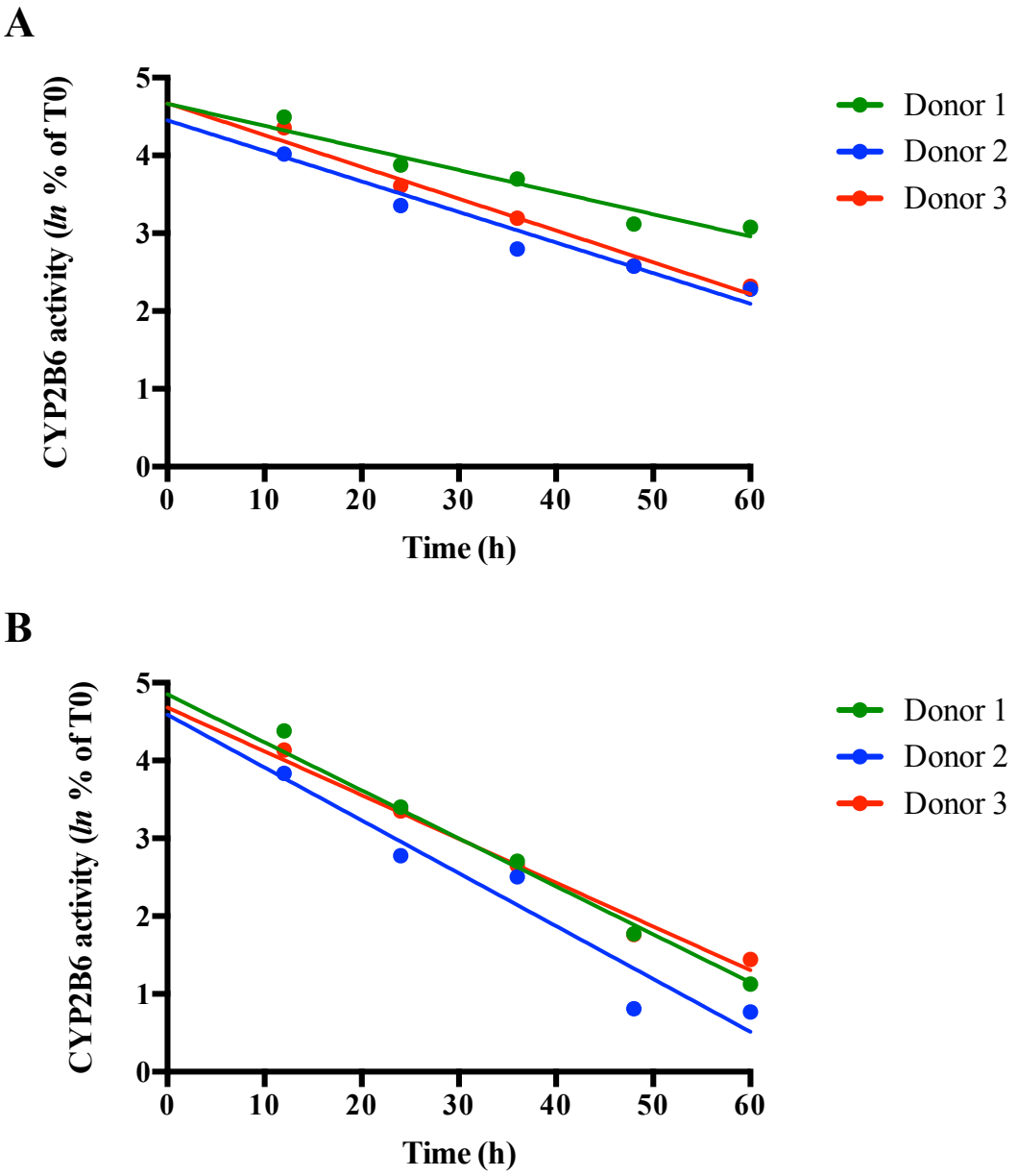

Figure 5.15 Determination of the CYP2B6 k_{deg} by (2S,3S)-hydroxybupropion formation. CYP2B6 activity was determined by formation of (2S,3S)-hydroxybupropion. CYP2B6 activity is expressed as a percentage of T0. **A.** CYP2B6 k_{deg} derived from untreated hepatocytes. **B.** CYP2B6 k_{deg} derived from siRNA-treated hepatocytes. The natural logarithm of the percent of T0 is given and the slope of the loss of enzyme activity is used to calculate the protein half-life, which is equal to the rate of degradation. Data represents 1 replicate from N=3 donors.

Table 5.5 Summary of the k_{deg} and $t_{1/2}$ values derived from protein and activity methods of analysis using untreated and siRNA treated samples.

Parameter	Donor 1	Donor 2	Donor 3
$t_{1/2}$ (h) derived from protein determined by Western blot in untreated samples	56.8	10.5	10.7
k_{deg} (h^{-1}) derived from protein determined by Western blot in untreated samples	0.0122	0.066	0.065
Average $t_{1/2}$ (h)	26.0 (± 26.7)		
Average k_{deg} (h^{-1})	0.048 (± 0.031)		
$t_{1/2}$ (h) derived from protein determined by Western blot in siRNA treated samples	9.50	7.62	8.77
k_{deg} (h^{-1}) derived from protein determined by Western blot in siRNA treated samples	0.073	0.091	0.079
Average $t_{1/2}$ (h)	8.63 (± 0.948)		
Average k_{deg} (h^{-1})	0.081 (± 0.009)		
$t_{1/2}$ (h) derived from activity determined by P450 Glo™ assay in untreated samples	31.5	23.1	19.3
k_{deg} (h^{-1}) derived from activity determined by P450 Glo™ assay in untreated samples	0.022	0.030	0.036
Average $t_{1/2}$ (h)	24.6 (± 6.24)		
Average k_{deg} (h^{-1})	0.029 (± 0.007)		
$t_{1/2}$ (h) derived from activity determined by P450 Glo™ assay in siRNA treated samples	14.7	10.2	12.0
k_{deg} (h^{-1}) derived from activity determined by P450 Glo™ assay in siRNA treated samples	0.047	0.068	0.058
Average $t_{1/2}$ (h)	12.3 (± 2.26)		
Average k_{deg} (h^{-1})	0.058 (± 0.010)		
$t_{1/2}$ (h) derived from activity determined by probe substrate metabolite formation in untreated samples	10.8	17.8	16.9
k_{deg} (h^{-1}) derived from activity determined by probe substrate metabolite formation in untreated samples	0.028	0.039	0.041
Average $t_{1/2}$ (h)	15.2 (± 3.81)		
Average k_{deg} (h^{-1})	0.036 (± 0.007)		
$t_{1/2}$ (h) derived from activity determined by probe substrate metabolite formation in siRNA treated samples	11.2	10.2	12.4
k_{deg} (h^{-1}) derived from activity determined by probe substrate metabolite formation in siRNA treated samples	0.062	0.068	0.056
Average $t_{1/2}$ (h)	11.3 (± 1.10)		
Average k_{deg} (h^{-1})	0.062 (± 0.006)		

5.4 Discussion

Accurate CYP enzyme k_{deg} values are vital for the correct prediction of time-dependent DDIs, but until now, most studies have focused on measuring the degradation rate of CYP3A4 (Table 1.3) with no consensus to the best approach. As CYP2B6 is highly polymorphic and inducible with an ever-growing list of new substrates, it is hypothesised that the enzyme has an important role in causing DDIs, especially in time-dependent induction interactions. In this Chapter, the siRNA-based methods used for deriving CYP3A4 $k_{deg,}$ which was utilised in Chapter 4, was applied to measure CYP2B6 k_{deg} with the addition of a different method of detecting CYP2B6 activity to further validate the approach.

Previous work conducted from our laboratory reported that CYP2B6 and CYP3A4 mRNA were inducible after treatment with PB for 24 h in Caco-2 and HepG2 cell lines, respectively (Martin et al. 2008). Due to the expense of using primary human hepatocytes for initial protein and activity assay optimisations (Faucette et al. 2004), HepG2 and Caco-2 cell lines were incubated with known inducer compounds RIF and PB over a time-course of 72 h with the aim of increasing CYP2B6 expression to detectable levels of protein and activity for use in experimental optimisations. After induction with RIF and PB, CYP2B6 mRNA was undetectable in HepG2 cells at all inducer concentrations and across all time-points. This was inconsistent with the findings of Choi et al. (2015) who reported 8-fold induction of CYP2B6 mRNA after treatment with PB for 24 h. Li et al. (2010) reported detectable CYP2B6 activity in HepG2 when transfected with PXR vector, whilst other studies reported little or no induction after RIF or PB treatment (Gerets et al. 2012; Westerink & Schoonen 2007). In this study, a low level of CYP2B6 mRNA expression was detected in Caco-2 cells after induction with both RIF and PB and

after culture for 72 h, however, this was not in agreement with the much higher levels of CYP2B6 induction with PB reported by Martin et al (2008). The main disparity between the protocol published by Martin et al. (2008) and the methodology used here was that a lower seeding density was used (3×10^5 vs. 5×10^6 cells) and this difference in cell numbers may well give rise to the discrepancies observed. Furthermore, protein binding was not assessed and this could impact on overall free drug concentrations able to exert effects.

Overall, insufficient levels of CYP2B6 expression was achieved after induction in both Caco-2 and HepG2 cell lines; therefore all protein and activity detection methods were optimised in primary human hepatocytes. In the wider context, Caco-2 and HepG2 are often used as cost-effective *in vitro* cell systems to study transporter activity and toxicity during human drug development (Brandon et al. 2006) but are not used for studying metabolism and PK. Caco-2 cells express many transporters representative of the *in vivo* human gut and are routinely used to study absorption (Artursson & Karlsson 1991; Angelis & Turco 2011). HepG2 cells are highly differentiated hepatoma cells that display many genotypic similarities with liver cells; they express many hepatic enzymes and are often used as screening for toxicity of parent compound during drug development (Gerets et al. 2012). Both Caco-2 and HepG2 cells are not generally used to study metabolism due to the low expression of phase I DMEs (Prueksaritanont et al. 1996; Westerink & Schoonen 2007) and caution must be exercised when using these cell systems as they may not be representative of the human situation or that of primary cells.

To date, there are only two studies that have reported a $t_{1/2}$ value for CYP2B6. Renwick et al. (2000) reported a $t_{1/2}$ of 32 h estimated based on using immunoblot detection of decreasing protein levels in human liver slices in culture from a single

donor. Dixit et al. (2016) reported a $t_{1/2}$ of 70 h and this was measured by induction of CYP2B6 in primary human hepatocytes to maximal levels then tracking the time taken to recover to basal pre-induced activity levels. The caveat to both approaches is that in order for the rates to be deemed accurate, it must be assumed that there was no further *de novo* synthesis during the time period investigated that would distort CYP abundance. The approach described in this study addresses this issue by introducing siRNA to impede *de novo* protein synthesis, thus rendering protein degradation as the rate-limiting step and therefore the loss of enzyme activity should be attributable to the $t_{1/2}$ of the specific protein measured. Interestingly, the hepatic CYP2B6 k_{deg} values derived from untreated hepatocytes by protein expression loss and activity loss measured by P450-Glo™ assay generated k_{deg} vales of 0.048 h^{-1} and 0.029 h^{-1} with $t_{1/2}$ of 26.0 h and 24.6 h, respectively, which were in reasonable agreement with values obtained by Renwick et al. (2000).

Overall, the k_{deg} values derived from untreated hepatocytes generated a longer $t_{1/2}$ value compared with siRNA treated. This is unsurprising given the purpose of using siRNA to inhibit mRNA translation and therefore reducing downstream protein translation and activity. However, it must be noted that less variability was observed for both CYP3A4 (see Chapter 4) and CYP2B6 when k_{deg} was derived from siRNA treated hepatocytes and that k_{deg} cannot be consistently derived from untreated hepatcoyes, as with CYP3A4 activity where loss over time was not observed (see Figure 4.15). Moreover, CYP3A4 k_{deg} values of 0.0189 (± 0.0043) h^{-1} and 0.0202 (± 0.0003) h^{-1} derived from siRNA treated hepatocytes in Chapter 4 were within the 0.017 - 0.028 h^{-1} range recommended by Mao et al. (2013) and closer to the recently reported k_{deg} values of 0.019 h^{-1} and 0.03 h^{-1} (see Table 1.3) which were used in PBPK models to predict TDIs. The CYP3A4 and CYP2B6 k_{deg} values derived from

untreated hepatocytes were in reasonable agreement with Renwick et al. (2000), who tracked CYP apoprotein loss in non-treated liver slices. It would appear that the siRNA treatment approach generated more accurate k_{deg} values compared with non-treated as *de novo* protein synthesis could be obscuring the true protein degradation rate. The k_{deg} values measured by all approaches ought to be incorporated into PBPK simulations of time-dependent CYP2B6 induction interactions and assessed in comparison to other available literature values, for DDI prediction accuracy to validate the physiological relevance and aid defining the best method.

Interestingly, in agreement with findings in Chapter 4, using activity analysis to derive CYP2B6 k_{deg} appeared to be the more robust method compared with quantifying protein loss by Western blotting. There was a larger variation in CYP2B6 k_{deg} calculated from protein compared to activity loss and this can be attributed to the semi-quantitative limitations of using Western blot to assess absolute protein abundance. Furthermore, there was good agreement of CYP2B6 k_{deg} 0.029 (± 0.007) h^{-1} and 0.036 (± 0.007) h^{-1} for untreated hepatocytes and 0.058 (± 0.010) h^{-1} and 0.062 (± 0.006) h^{-1} for siRNA treated hepaotyctes, derived from two different activity measurement approaches. This suggests that tracking activity loss rather than protein may be the more robust approach for measuring k_{deg}.

It should be noted that CYP2B6 is highly polymorphic and there can be large inter-individual variability in the expression and activity between donors (Zanger & Klein 2013) and this presents a limitation to the current study. Another potential limitation to our k_{deg} approach is that the quantification of a given protein with a long $t_{1/2}$ in monocultured primary human hepatocytes is likely to be problematic. Although primary human hepatocytes are regarded as the gold standard *in vitro* model for assessing drug metabolism (Gerets et al. 2012), our studies showed that after 120

hours of incubation CYP2B6 mRNA expression reduced to 7.6% (± 1.3) of the expression level at time 0 and this differential decline in CYP2B6 expression is consistent with the well-documented parallel CYP decline over time in cultured human hepatocytes (Renwick et al. 2000; Rodriguez-Antona et al. 2002; Heslop et al. 2016; LeCluyse 2001). Several studies have commented on the longevity and stabilisation of CYP expression in HepatoPac® model and indeed this model was used by Ramsden et al. (2015) and Dixit et al. (2016) to directly measure CYP k_{deg}. Thus, for proteins with $t_{1/2}$ over 120 hours an alternative liver model with prolonged CYP expression, such as the HepatoPac® model may be preferred. There are several conflicting reports regarding the expression of CYPs in monocultured primary hepatocytes. For example, Rodriguez-Antona et al. (2002) reported significant mRNA decrease (to below 20%) after 24 hours of culture whereas protein levels were detectable at 72 hours. Heslop et al. (2016) were able to detect multiple CYP mRNA expression up to 168 hours in culture. Runge et al. (2000) showed detectable CYP protein expression at 30 days of culture. It is therefore clearly difficult to define a cut-off; the current studies indicate that primary human hepatocytes can be used successfully up to 96 hours (in Chapter 4) but caution should be taken when investigating proteins beyond this time point. Where prior knowledge indicates that $t_{1/2}$ is likely to be less than 96 hours, the use of monocultured primary hepatocytes offers a cost-effective and robust approach but variability across systems and experiments warrant validation for an appropriate cut-off for each experimental set-up. In summary, a cost-effective and robust method for determination of protein degradation was validated by comparison to accepted values of CYP3A4 and employed to determine a value for CYP2B6.

CHAPTER 6

Exploring genetic polymorphisms in CYP3A4 protein degradation machinery on substrate pharmacokinetics

CONTENTS

6.1 Introduction

As discussed previously in chapter 1.6, much of what is known about the specific mechanisms of CYP3A4 protein degradation are derived from studies in *Sacchromyces cerevisae* and rat hepatocytes but there is a high degree of evolutionary conservation in degradation pathways between these systems (Wang et al. 2011). Consequently, they can be considered to provide reliable clues to the endogenous human pathways of degradation. CYP proteins are thought to undergo degradation via the ERAD-C pathway of degradation and different CYPs undergo varying degrees of ERAD/UPD or ERAD/ALD. Studies in cultured rat hepatocytes have revealed that CYP3A protein degradation occurs predominantly via the UPD pathway involving the Ub-mediated 26S proteasomal system, but the ALD pathway is likely to contribute to a smaller extent (Kim et al. 2016).

CYP3A4 is an integral monotopic type I ER-anchored protein with a cytosolic-facing haem active site that carries out oxidative reactions with a propensity to generate ROS; this makes it a model candidate for ERAD-C targeted degradation (Wang et al. 2015; Kim et al. 2016). CYP3A4 first undergoes post-translational phosphorylation by PKA and PKC protein kinases (Wang et al. 2009), followed by synergistic ubiquitination by two cytosolic E2/E3 Ub-ligase complexes: UbcH5a-CHIP-Hsc70-Hsp40 and UBC7-gp78/AMFR. Molecular recognition of CHIP substrates occurs though the Hsc70-Hsp40 co-chaperone complex (Pabarcus et al. 2009). gp78/AMFR complex recognition involves 'phosphodegrons' which are Lys residues within a negatively charged cluster of phosphorylatable DEST residues along cytosol-exposed surface loops and/or disordered regions within the CYP3A4 protein (Wang et al. 2015). Following ubiquitination by E2/E3 Ub-ligase complexes, the p97/VCP-AAA ATPase-Npl4-Ufd1 chaperone complex extracts the ubiquitinated

CYP3A4 protein from the ER membrane and translocates it to the cytosolic 26S proteasome for degradation (Faouzi et al. 2007; Acharya et al. 2011). CYP3A4's LIR motifs, which are hallmarks of ERAD/ALD, are concealed within the protein fold and have restricted cytosol accessibility for ERAD/ALD recognition. This is therefore consistent with the finding that the protein predominantly undergoes ERAD/UPD over ALD (Faouzi et al. 2007; Kim et al. 2016). A schematic for the current best hypothesis for the components involved in CYP3A4 protein ERAD/UPD pathway are shown in Figure 6.1.

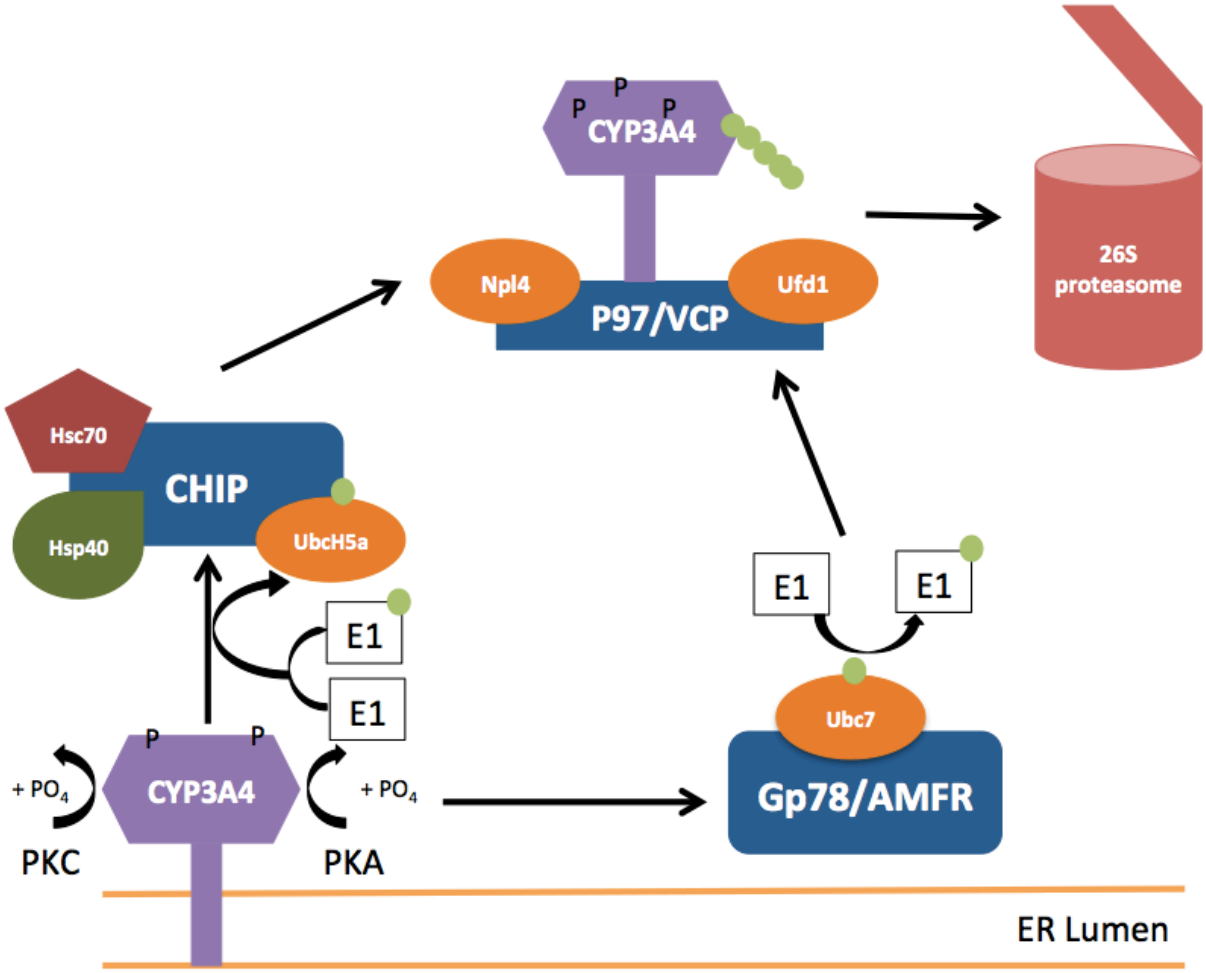

Figure 6.1 A schematic of CYP3A4 ERAD/UPD pathway of protein degradation (adapted from Kim et al 2016).

The gp78 (glycoprotein 78) protein, encoded by the AMFR gene, is an E2 ubiquitin-protein ligase that is involved in the degradation processes of not only CYP3A4, but also of human CD3D (T-cell surface glycoprotein CD3 delta chain), CFTR (cystic fibrosis transmembrane conductance regulator) and APOB (apolipoprotein B) proteins. Over 3,600 single nucleotide polymorphisms (SNPs) have been identified for the AMFR gene yet their propensity to cause drug interactions is not well studied. A handful of SNPs have been cited in published literature; Choi et al. (2011) found 3 SNPs (rs2440467, rs2432540 and rs6499837) to be significantly associated with AMFR protein expression levels. Cha et al. (2014) found rs2440472 to be associated with coronary artery disease in Chinese populations. UBE2G1 (ubiquitin-conjugating enzyme E2 G1) is the human homologue to yeast ubiquitin-conjugating enzyme E2 7 (UBC7) that has been previously found to be involved in the CYP3A4 ERAD-C pathway. Evangelou et al. recently found a significant association of UBE2G1 SNP rs9906760 with type 1 diabetes (Evangelou et al. 2014). As these SNPs identified in AMFR and UBE2G1 were likely to cause functional alterations to the gene product, it was hypothesised that these polymorphisms could potentially impact on CYP3A4 degradation.

SNPs are a single nucleotide variation within a gene sequence that can give rise to clinical interactions, by generating disease through a dysfunctional gene product or through alteration in response to drugs. For example, CYP3A4*22 has been linked to reduced hepatic expression (Okubo et al. 2013) and an altered response to statin drugs (D. Wang et al. 2011; Elens et al. 2011). CYP3A4*1B has been associated with enhanced CYP3A4 activity and affects tacrolimus PK in renal transplant patients (Shi et al. 2015). Clearly, SNPs that alter CYP3A4 expression levels can give rise to major clinical interactions, given its importance role in drug

metabolism. In theory, any SNP that elicits a significant impact on CYP3A4 protein degradation machinery may also alter its abundance and modify drug metabolism.

Atazanavir (ATV) is a protease inhibitor (PI) used in the treatment of HIV subtype 1 (HIV-1) infections. It can be administered at a dosage of 400 mg once a day (unboosted) or 300 mg coupled with 100 mg dose of ritonavir (RTV) once per day (boosted; ATV/r) in treatment naïve patients (Bristol-Myers Squibb 2003). The use of unboosted ATV is not licensed in Europe and is currently not recommended but it remains the PI of choice for special populations of patients who are unable to tolerate ritonavir, such as in the case of hyperbilirubinaemia and moderate liver insufficiency (Siccardi et al. 2012; Achenbach et al. 2011). Atazanavir is predominantly metabolised by CYP3A isoenzymes (Goldsmith & Perry 2003; Bristol-Myers Squibb Company, 2004) and therefore quantifying plasma concentrations of ATV can be an indicator of the extent of CYP3A activity correlating with treatment response. The aim of this chapter was to investigate the impact of known functional SNPs in AMFR (rs2432540 A>G, rs6499837 C>T, rs2440472 A>G and rs2440467 C>T) and UBE2G1 (rs9906760 A>G) genes on ATV plasma concentration in two cohorts of patients; one given unboosted ATV and the other ATV/r. Plasma concentrations of ATV were therefore used as a surrogate measure of CYP3A4 activity.

6.2 Materials and methods

6.2.1 Materials

TaqMan® Genotyping Master Mix and TaqMan® SNP Genotyping assays for AMFR: rs2432540 A>G (C__16014493_10), rs6499837 C>T (C__29285325_10), rs2440472 A>G (C__26354979_10) and rs2440467 C>T (C__16240734_10) and UBE2G1 rs9906760 A>G (C__29654285_20) were purchased from ThermoFisher Scientific Inc. (Loughborough, UK). 96-well polymerase chain reaction (PCR) plates and Microseal® 'B' PCR plate sealing film were obtained from Bio-Rad (Watford, UK). Nuclease-free water (W4502) was purchased from Sigma-Aldrich (Dorset, UK).

6.2.2 Patient samples

Cohort A consisted of 47 patients administered with unboosted ATV and these patients were recruited in Torino. Cohort B included 50 patients administered with RTV-boosted ATV (ATV/r) recruited in Liverpool and Torino. Inclusion criteria for cohorts were as follows: receipt of unboosted ATV (400 mg once per day) for cohort A, receipt of ATV/r (300 mg ATV with 100 mg RTV once per day) for cohort B, age > 18 years and no receipt of other drugs known to affect plasma concentrations of ATV (except tenofovir). Data for age, sex, body weight, time after dose, concomitant antiretroviral drugs and other medications were collected for both cohorts. For cohort B, the plasma ATV concentrations taken at 24 (±4) h post dose were included. Sampling was performed after written informed consent was obtained in accordance with local ethics committee instructions.

6.2.3 DNA extraction and atazanavir plasma concentration quantification

Dr Marco Siccardi previously extracted genomic DNA and quantified ATV plasma

concentrations using UV-HPLC and HPLC-MS/MS in patient blood samples, as detailed in his publications (Siccardi et al. 2012; Schipani et al. 2010). The extracted genomic DNA was stored at -20^{o}C until analysis. Upon analysis DNA was quantified using NanoDrop™ 1000 spectrophotometer (ThermoFisher Scientific Inc., Delaware, USA) to determine sample concentration and purity ratio. Only DNA samples with a 260:280 absorbance of >1.4 and concentration of >2 ng/µl were included in the analysis.

6.2.4 SNP genotyping

Real-time polymerase chain reactions (qPCR) were made up to a final volume of 25 µl per well on 96-well PCR plates. Each well consisted of 12.5 µl of 2X TaqMan® Genotyping Master Mix, 1.25 µl of 20X gene assay, 9.25 µl nuclease-free water and 2 µl of genomic DNA (at least 2 ng/µl concentration). Negative controls were included for each gene assay where 2 µl of nuclease-free water was added in place of genomic DNA. Each sample was completed in duplicates. The 96-well plates were then covered with Microseal® adhesive PCR plate sealing film and centrifuged briefly up to 2000 rpm to mix the reaction contents and to allow all reagents to collect at the bottom of the well to eliminate air bubbles from the solution mix.

Genotyping was performed using real-time PCR allelic discrimination assay on a DNA Engine Chromo4 system (Bio-Rad Laboratories, California, USA). Four AMFR polymorphisms rs2432540 A>G, rs6499837 C>T, rs2440472 A>G and rs2440467 C>T, and one UBE2G1 polymorphism rs9906760 A>G were assessed in 2 cohorts of patient samples (see Table 6.2). The PCR heat cycling protocol involved an initial enzyme activation step at 95^{o}C for 10 min, followed by 40 cycles of amplification with denaturation at 95^{o}C for 15 s, followed by final annealing at 60^{o}C

for 1 min. Allelic discrimination plots (Figure 6.2) and genotype assignments were performed using Opticon Monitor, version 3.1 (Bio-Rad Laboratories Inc., UK) according to VIC® and FAM™ fluorescence.

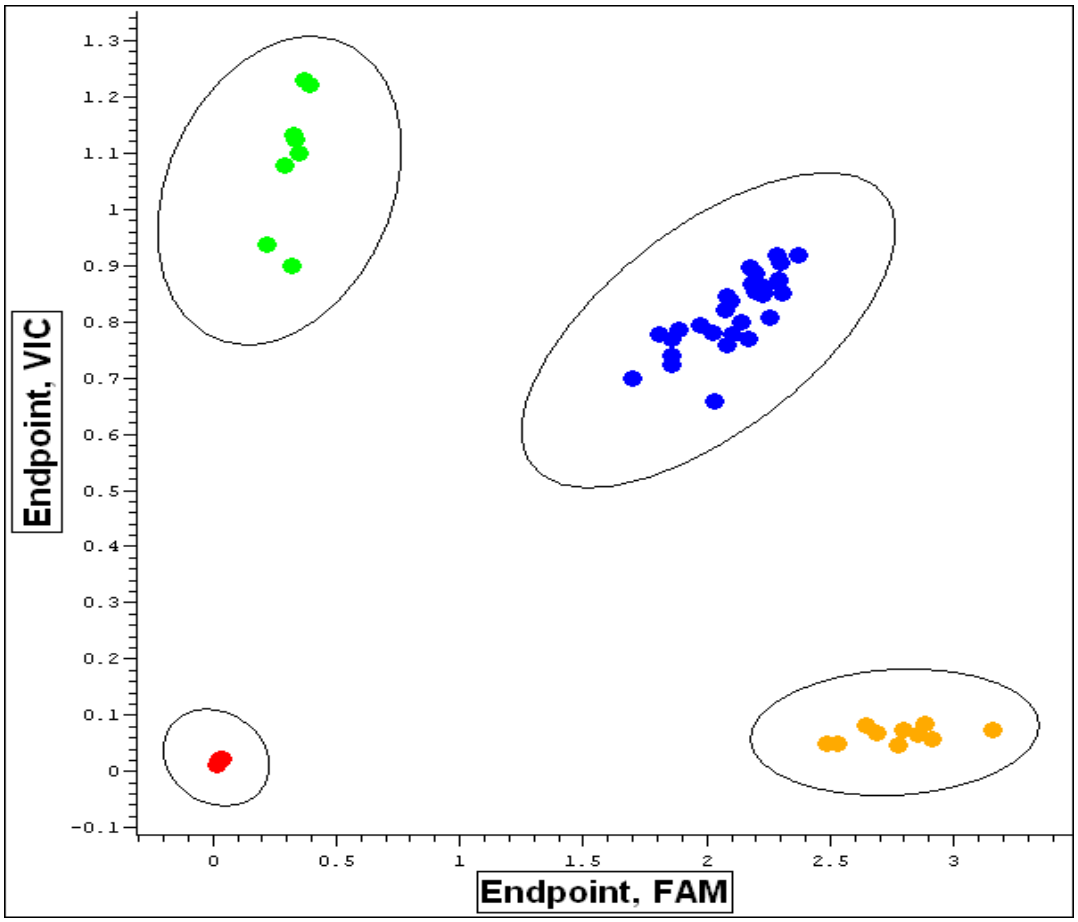

Figure 6.2 Representative allelic discrimination plot. Red dots indicate blanks with no expression. Green dots represent homozygous genotype for allele associated with VIC® dye. Blue dots represent heterozygous genotype. Orange dots represent homozygous genotype for allele associated with FAM™ dye.

Table 6.1 Applied Biosystem Assay IDs and sequence for selected SNPs (VIC® and FAM™ are TaqMan® reporter dyes)

Assay ID	SNP ID	Gene	SNP alleles	Assay sequence ([VIC/FAM])
C__16014493_10	rs2432540	AMFR	A/G	GTGTTCAGAAAAGGTTAGATTATCC**[A/G]**C CACAGAAATAAAATGAACGTTTCA
C__29285325_10	rs6499837	AMFR	C/T	CCCTTCCAGAATGGTTCTACTCTTC**[C/T]**A CTGGAGAAAACAGAAACTAAATTA
C__26354979_10	rs2440472	AMFR	A/G	GCAGTTTACAAACATACATTCTGAC**[A/G]**T ACTCTGGGATCTGCTGTTATTAAA
C__16240734_10	rs2440467	AMFR	C/T	AGCTCCCACTCATTTCAATCTACCA**[C/T]**A ATCTACTGTCCAACCCCTCGGGCA
C__29654285_20	rs9906760	UBE2G1	A/G	GGTCCTGTTGAGGTGGAAGAGTTGC**[A/G]**T GGTGTGAACACTAAATCAAGTAAG

6.2.5 Statistical analysis

All genotypes were assigned 0 or 1 binary coding based on homozygous for common allele, or carrier of at least one variant allele, respectively, for regression analyses. Patient characteristics were analysed and categorical variables were described using relative frequencies, whilst continuous variables were described using median and range. Compliance with Hardy-Weinberg equilibrium was tested by χ^2 test of observed and predicted genotype frequencies using an online Hardy-Weinberg equilibrium calculator (Rodriguez et al. 2009). The distribution of ATV plasma concentrations for both cohorts was determined individually by Shapiro-Wilk test for normality with $P<0.05$ considered significant. Categorical genotype data were compared using the Kruskal Walis one-way analysis of variance (ANOVA) and Mann-Whitney *U* test; $P<0.05$ was considered a significant association.

A univariate linear regression analysis was carried out to identify patient

demographic variables associated with mean ATV plasma concentrations. Independent variables with a P-value up to 0.2 in the univariate analysis were carried through to a multivariate stepwise linear regression analysis where $P<0.05$ was considered significant. Because no significant associations were detected for any of the demographic variables or genotypes against ATV plasma concentrations in both cohorts, further statistical analyses were not conducted. All statistical analyses were performed with SPSS Statistics Software, version 22 (IBM) and charts were produced using GraphPad Prism 6 (GraphPad Software, CA, USA).

6.3 Results

6.3.1 Patient characteristics

A total of 47 patients of cohort A and 50 patients of cohort B met the inclusion criteria. The data available for characteristics for patients included were assessed and are presented in Table 6.2.

Table 6.2 Patient characteristics for Cohorts A and B (values shown as median (range) or % of subjects).

Characteristics	Cohort A Total (n=47)	Cohort B Total (n=50)
Age (years)	45 (44)	45 (45)
Caucasian (%)	100	100
Gender: Female (%)	40	28
Weight (kg)	65 (47)	72 (70)
Height (cm)	168 (35)	172 (38)
BMI	23.74 (13.7)	23.81 (17.8)

6.3.2 Summary of genotype frequencies

Genotype was characterised for cohorts A and B for the 5 chosen SNPs and population frequencies were in agreement with published data, as shown in Table 6.3.

Table 6.3 Summary of genotype frequencies (EUR = European population)

Gene	SNP	EUR population allele frequency from 1000Genome	Cohort A genotype frequencies	Cohort B genotype frequencies
AMFR	rs2432540	C 0.53 : T 0.47	C 0.53 : T 0.47	C 0.59 : T 0.41
AMFR	rs6499837	T 0.45 : C 0.55	T 0.42 : C 0.58	T 0.35 : C 0.65
AMFR	rs2440472	C 0.53 : T 0.47	C 0.54 : T 0.46	C 0.59 : T 0.41
AMFR	rs2440467	T 0.45 : C0.55	T 0.43 : C 0.57	T 0.35 : C 0.65
UBE2G1	rs9906760	A 0.68 : G 0.32	A 0.62 : G 0.38	A 0.63 : G0.37

6.3.3 Assessment of compliance with Hardy-Weinberg equilibrium

The genotypes characterised for cohorts A and B were assessed for fit with the Hardy-Weinberg equilibrium by χ^2 test of observed and predicted genotype frequencies. This data is presented in Table 6.4. All genotypes characterised for the 5 SNPs in both cohorts displayed a P-value of >0.0001 and were therefore in compliance with the Hardy-Weinberg equilibrium.

Table 6.4 Compliance of patient samples with Hardy-Weinberg equilibrium

Gene	SNP	Cohort A (n=47)		Cohort B (n=50)	
		χ^2	P-value	χ^2	P-value
AMFR	rs2432540	0.58	P > 0.05	1.98	P > 0.05
AMFR	rs6499837	0.43	P > 0.05	1.74	P > 0.05
AMFR	rs2440472	0.24	P > 0.05	1.98	P > 0.05
AMFR	rs2440467	0.81	P > 0.05	1.76	P > 0.05
UBE2G1	rs9906760	5.78	0.05>P<0.01	3.66	P > 0.05

6.3.4 Non-association of SNPs with ATV plasma concentrations

The Shapiro-Wilk test for normality for ATV plasma concentration (dependent variable) displayed a significant P-value of $P=7.4x10^{-7}$ for cohort A and $P=3.4x10^{-7}$ for cohort B, therefore non-normal distributions were assumed. The effect of the 5 SNPs on ATV plasma concentrations was determined by Kruskal Walis non-parametric ANOVA test. No significant associations were found for all 5 SNPs for both cohorts (P>0.05) as depicted in Figures 6.3 and 6.4. Categorical data were assessed with Mann-Whitney *U* test for carrier and non-carrier genotype categories. No significance was detected for all 5 SNPs with Mann-Whitney *U* tests in both cohorts (P>0.05). Table 6.5 summarises the effect of the 5 selected SNPs on ATV plasma concentrations.

Table 6.5 Effect of SNPs on ATV plasma concentration

Gene	SNP	Cohort A			Cohort B		
		Kruskal Walis P-value	Mann-Whitney U Test P-value		Kruskal Walis P-value	Mann-Whitney U Test P-value	
			1-tailed	2-tailed		1-tailed	2-tailed
AMFR	rs2432540	0.44	0.11	0.22	0.36	0.18	0.37
AMFR	rs6499837	0.82	0.27	0.54	0.35	0.18	0.36
AMFR	rs2440472	0.65	0.22	0.44	0.59	0.29	0.60
AMFR	rs2440467	0.94	0.37	0.73	0.35	0.18	0.35
UBE2G1	rs9906760	0.32	0.08	0.16	0.87	0.43	0.87

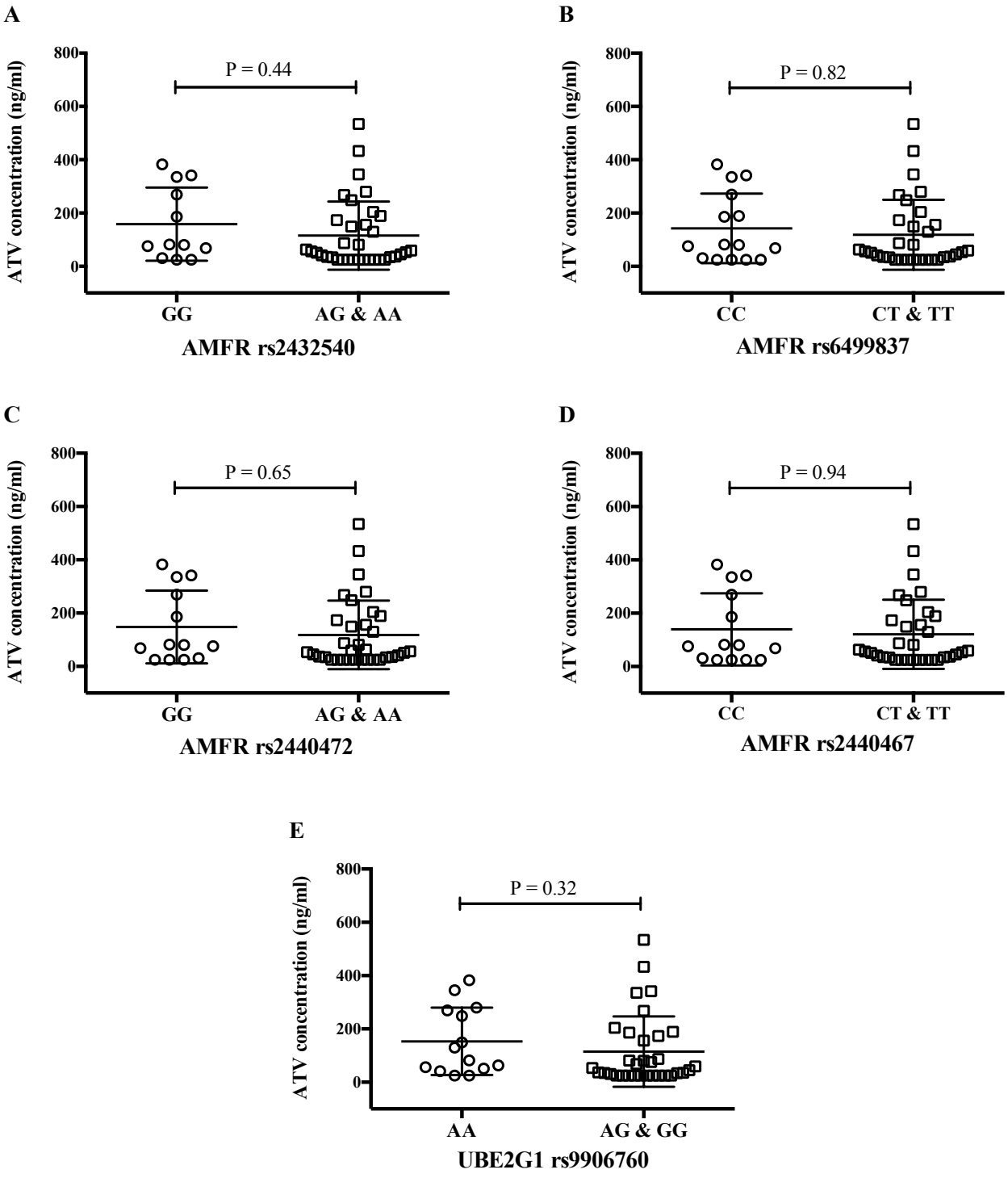

Figure 6.3 Comparison of ATV concentrations in carriers and non-carrier of selected SNPs in patient cohort A administered with unboosted ATV. A. AMFR A>G rs2432540, **B.** AMFR C>T rs6499837, **C.** AMFR A>G rs2440472, **D.** AMFR C>T rs2440467 and **E.** UBE2G1 A>G rs9906760. Statistical significance determined by Kruskal Walis ANOVA.

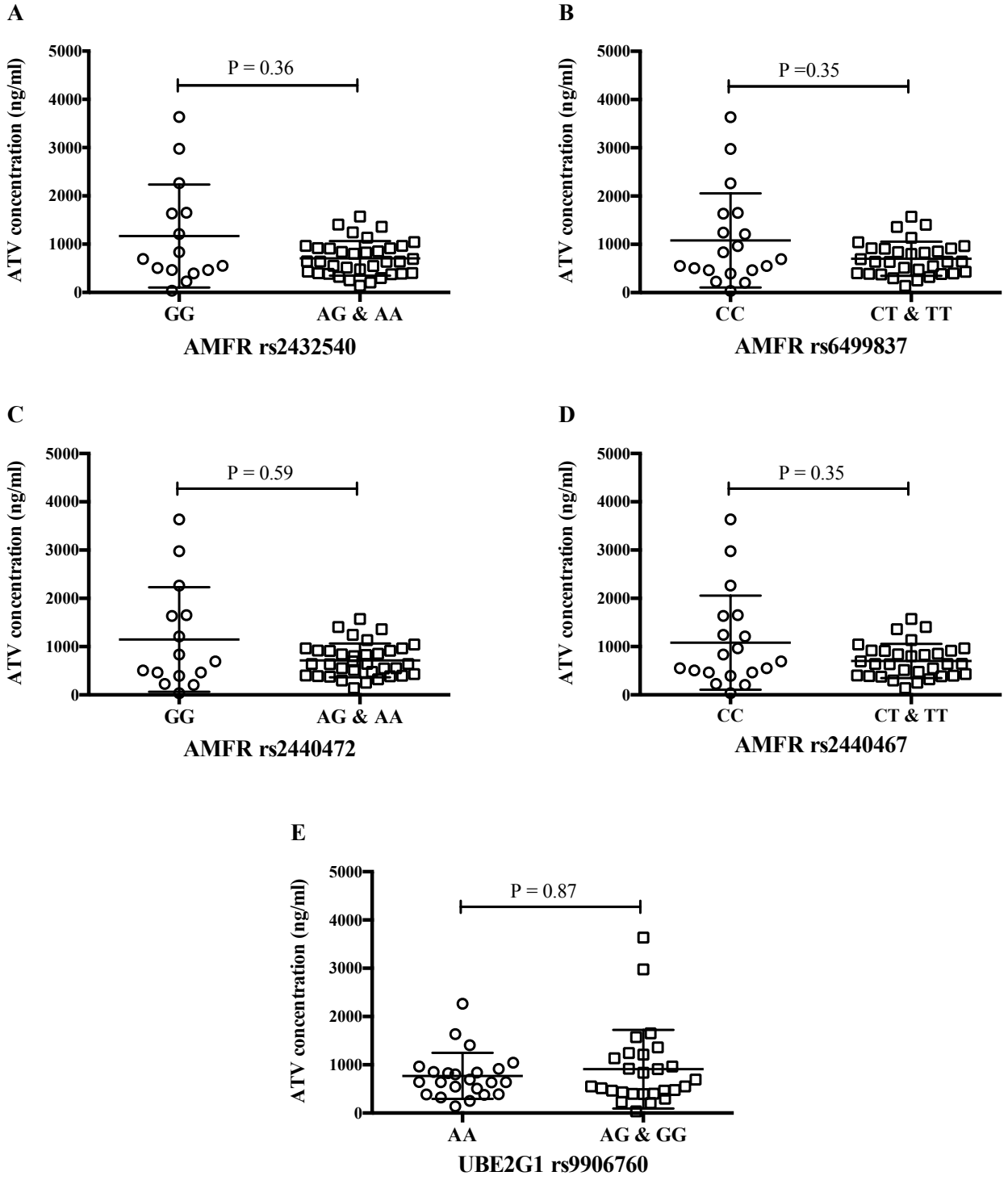

Figure 6.4 Comparison of ATV concentrations (24 ±4 h post dose) in carriers and non-carrier of selected SNPs in patient cohort B administered with boosted ATV/r. A. AMFR A>G rs2432540, **B.** AMFR C>T rs6499837, **C.** AMFR A>G rs2440472, **D.** AMFR C>T rs2440467 and **E.** UBE2G1 A>G rs9906760. Statistical significance determined by Kruskal Walis ANOVA.

6.3.5 Univariate and multivariate analysis for associations with ATV plasma concentrations in unboosted patient samples (cohort A)

Univariate regression analysis showed associations of gender (P=0.20), height (P=0.15) and rs9906760 (P=0.18) to ATV plasma concentrations for cohort A. Therefore, these characteristics were included in a stepwise multivariate regression analysis. Patient characteristics including age (P=0.97), weight (P=0.78) and body mass index (BMI; P=0.53) were not correlated to ATV concentrations in univariate analysis. No significant associations of gender, height or rs9906760 carrier/non-carrier status to ATV concentrations were found (P>0.05) upon multivariate analysis, so no further statistical analyses were conducted.

Table 6.6 Univariate and multivariate analysis of patient demographics and physical characteristics with plasma ATV concentrations for cohort A.

Characteristics	Univariate linear regression		Multivariate linear regression	
	P-value	β-value (95% CI)	P-value	β-value (95% CI)
Age (years)	0.970	0.000 (-0.014 – 0.014)	-	-
Gender	0.201	0.167 (-0.092 – 0.426)	0.627	0.073 (-0.228 – 0.374)
Weight (kg)	0.779	-0.002 (-0.013 - 0.010)	-	-
Height (cm)	0.146	-0.012 (-0.029 – 0.005)	0.146	-0.012 (-0.029 – 0.005)
BMI	0.526	0.013 (-0.027 – 0.053)	-	-
rs2432540	0.248	-0.170 (-0.462 – 0.122)	-	-
rs6499837	0.509	-0.091 (-0.367 – 0.185)	-	-
rs2440472	0.447	-0.109 (-0.397 – 0.178)	-	-
rs2440467	0.697	-0.055 (-0.337 – 0.227)	-	-
rs9906760	0.177	-0.189 (-0.466 – 0.088)	0.259	-0.159 (-0.438 – 0.121)

6.3.6 Univariate and multivariate analysis for associations with ATV plasma concentrations in RTV boosted patient samples (cohort B)

Univariate regression analysis showed no significant associations with demographics or physical characteristics including: age (P=0.72), gender (P=0.62), weight (P=0.82), height (P=0.33), BMI (P=0.38), tenofovir dose (P=0.99) and time post dose (P=0.85) to ATV plasma concentrations for cohort B (P>0.2). No significant associations were found with the 5 selected SNPs; therefore multivariate regression and further statistical analyses were not conducted for cohort B data.

Table 6.7 Univariate analysis of patient demographics and physical characteristics with plasma ATV concentrations for cohort B.

Characteristics	Univariate linear regression	
	P-value	β-value (95% CI)
Age (years)	0.722	0.002 (-0.009 – 0.013)
Gender	0.617	-0.055 (-0.275 – 0.165)
Weight (kg)	0.817	0.126 (-0.962 – 1.215)
Height (cm)	0.327	-0.006 (-0.017 – 0.006)
BMI	0.378	0.010 (-0.013 – 0.033)
Tenofovir dose	0.992	0.001 (-0.208 – 0.210)
Time post dose (h)	0.845	-0.005 (-0.059 – 0.048)
rs2432540	0.466	-0.077 (-0.289 – 0.134)
rs6499837	0.548	-0.060 (-0.261 – 0.140)
rs2440472	0.729	-0.037 (-0.250 – 0.176)
rs2440467	0.548	-0.060 (-0.261 – 0.140)
rs9906760	0.979	-0.003 (-0.198 – 0.193)

6.4 Discussion

Alterations to CYP3A4 abundance, whether through inhibition/induction or modulation of protein expression through genetic polymorphisms, can have significant impact on substrate drug metabolism and disposition. It was therefore hypothesised that any disruption to the CYP3A4 protein degradation machinery will alter overall protein abundance and subsequently impact on substrate PK. To test this hypothesis, four SNPs in the AMFR gene and one SNP in UBE2G1 gene, where both gene products were speculated to be involved in the human CYP3A4 ERAD/UPD pathway, were assessed for associations with substrate ATV plasma concentrations in two cohorts of HIV-1 infected patients. This study found that the 5 selected SNPs had no effect on plasma ATV concentrations in both cohorts of patients.

Cohort B included patients given RTV-boosted ATV regimens. RTV is a PI class drug and a potent inhibitor of CYP3A4. It is often prescribed with additional PI drugs to boost concomitant drug exposure. Its rationale for use as a 'booster' is due to its ability to inhibit CYP3A4, resulting in reduced metabolism and increased exposure of concomitant drugs and therefore a 'boosted' therapeutic effect (Zeldin & Petruschke 2004; Hull & Montaner 2011; Boffito 2004). Less significant associations of SNPs to ATV PK were expected in cohort B as RTV's effect on CYP3A4 and ATV PK could mask any effect of the AMFR or UBE2G1 SNPs. Both cohorts were included in this study with the ATV/r cohort B intended as a comparison with cohort A. However, no significant associations were found in either cohort. Our group had previously characterized an association of the *PXR* SNP rs2472677 C>T to reduced concentrations of unboosted ATV (cohort A) (Siccardi et al. 2008), however, associations *CYP3A4*22* (rs35599367 C>T), a well-known polymorphism resulting in reduced CYP3A4 expression, was not analysed for these cohorts.

Several sources have documented that altered states of protein degradation have been a principal cause of pharmacogenetic related loss of function of different DMEs. Enhanced proteasomal degradation has been reported as a principal mechanism for thiopurine S-methyltrasnferase (TPMT) deficiency in mutant TPMT*2 and TPMT*3 alleles (Tai et al. 1999). Li et al. (2008) reported on the importance of SNPs in autophagic machinery for the protein degradation of TPMT*3A, which is a well-characterised variant allozyme known to cause clinical pharmacogenetic interactions. Additionally, the human N-acetyltrasnferase 2 (NAT2) enzyme polymorphism NAT2*5 allozyme yields large reduction in NAT2 protein due to enhanced protein degradation, which results in a slow acetylator phenotype (Zang et al. 2004). For the sulfotransferase (SULT) 1A1*2 allozyme, enhanced proteasomal degradation can be attributed for reduced metabolism of carcinogens and increased risk of urinary tract cancer (Nagar et al. 2006). More recently, altered proteasomal degradation in p.P187S polymorphism of NADPH quinone oxidoreductase 1 (NQO1) has been identified as a mechanism contributing to loss of function and non-activation of cancer pro-dugs (Encarnación et al. 2016). Nakagawa et al. (2011) reviewed the impact of protein degradation on ABC transporter protein expression and consequent effects on drug disposition. It is evident that protein degradation mechanisms should be considered amongst mechanisms responsible for the effects of pharmacogenetically significant polymorphisms.

Polymorphisms in genes involved in protein degradation mechanisms give rise to clinical manifestations and disease. Deregulation of the UPD has been implicated in the pathology of many neurodegenerative disorders such as Alzheimer's disease, Parkinson's disease and Huntington disease, where inadequate degradation leads to aggregation of misfolded and dysfunctional proteins (Paul 2008; Schmidt & Finley

2014). Stintzing et al. (2015) reported that polymorphisms in genes involved in epidermal growth factor receptor (EGFR) turnover could be predictors of efficacy of cetuximab in colorectal cancer patients. This is the only published study, at the time of writing, which has validated a SNP in protein degradation machinery that is associated with disposition of a clinically used drug. Although polymorphisms in degradation proteins are a plausible mechanism for causing clinical interactions, clearly this area is under studied. This is perhaps due to the complexity of the signaling and protein cascades involved in the degradation process and paucity in the understanding of molecular interactions and mechanisms for target recognition.

To date, there are no published pharmacogenetic effects of protein degradation machinery on CYP degradation despite well-established associations of CYP protein abundance to clinical interactions (Nebert et al. 2013). This is perhaps due to insufficient understanding of the exact mechanisms of CYP protein degradation and further elucidation is needed to identify specific markers of degradation. CYP3A4 and CYP2E1 are the most extensively studied in terms of protein degradation and the pathways identified for these CYP proteins have provided clues to elucidate mechanisms for other CYPs. Human CYPs 3A4, 3A5 and 2B6 are likely to predominantly undergo ERAD/UPD whereas CYPs 2E1, 2C9, 2D6 showed biphasic turnover involving both UPD and ALD (Kim et al. 2016). As discussed previously gp78, the AMFR gene product, is involved in the ERAD/UPD degradation of many proteins other than CYP3A4, thus gp78 is specific but not limited to the CYP3A4 degradation pathway (Chen et al. 2012; Zhang et al. 2015). UBE2G1 is a human homologue of UBC7 and is a speculated component of the human CYP3A4 degradation pathway, however, the evidence of involvement of this protein is scarce compared with gp78. SNPs in UBE2G2 could be investigated instead, as it is another

UBC7 homologue and some studies have found this E2 protein to be clearly implicated in ERAD (Chen et al. 2006). As human CYP3A4 degradation is understudied, it is perhaps unsurprising that no associations of SNPs to ATV PK were found in this study. It must be noted that analysis for both cohorts across all 5 SNPs were also carried out using an additive model of inheritance, whereby alleles were coded as 0 (homozygous WT), 1 (heterozygous) and 2 (homozygous variant). However no significant associations were found correlating to ATV plasma concentrations and therefore the data was not presented. As the relative contributions of the identified components of the CYP3A4 degradation machinery to overall protein degradation are unknown, a limitation to this investigation was that only 5 SNPs in 2 genes were studied. More SNPs in more genes of the recognised degradation machinery is likely to be needed to find any significant associations, such as in the study by Stintzing et al. where they analysed 20 SNPs in 7 genes. However, this machinery is involved in degradation of many proteins and a high-impact genetic abnormality would therefore likely impact many biological processes. For this reason, one might expect these systems to be well conserved.

Characterising clinically relevant polymorphisms in the degradation process can provide predictive biomarkers of disease, provide new targets in treatments or inform treatment regimen design. The protein degradation pathway as a potential pathway for pharmacogenetics is a relatively new concept (Nakagawa et al. 2011). The UPD has been increasingly recognised as a potential pathway for biomarker and drug development but it is a field that requires further evaluation. Better elucidation of processes specific to CYP isozyme degradation will provide new targets for treatment and increase the likelihood of identifying significant pharmacogenetic relationships.

CHAPTER 7

FINAL DISCUSSION

DDIs may result in serious clinical consequences and therefore the potential of a NME causing or being a victim of an interaction needs to be carefully studied. The ability to quantitatively predict DDIs early in the drug development process is essential to reduce risks of adverse effects manifesting during clinical studies. The potential for a DDI interaction can be assessed using *in vitro*, *in vivo* and *in silico* methods. In early preclinical drug development, *in vitro* methods are used to determine the metabolic pathways involved in the clearance of a NME and for screening interaction potential, then IVIVE can be used for predicting the risk of clinical DDIs of the compound and where signs of interaction potential based on *in vitro* and *in silico* studies are identified, full drug interaction investigations may be carried out (Jones et al. 2012).

In silico approaches to predicting DDI potential can be applied at different points in the drug development process to aid drug candidate selection, inform drug trials and dosing regimen selection. The use of *in silico* approaches can reduce the costs of drug development considerably and in several instances simulations from PBPK models have been used in lieu of clinical studies (Bjornsson et al. 2003; Jones et al. 2012; Jamei 2016; Park et al. 2017).

The use of PBPK models to replace clinical studies has been particularly prevalent when the mechanism of DDI is due to competitive inhibition of CYP substrates (particularly when the CYP isozyme involved is CYP3A4). In irreversible or quasi-irreversible inhibition where manifestation and reversal of the interaction is slow and time-dependent, such as in the case of MBI interactions, accurate predictions of DDI potential and magnitude is problematic due to the lack of data for some parameters that are critical for prediction. In MBI, the perpetrator drug irreversibly binds to the enzyme forming an inactivated drug-enzyme complex that

permanently removes the enzyme from the pool of active enzymes and recovery of enzyme activity is gained only by re-synthesis of the enzyme protein. Therefore, the consequences of MBI persist longer and can be more profound than reversible inhibition. To predict MBI interactions, specific parameters such as k_{inact} and k_{deg} of the inhibited enzyme are essential for IVIVE. Using values only sufficient for reversible inhibition have resulted in under prediction or failure to identify MBI interactions. Although progress has also been made in predicting drug interactions caused by changes in the level of DMEs such as induction and MBI (Wagner et al. 2015), there is still more work that needs to be done to improve the accuracy of DDI predictions for these mechanisms (Jones et al. 2015).

The k_{deg} of CYP enzymes, characterising the *in vivo* turnover, is essential for the IVIVE of interactions caused by MBI. The first-order (where the rate is dependent on enzyme concentration) enzyme degradation rate is a physiological value depending on the enzyme, individual and species concerned. Ideally CYP k_{deg} ought to be derived *in vivo* in humans for effective IVIVE of human drug interactions. However, k_{deg} of DMEs cannot be easily measured directly *in vivo* therefore surrogate measures using *in vitro* systems have been used to obtain estimates. For many years, the prediction accuracy of MBI interactions have been hampered by the lack of a physiologically-relevant enzyme k_{deg} values and where they are available, the values vary widely because they are generated from many different *in vitro* approaches with no consensus as to the best method. As the half-lives of CYPs vary between species, for example they are shorter in rats compared to humans, using preclinical species to derive k_{deg} values can under predict the risk and magnitude of MBI interactions. One of the major aims of this thesis was to develop a robust *in vitro* method for measuring

DME k_{deg} in primary human hepatocytes as an accurate representation of the *in vivo* human condition.

Initially, the simplest and most widely used *in vitro* approach for measuring protein degradation was explored and this involved using pharmacological interference by protein synthesis inhibitor compounds to stop *de novo* protein synthesis followed by tracking protein expression decline over time. However, protein synthesis inhibitor drugs exert their effects through inhibiting fundamental components of the universal protein synthesis pathway, therefore cytotoxicity was expected with prolonged use. Four commonly used protein synthesis inhibitor compounds including actinomycin D, cycloheximide, emetine and puromycin, were assessed as single agents and also in two-, three- and four-agent combinations for their capacity to stop *de novo* protein synthesis without producing overt cytotoxicity. However, all four inhibitor drugs in all combinations were found to be unsuitable for further use in deriving CYP k_{deg} due to cytotoxicity determined through several different toxicity assays, that was frequently observed at lower concentrations than required for protein synthesis inhibition. Therefore, a different approach for stopping *de novo* protein synthesis was required. The protein synthesis inhibitor agents investigated are commonly used *in vitro* for analysis of protein or mRNA stability with applications in many fields of cellular biology and the concentrations used in these studies far exceed the toxic concentrations reported here (Table 2.1). Work herein shows that for proteins that are likely to have longer half-lives (over 24 h), the use of pharmacological interference is unsuitable for determining protein turnover. Caution should be exercised when using other protein synthesis inhibitor compounds in *in vitro* cellular systems and ideally, drug concentrations should first be optimised

and deemed non-toxic through the use of appropriate toxicity assays prior to being used in downstream applications.

It was hypothesised that introducing DME-specific siRNA to an *in vitro* culture system would exclusively knockdown expression of target gene mRNA and subsequent *de novo* protein synthesis with minimal cytotoxicity due to specificity of the siRNA target. A time-course of mRNA knockdown was validated in primary human hepatocytes and siRNA methods were found to be considerably less cytotoxic than using protein synthesis inhibitor agents. The CYP protein expression and activity decline through time was tracked by Western blotting and probe substrate metabolite formation, respectively, and the k_{deg} value was derived from the degradation curves assuming first-order kinetics in untreated and siRNA treated hepatocytes. The CYP3A4 k_{deg} values derived using the siRNA treated approach were found to be similar to recently published values (Ramsden et al 2015; Dixit et al 2016; Takahashi et al 2017) and within the range described by Mao et al. (2013). Therefore the same approach was applied to measure CYP2B6 k_{deg}, which is a less-well characterised CYP enzyme. There have only been two previous studies, at the time of writing, that have reported on the k_{deg} of CYP2B6 and both studies did not account for *de novo* protein synthesis during assessment of degradation and consequently the values varied widely. The CYP2B6 k_{deg} values derived in this study was closer to 0.022 h^{-1} ($t_{1/2}$ of 26 h) reported by Renwick et al (2000) than 0.010 h^{-1} ($t_{1/2}$ of 68 h) reported by Dixit et al (2016). The CYP2B6 k_{deg} values can now be incorporated into PBPK predictions of DDIs involving mechanism-based inactivators of CYP2B6 such as clopidogrel, ticlopidine (Richter et al. 2004; Nishiya et al. 2009), monoamine oxidase inhibitors (Sridar et al. 2012; Nirogi et al. 2015) and components of medicinal herbs (Cao et al. 2015; Ji et al. 2015; Lu et al. 2016).

A limitation to the use of cryopreserved primary hepatocytes as the *in vitro* model for deriving CYP k_{deg} is that several sources have documented significant decline of CYP expression over time in monolayer culture and thus they may not be representative of the endogenous human state. However, primary human hepatocytes are still regarded as the 'gold standard' for *in vitro* metabolism studies because they possess the full complement of DMEs and they have been found to be better predictors of *in vivo* drug clearance compared with liver microsome preparations in some studies. Moreover, cryopreserved hepatocytes express CYP proteins at levels comparable to freshly isolated hepatocytes (Smith et al. 2012). Indeed, better cell models that mimic the endogenous human liver will improve drug research and several models are under development to address this need. For example, 3D hepatocyte culture systems involving sandwich culture between an extracellular matrix and a scaffold-free approach in the self-aggregation of cells into spheroids with or without nutrient perfusion, have reported stable hepatocyte phenotype for longer duration (over weeks) compared with monoculture systems (Soldatow et al. 2013; Zeilinger et al. 2016). Other methods include co-culturing hepatocytes with non-parenchymal cells such as Kuppfer and endothelial cells, which promote cell-to-cell adhesion and have resulted in reduced de-differentiation during *in vitro* culture (Bhatia et al. 1999; Shulman & Nahmias 2013). Using such long-lived liver cell models to measure k_{deg} of hepatic proteins with long $t_{1/2}$ (days) may be more appropriate than the current monoculture hepatocyte system and indeed, drug metabolism studies have increasingly come away from using monocultured hepatocytes in favour of the 3D culture models, especially in transporter studies.

Of all the identified CYP enzymes, CYP3A4 is also the most extensively studied for its precise mechanisms of protein degradation. CYP3A4 predominantly undergoes

degradation via the ERAD/UPD degradation pathway that involves several components including the gp78 glycoprotein (encoded by AMFR gene) and the UBE2G1 enzyme (Correia et al. 2014). It was postulated that any dysregulation of the CYP enzyme degradation machinery would have an overall impact on steady-state protein abundance and therefore capacity to facilitate metabolism. Four SNPs in the AMFR gene and one in UBE2G1 were selected based on their reported likelihood of affecting the gene product function and were assessed for associations with CYP3A4-mediated PK changes in the known substrate ATV plasma concentrations in two cohorts of HIV-1 infected patients. Significant associations were not observed with any of the 5 SNPs. The ERAD/UPD pathway for CYP enzymes has been more extensively studied compared with the ERAD/ALD pathway; the factors targetting CYP proteins to be degraded by ALD pathway remains mostly obscure (Kim et al. 2016). Further elucidation of the precise mechanisms that target DME proteins for degradation may identify new targets to measure to better characterise DME k_{deg} values. Stintzing et al. (2015) identified associations between polymorphisms in the EGFR degradation machinery and PK of cetuximab in colorectal cancer patients. This presents the only study, at the time of writing, to identify associations between SNPs of proteins involved in protein degradation to drug disposition. Clearly, dysregulation of the protein degradation machinery offers a plausible mechanism for altering drug disposition but the magnitude of effect and whether they contribute to significant changes in PK remains understudied.

Confidence in the prediction of DDIs for drugs eliminated via CYP enzymes, especially those mediated by CYPs 1A2, 2C8, 2C9, 2C19, 2D6 and 3A4, is generally high compared with those for transporter-based DDIs and non-CYP enzymes (Fowler et al. 2017). Significant challenges are still present in the prediction of complex drug

interactions where perpetrator drugs and metabolites affect both transporter and enzyme-mediated disposition processes, where multiple forms of interaction such as time-dependent inhibition, active uptake and enzyme induction occur simultaneously (Varma et al. 2014; Fowler et al. 2017). The HIV drug ritonavir, is one such example of a complex case where as well as being a CYP3A4 substrate, it inhibits, inactivates and induces CYP3A4 and also inhibits and induces other DMEs. Model validation for accurate prediction of DDIs is more difficult concerning non-CYP enzymes such as aldehyde oxidase (AO), flavin monooxygenases (FMO) and UGTs because PK data for specific substrates and *in vivo* interactions with inhibitors are lacking. Currently, much effort is focused on dissecting the relative contributions of DMEs and drug transporters on drug PK and therefore the potential for the DMEs and transporters to mediate DDIs. Increased knowledge in enzymology and better cellular models to investigate DDIs will overcome some of these problems. The methods presented in this thesis can be used to characterise k_{deg} for less well-characterised CYPs or non-CYP DMEs. The data and discussions presented in this thesis will hopefully contribute to improving prediction accuracy of DDIs in the near future.

References

Aagaard, L. & Rossi, J.J., 2007. RNAi therapeutics: principles, prospects and challenges. *Advanced drug delivery reviews*, 59(2–3), pp.75–86.

Acharya, P. et al., 2011. Liver Cytochrome P450 3A endoplasmic reticulum-associated degradation: A major role for the P97 AAA ATPase in cytochrome P450 3A extraction into the cytosol. *Journal of Biological Chemistry*, 286(5), pp.3815–3828.

Achenbach, C.J. et al., 2011. Atazanavir/ritonavir-based combination antiretroviral therapy for treatment of HIV-1 infection in adults. *Future virology*, 6(2), pp.157–177.

Akinboye, E., 2011. Biological Activities of Emetine. *The Open Natural Products Journal*, 4(1), pp.8–15.

Alarid, E.T., 2006. Lives and times of nuclear receptors. *Mol Endocrinol*, 20(9), pp.1972–1981.

Almira Correia, M., Sinclair, P.R. & De Matteis, F., 2011. Cytochrome P450 regulation: the interplay between its heme and apoprotein moieties in synthesis, assembly, repair, and disposal. *Drug Metabolism Reviews*, 43(1), pp.1–26.

Almond, L.M. et al., 2016. Prediction of drug-drug interactions arising from CYP3A induction using a physiologically-based dynamic model. *Drug metabolism and disposition: the biological fate of chemicals*, 44(6), pp.821–32.

Almond, L.M. et al., 2009. Towards a quantitative framework for the prediction of DDIs arising from cytochrome P450 induction. *Current drug metabolism*, 10(4), pp.420–32.

Alvarez-Castelao, B., Ruiz-Rivas, C. & Castaño, J.G., 2012. A critical appraisal of quantitative studies of protein degradation in the framework of cellular proteostasis. *Biochemistry Research International*, 2012.

Angelis, I. De & Turco, L., 2011. Caco-2 cells as a model for intestinal absorption. *Current protocols in toxicology*, Chapter 20, p.Unit20.6.

Artursson, P. & Karlsson, J., 1991. Correlation between oral drug absorption in humans and apparent drug permeability coefficients in human intestinal epithelial (Caco-2) cells. *Biochemical and Biophysical Research Communications*, 175(3), pp.880–885.

Azzam, M.E. & Algranati, I.D., 1973. Mechanism of puromycin action: fate of ribosomes after release of nascent protein chains from polysomes. *Proceedings of the National Academy of Sciences of the United States of America*, 70(12), pp.3866–9.

Bachmann, K., 2009a. *Drug-Drug Interactions with an Emphasis on Drug Metabolism and Transport* 1st ed., Elsevier Inc.

Bachmann, K., 2009b. *Drug Metabolism* 1st ed., Elsevier Inc.

Backman, J.T. et al., 2009. CYP2C8 activity recovers within 96 hours after gemfibrozil dosing: Estimation of CYP2C8 half-life using repaglinide as an in vivo probe. *Drug Metabolism and Disposition*, 37(12), pp.2359–2366.

Von Bahr, C. et al., 1998. Time course of enzyme induction in humans: Effect of pentobarbital on nortriptyline metabolism. *Clinical Pharmacology and Therapeutics*, 64(1), pp.18–26.

Bains, R.K., 2013. African variation at Cytochrome P450 genes: Evolutionary aspects and the implications for the treatment of infectious diseases. *Evolution, medicine, and public health*, 2013(1), pp.118–34.

Bedford, L. et al., 2010. Assembly, structure, and function of the 26S proteasome.

Trends in Cell Biology, 20(7), pp.391–401.
Belle, A. et al., 2006. Quantification of protein half-lives in the budding yeast proteome. *Proceedings of the National Academy of Sciences of the United States of America*, 103(35), pp.13004–9.
Bento, C.F. et al., 2016. Mammalian Autophagy: How Does It Work? *Annual Review of Biochemistry*, 85(1), pp.685–713.
Berridge, M.V. & Tan, A.S., 1993. Characterization of the Cellular Reduction of 3-(4,5-dimethylthiazol-2-yl)-2,5-diphenyltetrazolium bromide (MTT): Subcellular Localization, Substrate Dependence, and Involvement of Mitochondrial Electron Transport in MTT Reduction. *Archives of Biochemistry and Biophysics*, 303(2), pp.474–482.
Bhatia, S.N. et al., 1999. Effect of cell-cell interactions in preservation of cellular phenotype: cocultivation of hepatocytes and nonparenchymal cells. *FASEB journal : official publication of the Federation of American Societies for Experimental Biology*, 13(14), pp.1883–900.
Bjornsson, T.D. et al., 2003. The conduct of in vitro and in vivo drug-drug interaction studies: a PhRMA perspective. *Journal of clinical pharmacology*, 43(5), pp.443–469.
Boddy, A. V. et al., 1995. The kinetics of the auto-induction of ifosfamide metabolism during continuous infusion. *Cancer Chemotherapy and Pharmacology*, 36(1), pp.53–60.
Boffito, M., 2004. From Concept to Care : Pharmacokinetic Boosting of Protease Inhibitors. *Physicians' Research Network*, 9(4), pp.15–19.
Boisvert, F.-M. et al., 2012. A Quantitative Spatial Proteomics Analysis of Proteome Turnover in Human Cells. *Molecular & Cellular Proteomics : MCP*, 11(3), p.M111.011429.
Bouligand, J. et al., 2010. Familial Glucocorticoid Receptor Haploinsufficiency by Non-Sense Mediated mRNA Decay, Adrenal Hyperplasia and Apparent Mineralocorticoid Excess P. H. Reitsma, ed. *PLoS ONE*, 5(10), p.e13563.
Brandon, E.F.A. et al., 2006. Validation of in vitro cell models used in drug metabolism and transport studies; genotyping of cytochrome P450, phase II enzymes and drug transporter polymorphisms in the human hepatoma (HepG2), ovarian carcinoma (IGROV-1) and colon carcinoma (CaCo-2, LS. *Toxicology and applied pharmacology*, 211(1), pp.1–10.
Bristol-Myers Squibb, 2003. Atazanavir Briefing Document May-2003. , pp.1–226.
Burt, H.J. et al., 2012. Progress curve mechanistic modeling approach for assessing time-dependent inhibition of CYP3A4. *Drug Metabolism and Disposition*, 40(9), pp.1658–1667.
Cao, J. et al., 2015. Mechanism-based inactivation of cytochrome P450 2B6 by isoimperatorin. *Chemico-biological interactions*, 226, pp.23–29.
Carthew, R.W. & Sontheimer, E.J., 2009. Origins and Mechanisms of miRNAs and siRNAs. *Cell*, 136(4), pp.642–655.
Cha, E. et al., 2014. A novel polymorphism of the GP78 gene is associated with coronary artery disease in Han population in China. *Lipids in Health and Disease*, 13(1), p.147.
Chan, C. et al., 2017. Incompatibility of chemical protein synthesis inhibitors with accurate measurement of extended protein degradation rates. *Pharmacology research & perspectives*, 5(5).
Chan, T.Y., 1995. Adverse Interactions Between Warfarin and Nonsteroidal Antiinflammatory Drugs: Mechanisms, Clinical Significance, and Avoidance.

Annals of Pharmacotherapy, 29(12), pp.1274–1283.
Chang, T.Y., Limanek, J.S. & Chang, C.C.Y., 1981. Evidence indicating that inactivation of 3-hydroxy-3-methylglutaryl coenzyme A reductase by low density lipoprotein or by 25-hydroxycholesterol requires mediator protein(s) with rapid turnover rate. *Journal of Biological Chemistry*, 256(12), pp.6174–6180.
Chen, B. et al., 2006. The activity of a human endoplasmic reticulum-associated degradation E3, gp78, requires its Cue domain, RING finger, and an E2-binding site. *Proceedings of the National Academy of Sciences of the United States of America*, 103(2), pp.341–346.
Chen, C.C. & Feigelson, P., 1979. Cycloheximide inhibition of hormonal induction of a2u-globulin mRNA. , 76(6), pp.2669–2673.
Chen, L. & Madura, K., 2008. Centrin/Cdc31 is a novel regulator of protein degradation. *Molecular and cellular biology*, 28(5), pp.1829–1840.
Chen, Y. et al., 2011. Determination of time-dependent inactivation of CYP3A4 in cryopreserved human hepatocytes and assessment of human drug-drug interactions. *Drug Metabolism and Disposition*, 39(11), pp.2085–2092.
Chen, Z., Du, S. & Fang, S., 2012. gp78: a multifaceted ubiquitin ligase that integrates a unique protein degradation pathway from the endoplasmic reticulum. *Current protein & peptide science*, 13(5), pp.414–24.
Chistyakov, D. V et al., 2014. Regulation of peroxisome proliferator-activated receptor β/δ expression and activity levels by toll-like receptor agonists and MAP kinase inhibitors in rat astrocytes. *Journal of neurochemistry*, 130(4), pp.563–74.
Choi, J.M. et al., 2015. HepG2 cells as an in vitro model for evaluation of cytochrome P450 induction by xenobiotics. *Archives of Pharmacal Research*, 38(5), pp.691–704.
Choi, K.H. et al., 2011. Gene Expression and Genetic Variation Data Implicate PCLO in Bipolar Disorder. *Biological Psychiatry*, 69(4), pp.353–359.
Chou, T.C., 2010. Drug combination studies and their synergy quantification using the chou-talalay method. *Cancer Research*, 70(2), pp.440–446.
Chu, V. et al., 2009. Perspective In Vitro and in Vivo Induction of Cytochrome P450: A Survey of the Current Practices and Recommendations: A Pharmaceutical. *Pharmacology*, 37(7), pp.1339–1354.
Ciechanover, A., 2005. Proteolysis: from the lysosome to ubiquitin and the proteasome. *Nature reviews. Molecular cell biology*, 6(1), pp.79–87.
Ciechanover, A., 1998. The ubiquitin-proteasome pathway: On protein death and cell life. *EMBO Journal*, 17(24), pp.7151–7160.
Cole, N.H., 2001. Compendium of drugs commonly used in cell biology research. *Current protocols in cell biology*, Appendix 1, p.Appendix 1B.
Correia, M.A., 1991. Cytochrome P450 Turnover. *Methods in Enzymology*, 206(C), pp.315–325.
Correia, M.A., 2003. Hepatic cytochrome P450 degradation: mechanistic diversity of the cellular sanitation brigade. *Drug Metab. Rev.*, 35(2–3), pp.107–143.
Correia, M.A. et al., 2014a. Hepatic cytochrome P450 ubiquitination: Conformational phosphodegrons for E2/E3 recognition? *IUBMB Life*, 66(2), pp.78–88.
Correia, M.A. et al., 2014b. Hepatic cytochrome P450 ubiquitination: Conformational phosphodegrons for E2/E3 recognition? *IUBMB Life*, 66(2), pp.78–88.
Curfman, G.D. et al., 1980. Suppression of myocardial protein degradation in the rat during fasting. Effects of insulin, glucose, and leucine. *Circulation research*,

46(4), pp.581–9.
Dai, C.-L. et al., 2013. Inhibition of protein synthesis alters protein degradation through activation of protein kinase B (AKT). *The Journal of biological chemistry*, 288(33), pp.23875–83.
Danielson, P.B., 2002. The Cytochrome P450 Superfamily : Biochemistry, Evolution and Drug Metabolism in Humans. *Curr Drug Metab*, 3(6), pp.561–597.
Darwich, A.S. et al., 2012. Trends in oral drug bioavailability following bariatric surgery: Examining the variable extent of impact on exposure of different drug classes. *British Journal of Clinical Pharmacology*, 74(5), pp.774–787.
Delgado-Vega, A.M. et al., 2012. Fine mapping and conditional analysis identify a new mutation in the autoimmunity susceptibility gene BLK that leads to reduced half-life of the BLK protein. *Annals of the rheumatic diseases*, 71(7), pp.1219–26.
Diaz, D. et al., 1990. Omeprazole is an aryl hydrocarbon-like inducer of human hepatic cytochrome P450. *Gastroenterology*, 99(3), pp.737–47.
Dixit, V. et al., 2016. Application of micropatterned cocultured hepatocytes to evaluate the inductive potential and degradation rate of major xenobiotic metabolizing enzymes. *Drug Metabolism and Disposition*, 44(2), pp.250–261.
Doherty, M.K. et al., 2009. Turnover of the human proteome: determination of protein intracellular stability by dynamic SILAC. *Journal of proteome research*, 8(1), pp.104–12.
Doherty, M.K. & Beynon, R.J., 2006. Protein turnover on the scale of the proteome. *Expert review of proteomics*, 3(1), pp.97–110.
Dorsett, Y. & Tuschl, T., 2004. siRNAs: applications in functional genomics and potential as therapeutics. *Nature reviews. Drug discovery*, 3(4), pp.318–329.
Dresser, G.K., Spence, J.D. & Bailey, D.G., 2000. Consequences and Clinical Relevance of Cytochrome P450 3A4 Inhibition. *Clinical Pharmacokinetics*, 38(1), pp.41–57.
Dudani, A.K., Gupta, R.S. & Gupta, R., 1988. Species-specific differences in the toxicity of puromycin towards cultured human and Chinese hamster cells. *FEBS Letters*, 234(1), pp.141–144.
Eden, E. et al., 2011. Proteome half-life dynamics in living human cells. *Science (New York, N.Y.)*, 331(6018), pp.764–8.
Einolf, H.J., 2007. Comparison of different approaches to predict metabolic drug-drug interactions. *Xenobiotica; the fate of foreign compounds in biological systems*, 37(10–11), pp.1257–94.
Elens, L. et al., 2011. Novel CYP3A4 intron 6 single nucleotide polymorphism is associated with simvastatin-mediated cholesterol reduction in the Rotterdam Study. *Pharmacogenetics and genomics*, 21(12), pp.861–866.
EMA, 2012. Guideline on the investigation of drug interactions. *Guidance Document*, 44(June), p.59.
Emery, M.G. et al., 1999. Duration of cytochrome P-450 2E1 (CYP2E1) inhibition and estimation of functional CYP2E1 enzyme half-life after single-dose disulfiram administration in humans. *The Journal of pharmacology and experimental therapeutics*, 291(1), pp.213–219.
Encarnación, M.-C. et al., 2016. Conformational dynamics is key to understanding loss-of-function of NQO1 cancer-associated polymorphisms and its correction by pharmacological ligands. *Scientific reports*, 6(February), p.20331.
Eskelinen, E.-L. & Saftig, P., 2009. Autophagy: a lysosomal degradation pathway with a central role in health and disease. *Biochimica et biophysica acta*, 1793(4),

pp.664–673.
Evangelou, M. et al., 2014. A Method for Gene-Based Pathway Analysis Using Genomewide Association Study Summary Statistics Reveals Nine New Type 1 Diabetes Associations. *Genetic Epidemiology*, 38(8), pp.661–670.
Faber, M.S. & Fuhr, U., 2004. Time response of cytochrome P450 1A2 activity on cessation of heavy smoking. *Clinical Pharmacology and Therapeutics*, 76(2), pp.178–184.
Fahmi, O.A. et al., 2008. A combined model for predicting CYP3A4 clinical net drug-drug interaction based on CYP3A4 inhibition, inactivation, and induction determined in vitro. *Drug metabolism and disposition: the biological fate of chemicals*, 36(8), pp.1698–708.
Fahmi, O. a & Ripp, S.L., 2010. Evaluation of models for predicting drug-drug interactions due to induction. *Expert opinion on drug metabolism & toxicology*, 6(11), pp.1399–416.
Faouzi, S. et al., 2007. Characterization of the physiological turnover of native and inactivated cytochromes P450 3A in cultured rat hepatocytes: A role for the cytosolic AAA ATPase p97? *Biochemistry*, 46(26), pp.7793–7803.
Faucette, S.R. et al., 2004. Regulation of CYP2B6 in primary human hepatocytes by prototypical inducers. *Drug metabolism and disposition: the biological fate of chemicals*, 32(3), pp.348–58.
Fayadat, L. et al., 2000. Degradation of human thyroperoxidase in the endoplasmic reticulum involves two different pathways depending on the folding state of the protein. *Journal of Biological Chemistry*, 275(21), pp.15948–15954.
FDA, 2012. Guidance for industry. Drug interaction studies study design, data analysis, implications for dosing, and labeling recommendations. *Guidance Document*, (February), p.79.
FDA, 2017. In Vitro Metabolism- and Transporter- Mediated Drug-Drug Interaction Studies (Draft). *Guidance*, (October).
Fierro-Monti, I. et al., 2013. A Novel Pulse-Chase SILAC Strategy Measures Changes in Protein Decay and Synthesis Rates Induced by Perturbation of Proteostasis with an Hsp90 Inhibitor L. Martens, ed. *PLoS ONE*, 8(11), p.e80423.
Fivelman, Q.L., Adagu, I.S. & Warhurst, D.C., 2004. Modified fixed-ratio isobologram method for studying in vitro interactions between atovaquone and proguanil or dihydroartemisinin against drug-resistant strains of Plasmodium falciparum. *Antimicrobial Agents and Chemotherapy*, 48(11), pp.4097–4102.
Foisy, M.M., Yakiwchuk, E.M. & Hughes, C.A., 2008. Induction effects of ritonavir: implications for drug interactions. *The Annals of pharmacotherapy*, 42(7), pp.1048–59.
Foucquier, J. & Guedj, M., 2015. Analysis of drug combinations: current methodological landscape. *Pharmacology Research & Perspectives*, 3(3), p.e00149.
Fowler, S. et al., 2017. Progress in Prediction and Interpretation of Clinically Relevant Metabolic Drug-Drug Interactions: a Minireview Illustrating Recent Developments and Current Opportunities. *Current Pharmacology Reports*, 3(1), pp.36–49.
Friedman, E.J. et al., 2011. Effect of Different Durations and Formulations of Diltiazem on the Single-Dose Pharmacokinetics of Midazolam: How Long Do We Go? *The Journal of Clinical Pharmacology*, 51(11), pp.1561–1570.
Fromm, M.F. et al., 1996. Differential induction of prehepatic and hepatic metabolism

of verapamil by rifampin. *Hepatology*, 24(4), pp.796–801.
Fujioka, Y., Kunze, K.L. & Isoherranen, N., 2012. Risk Assessment of Mechanism-Based Inactivation in Drug-Drug Interactions. *Drug Metabolism and Disposition*, 40(9), pp.1653–1657.
Galetin, A. et al., 2006. Prediction of time-dependent CYP3A4 drug-drug interactions: impact of enzyme degradation, parallel elimination pathways, and intestinal inhibition. *Drug metabolism and disposition: the biological fate of chemicals*, 34(1), pp.166–75.
Galetin, a, Burt, H. & Houston, J.B., 2005. Prediction of time-dependent drug-drug interactions - Impact of parallel pathways, enzyme degradation and intestinal inhibition. *Drug Metabolism Reviews*, 37(1), p.38.
Gelman, M.S., Kannegaard, E.S. & Kopito, R.R., 2002. A principal role for the proteasome in endoplasmic reticulum-associated degradation of misfolded intracellular cystic fibrosis transmembrane conductance regulator. *Journal of Biological Chemistry*, 277(14), pp.11709–11714.
Gerets, H.H.J. et al., 2012. Characterization of primary human hepatocytes, HepG2 cells, and HepaRG cells at the mRNA level and CYP activity in response to inducers and their predictivity for the detection of human hepatotoxins. *Cell Biology and Toxicology*, 28(2), pp.69–87.
Ghanbari, F. et al., 2006. A critical evaluation of the experimental design of studies of mechanism based enzyme inhibition, with implications for in vitro-in vivo extrapolation. *Current drug metabolism*, 7(3), pp.315–34.
Goldberg, A.L. & Dice, J.F., 1974. Intracellular protein degradation in mammalian and bacterial cells. *Annual review of biochemistry*, 43, pp.835–69.
Goldsmith, D.R. & Perry, C.M., 2003. Atazanavir. *Drugs*, 63(16), pp.1679-93–5.
Gorka, A.P., Jacobs, L.M. & Roepe, P.D., 2013. Cytostatic versus cytocidal profiling of quinoline drug combinations via modified fixed-ratio isobologram analysis. *Malaria journal*, 12(1), p.332.
Gottesman, S. & Maurizi, M.R., 1992. Regulation by proteolysis: energy-dependent proteases and their targets. *Microbiological reviews*, 56(4), pp.592–621.
Greenblatt, D., 2003. Time course of recovery of cytochrome p450 3A function after single doses of grapefruit juice. *Clinical Pharmacology & Therapeutics*, 74(2), pp.121–129.
Grimm, S.W. et al., 2009. The conduct of in vitro studies to address time-dependent inhibition of drug-metabolizing enzymes: A perspective of the Pharmaceutical Research and Manufacturers of America. *Drug Metabolism and Disposition*, 37(7), pp.1355–1370.
Guengerich, F.P., 2008. Cytochrome P450 and Chemical Toxicology Cytochrome P450 and Chemical Toxicology. *Perspective*, 21(December 2007), pp.70–83.
Guillouzo, A. et al., 1985. Maintenance of cytochrome p-450 in cultured adult human hepatocytes. *Biochemical Pharmacology*, 34(16), pp.2991–2995.
Guzelian, P.S. & Barwick, J.L., 1979. Inhibition By Cyclohexmide of Degradation of Cytochrome P-450 in Primary Cultures of Adult Rat Liver Parenchymal Cells and (iin vivo). *Biochemical Journal*, 180, pp.621–630.
Handschin, C. & Meyer, U.A., 2003. Induction of drug metabolism: the role of nuclear receptors. *Pharmacological reviews*, 55(4), pp.649–73.
Hanna, J., Leggett, D.S. & Finley, D., 2003. Ubiquitin depletion as a key mediator of toxicity by translational inhibitors. *Molecular and Cellular Biology*, 23(24), pp.9251–9261.
Hattori, Y. & Gross, S.S., 1995. Cycloheximide induces nitric oxide synthase mRNA

in vascular smooth muscle cells by prolonging mRNA lifetime. *Biochemistry and molecular biology international*, 37(3), pp.439–45.
Hedrich, W.D., Hassan, H.E. & Wang, H., 2016. Insights into CYP2B6-mediated drug-drug interactions. *Acta Pharmaceutica Sinica B*, 6(5), pp.413–425.
Hemeryck, A., De Vriendt, C.A. & Belpaire, F.M., 2001. Metoprolol-paroxetine interaction in human liver microsomes: Stereoselective aspects and prediction of the in vivo interaction. *Drug Metabolism and Disposition*, 29(5), pp.656–663.
Henderson, C.J. et al., 2003. Inactivation of the hepatic cytochrome P450 system by conditional deletion of hepatic cytochrome P450 reductase. *The Journal of biological chemistry*, 278(15), pp.13480–13486.
Heslop, J.A. et al., 2016. Mechanistic evaluation of primary human hepatocyte culture using global proteomic analysis reveals a selective dedifferentiation profile. *Archives of Toxicology*, 91(1), pp.1–14.
Hewitt, N.J., Lecluyse, E.L. & Ferguson, S.S., 2007. Induction of hepatic cytochrome P450 enzymes: Methods, mechanisms, recommendations, and in vitro-in vivo correlations. *Xenobiotica*, 37(10–11), pp.1196–1224.
Houston, J.B. & Galetin, A., 2010. *Enzyme- and Transporter-Based Drug-Drug Interactions* K. S. Pang, A. D. Rodrigues, & R. M. Peter, eds., New York, NY: Springer New York.
Hsu, A. et al., 1997. Multiple-dose pharmacokinetics of ritonavir in human immunodeficiency virus-infected subjects. *Antimicrobial Agents and Chemotherapy*, 41(5), pp.898–905.
Hull, M.W. & Montaner, J.S., 2011. Ritonavir-boosted protease inhibitors in HIV therapy. *Annals of Medicine*, 43(5), pp.375–388.
Hummon, A.B. et al., 2007. Isolation and solubilization of proteins after TRIZOL?? extraction of RNA and DNA from patient material following prolonged storage. *BioTechniques*, 42(4), pp.467–472.
Hutzler, M.J., Cook, J. & Fleishaker, J.C., 2011. *Drug–Drug Interactions: Designing Development Programs and Appropriate Product Labeling* P. L. Bonate & D. R. Howard, eds., Springer US.
Imai, H. et al., 2008. The recovery time-course of CYP3A after induction by St John's wort administration. *British Journal of Clinical Pharmacology*, 65(5), pp.701–707.
Iwano S, S.C., 2015. Species Differences in the Pharmacokinetic Parameters of Cytochrome P450 Probe Substrates between Experimental Animals, such as Mice, Rats, Dogs, Monkeys, and Microminipigs, and Humans. *Journal of Drug Metabolism & Toxicology*, 5(6).
Jamei, M., 2016. Recent Advances in Development and Application of Physiologically-Based Pharmacokinetic (PBPK) Models : a Transition from Academic Curiosity to Regulatory Acceptance. *Current Pharmacology Reports*, pp.161–169.
Jansens, A. & Braakman, I., 2003. Pulse-Chase Labeling Techniques for the Analysis. *Methods in Molecular Biology, vol 232: Protein Misfolding and Disease: Principles and Protocols*, 232, pp.133–145.
Jayapal, K.P. et al., 2010. Multitagging proteomic strategy to estimate protein turnover rates in dynamic systems. *Journal of Proteome Research*, 9(5), pp.2087–2097.
Jeong, W.-S. et al., 2005. Differential expression and stability of endogenous nuclear factor E2-related factor 2 (Nrf2) by natural chemopreventive compounds in HepG2 human hepatoma cells. *Journal of biochemistry and molecular biology*,

38(2), pp.167–176.
Ji, L. et al., 2015. Psoralen, a mechanism-based inactivator of CYP2B6. *Chemico-biological interactions*, 240, pp.346–352.
Jia, J. et al., 2009. Mechanisms of drug combinations: interaction and network perspectives. *Nature reviews. Drug discovery*, 8(2), pp.111–28.
Joiakim, A. et al., 2004. Superinduction of CYP1A1 in MCF10A cultures by cycloheximide, anisomycin, and puromycin: a process independent of effects on protein translation and unrelated to suppression of aryl hydrocarbon receptor proteolysis by the proteasome. *Molecular pharmacology*, 66(4), pp.936–947.
Jones, H. & Rowland-Yeo, K., 2013. Basic concepts in physiologically based pharmacokinetic modeling in drug discovery and development. *CPT: pharmacometrics & systems pharmacology*, 2(August), p.e63.
Jones, H.M. et al., 2012. Application of PBPK modelling in drug discovery and development at Pfizer. *Xenobiotica; the fate of foreign compounds in biological systems*, 42(1), pp.94–106.
Jones, H.M. et al., 2015. Physiologically based pharmacokinetic modeling in drug discovery and development: a pharmaceutical industry perspective. *Clinical pharmacology and therapeutics*, 97(3), pp.247–262.
Ke, A. et al., 2016. Towards a Best Practice Approach in PBPK Modeling: Case Example of Developing a Unified Efavirenz Model Accounting for Induction of CYPs 3A4 and 2B6 (CPT: Pharmacometrics and Systems Pharmacology (2014) 3 (e122))). *CPT: Pharmacometrics and Systems Pharmacology*, 5(7), pp.367–376.
Kern, A. et al., 1997. Drug metabolism in hepatocyte sandwich cultures of rats and humans. *Biochemical pharmacology*, 54(7), pp.761–72.
Kharasch, E.D. et al., 2012. Mechanism of Efavirenz Influence on Methadone Pharmacokinetics and Pharmacodynamics. *Clinical Pharmacology & Therapeutics*, 91(4), pp.673–684.
Kim, H.S.H.J. et al., 2014. Evaluation of protein expression in housekeeping genes across multiple tissues in rats. *Korean Journal of Pathology*, 48(3), pp.193–200.
Kim, S.-M. et al., 2016. Hepatic cytochromes P450: structural degrons and barcodes, posttranslational modifications and cellular adapters in the ERAD-endgame. *Drug metabolism reviews*, 48(3), pp.405–33.
Koeller, D.M. et al., 1991. Translation and the stability of mRNAs encoding the transferrin receptor and c-fos. *Proceedings of the National Academy of Sciences*, 88(17), pp.7778–7782.
Kuhlmann, J. & Mück, W., 2001. Clinical-Pharmacological Strategies to Assess Drug Interaction Potential During Drug Development. *Drug safety*, 24(10), pp.715–725.
Kuramoto, S. et al., 2017. Simple evaluation method for CYP3A4 induction from human hepatocytes; the relative factor approach with an induction detection limit concentration based on the Emax model. *Drug Metabolism and Disposition*.
Lacsina, J.R. et al., 2012. Premature Translational Termination Products Are Rapidly Degraded Substrates for MHC Class I Presentation. *PLoS ONE*, 7(12).
Lamba, J. et al., 2012. PharmGKB summary. *Pharmacogenetics and Genomics*, 22(7), pp.555–558.
Lamba, V. et al., 2010. Genetic predictors of interindividual variability in hepatic CYP3A4 expression. *The Journal of pharmacology and experimental therapeutics*, 332(3), pp.1088–99.
Lecker, S.H., 2006. Protein Degradation by the Ubiquitin-Proteasome Pathway in

Normal and Disease States. *Journal of the American Society of Nephrology*, 17(7), pp.1807–1819.
Leclerc, G.J., Leclerc, G.M. & Barredo, J.C., 2002. Real-time RT-PCR analysis of mRNA decay: half-life of Beta-actin mRNA in human leukemia CCRF-CEM and Nalm-6 cell lines. *Cancer Cell International*, 2(1), p.1.
LeCluyse, E.L., 2001. Human hepatocyte culture systems for the in vitro evaluation of cytochrome P450 expression and regulation. *European Journal of Pharmaceutical Sciences*, 13(4), pp.343–368.
Lee, A.J. & Maddix, D.S., 2001. Rhabdomyolysis secondary to a drug interaction between simvastatin and clarithromycin. *Annals of Pharmacotherapy*, 35(1), pp.26–31.
Lee, W. & Wayne, N.L., 1998. The roles of transcription and translation in mediating the effect of electrical afterdischarge on neurohormone synthesis in Aplysia bag cell neurons. *Endocrinology*, 139(12), pp.5109–5115.
Leong, R. et al., 2012. Regulatory experience with physiologically based pharmacokinetic modeling for pediatric drug trials. *Clinical pharmacology and therapeutics*, 91(5), pp.926–31.
Levy, G. et al., 2015. Long-term culture and expansion of primary human hepatocytes. *Nature biotechnology*, 33(12), pp.1264–1271.
Li, F. et al., 2008. Thiopurine S-methyltransferase pharmacogenetics: autophagy as a mechanism for variant allozyme degradation. *Pharmacogenetics and genomics*, 18(12), pp.1083–94.
Li, H., Ferguson, S.S. & Wang, H., 2010. Synergistically enhanced CYP2B6 inducibility between a polymorphic mutation in CYP2B6 promoter and pregnane X receptor activation. *Molecular pharmacology*, 78(4), pp.704–13.
Li, X. et al., 2011. Synergy of the antiretroviral protease inhibitor indinavir and chloroquine against malaria parasites in vitro and in vivo. *Parasitology Research*, 109(6), pp.1519–1524.
Liao, M. et al., Cytochrome P450 Degradation and Its Clinical Relevance. In *Enzyme Inhibition in Drug Discovery and Development*. Hoboken, NJ, USA: John Wiley & Sons, Inc., pp. 363–406.
Liao, W., Yeung, S.C.J. & Chan, L., 1998. Proteasome-mediated degradation of apolipoprotein B targets both nascent peptides cotranslationally before translocation and full-length apolipoprotein B after translocation into the endoplasmic reticulum. *Journal of Biological Chemistry*, 273(42), pp.27225–27230.
Lindley, C. et al., 2002. The effect of cyclophosphamide with and without dexamethasone on cytochrome P450 3A4 and 2B6 in human hepatocytes. *Drug Metabolism and Disposition*, 30(7), pp.814–822.
Liston, H.L. et al., 2002. Differential Time Course of Cytochrome P450 2D6 Enzyme Inhibition by Fluoxetine, Sertraline, and Paroxetine in Healthy Volunteers HEIDI. *Journal of Clinical Psychopharmacology*, 22(2), pp.169–173.
Loboz, K.K. et al., 2005. HPLC assay for bupropion and its major metabolites in human plasma. *Journal of Chromatography B: Analytical Technologies in the Biomedical and Life Sciences*, 823(2), pp.115–121.
Lu, D. et al., 2016. Mechanism-based inactivation of cytochrome P450 2B6 by isopsoralen. *Xenobiotica*, 46(4), pp.335–341.
Lucas, D. et al., 1995. Decrease in cytochrome P452E1 as assessed by the rate of chlozoxazone hydroxylation in alcoholics during the withdrawal phase. *Alcohol Clin Exp Res*, 19(2), pp.362–6.

Lugowski, A., Nicholson, B. & Rissland, O.S., 2017. Determining mRNA half-lives on a transcriptome-wide scale. *Methods*, pp.4–12.
Lutz, J.D. et al., 2013. Stereoselective inhibition of CYP2C19 and CYP3A4 by fluoxetine and its metabolite: implications for risk assessment of multiple time-dependent inhibitor systems. *Drug metabolism and disposition: the biological fate of chemicals*, 41(12), pp.2056–65.
Magnusson, M.O. et al., 2007. Pharmacodynamics of Carbamazepine-mediated induction of CYP3A4, CYP1A2, and Pgp as assessed by probe substrates midazolam, caffeine and digoxin. *Clinical Pharmacology And Therapeutics*, 84(1), pp.52–62.
Mahmood, T. & Yang, P.C., 2012. Western blot: Technique, theory, and trouble shooting. *North American Journal of Medical Sciences*, 4(9), pp.429–434.
Majumder, P. et al., 2012. TDP-43 regulates the mammalian spinogenesis through translational repression of Rac1. *Acta neuropathologica*, 124(2), pp.231–45.
Mann, M., 2006. Functional and quantitative proteomics using SILAC. *Nature Reviews Molecular Cell Biology*, 7(12), pp.952–958.
Mao, J. et al., 2013. Prediction of crizotinib-midazolam interaction using the simcyp population-based simulator: Comparison of CYP3A time-dependent inhibition between human liver microsomes versus hepatocytes. *Drug Metabolism and Disposition*, 41(2), pp.343–352.
Marroquin, C.E. et al., 2004. Osteopontin increases CD44 expression and cell adhesion in RAW 264.7 murine leukemia cells. *Immunology Letters*, 95(1), pp.109–112.
Martin, P. et al., 2008. Comparison of the induction profile for drug disposition proteins by typical nuclear receptor activators in human hepatic and intestinal cells. *British journal of pharmacology*, 153(4), pp.805–19.
Masaki, R., Yamamoto, A. & Tashiro, Y., 1987. Cytochrome P-450 and NADPH-cytochrome P-450 reductase are degraded in the autolysosomes in rat liver. *Journal of Cell Biology*, 104(5), pp.1207–1215.
Matthews, H. et al., 2017. Investigating antimalarial drug interactions of emetine dihydrochloride hydrate using CalcuSyn-based interactivity calculations. *Plos One*, 12(3), p.e0173303.
Maurel, P., 1996. The use of adult human hepatocytes in primary culture and other in vitro systems to investigate drug metabolism in man. *Adv Drug Deliv Rev*, 22(96), pp.105–132.
Mayhew, B.S., Jones, D.R. & Hall, S.D., 2000. An in vitro model for predicting in vivo inhibition of cytochrome P450 3A4 by metabolic intermediate complex formation. *Drug metabolism and disposition: the biological fate of chemicals*, 28(9), pp.1031–1037.
Merry, C. et al., 1997. Saquinavir pharmacokinetics alone and in combination with ritonavir in HIV-infected patients. *Aids*, 11(15), pp.F29–F33.
Meunier, B., de Visser, S.P. & Shaik, S., 2004. Mechanism of Oxidation Reactions Catalyzed by Cytochrome P450 Enzymes. *Chemical Reviews*, 104(9), pp.3947–3980.
Millward, D.J., Bates, P.C. & Rosochacki, S., 1981. The extent and nature of protein degradation in the tissues during development. *Reproduction Nutrition Development*, 21(2), pp.265–277.
Montgomery, J.L. et al., 2003. Measurement of protein synthesis and degradation in C2C12 myoblasts using extracts of muscle from hormone treated bovine. *Methods in Cell Science*, 24(4), pp.123–129.

Morel, F. et al., 1990. Expression of cytochrome P-450 enzymes in cultured human hepatocytes. *Eur J Biochem*, 191(2), pp.437–444.
Murray, B.P., Zgoda, V.G. & Correia, M.A., 2002. Native CYP2C11: heterologous expression in Saccharomyces cerevisiae reveals a role for vacuolar proteases rather than the proteasome system in the degradation of this endoplasmic reticulum protein. *Molecular pharmacology*, 61(5), pp.1146–53.
Nagar, S., Walther, S. & Blanchard, R.L., 2006. Sulfotransferase (SULT) 1A1 Polymorphic Variants *1, *2, and *3 Are Associated with Altered Enzymatic Activity, Cellular Phenotype, and Protein Degradation. *Molecular Pharmacology*, 69(6), pp.2084–2092.
Nakagawa, H. et al., 2011. Ubiquitin-mediated proteasomal degradation of ABC transporters: A new aspect of genetic polymorphisms and clinical impacts. *Journal of Pharmaceutical Sciences*, 100(9), pp.3602–3619.
Nakayama, K.I. & Nakayama, K., 2006. Ubiquitin ligases: cell-cycle control and cancer. *Nature reviews. Cancer*, 6(5), pp.369–81.
Nebert, D.W., Wikvall, K. & Miller, W.L., 2013. Human cytochromes P450 in health and disease. *Philosophical Transactions of the Royal Society, B: Biological Sciences*, 368(1612), p.20120431/1-20120431/21.
Van Nguyen, T. et al., 1996. In vivo degradation of RNA polymerase II largest subunit triggered by α-amanitin. *Nucleic Acids Research*, 24(15), pp.2924–2929.
Nirogi, R. et al., 2015. Evaluation of metabolism dependent inhibition of CYP2B6 mediated bupropion hydroxylation in human liver microsomes by monoamine oxidase inhibitors and prediction of potential as perpetrators of drug interaction. *Chemico-Biological Interactions*, 230, pp.9–20.
Nishiya, Y. et al., 2009. Mechanism-based inhibition of human cytochrome P450 2B6 by ticlopidine, clopidogrel, and the thiolactone metabolite of prasugrel. *Drug Metabolism and Disposition*, 37(3), pp.589–593.
O'Mathúna, B. et al., 2008. The consequences of 3,4-methylenedioxymethamphetamine induced CYP2D6 inhibition in humans. *Journal of clinical psychopharmacology*, 28(5), pp.523–529.
O'Shaughnessy, J. et al., 2002. Superior survival with capecitabine plus docetaxel combination therapy in anthracycline-pretreated patients with advanced breast cancer: phase III trial results. *Journal of clinical oncology : official journal of the American Society of Clinical Oncology*, 20(12), pp.2812–23.
Obach, R.S., Walsky, R.L. & Venkatakrishnan, K., 2006. Mechanism-Based Inactivation of Human Cytochrome P450 Enzymes and the Prediction of Drug-Drug Interactions. *Drug Metabolism and Disposition*, 35(2), pp.246–255.
Okubo, M. et al., 2013. CYP3A4 intron 6 C>T polymorphism (CYP3A4*22) is associated with reduced CYP3A4 protein level and function in human liver microsomes. *The Journal of toxicological sciences*, 38(3), pp.349–54.
Ono, S. et al., 1995. Chlorzoxazone is metabolized by human CYP1A2 as well as by human CYP2E1. *Pharmacogenetics*, 5(3), p.143–50.
Pabarcus, M.K. et al., 2009. CYP3A4 ubiquitination by gp78 (the tumor autocrine motility factor receptor, AMFR) and CHIP E3 ligases. *Archives of Biochemistry and Biophysics*, 483(1), pp.66–74.
Paine, A.J., 1990. The maintenance of cytochrome P-450 in rat hepatocyte culture: Some applications of liver cell cultures to the study of drug metabolism, toxicity and the induction of the P-450 system. *Chemico-Biological Interactions*, 74(1–2), pp.1–31.
Pan, Y. & Haines, D.S., 1999. The pathway regulating MDM2 protein degradation

can be altered in human leukemic cells. *Cancer Research*, 59(9), pp.2064–2067.
Park, M.H. et al., 2017. Prediction of pharmacokinetics and drug-drug interaction potential using physiologically based pharmacokinetic (PBPK) modeling approach: A case study of caffeine and ciprofloxacin. *Korean Journal of Physiology and Pharmacology*, 21(1), pp.107–115.
Parkinson, A. et al., 2011. An evaluation of the dilution method for identifying metabolism-dependent inhibitors of cytochrome P450 enzymes. *Drug metabolism and disposition: the biological fate of chemicals*, 39(8), pp.1370–87.
Paul, S., 2008. Dysfunction of the ubiquitin-proteasome system in multiple disease conditions: Therapeutic approaches. *BioEssays*, 30(11–12), pp.1172–1184.
Pelkonen, O. et al., 2008. Inhibition and induction of human cytochrome P450 enzymes: Current status. *Archives of Toxicology*, 82(10), pp.667–715.
Peters, S.A. et al., 2012. Evaluation of the use of static and dynamic models to predict drug-drug interaction and its associated variability: impact on drug discovery and early development. *Drug metabolism and disposition: the biological fate of chemicals*, 40(8), pp.1495–507.
Pfaffl, M.W., 2001. A new mathematical model for relative quantification in real-time RT-PCR. *Nucleic acids research*, 29(9), p.e45.
Pichard, L. et al., 1992. Effect of corticosteroids on the expression of cytochromes P450 and on cyclosporin A oxidase activity in primary cultures of human hepatocytes. *Molecular pharmacology*, 41(6), pp.1047–1055.
Pitlick, W.H. et al., 1976. Pharmacokinetic Model to Describe Self-Induced Decreases in Steady-State Concentrations of Carbamazepine. *Journal of Pharmaceutical Sciences*, 65(3), pp.462–463.
Posimo, J.M. et al., 2014. Viability assays for cells in culture. *Journal of visualized experiments : JoVE*, 2(83), pp.1–14.
Pratt, J.M. et al., 2002. Dynamics of Protein Turnover, a Missing Dimension in Proteomics. *Molecular & Cellular Proteomics*, 1(8), pp.579–591.
Princiotta, M.F. et al., 2003. Quantitating protein synthesis, degradation, and endogenous antigen processing. *Immunity*, 18(3), pp.343–54.
Prueksaritanont, T. et al., 1996. Comparative studies of drug-metabolizing enzymes in dog, monkey, and human small intestines, and in Caco-2 cells. *Drug metabolism and disposition: the biological fate of chemicals*, 24(6), pp.634–42.
Prueksaritanont, T. et al., 2013. Drug-drug interaction studies: regulatory guidance and an industry perspective. *The AAPS journal*, 15(3), pp.629–45.
Punyawudho, B. et al., 2009. Characterization of the time course of carbamazepine deinduction by an enzyme turnover model. *Clinical Pharmacokinetics*, 48(5), pp.313–320.
Puskarjov, M. et al., 2012. Activity-Dependent Cleavage of the K-Cl Cotransporter KCC2 Mediated by Calcium-Activated Protease Calpain. *Journal of Neuroscience*, 32(33), pp.11356–11364.
Rakhmanina, N.Y. & van den Anker, J.N., 2011. Efavirenz in the Therapy of HIV Infection. *National Institutes of Health*, 6(1), pp.95–103.
Ramsden, D., Zhou, J. & Tweedie, D.J., 2015. Determination of a degradation constant for CYP3A4 by direct suppression of mRNA in a novel human hepatocyte model, HepatoPac. *Drug Metabolism and Disposition*, 43(9), pp.1307–1315.
Ravid, T. & Hochstrasser, M., 2008. Diversity of degradation signals in the ubiquitin–proteasome system. *Nature Reviews Molecular Cell Biology*, 9(9), pp.679–689.
Reitman, M.L. et al., 2011. Rifampin's acute inhibitory and chronic inductive drug

interactions: Experimental and model-based approaches to drug-drug interaction trial design. *Clinical Pharmacology and Therapeutics*, 89(2), pp.234–242.
Renwick, A.B. et al., 2000. Differential maintenance of cytochrome P450 enzymes in cultured precision-cut human liver slices. *Drug metabolism and disposition: the biological fate of chemicals*, 28(10), pp.1202–9.
Richter, T. et al., 2004. Potent mechanism-based inhibition of human CYP2B6 by clopidogrel and ticlopidine. *The Journal of pharmacology and experimental therapeutics*, 308(1), pp.189–97.
Riley, R.J. & Wilson, C.E., 2015. Cytochrome P450 time-dependent inhibition and induction: advances in assays, risk analysis and modelling. *Expert Opinion on Drug Metabolism & Toxicology*, 11(4), pp.557–572.
Riss, T.L. et al., 2004. *Cell Viability Assays*,
Roberts, B.J. et al., 1995. Ethanol induces CYP2E1 by protein stabilization: Role of ubiquitin conjugation in the rapid degradation of CYP2E1. *Journal of Biological Chemistry*, 270(50), pp.29632–29635.
Rodriguez-Antona, C. et al., 2002. Cytochrome P450 expression in human hepatocytes and hepatoma cell lines: molecular mechanisms that determine lower expression in cultured cells. *Xenobiotica*, 32(6), pp.505–520.
Rodriguez, S., Gaunt, T.R. & Day, I.N.M., 2009. Hardy-Weinberg Equilibrium Testing of Biological Ascertainment for Mendelian Randomization Studies. *American Journal of Epidemiology*, 169(4), pp.505–514.
Ronis, M.J. et al., 1991. Acetone-regulated synthesis and degradation of cytochrome P4502E2 and cytochrome P4502B1 in rat liver. *Eur J Biochem*, 198, pp.383–389.
Ronis, M.J.J. & Ingelman-Sundberg, M., 1989. Acetone-dependent regulation of cytochrome P-450j (IIE1) and P-450b (IIB1) in rat liver. *Xenobiotica*, 19(10), pp.1161–1165.
Rostami-Hodjegan, A., 2012. Physiologically based pharmacokinetics joined with in vitro-in vivo extrapolation of ADME: a marriage under the arch of systems pharmacology. *Clinical pharmacology and therapeutics*, 92(1), pp.50–61.
Rostami-Hodjegan, A. et al., 1999. Population pharmacokinetics of methadone in opiate users: Characterization of time-dependent changes. *British Journal of Clinical Pharmacology*, 48(1), pp.43–52.
Rowland Yeo, K. et al., 2011. Prediction of time-dependent CYP3A4 drug-drug interactions by physiologically based pharmacokinetic modelling: Impact of inactivation parameters and enzyme turnover. *European Journal of Pharmaceutical Sciences*, 43(3), pp.160–173.
Ruggiano, A., Foresti, O. & Carvalho, P., 2014. ER-associated degradation: Protein quality control and beyond. *The Journal of Cell Biology*, 204(6), pp.869–879.
Runge, D. et al., 2000. Serum-Free, Long-Term Cultures of Human Hepatocytes: Maintenance of Cell Morphology, Transcription Factors, and Liver-Specific Functions. *Biochemical and Biophysical Research Communications*, 269(1), pp.46–53.
Sawicki, S.G. & Godman, G.C., 1971. On the differential cytotoxicity of actinomycin D. *The Journal of cell biology*, 50(3), pp.746–61.
Schipani, A. et al., 2010. Population pharmacokinetic modeling of the association between 63396C→T pregnane X receptor polymorphism and unboosted atazanavir clearance. *Antimicrobial Agents and Chemotherapy*, 54(12), pp.5242–5250.
Schmidt, M. & Finley, D., 2014. Regulation of proteasome activity in health and

disease. *Biochimica et biophysica acta*, 1843(1), pp.13–25.
Schneider-Poetsch, T. et al., 2010. Inhibition of eukaryotic translation elongation by cycloheximide and lactimidomycin. *Nature chemical biology*, 6(3), pp.209–217.
Schuetz, J.D., Strom, S.C. & Schuetz, E.G., 1995. Induction of P-glycoprotein mRNA by protein synthesis inhibition is not controlled by a transcriptional repressor protein in rat and human liver cells. *Journal of cellular physiology*, 165(2), pp.261–72.
Scripture, C.D. & Figg, W.D., 2006. Drug interactions in cancer therapy. *Nature reviews. Cancer*, 6(7), pp.546–58.
Shi, W.-L., Tang, H.-L. & Zhai, S.-D., 2015. Effects of the CYP3A4*1B Genetic Polymorphism on the Pharmacokinetics of Tacrolimus in Adult Renal Transplant Recipients: A Meta-Analysis. *PloS one*, 10(6), p.e0127995.
Shou, M. et al., 2008. Modeling, prediction, and in vitro in vivo correlation of CYP3A4 induction. *Drug Metabolism and Disposition*, 36(11), pp.2355–2370.
Shulman, M. & Nahmias, Y., 2013. Long-term culture and coculture of primary rat and human hepatocytes. *Methods in molecular biology (Clifton, N.J.)*, 945, pp.287–302.
Siccardi, M. et al., 2008. Association of a Single-Nucleotide Polymorphism in the Pregnane X Receptor (PXR 63396C→T) with Reduced Concentrations of Unboosted Atazanavir. *Clinical Infectious Diseases*, 47(9), pp.1222–1225.
Siccardi, M. et al., 2012. Pharmacokinetic and pharmacodynamic analysis of efavirenz dose reduction using an in vitro-in vivo extrapolation model. *Clinical pharmacology and therapeutics*, 92(4), pp.494–502.
Silverman, R.B., 1995. [10] Mechanism-based enzyme inactivators. In pp. 240–283.
Simões, A.E. et al., 2013. Efficient recovery of proteins from multiple source samples after trizol® or trizol®LS RNA extraction and long-term storage. *BMC Genomics*, 14(1), p.181.
Smith, C.M. et al., 2012. A comprehensive evaluation of metabolic activity and intrinsic clearance in suspensions and monolayer cultures of cryopreserved primary human hepatocytes. *Journal of Pharmaceutical Sciences*, 101(10), pp.3989–4002.
Soars, M.G., Grime, K. & Riley, R.J., 2006. Comparative analysis of substrate and inhibitor interactions with CYP3A4 and CYP3A5. *Xenobiotica; the fate of foreign compounds in biological systems*, 36(4), pp.287–99.
Sobell, H.M., 1985. Actinomycin and DNA transcription. *Proceedings of the National Academy of Sciences of the United States of America*, 82(16), pp.5328–31.
Soldatow, V.Y. et al., 2013. In vitro models for liver toxicity testing. *Toxicol. Res.*, 2(1), pp.23–39.
Sridar, C., Kenaan, C. & Hollenberg, P.F., 2012. Inhibition of bupropion metabolism by selegiline: Mechanism-based inactivation of human CYP2B6 and characterization of glutathione and peptide adducts. *Drug Metabolism and Disposition*, 40(12), pp.2256–2266.
Stintzing, S. et al., 2015. Polymorphisms in Genes Involved in EGFR Turnover Are Predictive for Cetuximab Efficacy in Colorectal Cancer. *Molecular cancer therapeutics*, 14(October), pp.1–9.
Stordeur, P. et al., 1995. Spontaneous and cycloheximide-induced interleukin-10 mRNA expression in human mononuclear cells. *Molecular immunology*, 32(4), pp.233–9.
Strober, W., 2001. Trypan blue exclusion test of cell viability. *Current protocols in immunology*, Appendix 3, p.Appendix 3B.

Su Yin Low, J. et al., 2009. Antiviral Activity of Emetine Dihydrochloride Against Dengue Virus Infection. *Journal of Antivirals & Antiretrovirals*, 1(1), pp.062–071.
Tai, H.L. et al., 1999. Enhanced proteasomal degradation of mutant human thiopurine S-methyltransferase (TPMT) in mammalian cells: mechanism for TPMT protein deficiency inherited by TPMT*2, TPMT*3A, TPMT*3B or TPMT*3C. *Pharmacogenetics*, 9(5), pp.641–50.
Takahashi, R.H. et al., 2017. Applying Stable Isotope Labeled Amino Acids in Micropatterned Hepatocyte Coculture to Directly Determine the Degradation Rate Constant for CYP3A4. *Drug Metabolism and Disposition*, 45(6), p.581 LP-585.
Takei, S. et al., 2000. Destabilization of tumor necrosis factor-alpha mRNA by 5-alpha dihydrotestosterone in Jurkat cells. *Life sciences*, 66(20), p.PL277-82.
Tallarida, R.J., 2006. An overview of drug combination analysis with isobolograms. *The Journal of pharmacology and experimental therapeutics*, 319(1), pp.1–7.
Tallarida, R.J., 2010. Combination analysis. *Advances in Experimental Medicine and Biology*, 678, pp.133–137.
Tallarida, R.J., 2011. Quantitative methods for assessing drug synergism. *Genes & cancer*, 2(11), pp.1003–8.
Tan, D. & Walker, A.M., 2010. Short form 1b human prolactin receptor down-regulates expression of the long form. *Journal of Molecular Endocrinology*, 44(3), pp.187–197.
Tanaka, E., 1998. Clinically important pharmacokinetic drug-drug interactions: role of cytochrome P450 enzymes. *J.Clin.Pharm.Ther.*, 23(0269–4727), pp.403–416.
Thoene, J.G. et al., 1985. Inhibitors of Protein Synthesis Also Inhibit Lysosomal Proteolysis. *Journal of Clinical Investigation*, 75(February), pp.370–376.
Tokunaga, F., Hara, K. & Koide, T., 2003. N-Linked oligosaccharide processing, but not association with calnexin/calreticulin is highly correlated with endoplasmic reticulum-associated degradation of antithrombin Glu313-deleted mutant. *Archives of Biochemistry and Biophysics*, 411(2), pp.235–242.
Tolson, A.H. et al., 2009. Methadone induces the expression of hepatic drug-metabolizing enzymes through the activation of pregnane X receptor and constitutive androstane receptor. *Drug metabolism and disposition: the biological fate of chemicals*, 37(9), pp.1887–94.
Toyama, B.H. & Hetzer, M.W., 2013. Protein homeostasis: live long, won't prosper. *Nature reviews. Molecular cell biology*, 14(1), pp.55–61.
Tran, J.Q. et al., 1999. Morning spot and 24-hour urinary 6 beta-hydroxycortisol to cortisol ratios: intraindividual variability and correlation under basal conditions and conditions of CYP 3A4 induction. *Journal of clinical pharmacology*, 39(5), pp.487–494.
Tsao, D.C. et al., 2012. Prolonged -amanitin treatment of cells for studying mutated polymerases causes degradation of DSIF160 and other proteins. *RNA*, 18(2), pp.222–229.
Varma, M. V et al., 2014. Quantitative prediction of transporter- and enzyme-mediated clinical drug-drug interactions of organic anion-transporting polypeptide 1B1 substrates using a mechanistic net-effect model. *J Pharmacol Exp Ther*, 351(1), pp.214–223.
Venkatakrishnan, K. & Obach, R.S., 2007. Drug-drug interactions via mechanism-based cytochrome P450 inactivation: points to consider for risk assessment from in vitro data and clinical pharmacologic evaluation. *Current drug metabolism*,

8(5), pp.449–62.
Venkatakrishnan, K. & Obach, R.S., 2005. In vitro-in vivo extrapolation of CYP2D6 inactivation by paroxetine: prediction of nonstationary pharmacokinetics and drug interaction magnitude. *Drug metabolism and disposition: the biological fate of chemicals*, 33(6), pp.845–52.
Venkatakrishnan, K., Obach, R.S. & Rostami-Hodjegan, A., 2007. Mechanism-based inactivation of human cytochrome P450 enzymes: strategies for diagnosis and drug-drug interaction risk assessment. *Xenobiotica; the fate of foreign compounds in biological systems*, 37(10–11), pp.1225–56.
Verma, S. et al., 2005. Capecitabine plus Docetaxel Combination Therapy. *Cancer*, 103(12), pp.2455–2465.
Vilei, M.T. et al., 2001. Comparison of pig, human and rat hepatocytes as a source of liver specific metabolic functions in culture systems--implications for use in bioartificial liver devices. *The International journal of artificial organs*, 24(6), pp.392–6.
Vozza-brown, L., Grepper, S. & Sahi, J., 2005. Suppression of OATP1B1 , OATP1B3 , and OATP2B1 Transporters in Primary Cryopreserved Human Hepatocytes Following Lipid Delivery of Stealth siRNA ™. , 1(1999), p.92008.
Wagner, C. et al., 2015. Predicting the effect of cytochrome P450 inhibitors on substrate drugs: analysis of physiologically based pharmacokinetic modeling submissions to the US Food and Drug Administration. *Clinical pharmacokinetics*, 54(1), pp.117–27.
Walsky, R.L., Astuccio, A. V & Obach, R.S., 2006. Evaluation of 227 drugs for in vitro inhibition of cytochrome P450 2B6. *Journal of clinical pharmacology*, 46(12), pp.1426–1438.
Wang, A. et al., 2012. Crystal Structure of Human Cytochrome P450 2D6 with Prinomastat Bound. *Journal of Biological Chemistry*, 287(14), pp.10834–10843.
Wang, D. et al., 2011. Intronic polymorphism in CYP3A4 affects hepatic expression and response to statin drugs. *The pharmacogenomics journal*, 11(4), pp.274–86.
Wang, H. & Tompkins, L.M., 2008. CYP2B6: new insights into a historically overlooked cytochrome P450 isozyme. *Current drug metabolism*, 9(7), pp.598–610.
Wang, Y. et al., 2009. A role for protein phosphorylation in cytochrome P450 3A4 ubiquitin-dependent proteasomal degradation. *The Journal of biological chemistry*, 284(9), pp.5671–5684.
Wang, Y. et al., 2015. Human liver cytochrome P450 3A4 ubiquitination: molecular recognition by UBC7-gp78 autocrine motility factor receptor and UbcH5a-CHIP-Hsc70-Hsp40 E2-E3 ubiquitin ligase complexes. *The Journal of biological chemistry*, 290(6), pp.3308–32.
Wang, Y. et al., 2011. Ubiquitin-dependent proteasomal degradation of human liver cytochrome P450 2E1: identification of sites targeted for phosphorylation and ubiquitination. *The Journal of biological chemistry*, 286(11), pp.9443–56.
Wang, Y.H., 2010. Confidence assessment of the Simcyp time-based approach and a static mathematical model in predicting clinical drug-drug interactions for mechanism-based CYP3A inhibitors. *Drug Metabolism and Disposition*, 38(7), pp.1094–1104.
Warren, J.W. et al., 1980. Kinetics of a carbamazepine-ethosuximide interaction. *Clinical Pharmacology & Therapeutics*, 28(5), pp.646–651.
Waterlow, J.C., 1984. Protein turnover with special reference to man. *Quarterly Journal of Experimental Physiology*, 69(3), pp.409–438.

Watkins, P.B. et al., 1985. Identification of an inducible form of cytochrome P-450 in human liver. *Proceedings of the National Academy of Sciences of the United States of America*, 82(18), pp.6310–6314.
Weitzel, H.E. et al., 2004. Differential stability of beta-catenin along the animal-vegetal axis of the sea urchin embryo mediated by dishevelled. *Development (Cambridge, England)*, 131, pp.2947–2956.
Welch, P.J. & Wang, J.Y., 1992. Coordinated synthesis and degradation of cdc2 in the mammalian cell cycle. *Proceedings of the National Academy of Sciences of the United States of America*, 89(7), pp.3093–3097.
Westerink, W.M.A. & Schoonen, W.G.E.J., 2007. Cytochrome P450 enzyme levels in HepG2 cells and cryopreserved primary human hepatocytes and their induction in HepG2 cells. *Toxicology in vitro : an international journal published in association with BIBRA*, 21(8), pp.1581–91.
Whitehead, K. a, Langer, R. & Anderson, D.G., 2009. Knocking down barriers: advances in siRNA delivery. *Nature reviews. Drug discovery*, 8(2), pp.129–38.
Wienkers, L.C. & Heath, T.G., 2005. Predicting in vivo drug interactions from in vitro drug discovery data. *Nat Rev Drug Discov*, 4(10), pp.825–833.
Williams, J.A. et al., 2004. Drug-drug interactions for UDP-glucuronosyltransferase substrates: a pharmacokinetic explanation for typically observed low exposure (AUCi/AUC) ratios. *Drug metabolism and disposition: the biological fate of chemicals*, 32(11), pp.1201–8.
Williams, P. A. et al., 2000. Mammalian microsomal cytochrome P450 monooxygenase: structural adaptations for membrane binding and functional diversity. *Molecular cell*, 5(1), pp.121–131.
Wittrup, A. & Lieberman, J., 2015. Knocking down disease: a progress report on siRNA therapeutics. *Nature reviews. Genetics*, 16(9), pp.543–52.
Wong, S.G., Lee, M. & Wong, B.K., 2016. Single concentration loss of activity assay provides an improved assessment of drug–drug interaction risk compared to IC50-shift. *Xenobiotica*, 8254(March), pp.1–14.
Woosley, R.L. et al., 1993. Mechanism of the cardiotoxic actions of terfenadine. *JAMA*, 269(12), pp.1532–6.
Xie, F., Ding, X. & Zhang, Q.-Y., 2016. An update on the role of intestinal cytochrome P450 enzymes in drug disposition. *Acta pharmaceutica Sinica. B*, 6(5), pp.374–383.
Xu, Y. et al., 2015. Physiologically Based Pharmacokinetic Model to Assess the Influence of Blinatumomab-Mediated Cytokine Elevations on Cytochrome P450 Enzyme Activity. *CPT: Pharmacometrics & Systems Pharmacology*, 4(9), pp.507–515.
Yamashita, F. et al., 2013. Modeling of Rifampicin-Induced CYP3A4 Activation Dynamics for the Prediction of Clinical Drug-Drug Interactions from In Vitro Data. *PLoS ONE*, 8(9).
Yang, J. et al., 2008. Cytochrome P450 Turnover: Regulation of Synthesis and Degradation, Methods for Determining Rates, and Implications for the Prediction of Drug Interactions. *Curr Drug Metab*, 9, pp.384–393.
Yang, J. et al., 2005. Kinetic values for mechanism-based enzyme inhibition: Assessing the bias introduced by the conventional experimental protocol. *European Journal of Pharmaceutical Sciences*, 26(3–4), pp.334–340.
Yen, H.C. et al., 2008. Global protein stability profiling in mammalian cells. *Science*, 322(5903), pp.918–923.
Yeo, K.R., Jamei, M. & Rostami-Hodjegan, A., 2013. Predicting drug-drug

interactions: application of physiologically based pharmacokinetic models under a systems biology approach. *Expert review of clinical pharmacology*, 6(2), pp.143–57.
Yewdell, J.W. et al., 2011. Out with the old, in with the new? Comparing methods for measuring protein degradation. *Cell biology international*, 35(5), pp.457–62.
Yubero-lahoz, S. et al., 2000. Sex Differences in 3,4-Methylenedioxymethamphetamine (MDMA; Ecstasy)-Induced Cytochrome P450 2D6 Inhibition in Humans. *Clinical Pharmacokinetics*, 50(5), pp.319–329.
Zang, Y. et al., 2004. The T341C (Ile114Thr) polymorphism of N-acetyltransferase 2 yields slow acetylator phenotype by enhanced protein degradation. *Pharmacogenetics*, 14(11), pp.717–723.
Zanger, U.M. & Klein, K., 2013. Pharmacogenetics of cytochrome P450 2B6 (CYP2B6): Advances on polymorphisms, mechanisms, and clinical relevance. *Frontiers in Genetics*, 4(MAR), pp.1–12.
Zanger, U.M. & Schwab, M., 2013. Pharmacology & Therapeutics Cytochrome P450 enzymes in drug metabolism : Regulation of gene expression , enzyme activities , and impact of genetic variation. *Pharmacology and Therapeutics*, 138(1), pp.103–141.
Zeilinger, K. et al., 2016. Cell sources for *in vitro* human liver cell culture models. *Experimental Biology and Medicine*, 241(15), pp.1684–1698.
Zeldin, R.K. & Petruschke, R.A., 2004. Pharmacological and therapeutic properties of ritonavir-boosted protease inhibitor therapy in HIV-infected patients. *Journal of Antimicrobial Chemotherapy*, 53(1), pp.4–9.
Zhang, H. et al., 2016. Content and activity of human liver microsomal protein and prediction of individual hepatic clearance in vivo. *Scientific Reports*, 5(1), p.17671.
Zhang, L. et al., 2007. Method for real-time monitoring of protein degradation at the single cell level. *BioTechniques*, 42(4), pp.446–450.
Zhang, T. et al., 2015. gp78 functions downstream of Hrd1 to promote degradation of misfolded proteins of the endoplasmic reticulum. *Molecular biology of the cell*, pp.5–6.
Zhang, X. et al., 2010. Inhibition of CYP3A by erythromycin: in vitro-in vivo correlation in rats. *Drug metabolism and disposition: the biological fate of chemicals*, 38(1), pp.61–72.
Zhang, Z.-Y. & Wong, Y.N., 2005. Enzyme kinetics for clinically relevant CYP inhibition. *Current drug metabolism*, 6(3), pp.241–257.
Zhao, P., Rowland, M. & Huang, S.-M., 2012. Best practice in the use of physiologically based pharmacokinetic modeling and simulation to address clinical pharmacology regulatory questions. *Clinical pharmacology and therapeutics*, 92(1), pp.17–20.
Zhou, P., 2004. Determining protein half-lives. *Methods in molecular biology (Clifton, N.J.)*, 284, pp.67–77.
Zhou, S.-F., 2008. Drugs behave as substrates, inhibitors and inducers of human cytochrome P450 3A4. *Current drug metabolism*, 9(4), pp.310–22.
Zhou, X. et al., 2016. Synergistic effects of Chinese herbal medicine: A comprehensive review of methodology and current research. *Frontiers in Pharmacology*, 7(JUL), pp.1–16.